Développement de biopuces dédiées au tri d'échantillons cellulaires

Radoslaw Bombera

▶ **To cite this version:**

Radoslaw Bombera. Développement de biopuces dédiées au tri d'échantillons cellulaires. Autre [q-bio.OT]. Université de Grenoble, 2011. Français. NNT : 2011GRENV065 . tel-00680029

HAL Id: tel-00680029
https://theses.hal.science/tel-00680029

Submitted on 17 Mar 2012

UNIVERSITÉ DE GRENOBLE

THÈSE

Pour obtenir le grade de

DOCTEUR DE L'UNIVERSITÉ DE GRENOBLE

Spécialité : **Chimie - Biologie**

Arrêté ministériel : 7 août 2006

Présentée par

Radoslaw BOMBERA

Thèse dirigée par **Thierry LIVACHE** et
codirigée par **Yoann ROUPIOZ**

préparée au sein du **CEA Grenoble
Institut Nanosciences et Cryogènie (INAC)
Service : Structures et Propriétés d'Architectures Moléculaires (SPrAM)
Groupe : Chimie pour la Reconnaissance et l'Etude d'Assemblages
Biologiques (CREAB)**
dans **l'École Doctorale Chimie et Sciences du Vivant**

Développement de biopuces dédiées au tri d'échantillons cellulaires

Thèse soutenue publiquement le **5 décembre 2011**,
devant le jury composé de :

M. Eric DEFRANCQ
Professeur (Université de Grenoble), Président
Mme Carole CHAIX
Directeur de recherche CNRS (Université Lyon 1), Rapporteur
M. Pascal COLPO
Directeur de recherche (Commission Européenne, JRC – Ispra, Italie), Rapporteur
M. Ali LAAYOUN
Directeur de recherche (bioMérieux S.A., Grenoble), Membre
M. Thierry LIVACHE
Directeur de recherche CEA (CEA Grenoble), Membre
M. Yoann ROUPIOZ
Chargé de recherche CNRS (CEA Grenoble), Membre

UNIVERSITÉ DE GRENOBLE

Development of biochips for blood cell sorting

PhD thesis by

Radoslaw BOMBERA

Grenoble 2011

Remerciements

La thèse est une étape particulière de la vie professionnelle, pleine de découvertes scientifiques et discussions intéressantes accompagnées par des longues heures de manipes et de rédaction. Hormis l'épanouissement intellectuel, c'est une période riche au niveau relationnel grâce aux différents gens qui contribuent à ce travail de façon directe ou indirecte. Pendant, les trois années de thèse j'ai eu l'occasion de côtoyer plusieurs personnes qui m'ont permis d'enrichir cette expérience et dont je tiens à remercier en quelques mots.

Tout d'abord, j'aimerais exprimer ma grande reconnaissance à mes deux directeurs de thèse Yoann Roupioz et Thierry Livache sans lesquels ce travail n'aurait pas la présente forme. Ainsi, je remercie Toi Thierry de m'avoir accueilli dans le laboratoire CREAB où j'ai pu apprendre beaucoup et où tu crées une ambiance inoubliable. Merci d'avoir toujours trouvé du temps malgré tes nombreuses obligations, pour partager ton expérience scientifique et ton vécu professionnel, participer à des discussions intéressantes (parfois agrémentées avec tes anecdotes) ou bien remonter le moral d'un jeune chercheur lorsqu'il a l'impression que rien ne marche… Je remercie également Yoann pour l'accompagnement pendant toute mon expérience au CREAB. Je te remercie de m'avoir guidé dans les méandres du monde de la recherche et ramené là où je suis aujourd'hui. J'ai appris beaucoup de choses à tes côtés et je t'en remercie. Merci du temps que tu as consacré pour me transmettre ton savoir et ton expérience aussi bien que pour corriger mes dissertations en français (mon expression écrite est au top grâce à Toi !). Ici, j'aimerais adresser mes remerciements à Loïc Leroy qui est naturellement devenu mon non-officiel co-directeur de thèse. Je te suis reconnaissant pour ton aide inestimé dans la partie optique du projet et ton implication dans ma thèse allant de l'accompagnement pendant les manipes, la réalisation de mesures optiques et jusqu'à la lecture de mon manuscrit. Merci pour ton approche très pédagogique, ta patience et ta motivation d'expliquer la physique à tout moment (même pendant le repas). Un grand MERCI à tous les trois – c'a été un énorme plaisir de vous connaître et avoir la possibilité de travailler avec vous.

Je remercie par la suite les membres du jury qui ont accepté de juger mon travail et moi-même en qualité de chercheur. Merci à madame Carole Chaix et monsieur Pascal Colpo pour le temps qu'ils ont consacré à la lecture détaillée de mon manuscrit de thèse et de leur appréciation pour ce travail. Merci à professeur Eric Defrancq d'avoir présidé le jury de soutenance (la deuxième fois pour moi) et ses commentaires très pertinents concernant la chimie. Merci aussi à monsieur Ali Laayoun dont la rencontre et l'approche industrielle m'ont été très profitable. Je remercie l'ensemble du jury d'avoir trouvé du temps parmi leurs nombreuses contraintes professionnelles et de l'intérêt qu'ils ont porté à mon travail.

Je tiens à remercier la Fondation Nanosciences, y compris la Direction, les comités scientifiques et l'équipe administrative de m'avoir apporté le soutien financier grâce auquel j'ai pu réaliser mon doctorat en France. Plus particulièrement, je remercie Stéphanie Monfront que j'ai eu un grand plaisir de connaître en dehors du cadre professionnel.

J'adresse mes remerciements à quelques personnes de la communauté scientifique de Grenoble qui ont apporté leur expertise à différentes étapes de cette thèse : Sylvie Elsen pour les conseils concernant la purification des protéines, Christine Saint-Pierre et Michel Jaquinod pour les analyses en spectrométrie de masse ainsi que Patrice Marche et son équipe pour la préparation des échantillons cellulaires. Je remercie également certains collègues du laboratoire qui ont eu envie de faire le lien entre nos projets respectifs et donner lieu à des expériences intéressantes. Merci à Jie Liu pour les manipes réalisées ensemble et la détermination que nous avons partagé pour capturer

Contents

Abbreviations

ATP	Adenosine triphosphate
Au	Gold
BCR	B-cell receptor
bp	Base pair
BSA	Bovine serum albumin
CbpE	Choline binding protein E
CD	Cluster of differentiation
CE	Counter electrode
CEA	French Atomic Energy Commission (fr. *Commissariat à l'Energie Atomique*)
cfu	Colony forming unit
CK	Creatine kinase
CKBB	Creatine kinase BB human brain fraction
CKMM	Creatine kinase MM human muscle fraction
CLEF	Contactless electrofunctionalization
CNRS	*Centre Nationale de la Recherche Scientifique* (fr.)
ConA	Concanavalin A
CPK	Creatine phosphokinase
CREAB	Research group: *Chimie pour la Reconnaissance et l'Etude d'Assemblages Biologiques* (fr.)
CTC	Circulating tumor cells
DDI	DNA-directed immobilization
DEP	Dielectrophoresis
DMEM	*Dulbecco's Modified Eagle Medium*
DMF	N,N-Dimethylformamide
DMF	N,N-dimethylformamide
DNA	Deoxyribonucleic acid
dsDNA	Double-stranded DNA
DSS	Disuccinimidyl suberate
DTT	Dithiothreitol
EDC	1-Ethyl-3-(3-dimethylaminopropyl)carbodiimide hydrochloride
EDTA	Ethylenediaminetetraacetic acid
ELISA	Enzyme-linked immunosorbent assay
ELISPOT	Enzyme-linked immunosorbent spot assay
ESI	Electrospray ionization
Fab	Fragment antigen-binding
FACS	Fluorescence-activated cell sorting

FBS	Fetal bovine serum
Fc	Fragment crystallizable
h	Hour
HPLC	High-performance liquid chromatography
IAB	Institut Albert Bonniot
IARC	International Agency for Research on Cancer
IBEB	Institute of environmental biology and biotechnology
IBS	*Institut de Biologie Structurale* (fr.)
ICS	Intracellular cytokine staining
ID	Inside diameter
IFN	Interferon
IgG	Immunoglobulin G
IL	Interleukin
LAAS	*Laboratoire d'Analyse et d'Architecture des Systèmes* (fr.)
LAN	Nucleic Acid Lesions laboratory; *Lésions des Acides Nucléiques* (fr.)
LED	Light emitting diode
LOC	Lab-on-a-chip
MACS	Magnetic-activated cell sorting
MALDI	Matrix assisted laser desorption ionisation
min	Minute
mL	Milliliter
MS	Mass spectrometry
MW	Molecular weight
MWCO	Molecular weight cut-off
NHS	N-hydroxysuccinimidyl
NIH	The National Institutes of Health
NK	Natural killer
NP	Nanoparticle
NTA	Nitrilotriacetic acid
OD	Optical density
PBS	Phosphate buffer saline
PCR	Polymerase chain reaction
PDB	Protein Data Bank
PDMS	Polydimethylsiloxane
PEEK	Polyether ether ketone
PEG	Polyethylene glycol
PhD	Doctor of Philosophy (lat. *philosophiae doctor*)
Py	Pyrrole
Ppy	Polypyrrole
PS	Polystyrene

PTFE	Polytetrafluoroethylene
Py	Pyrrole
R	Reflectivity
Rab-IgG	IgG from rabbit serum
RBC	Red blood cells
RNA	Ribonucleic acid
RPMI	*Roswell Park Memorial Institute medium*
RT	Room temperature
SAM	Self assembled monolayer
siRNA	Small interfering RNA
SM(PEG)$_{12}$	Succinimidyl-[(N-maleimidopropionamido)-dodecaethyleneglycol
SP	Surface plasmon
SPR	Surface plasmon resonance
SPRAM	Research laboratory: *Structures et Propriétés d'Architectures Moléculaires* (fr.)
SPRi	Surface plasmon resonance imaging
ssDNA	Single-stranded DNA
STV	Streptavidin
STV-PE	Streptavidin and R-phycoerythrin conjugate
TCEP	Tris(2-carboxyethyl) phosphine
TCR	T-cell receptor
TE	Transverse electric mode
TH	Todd Hewitt broth
TIR	Total internal reflection
T_m	Melting temperature
TM	Transverse magnetic mode
t_R	Retention time
WBC	White blood cells
WE	Working electrode
*	Complementary DNA strand

Introduction

Au début du présent manuscrit, il est important d'établir les motivations et les principaux objectifs de ce travail de thèse. Nous nous concentrons ainsi sur l'échantillon sanguin en tant que riche source d'information, essentielle du point de vue du diagnostic et de la recherche. Ceci implique un fort intérêt d'études sur cet échantillon biologique et sur les cellules sanguines en particulier. Parmi les différents composants du sang, les lymphocytes représentent une fraction cellulaire qui joue une des rôles primordiaux dans le fonctionnement de l'organisme humain. Ils sont responsables des mécanismes de défense immunitaire qui constituent la barrière de protection contre les différents pathogènes. Les acquis en immunologie montrent la complexité des réponses immunitaires générées par les lymphocytes et indiquent un réel besoin d'une recherche plus approfondie sur ces divers phénomènes. Cette approche doit néanmoins faire face à de nombreux défis comme une grande diversité des lymphocytes, leur faible quantité dans un échantillon de sang total ainsi qu'une grande sensibilité aux variations des conditions extérieures.

Afin de découvrir les aspects fondamentaux de l'immunologie, il est particulièrement intéressant d'examiner une population de lymphocytes bien définie. C'est pourquoi nous avons besoin d'outils de recherche capables de réaliser un tri cellulaire efficace. Dans ce domaine, il existe de nombreuses techniques utilisées en routine à l'échelle du laboratoire (*e.g.* FACS$^{®}$) mais ces procédures sont souvent longues, coûteuses et nécessitent une quantité d'échantillon importante. Un développement récent des systèmes miniaturisés ouvre de nouvelles voies de fractionnement de cellules vivantes à l'échelle micrométrique. L'exemple d'une biopuce est ainsi proposé par ce travail de thèse.

En effet, ce projet vise à construire une microplateforme capable d'immobiliser spécifiquement les cellules sanguines et par la suite d'effectuer leur relargage contrôlé depuis la surface. Dans ce cadre, deux stratégies indépendantes seront ici explorées : la première basée sur le clivage enzymatique et la deuxième exploitant une approche originale de désorption par chauffage localisée. Nous démontrerons ainsi la faisabilité du tri cellulaire à partir d'un mélange de lymphocytes primaires. Une technique basée sur la résonance plasmonique de surface (*Surface Plasmon Resonance* ou *SPR*) assurera la détection de phénomènes moléculaires et cellulaires en temps réel et sans marquage.

Le travail de thèse décrit par le présent manuscrit est une approche pluridisciplinaire qui touche à des domaines à l'interface entre la Chimie, la Biologie et la Physique. En vue de cela, la bibliographie nécessaire à la compréhension des résultats sera introduite au fur et à mesure. Ainsi, suite à l'introduction générale, le lecteur trouvera trois grandes parties (chapitre 2 à 4) qui décrivent les résultats obtenus dans le cadre de ce projet. Chapitre 2 sera principalement consacré à la construction de l'assemblage moléculaire formant la base de la biopuce proposée. Ensuite, le Chapitre 3 détaillera la stratégie de relargage contrôlé par la voie enzymatique alors que le Chapitre 4 présentera la désorption des protéines et des cellules vivantes par un faisceau laser couplé au SPR. Nous terminerons avec les conclusions et perspectives sur lesquelles la biopuce capable de tri cellulaire pourra s'ouvrir, notamment dans le domaine de la recherche immunologique. Enfin, le lecteur aura connaissance de procédures expérimentales et des références citées dans le travail. Les informations complémentaires aux résultats décrits dans le corps du texte seront comprises dans la partie Annexes.

Résumé Chapitre 2

Concept de l'assemblage moléculaire sur biopuce

Ce chapitre sera consacré au développement de l'assemblage moléculaire sur lequel s'appuie la fonctionnalité de la biopuce. Parmi les différentes stratégies de relargage contrôlé à multiéchelles proposées dans la littérature, celles qui impliquent l'utilisation de molécules d'ADN offrent plusieurs avantages comme : la facilité de fabrication des puces à ADN et leur stabilité dans le temps, l'accès à de nombreuses séquences d'oligonucléotides et finalement leur susceptibilité à la manipulation chimique, enzymatique ou physique. Pour le besoin de cette étude, nous proposerons une approche particulière qui permet de transformer une simple matrice d'ADN en une puce à anticorps capable de réaliser la capture spécifique de cellules. La microplateforme en question sera ainsi basée d'une part sur une surface d'or fonctionnalisée par différentes séquences d'oligonucléotides et d'autre part sur la conception d'une molécule hybride composée d'un anticorps (IgG) conjugué avec une courte séquence complémentaire d'ADN. Cette approche nécessite l'établissement d'un protocole de couplage qui sera ici discuté. En utilisant un agent hétéro-bifunctionnel, l'IgG sera covalemment lié à l'ADN puis purifié par la chromatographie échangeuse d'anions. Le produit final étant une molécule IgG-ADN monoconjuguée sera ainsi isolé et par la suite caractérisé par mesure d'absorbance et suivi d'un test de révélation en fluorescence.

Dans la partie finale du présent chapitre, le lecteur fera connaissance avec le principe de détection utilisée et les détails instrumentaux de l'imagerie SPR. Cette technique servira alors à confirmer la fonctionnalité de l'assemblage moléculaire sur biopuce dont la construction étape par étape sera mise en évidence.

Résumé Chapitre 3

Relargage contrôlé par clivage enzymatique

Dans ce chapitre nous explorerons la première stratégie de relargage contrôlé basée sur le clivage enzymatique réalisé dans le format de biopuce. Cette approche repose sur l'utilisation de l'assemblage moléculaire décrit dans le chapitre précédent. En effet, les oligonucléotides utilisés pour le montage fonctionnel sur biopuce contiennent des séquences qui peuvent être spécifiquement reconnues par les endonucleases (les sites de restriction). En utilisant une série de séquences de restriction associées à des enzymes bien définies, une libération spécifique de différentes cibles pourra avoir lieu.

Le concept sera dans un premier temps validé sur des cibles moléculaires correspondantes à plusieurs séquences de restriction, chacune conjuguée à un anticorps modèle – IgG du lapin. Ainsi, nous nous pencherons sur l'optimisation des conditions expérimentales afin d'établir un protocole permettant de réaliser une digestion efficace du substrat d'ADN immobilisé sur la surface. La spécificité du clivage enzymatique sera mise en évidence par suivi en temps réel permis par la technique SPRi. Par la suite, le système de relargage contrôlé sera expérimenté lors de tests sur des cellules vivantes.

Tout d'abord, nous adresserons les lymphocytes sur la biopuce à l'aide de molécules conjuguées composées de l'anticorps spécifique à l'antigène cellulaire bien défini couplé à la séquence d'ADN. Des premiers essais de désorption par les enzymes de restriction seront menés sur des cellules-modèles issues de lignées cellulaires (les hybridomes des cellules du type B et T). A l'occasion de ces tests préliminaires, nous discuterons des conditions expérimentales qui sont cruciales pour limiter l'adsorption non-spécifiques de cellules (traitement de surface, paramètres hydrodynamiques). Un protocole optimal sera ainsi développé et par la suite appliqué à des tests avec des cellules primaires – les lymphocytes B et T issues de la rate de souris. Cette étude montrera une reconnaissance spécifique des lymphocytes sur les plots concernés et leur relargage subséquent par clivage enzymatique. La SPRi permettra non seulement de suivre les étapes de l'expérimentation à l'échelle des biomolécules mais également de détecter les phénomènes cellulaires.

A la fin de ce chapitre, une étude supplémentaire sera présentée. Elle sera axée sur l'application de la méthodologie développée à d'autres échantillons cellulaires. Ainsi, nous montrerons une capture spécifique de bactéries et mettrons ensuite en évidence leur relargage contrôlé par la voie enzymatique. Cette étude est proposée comme une approche originale à l'analyse d'échantillons pour des applications microbiologiques.

Résumé Chapitre 4

Désorption par chauffage localisé

Le chapitre 4 présentera une approche originale de désorption de biomolécules et d'objets biologiques immobilisés sur la surface de la biopuce selon le montage moléculaire développé précédemment. Le relargage contrôlé des différentes cibles repose sur la dissociation des doubles brins d'ADN générée par un chauffage localisé. Ce phénomène résulte de l'effet photothermique induit par un faisceau laser sur la surface du métal (l'or en l'occurrence) dans les conditions de SPR. Dans un premier temps, nous expliquerons ce phénomène particulier en nous basant sur des exemples tirés de la littérature. L'effet photothermique trouve notamment de potentielles applications dans les domaines des nanobiotechnologies et la médecine qui seront brièvement décrites pour en apprécier les potentialités. Le chauffage localisé assisté par le plasmon de surface peut également être très utile dans le champ des biocapteurs. Ainsi, cette approche sera explorée dans le cadre du présent projet.

Tout d'abord, nous détaillerons la configuration instrumentale que ce concept nécessite. Par la suite, nous procéderons à l'exploration de l'approche qui repose sur le relargage contrôlé des espèces moléculaires et cellulaires préalablement immobilisées sur la biopuce. Cette stratégie est basée d'une part sur l'emploi d'un faisceau laser focalisé sur la surface d'or dont l'énergie est couplée aux plasmons de surface et d'autre part sur l'exploitation du caractère thermolabile du double brin d'ADN. Dans un premier temps, ce concept sera utilisé lors de tests à l'échelle moléculaire où l'optimisation des paramètres expérimentaux sera discutée. La spécificité de la désorption de différentes protéines sera confirmée par l'analyse en aval en spectrométrie de masse des échantillons relargués. Une fois la capture et le relargage des biomolécules mis en évidence, les résultats concernant des objets de taille micrométrique seront présentés. Nous observerons d'abord les résultats d'un test de désorption de microparticules capturées sur la surface de la biopuce et avant de discuter des résultats obtenus lors d'une étude similaire avec des cellules vivantes – les lymphocytes en l'occurrence. La réversibilité du système basée sur les propriétés intrinsèques de l'ADN sera également confirmée. Les cellules (ou les protéines selon le cas) pourront en effet être de nouveau immobilisées en des endroits où la matière aura été précédemment décrochée par le faisceau laser.

Résumé Chapitre 5

Conclusions et perspectives

Suite aux résultats obtenus dans le cadre de la présente thèse, nous présenterons les conclusions générales ainsi que les perspectives sur lesquelles ce travail peut finalement s'ouvrir. A travers ce projet nous avons développé une biopuce permettant d'effectuer une capture spécifique de lymphocytes et leur relargage subséquent suivi en temps réel. Cette étude propose ainsi un outil miniaturisé capable de réaliser un tri cellulaire à partir d'un mélange hétérogène de cellules. Ici, nous avons mis en évidence une séparation de lymphocytes B et T qui ont été spécifiquement répartis sur la surface de la biopuce selon un montage moléculaire particulier. En effet, les cellules ont été adressées sur une matrice d'ADN via une reconnaissance avec des anticorps spécifiques aux lymphocytes conjugués avec les oligonucléotides. Par la suite le relargage des cellules ciblées a été réalisé selon deux stratégies indépendantes.

Premièrement, nous avons démontré que les différentes cibles immobilisées sur la surface peuvent être décrochées sélectivement par des enzymes de restriction. La multitude de séquences d'oligonucléotides associées à des endonucleases différentes ouvre la possibilité d'élargir la désorption sur plusieurs cibles. Néanmoins, l'extension de ce système peut engendrer l'augmentation des coûts ainsi qu'entraîner un risque de réactivité croisée. Une deuxième méthode pouvant servir à un tri sélectif de cellules a été également développée. Elle consiste à une désorption depuis la surface basée sur les propriétés thermolabiles du double brin d'ADN. Cette stratégie est donc plus directe et peut également être étendue en utilisant des substrats d'ADN avec un équilibre thermodynamique différent (*e.g.* mutations ponctuelles, séquences de différentes longueurs). Cette deuxième approche nécessite toutefois l'utilisation d'une configuration instrumentale sophistiquée qui comprend l'optique SPRi, une source laser ainsi qu'un système de pilotage du faisceau laser. Dans le cadre du futur développement de ce dispositif expérimental, le laser travaillant en mode continu pourra être remplacé par un laser pulsé et mis en place de façon à pouvoir réaliser simultanément les étapes du décrochage et de la détection.

Les deux méthodologies proposées par le présent travail offrent plusieurs avantages sur le plan de la réalisation d'un tri cellulaire. Elles reposent sur la reconnaissance spécifique de cellules qui sont adressées sur la surface grâce à des anticorps pour être ensuite libérées de façon contrôlée par clivage enzymatique ou chauffage localisé. Toutes les étapes sont réalisées dans le format d'une microplateforme basée sur une matrice d'ADN et des molécules conjuguées IgG-ADN. L'assemblage particulier sur puce permet la régénération et l'utilisation de la matrice originelle de nouveau. En outre, le système est

accompagné par la détection en temps réel et sans marquage. Ceci n'implique pas d'étape de prétraitement de l'échantillon contrairement à des méthodes de laboratoire utilisées en routine comme par exemple FACS® ou MACS®, et offre ainsi l'opportunité de travailler avec des échantillons cellulaires bruts.

L'étude réalisée dans le cadre de cette thèse nous mène à de potentielles applications dans les domaines de la recherche et du diagnostic. En effet, le système de biopuce que nous proposons permet de réaliser un tri des cellules sanguines qui ouvre des perspectives d'études plus poussées sur une population des cellules du sang bien définie (*e.g.* lymphocytes d'un phénotype particulier). Ceci consiste ainsi en une brique élémentaire de la recherche avancée dans le champ de l'immunologie humaine qui permettrait d'avoir un aperçu plus large sur les complexes mécanismes de l'immunité (lors d'infection ou de cancer, rejet de greffe ou maladies auto-immunes). Les études fonctionnelles des lymphocytes du même type (l'activité sécrétrice) ou les investigations sous l'angle protéomique et transcriptomique concernant une famille individuelle de lymphocytes pourront ouvrir des nouvelles voies de développement thérapeutique (*e.g.* nouveaux vaccins) et du monitoring médical (*e.g.* suivi de marqueurs cancéreux, de l'effet des drogues).

Dans ce domaine, une approche permettant d'étudier une cellule individuelle est extrêmement intéressante. En perspective, nous présenterons ainsi des études préliminaires qui ont déjà permis de capturer des lymphocytes individuels dans un micropore fonctionnalisé selon le montage moléculaire développé par ce travail de thèse. Cette méthodologie exige néanmoins des étapes d'optimisation qui feront l'objet de travaux réalisés dans un proche avenir.

Résumé Chapitre 6

Partie expérimentale

Ce chapitre constituera la partie expérimentale du présent travail de thèse. Elle détaillera tous les aspects de l'expérimentation qui ont fait l'objet des chapitres précédents. Une liste exhaustive des réactifs sera ainsi présentée comprenant les séquences d'oligonucléotides, les anticorps et autres protéines, les tampons utilisés ainsi que les échantillons cellulaires testés. Par la suite, le lecteur aura connaissance de protocoles expérimentaux concernant différentes étapes de l'expérimentation mentionnées dans le corps du présent manuscrit : fabrication de puce à ADN, couplage et purification de l'IgG-oligonucleotide, validation des produits conjugués par test d'immunofluorescence, préparation des échantillons (microparticules, lymphocytes, bactéries), capture et relargage par clivage enzymatique et par l'effet photothermique, analyse en spectrométrie de masse. La description détaillée des procédures expérimentales permettra de mieux comprendre les résultats obtenus ainsi que leur éventuelle reproduction dans le futur.

Chapter 1

Project background and state of the art

At the beginning of the present PhD thesis, the reader will be introduced to the general scientific context that lays a motivation for the given work. Firstly, the complexity of a biological specimen will be stated by giving the example of blood sample. Significance of profound analysis of this particular sample will be stressed in terms of its utility not only for clinical diagnostics but also for research purposes. A special attention will be focused on studies carried out on complex processes of the immunological response that are of a great interest in the field of biological and medical sciences. Natural complexity of immune defense mechanisms makes such studies difficult and we therefore need novel high-throughput methods guaranteeing a wider insight. Exhaustive investigations of immune response phenomena can drive to better understanding of various processes that human body is involved in (*e.g.* infections, cancer) and thus help to improve existing methods of treatment and elaborate new medicines or vaccines. An important step in acquiring new knowledge on the functionality of different immune cells consists in the efficient out-of-sample extraction of lymphocytes implied in the immunological response. This approach enables profound investigation at the specific cell population level.

Several methods of cell sorting from heterogeneous samples have been used for many years but they frequently imply considerable sample volumes, preparation steps, long-time analysis or non-negligible costs. I will thus make an overview of existing cell analysis and sorting methods, giving the purpose to engineer new and efficient devices. In this matter, recent achievements in the field of microtechnologies arise as a solution in the construction of new tools for cell sorting purposes. Such microfluidic platforms or lab-on-a-chip systems remain more interesting because of their attractive features represented by rapidity, precise control of microenvironment, analysis parallelization, multiplexed detection and finally tiny quantity of biological material needed. Therefore, the present manuscript will describe the development of such exemplary micro-device capable of specific isolation and sorting of B and T lymphocytes. The proposed biochip shall be thus explored as a potential tool for advanced research or medical diagnostics.
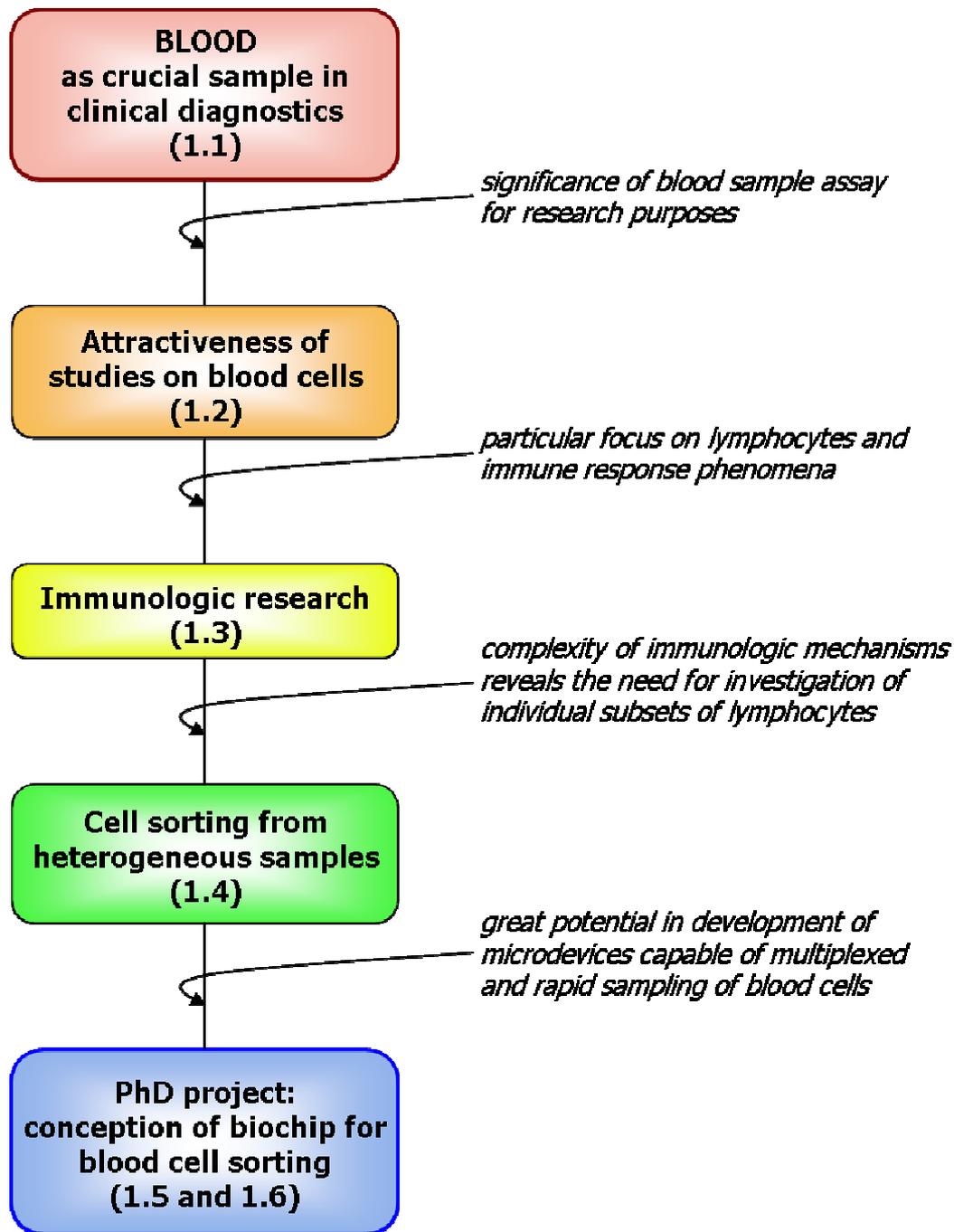
Figure 1.1 Flowchart of the introduction chapter

1.1 Blood sample diagnostics

Common biological samples such as blood or biopsy specimen are extracted from living organisms as heterogeneous mixtures composed of various molecular and cellular components. Their qualitative and quantitative assessment is of great importance in the field of clinical diagnostics and basic biological research. Among many examples of biological extracts, human blood represents a specimen of prime interest for medical and scientific applications. Indeed, it is an essential source of extremely important information concerning the functioning of the whole organism. As we all know, thanks to heart and blood vessels this life-sustaining fluid circulates throughout the body in order to deliver oxygen and nutritional elements to all cells structuring an organism. Among many important functions, blood flow enables also an efficient transport of metabolism substances produced by different organs to other tissues where they might be consumed (*e.g.* glucose in brain) or removed from the body (assisted by lungs, kidney or liver). Moreover, blood plays an essential role in human immune defense since it provides distribution of the immune cells to different anatomical compartments where they might produce specific immune responses or provide immuno-surveillance function. That is why, a quantitative and qualitative analysis of blood sample is needed to access many elements conditioning a patient's state (pathological or not). Monitoring of blood component concentration (cells, molecular entities) gives us the essential data concerning numerous diseases and is of great importance for both medical and research purposes.
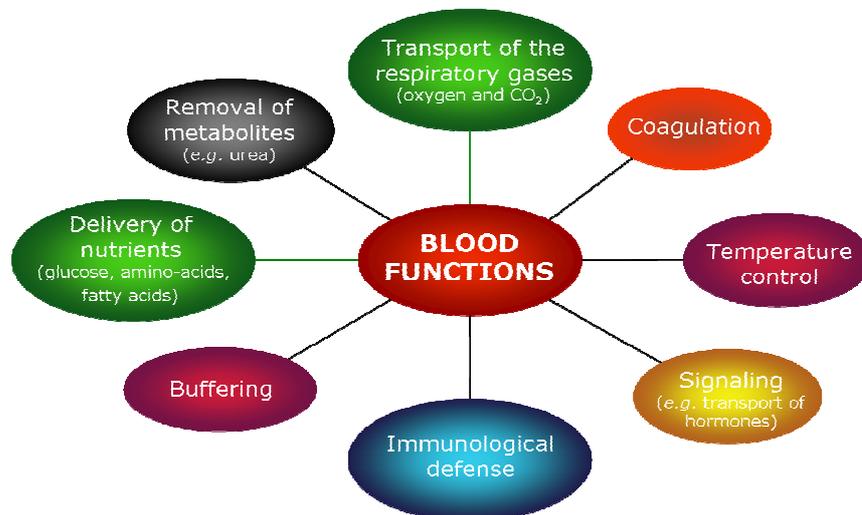
Figure 1.2 Main functions of blood in a human organism

The numerous functions of blood make this tissue an extremely rich source of clinical and scientific information. The blood sample consists of two main fractions: live cells and plasma. The latter one is a water-based mixture containing various molecular items such as antibodies, hormones or glucose and is considered as the largest

representation of the human proteome.[1] Furthermore, whole blood volume is almost in a half composed of cells predominating in erythrocytes (red blood cells - RBC) complemented by reticulocytes (immature RBCs), thrombocytes (platelets) and white blood cells (WBCs) of different kind (leukocytes). Classical approach for blood sampling relies on assessment of standard diagnostic parameters such as hemoglobin level, leukocyte count or biochemical profile (*e.g.* cholesterol level, hormones). However, currently employed techniques of blood sample preparation are usually time- and sample-consuming, and require laborious preparations. That is why, novel technological solutions are being developed in order to provide high-throughput analysis in shorter time (several minutes) and starting from barely few microlitres of a sample.

Cell type	Average/μL	Percent of WBC
All leukocytes (total)	5000–10,000	100%
Neutrophils	4000–8000	40%–66%
Monocytes	200–800	4%–8%
Eosinophils	50–300	1%–3%
Basophils	0–100	0%–1%
Lymphocytes (total)	1000–4000	20%–40%
CD4 + T Cell	400–1600	15%–20%
CD8 + T Cell	200–800	7%–10%
B-Cell	200–800	8%–12%
NK	100–500	4%–6%
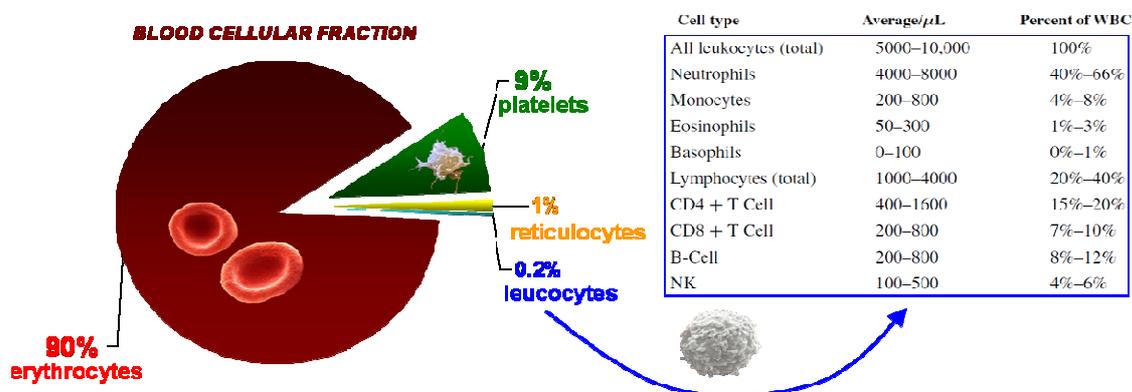
Figure 1.3 Composition of cellular fraction in healthy blood. The images adapted from www.sciencephoto.com and the table issued from Toner *et al.*[2]

Over the last few years, a considerable progress in the field of blood sampling microsystems is made and prone to revolutionize the world of laboratory diagnostics, by introducing in the near future "point-of-care" devices (available immediately at the site of patient care).[2-4] Among many potential candidates for such microsystems, we can point out *e.g.* a microfluidic biochip capable of rapid blood typing,[5] a micro-platform providing *in situ* profiling of plasma proteins[6, 7] or a lab-on-a-chip system that enables fast and simultaneous assessment of the hematocrit (erythrocyte volume fraction) and plasma protein profile.[8] In terms of blood sample preparation for diagnostics, an interesting study by E. Sollier (CEA Grenoble/LETI, France) explores new microfluidic solutions allowing efficient isolation of blood plasma from cellular components.[9] All these examples represent an energetically developing domain that aims to conceive novel blood sampling technologies able to rapidly furnish the most important diagnostic parameters. Apart from giving a deep insight into physiological or pathological state of the examined patient, these data may be helpful to clarify functional aspects of blood (*e.g.* immunological function) and thus are attractive for scientific research as well.

1.2   Blood cell samples in the scientific research scope

Profound analysis of blood sample components is a crucial point not only for clinical needs but may also serve to understand different physiological mechanisms, especially those involving blood cells. That is why cell-based blood sampling is naturally desired for research purposes. Isolation of pure fractions containing well-defined cell populations is of particular interest but constitutes a challenging approach if large diversity of blood cells and disproportionate cellular content in whole blood are taken into account. In fact, a normal blood sample is composed of a predominant fraction represented by erythrocytes. Although RBC examination is precious from the biomedical point of view (evaluation of the hematocrit, hemoglobin level or blood group typing), the erythrocyte physiology is not widely explored in the scientific research. In this matter, more fruitful is to assay white blood cells that are responsible for the functionality of the human immune defense characterized by a complex nature.
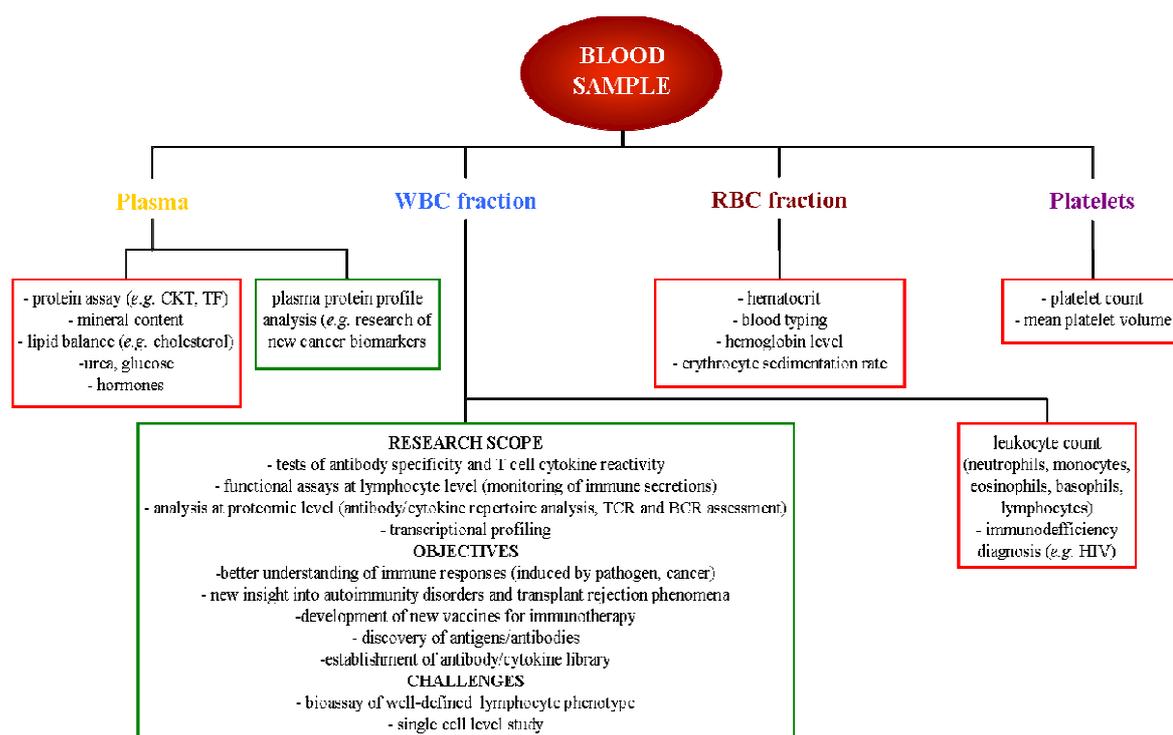
Figure 1.4 Exploration of the blood sample for diagnostic purposes (red-framed boxes) and biological research (green-framed boxes).

Analytic strategies aiming to interrogate white blood cells may appear problematic if we consider the fact that leukocytes represent only a small fraction of the total cell number in whole blood. Furthermore, an extremely challenging approach is to provide an exclusive examination of the lymphocyte fraction (less than 0.1 % of whole blood), especially because lymphocytes are themselves divided into several subpopulations. Since they play a major role in the adaptive immune response and their participation in immunologic defense processes is complex, these studies are of great interest for modern immunology and appoint main motivation of the present PhD work. Efficient isolation and characterization of lymphocytes of a precise phenotype may open up new horizons for more exhaustive studies on immune functionality at the level of well-defined cell populations. In the following section, we will therefore discuss the significance of profound studies on immune response phenomenon, mainly justified by its complex character still not integrally discovered.

1.3 Exploration of immune defense phenomena

The immunologic system is undoubtedly of great importance for a living unit since it plays an essential role in protecting host organism from a whole gamut of pathogens ranging from viruses and bacteria to infectious fungi and parasites. It is also responsible for responding in presence of foreign molecules (*e.g.* some vaccines), tumor cells or even own antigens (autoimmunity disorders). Human defense consists in biochemical or cellular mechanisms mediated by early reactions of the innate (natural) immune system or later responses generated by the adaptive immune system acquired over time.[10] These reactions are provided by different molecules (*e.g.* cytokines, antibodies) and cells of various types (leukocytes). The innate immune system provides an early line of defense against microbes and is based on recognition of common pathogen features (thanks to receptors encoded in a germline). Although these natural mechanisms are executed rapidly, they act in essentially the same way and may be evaded by many pathogenic elements. Hence, each human organism benefits from the adaptive immunity reactions that provide protection from a constant barrage of potentially large variety of pathogens.

The key elements of adaptive immune system are different populations of B and T lymphocytes. These immune cells are able to recognize and distinguish a large spectrum of antigens. Such particular ability lays the foundation for two main features of the immune response: **specificity** (high affinity to precise antigen) and **memory** (rapid response to formerly encountered antigen). The functionality of lymphocytes is based on an extensive outfit of cell surface receptors (B cell receptors, or BCRs; T cell receptors, or TCRs) providing characteristic response to an antigenic determinant. The cellular membranes within different lymphocyte populations are decorated with an incredible diversity of receptors. Unlike other leukocytes, B and T lymphocytes bear distinct cell receptors which result from somatic recombination of receptor gene segments.[11] The adaptive immunity reactions are thus enabled by a large total repertoire of receptors that can virtually recognize any antigen. Complex nature of the immunological system is thus exemplified by wide molecular diversity of antibodies and T-cell receptors which reflect a multitude of mutual dependences and interconnections (*e.g.* signaling by cytokine network, *cf.* Fig.1.5). Furthermore, circulating lymphocytes may be divided into several subclasses characterized by a specific set of cell surface molecules identified as cluster of differentiation (CD). Presence of this distinct surface marker depends on the function of a single lymphocyte (*e.g.* cytotoxic CD8+, helper CD4+), its differentiation state (*e.g.* naïve, memory) and even housing tissue (*e.g.* spleen, blood, thymus). Hence, such large diversity helps to imagine how multifaceted immune response process may be and evokes an unquestionable need for deep understanding of immunity mechanisms.

The recent years have brought many important advances in the field of immunology and point out the usefulness of research in this area in spite of funding challenges in different countries.[12-14] For 2011, the National Institutes of Health (NIH) provided almost $13 billion of financial support for research related to immunology which is more than for the general clinical research ($11 billion).[15] The main research scopes are therefore focused on better understanding of such processes like infections (including emerging infectious diseases *e.g.* pandemic influenza virus H1N1), autoimmunity or transplant rejection phenomena[16] as well as on development of new therapeutic vaccines (AIDS, cancer)[17] and discovery of new immunological biomarkers.[18] Different immunity phenomena can be studied by classical techniques or advanced high-throughput technologies recently reported.
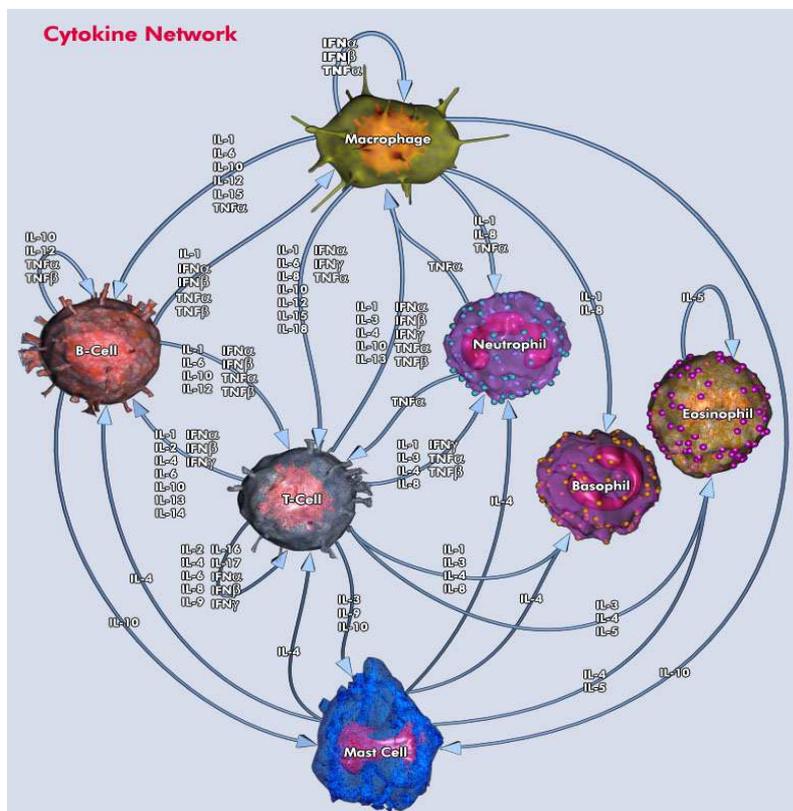
Figure 1.5 Complexity of the immune response process on the example of cytokine network. Different immune cells mutually communicate by secreted cytokines (*e.g.* interleukins ILs or interferons IFNs) acting in networks or cascades. Image adapted from QIAGEN GmbH (www.qiagen.com).

As conventional methods used for assessment of immune response, two approaches of different level of study can be generally discerned: molecular and cellular (*cf.* Table 1.1). The first of the mentioned strategies makes use of standard biochemical techniques of immunoassaying based on antibody titration to an antigen of interest. Classical ELISA (Enzyme-Linked Immunosorbent Assay), Electro-ChemiLuminescence (ECL) immunoassay[19] or recently developed immuno-PCR (Imperacer®)[20] can be here enumerated as exemplary methods. By dint of these methodologies, antibody-antigen recognition events can be detected, given by colorimetric read-out (ELISA), electric energy transfer (ECL) or, as the most efficient, exponential amplification of DNA in immuno-PCR approach.[21] The second family of currently employed immuno-methods is directly founded upon lymphocyte assays and aims the detection of cell specific secretions (antibodies or cytokines) that are generated during immune or inflammatory responses. ELISPOT is a flagship technique developed by C. Czerkinsky and inspired from ELISA test that enables indeed to measure single cytokine or antibody produced by T or B cells, respectively.[22, 23] In order to assess multiple cytokines expressed by T lymphocytes, an intracellular staining approach (ICS) can be put into action. This method exploits flow cytometry technique to detect intracytoplasmatic cytokines produced in permeabilized cells.[24, 25] Even if such approach provides multiple detection of immunologically involved molecules, it is however harmful for physiological integrity of cells that are eventually submitted to death. As an alternative, whole living lymphocytes of a particular functionality may be characterized by means of fluorescence- or magnetic-activated flow cytometry (FACS or MACS) according to secreted cytokine or expressed antibody.[26, 27]

The spectrum of the above specified methods for immunological investigation is based on end-point analyses which give only punctual data related to secretory activity of assayed lymphocytes. Indeed, conventional immunoassays such as ELISPOT or ICS are able to interrogate only a subset of lymphocytes thus providing only partial immunological information. Immunity mechanisms involve though many different molecules and/or cells and therefore need thorough characterization at a larger scale. Taking into account the heterogeneity of lymphocyte populations and the possible interdependence of their functional properties, new high-performance immunoassays providing a wide insight into human immunity aspects need to be established. This goal might be achieved by the development of miniaturized devices that emerge as versatile tools to conduct fast and multiplexed studies on different lymphocyte populations.

Technique	Performance	Features
molecular level (antibody-antigen titration)		
ELISA	colorimetric read-out of immunorecognition	- end-point analysis - punctual data, limited immuno-information
ECL[19]	electro-chemiluminescence signal upon antigen-antibody interaction	
Immuno-PCR[20]	DNA amplification	
lymphocyte level (secretory activity)		
ELISPOT[22, 23]	detection of single antibody (B cell) or cytokine (T cell)	- qualitative information (number of secreting cells) - single cytokine/antibody assayed within one assay
ICS[24, 25]	detection of intracytoplasmatic cytokines	- cell permeabilization - loss of cell integrity
FACS®[26]	fluorescence or magnetic detection of secreted cytokine or expressed antibody	- need for pre-labeling of a cellular sample - limited amount of fluorescence or magnetic tags
MACS®[27]		
immunoassays at a micro-scale		
microarray	immunofluorescence read-out of T-cell secretory activity[28, 29]	- high-throughput assay - multiparametric detection of several antibodies or secreted cytokines - real-time detection (SPR) - possibility of single-cell assaying
biochip combined with SPR	real-time detection of cytokines[30, 31]	
microfluidic platform	simultaneous detection of several secretory products[32]	
single-cell immunoassay	B-cell immunoassay[33, 34]	
	T-cell immunoassay[35, 36]	

Table 1.1 Tools for immunological examination used in biological and clinical research

Recent review by Reddy and Georgiou reports on up-to-date advances in the field of high-throughput technologies amenable to studying adaptive immunity processes.[37] Microscale platforms are stated as an attractive opportunity to realize detailed and quantitative characterization of lymphocyte functional properties (*e.g.* secretory activity), up to acquisition of deep information at proteomic (*e.g.* serological profiling) or genomic (*e.g.* sequencing of immune repertoires) level. For example, with help of antibodies specific to lymphocyte membrane markers or to immune secreted proteins, the secretory activity of a well-specified subset of lymphocytes can be detected.[28, 29] Knowing that lymphocyte functional activity may be altered in relation to changing cell environment, a

more attractive strategy is to follow kinetics of cytokine or antibody production by immune cells. Such solution offers rich and time-resolved information concerning immune response and generated in presence of a mitogenic agent or defined pathogen. A potentially useful tool capable of monitoring molecular[38, 39] or cellular[40] interactions in real time is represented by techniques based on optical phenomenon of surface plasmon resonance (SPR). Indeed, some groups report that label-free SPR-based analysis may be applied to explore immune responses in a continuous way, *e.g.* by monitoring lymphocyte secretions: B lymphocytes antibodies[30] and cytokines (*e.g.* interferon) produced by T-type lymphocytes.[31] In this matter, further step is to provide similar studies at single cell level which may open up to novel opportunities for detailed characterization of immune cell effector function.[33-36]

In conclusion, the understanding of immunological phenomena at a greater resolution is extremely attractive not only for research purposes but also from a biomedical point of view. Among various applications, detailed and quantitative immunologic monitoring leads to reliable assessment of humoral and cell-mediated immunity and is a crucial element of efficient immunotherapy.[16, 17, 41] High-throughput microscale platforms are considered as versatile tools for clinical assays. Microdevice approach enables high-informative evaluation of immune response provided by all individual subsets of lymphocytes. Furthermore, recent findings evidence that T lymphocytes result in production of heterogeneous response in terms of secreted cytokines, even if they represent similar T cell phenotype.[32] It proves therefore how intricate immune cell responses are and gives motivation for exhaustive investigations of well-defined lymphocyte populations. Taking into account complexity of blood sample as well as phenotypical and functional diversity of lymphocytes, we thus need efficient techniques to extract an exclusive lymphocyte family in order to realize downstream analyses. The approach of that kind will certainly lead to a more comprehensive insight into fundamental aspects of the human immunology.

1.4 Cell sorting methods

Taking into consideration the aforementioned statement, one may realize that development of reliable cell sorting methods is of great demand when willing to extract individual cellular subsets from a heterogeneous biological sample. Such approach needs to rise to a few important challenges such as extreme diversity of blood cells (even lymphocytes themselves) and their responsive character to the surrounding environment. Cell sorting should fulfill the requirement of precise control of a cell microenvironment and finally result in recovery of a cell sample of high purity. Even if these conditions seem to be demanding, this particular need for conception of reliable cell sorting methodology becomes a leading objective of the present PhD work where alternative strategies to various existing methods are proposed. That is why this section makes an overview of cell sorting approaches currently being developed as well as those widely employed for scientific or clinical purposes.

The cell sorting procedure is frequently an integral element of basic biological research, advanced biotechnology and biomedical applications. As a cell sorting technique, it may be considered a procedure that allows the obtention of defined cell subpopulations from a heterogeneous sample and according to cell physicochemical, morphological or physiological properties.[42] This analytical strategy results in separation, isolation or enrichment of a specific cell type and meets the requirements of several essential applications such as screening at genetic or proteomic level as well as further investigation on a purified cell sample (*e.g.* immunoassays). In general, cell sorting methods rely on the individual characteristics of cells founded on parameters of mechanical nature (*e.g.* density, size), reaction to the external environment (electrical, magnetic or optical stimulus) and more specifically on adhesion aptitude specific to each cell type (*e.g.* immunoaffinity). Conventional filtration or centrifugation methods, based on cell size or density are frequently used in standard research or biomedical protocols. They require however large scale sampling and are therefore inappropriate for small volume samples and with a narrow distribution of cell size. Other commonly employed methods rely on flow cytometry approach combined with fluorescence (FACS) or magnetic (MACS) activation of a cellular sample.[27] These analytical strategies often need laborious pre-processing of specimens and the analysis itself is costly and time-consuming. Hence, recent progress in the development of miniaturized systems could bring new technological solutions to efficient separation of cellular samples.

Cell-based system miniaturization has recently emerged as an energetically evolving concept of efficient bioanalytic tools that may be widely applied for modern cell biology goals.[43] Miniaturized platforms offer numerous possibilities of multifunctional analysis of cellular sample such as cultivation in controlled conditions, monitoring of metabolism and secretory activity up to cell counting and separation to defined subsets. In the last years several reviews appeared and revealed multifaceted usefulness of

microdevices in the field of cellomics – high-throughput studies of cells.[43-45] "Lab-on-a-chip" (LOC) systems have several advantages which are also attractive in the development of micro-technologies for cell sorting. Apart from reducing cost and time input, other benefits can be listed such as precisely controlled microenvironment, gentle handling of cellular samples and multiparametric sampling which provides analysis of complex biological specimens. Taking into account recent expansion of studies on novel micro-scale cell sorting technologies, I herein propose a short overview of available methodologies, accompanied by adequate literature references where detailed information can be found.

The first family of microdevices capable of cell sorting is founded on physical separation events as an analogy to classical filtration, sedimentation and centrifugation methods. Functionality of such systems is mainly related to size and density that differentiate targeted cells from the others. Microtools of this type are exemplified by microfabricated filters capable of mechanical cell trapping[46] or microstructured fluidic channels where selective sorting results from hydrodynamic flow conditions.[47] Kim *et al.* give a wide insight into microfluidic devices of various geometries resulting in a set of different mechanical constrains exercised on cells and potentially deployed in the separation approach.[48] Physical-based cell sorting methodologies are however limited to morphological discrimination and are not suitable to precisely separate cells of similar physical parameters (*e.g.* B lymphocytes versus T lymphocytes).

In order to increase the level of precision in the separation of well-defined cell subsets, we may benefit from inherent reactivity of living cells to external manipulation of physical or chemical nature. One possible solution is to impose an electric stimulus being relatively easy to produce in micro-scale devices within microfabricated electrodes. The difference of the electric potential applied between two electrodes may create localized and switchable traps for cell sorting purposes. It can be realized by an electro-osmotic flow of charged cellular entities within a microchannel[49, 50] or dynamic dielectrophoresis (DEP) when application of an external electric field results in generation of polarized particles.[51] The electro-osmosis approach has however limited use in separation of several cells because most of them have similar electrophoretic mobility. DEP appears as a more practical solution since it allows the separation of different biological cells in microfluidic or microchip devices. This method is reported as a cell friendly separation technique and can be potentially employed for effective enrichment of rare cells.[52]
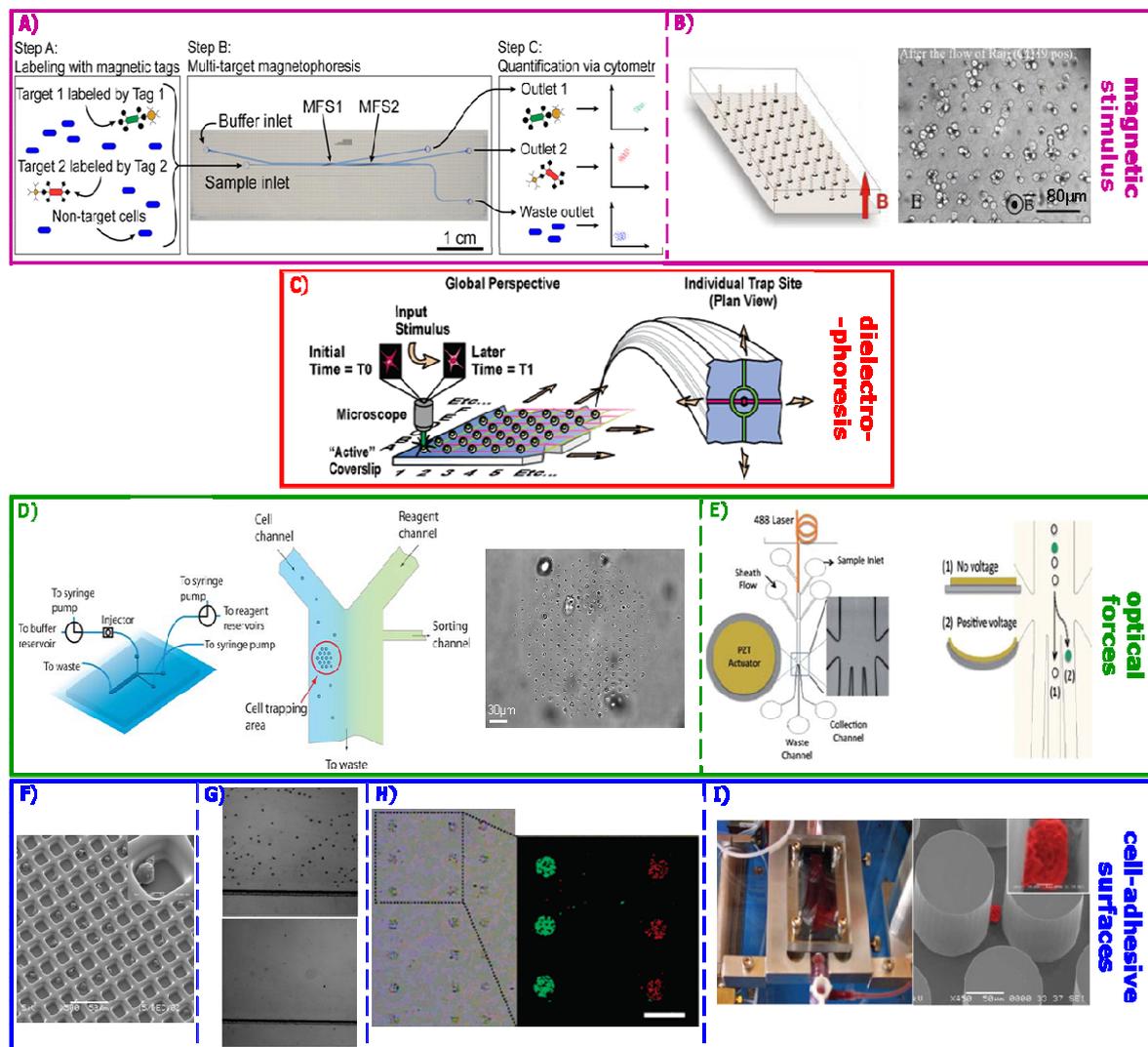
Figure 1.6 Development of microdevices devoted to cell sorting purposes.
A) Multitarget microMACS system. Magnetically tagged cells are sorted from a continuous flow by applying magnetic fields at the level of microfabricated magnetic strips (MFS);[53] **B)** *Ephesia* system developed by Saliba *et al.* Cells of interest are sorted from the microfluidic flow onto magnetic microbead columns covered by a specific antibody;[54] **C)** Microarray composed of individual dielectrophoretic (DEP) traps devoted to cell sorting and imaging;[51] **D)** Micro-scale optical tweezers. Cells are optically trapped from a microfluidic channel on a set of microlenses;[55] **E)** MicroFACS platform capable of separation at single cell level. Fluorescent cells are excited by a laser light guided through a microfluidic channel and manipulated at the sorting junction by a piezoelectric actuator (PZT);[56] **F)** Lymphocyte capture into individual microwells coated with poly-*L*-lysine (PLL);[57] **G)** Capture and release of cardiac fibroblasts on peptide-modified alginate gel in a microfluidic channel;[58] **H)** Spatial separation of lymphocytes onto an antibody microarray – within DNA-directed immobilization (DDI);[59] **I)** Isolation of circulating tumor cells (CTC) on antibody-covered microposts coupled to a microfluidic device.[60]

Another group of stimuli-based cell sorting methods consists in the manipulation of cell microenvironment by an external magnetic field. This strategy can be readily employed in microsystems since it does not require high power input and ensures biocompatibility with living cells.[61] As an example, the cell sorting task may be accomplished in a rapid and label-free manner by using ferrofluids being colloidal suspensions of ferrite nanoparticles. Application of a magnetic gradient within the microchannel enables therefore efficient separation of different cells driven by differences in their velocity.[62] A more frequent approach takes advantage of magnetic-activated cell sorting (MACS) realized in miniaturized format. MicroMACS strategy involves preliminary conjugation of cells with magnetic tags which are subsequently introduced to microfluidic chip where separated upon magnetic field gradient.[53, 63, 64] Target cells are tagged by magnetic particles (having different magnetic properties for multiple target sorting) coated with a cell-specific antibody. The use of non-modified cellular targets is however more attractive since it allows sampling of crude biological extract. Accordingly, Saliba *et al.* propose a particular cell sorting method called *Ephesia* which provides the separation of a desired cell type directly on microarray by the means of magnetically induced anchors (micro-bead columns) covered by cell-specific antibodies.[54]

Apart from application of electric or magnetic field, some other physical stimuli may be deployed to perform cell sorting in biological samples. An intriguing solution is represented by acoustic stimulation capable of cell trapping and transporting throughout microfluidic channel submitted to ultrasound fields.[65, 66] Other more practical possibilities of cell micro-manipulation are ascribed to optical forces.[67] Sorting tasks may be thus accomplished for example by using microscale optical tweezers – focused laser beam providing attractive or repulsive forces. This strategy can be illustrated by a sophisticated optical microsystem relying on set of silica microlenses arranged on a chip.[55] Application of a laser focused by each microlens generates multiple optical tweezers creating a steerable optical trap capable of cell capture from microfluidic channel. Analogically to large-scale cell sorting tool based on classical flow cytometry assisted by fluorescence read-out (FACS), microfabrication also opens an opportunity to realize similar protocols in devices of miniaturized format. Indeed, microfluidic geometry may provide a robust strategy based on optically mediated sorting on microchannel junctions.[68, 69] An example of highly developed Lab-on-a-chip FACS system is given by Cho *et al.*[56] They report on an integrated microfluidic device capable of single cell level separation provided by a piezoelectric actuator installed at the sorting junction. High-speed response generated by the piezoelectric module as well as an excitation light guided along microfluidic channel makes this microFACS system a versatile tool for high-throughput cell sorting, particularly interesting for rare cell enrichment.

Although the aforementioned methods offer large spectrum of potential applications for cell sorting purposes, microdevices of this type require the integration of microstructured chip or channels with external manipulation or detection modules made of

optical, electronic or magnetic elements. They are also less flexible regarding to multiplexed sampling and in some cases need preliminary preparation of cellular sample involving photo- or magneto-sensitive labels (μFACS and μMACS). That is why a definitely more attractive strategy is to conceive microsystems based on adhesive surfaces modified with ligands specific to each cell type.[70]

Hence, sorting of living cells of an exclusive type from a complex sample may be achieved in a label-free manner based on proper biomolecular interactions. This strategy is achieved by immobilization of specific ligands on localized surfaces. A flagship model of cell-ligand interaction is represented by recognition of cell surface biomarker by a molecule of specific antibody. When separating biological cells, we can thus benefit from a great diversity of the cell membrane decoration proper to each cellular type. One of the first examples of cell separation founded on binding to antibody was proposed by Wysocki *et al.* as an efficient procedure to isolate B lymphocytes from a heterogeneous mixture.[71] However since miniaturization has entered the field of analytics, development of immunorecognition-based systems for separation and enrichment of cellular samples has gained impetus. Antibody micro-patterns are explored as effective cytometry platforms capable of selective cell sorting to predetermined chip localizations.[59, 72] They have been reported to efficiently trap rare cells from complex medium as it was demonstrated on example of circulating tumor cells (CTC) in whole blood.[60] Selective cell isolation on well-defined regions of a microfluidic channel surface may be also achieved with other adhesive molecules. Indeed, different cells are reported to express a certain level of affinity with such substrates like peptides[73] or even DNA-aptamers[74] which can be successfully employed to isolate biological cells from microfluidic flow.

As we can see, the miniaturization of cell-based bioanalytic systems creates a wide field for development of efficient and poorly invasive procedures for cell sorting purposes. The example of high-throughput devices might be particularly assigned to strategies of specific cell adsorption realized in a micro-array format. By dint of parallelized proper interactions with cells, these systems provide spatial organization of a few cellular targets on high-density arrays. Furthermore, once the cell micropatterning has been accomplished, target cells may be subsequently released from the surface by using selective biocompatible methods.[57, 75, 76] Such approach permits to obtain fractions of individual cell subsets from a heterogeneous biological sample. The isolated well-defined populations of immune cells may be potentially submitted to downstream analysis in order to provide better understanding of complex immunologic processes. This particular concept of specific on chip cell sorting and subsequent release makes object of the present PhD project.

1.5 Presentation of the PhD project

This work is motivated by the fact that the immune response is an extremely complex biological process and isolation of specified population of lymphocytes remains a challenging step of sample exploration. That is why, **the present PhD thesis is devoted to the development of an alternative methodology providing an efficient sampling of lymphocyte mixture in a biochip format. The main goal is to enable SPECIFIC CAPTURE of phenotypically different immune cells and their SUBSEQUENT RELEASE under spatio-temporal control. This approach aims to perform the cell sorting task at a microscale and thus generate isolated fractions of individual subsets of lymphocytes prone to become an object of further analyses.** Similar studies could offer a priceless insight into various immunological mechanisms at molecular or cellular level and are of great interest for clinical and research purposes.

More precisely, we herein explore two different strategies leading to cell-specific separation of B and T primary lymphocytes. A cell-based miniaturized tool is developed to ensure addressing of defined B and T lymphocytes onto a DNA microarray. By means of hybrid molecules composed of short DNA oligomers combined with lymphocyte-specific antibodies, cells are sorted into spatially resolved locations of the functional matrix. In a further step, we realize orthogonal release of thus captured cells which sequential desorption potentially leads to obtain isolated fractions of B and T cell populations. To achieve this final goal, two independent strategies are put forward and based on a proper molecular assembly built on the biochip surface. Both of the developed approaches take advantage of intrinsic properties of the DNA substrate underlaying lymphocytes immobilized by dint of specified antibodies. The first of proposed strategies makes use of restriction enzymes capable of highly effective recognition of an exclusive nucleic acid sequences and subsequent cleavage to separate fragments. The latter concept of controlled release is driven by straightforward melting of the double stranded DNA generated by locally confined heating and produced by an external laser source. Both of the explored methodologies benefit from label-free detection provided by Surface Plasmon Resonance Imaging (SPRi). The technique here employed enables therefore a real-time monitoring of molecular and cell-involving phenomena that take place in the vicinity of the biochip surface.
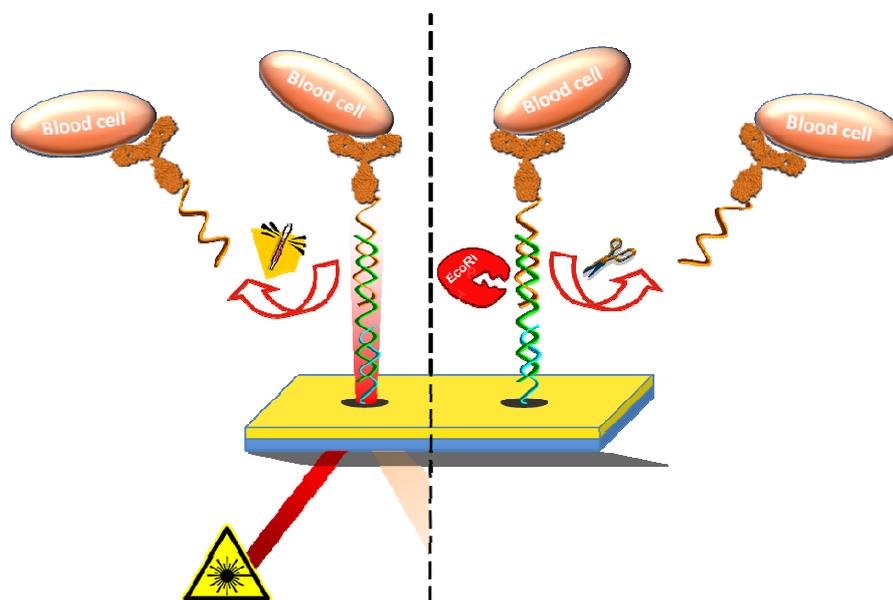
Figure 1.7 Schematic representation of the two strategies developed by the present PhD thesis. Lymphocytes are immobilized on a DNA biochip via specific antibody combined with a DNA complementary strand. Cell sorting task is accomplished either through local heating induced by a laser beam (on the left) or enzymatic digestion (on the right).

The reported study requires evaluation of different elements that are explicitly introduced within the body of the present manuscript. It thus comprises: adaptation of chemistry for biochip functionalization, elaboration and optimization of both proposed release strategies, accommodation of experimental conditions to work with living cells and finally configuration of necessary instrumental set-up. The reader may easily remark that this work is focused on different aspects corresponding to various domains of competences ranging from biomolecular engineering, cell sample handling up to optical physics. In order to provide high level of presentation clarity, I decided to introduce all necessary information accompanied by adequate bibliographic references along with discussed results and throughout the given manuscript. I hope this composition will clearly guide the reader to comprehensive understanding of the reported work.

Chapter 2

Conception of the biochip molecular assembly

2.1 Introduction

2.1.1 Specific capture and controlled release methodology in a micro-scale

This chapter is essentially devoted to explore the molecular aspects of the biochip system construction which constitutes a basic issue of the biosensor functionality exploited in the present work. The objective is to propose a biosensing surface capable of selective immobilization of cells and their sequential release. Such achievement would fulfill the need of novel methodologies ensuring controlled cell capture and desorption steps in one single micro-scale device. Though, an important issue related to this development is to provide optimal operating conditions deprived of extensive physical or chemical perturbations that may possibly influence the live cell viability. The target cell immobilization in a microarray or microfluidic format can be achieved by cell-adhesive surfaces of several types frequently reported in the scientific literature. Ones can be therefore directed by the cell-specific biomolecules like for instance proteins of extracellular matrix (*e.g.* fibronectin),[77, 78] specific antibodies,[29, 79] peptides,[73, 80] aptamers[74, 81] or even DNA if using cells tagged with complementary strand.[82, 83] Consequently, live cells trapped on a solid substrate may be released from their microenvironment and thus achieve the final goal of such biosystem ranging from fundamental research to advanced diagnostic applications. Straightforward methods of cell detachment may be exemplified by enzymatic digestion of binding protein (*e.g.* by using trypsin treatment),[76] direct cell removal by optical forces,[84] micromanipulation,[85] microfluidic shear forces,[86, 87] or even *in situ* cell lysis if further determination of genomic/proteomic characteristics is needed.[60] Nevertheless, when developing new cell sorting strategies, the key point is to realize spatio-temporal control of capture/release steps under physiological conditions. It is particularly advisable to ensure the cell integrity before running downstream analyses. To attain these goals, multiple strategies are proposed in the literature and their short overview is hereafter presented. These methodologies may find an application in micro-scale tunable devices providing an efficient capture of living cells and their subsequent recovery with possibly minimal perturbation for cell viability and functionality.

When engineering remotely tunable biomaterials, a great challenge is to ensure precise control of adhesive properties between the developed substrate and a cellular sample. In order to allow controlled attachment and detachment of naturally adhesive or non-adhesive cells, leading development is focused on the design of specific molecular motifs incorporated in the biosensing solid support.[88, 89] Different chemistries are therefore worked out to generate stimuli-responsive surfaces that are or may be subsequently deployed for cell release. One of the solution found in the scientific literature is to perform spatially controlled cell desorption from antibody-modified self assembled monolayers (SAMs) generated on gold microelectrode surfaces.[90] Applying reductive potential difference of -1.2 to -0.9 V results in electrochemical desorption of cells captured by the

47

underlying antibody layer that can be easily regenerated with high level of reproducibility.[91] Some other groups propose to introduce an electro-sensitive modification to SAMs forming the adhering surface. Electrochemical oxidation/reduction is enabled by incorporation of such redox-active functions like for example hydro(quinone)[92-94] or ferrocene.[95] Therefore, the applied electrical potential fires gentle release of a live cell previously trapped by the modified monolayer into the bulk medium. According to this strategy, Mrksich's group reports on an orthogonal release of two cellular samples captured on a single micro-device, depending on the electrical stimulus (positive or negative potential).[96] This approach is however limited to only two target species since their release is enabled by either oxidation or reduction process. Alternatively to electrical stimulation, remotely triggered release may be achieved over other physical stimuli such as electromagnetic field (*e.g.* release from modified magnetic particles embedded in hydrogel),[97] temperature variation (by using designed thermoresponsive surfaces)[98-100] or UV illumination.[101] In each case, efficient cell detachment is observed upon external stimulation, although potential stress generation (*e.g.* thermal or UV) may influence further biomolecular investigations carried out on a cellular sample.

Some other strategies that might be potentially explored for controlled cell desorption are based on chemically or biochemically switchable substrates. Indeed, capability of a bioadhesive surface to smartly release living cells for biosensing applications is obtainable by an impulse of chemical or biochemical nature. An example of such approach, however not explored so far on a planar surface, exemplifies the release of physicochemically bound target upon rising of the pH value that switches off the electrostatic interactions with structured substrate.[102] Another interesting strategy may provide cell detachment by addition of chelating or metal binding agent (*e.g.* EDTA, imidazole) to a substrate based on Ni^{2+} ion complexed in nitrilotriacetic acid (NTA) and polyhistidine tag assembly.[103, 104] Employment of strong chelator is reported as an example of highly biocompatible strategy deployed to release fibroblasts from peptide-functionalized hydrogels formed with Ca^{2+} ions.[58] However, these methodologies may be hardly applied to design of remotely controlled systems where high throughput performance is desired.

Advanced approaches to tunable bio-adhesive surfaces are focused on a conception of more developed chemistries that enable cell specific addressing and controlled spatio-temporal release of several cellular targets bound on a biochip. In this scope, a great interest may be assigned to DNA-based substrates. Indeed, a multiple choice of DNA sequences, their automated synthesis and robust attachment on solid surface make them ideal tool for multiplexed analysis. Moreover, microdevices based on DNA matrix may be exploited to realize selective and programmable release of bound analyte – cellular target in particular – by the means of enzymatic cleavage[75, 105, 106] or thermal desorption.[99] We therefore benefit from the intrinsic properties of double stranded DNA that is susceptible to be precisely cut by restriction enzymes or to dissociate if adequate temperature is reached.

As we will see in the subsequent chapters, these two approaches are explored within the scope of the present work as potential strategies for cell sorting purposes.

2.1.2 DNA-driven cell capture

In the recent years, cell-based microsystems aroused tremendous interest in the field of modern biotechnologies aiming both research and biomedical application.[43, 107] A decade ago, the very fist example of cell biochip was published, demonstrating that solid support can be turned into a versatile miniaturized platform capable of highly parallelized investigations at cellular level.[108] Among efficient strategies to address biological cells of multiple type on well-defined locations of a microarray surface, many efforts have been deployed for the fabrication of protein biochips.[109] The cell-specific immobilization is mainly achieved within immunorecognition process by dint of accessible repertoires of antibodies produced for cell immunophenotyping.[110-112] However, some recent works show that DNA-based architectures may become a versatile way to achieve robust, fast and reliable cell-based microarray fabrication.[59, 75, 80, 82, 83, 113, 114] In order to ensure specific cell capture on a biochip provided by DNA hybridization step, we may generally proceed according to two strategies. The first approach involves a preliminary synthetic modification of the cell membrane by DNA motifs introduced under surface bioengineering protocol found in the literature[82, 83, 113] or proposed by a commercially available methodology (*e.g.* KODE^{TM} technology).[115] Once the cell decoration with oligonucleotides is achieved, their subsequent hybridization on a DNA-biochip may be realized. The second approach relies on conception of a protein-DNA conjugate (in a covalent or non-covalent coupling) and its immobilization on the microarray, followed by incubation and specific capture of cells.[80, 114] By comparing these two strategies, the latter one appears more straightforward since crude cellular sample might be directly loaded on a biosensing surface built out of properly organized and functional cell-specific architectures.

The strategy based on protein conjugation to DNA may be successfully used to specifically address several cellular targets on a DNA microarray. The on-chip capture of living cells according to so-called "DNA Directed Immobilization" (DDI)[114, 116] is therefore achieved and assisted by regular hybridizations between complementary strands. Such approach is more suitable for biochip design because it avoids direct grafting of structurally fragile proteins (often antibodies) on a surface. The main advantage of DDI method is the much higher stability of DNA microarrays, by comparison to protein microarrays, and the infinite number of oligonucleotide sequences potentially deployed to fabricate dense microarrays. Niemeyer, who pioneered in this method,[117] reports that DNA-directed protein microarrays characterize spot homogeneity as well as intra- and inter-experimental reproducibility in comparison to responses issued from direct grafting of proteins on a microarray.[116]
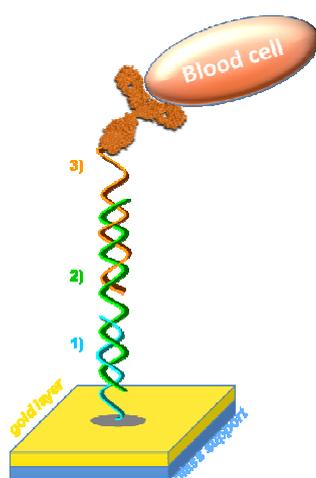
Figure 2.1 Schematic representation of living cell immobilization on DNA-based biochip. The specific capture is achieved by three-level molecular architecture: 1) oligonucleotide probe immobilized on the gold surface, 2) intermediate DNA strand, 3) hybrid IgG–DNA molecule bridging the target cell through a cell-specific antibody.

Therefore, the protein-DNA conjugate approach (or more precisely antibody-DNA conjugate) is explored in the present study, in order to develop biochip system suitable for primary cell sorting. Briefly, we create a DNA matrix by deposition of an oligonucleotide-modified conducting film of polypyrrole on a gold surface. (*cf.* Fig.2.1) Subsequently, the biochip molecular edifice is elevated with an intermediate DNA strand and finally completed by an antibody-DNA conjugate. Since the antibody molecule (IgG) is directed to a precise marker situated on a particular cell membrane, such biochip construction provides specific immobilization of well-defined cell types. In the final step, captured cells are remotely released from the platform according to one of two programmable strategies based on the properties of double stranded DNA. In the former one (*cf.* Chapter 3), cellular target release is fired by dint of enzymatic cleavage provided by DNA restriction site which is precisely recognized by specific endonucleases (restriction enzymes). The latter desorption approach is directly realized within dsDNA dissociation induced by local heating and based on a photothermal phenomenon described in Chapter 4. Moreover, both strategies guarantee reproducibility of the capture/release process thanks to DNA-based construction that may be eventually regenerated and the original DNA matrix retrieved for further use. In this chapter, the reader will thus become acquainted with the designed biomolecular on-chip assembly involving construction of the hybrid antibody-DNA molecule addressed onto DNA-functionalized biochip according to complementarity rules. Overall construction is monitored in a real-time and a label-free manner by using Surface Plasmon Resonance (SPR) imaging.

2.2   Fabrication of the DNA biochip

Nucleic acids as well as other biomolecules may be addressed onto the surface within many available functionalization methods ranging from one-step deposition by contact to more developed lithographic techniques.[118] In the scientific literature, we may find many examples of solid substrates deployed in biosensor applications like for example glass, silicon, indium tin oxide (ITO), gold or even crystalline carbon (*e.g.* diamond). The immobilization of a probe matrix may be achieved within covalent linking (*e.g.* EDC-mediated attachment) or physicochemical interaction (SAMs,[119] STV-biotin bridge). Deposition of probe-modified conducting polymers is an example of stable and robust biochip fabrication method.[120, 121] Therefore, for the need of the present study, pyrrole-modified DNA probes are specifically addressed to gold surface in form of polypyrrole films generated with help of an electrochemical impulse.
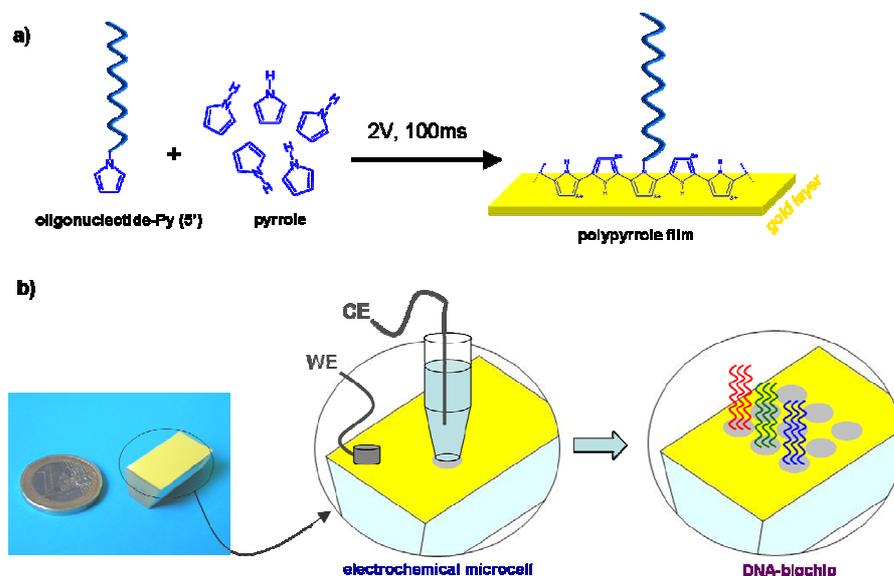
Figure 2.2 Fabrication of a DNA biochip by the electrospotting process.
a) electropolymerization reaction: pyrrole-modified DNA probe is copolymerized with pyrrole moieties upon an electric pulse and deposited on the gold surface in form of a polypyrrole film (~ 5 nm in thickness).
b) electrochemical microcell: 2 V potential difference is applied between the gold surface (WE - working electrode) and platinum wire (CE - counter electrode) immerged in the spotting solution (DNA-Py + Py monomer). Spot size is determined by the plastic tip opening (400-1200 µm in diameter) and spot position is controlled by external motors.

In order to immobilize the molecules of interest over a metallic layer, a home-made instrumental set-up is employed[122, 123] which enables multiple deposition (spotting) of several probes by dint of motile electrochemical cell (*cf.* Fig. 2.2) The DNA biochip matrix is fabricated on a solid material based on a glass prism or slide covered by thin gold layer (~50 nm). In fact, gold is a support substrate of choice for the biochip design because of its interesting properties - the metal is poorly oxidable, chemically stable in the presence

51

of biologic samples and easily undergoes functionalization by organic molecules (*e.g.* thiol-based probes). Moreover, it can be readily used as a working electrode (WE) which constitutes an integral part of the electrodeposition system here exploited.

The biochip surface is microarrayed with a few DNA probes by using the microcell composed of a micropipette tip equipped with a thin platinum filament (counter electrode or CE). The electrodes are connected to the external potentiostat which generates a 2-V potential diffference during the deposition step. Electrochemically driven synthesis of the polypyrrole (Ppy) film lays a foundation for the fabrication of DNA spots.[121] Namely, pyrrole (Py) molecules and 5' pyrrole-modified oligonucleotides are copolymerized upon the electrical stimulation. The electro-oxidization of Py monomers is very fast and results in a metal-adherent polymer film of nanometric thickness, deposited on the surface of working electrode (gold).[123] Such strategy ensures efficient linkage of DNA probes with the biochip surface provided by high stability of the Ppy film and its resistance to experimental conditions. Since the polymer growth is spatially defined by the electrochemical cell size (400-1200 µm in diameter), successive polymerizations of several oligonucleotide probes enable to obtain a functional matrix of DNA spots.

2.3   Chemistry of antibody-DNA conjugate

2.3.1   Overview of protein-to-DNA conjugation methods

From the introduction to this chapter, we have learnt that protein-DNA conjugates, thanks to their combined properties, may become versatile molecular tools of great interest for immunoassay and biosensing applications. Synthetic oligonucleotides have been modified for years to bridge their intrinsic properties to those borne by partner molecules.[124-126] Therefore, we may discern many examples of an efficient conjugation of semisynthetic DNA oligomers with polypeptides and proteins of different sort (including enzymes,[127-130] antibodies[131, 132] and other functional proteins).[117, 133-135] This bioengineering approach finds an application in such developments like new biological fluorophores for optical detection in nanobiotechnology,[134, 136] cell-based microarrays[59, 114] or multiplexed immunoassays (*e.g.* immuno-PCR).[20, 137] Thus, I would like to outline the most pertinent strategies of protein-DNA conjugation which have been recently deployed for biosensing needs and both for diagnostic and research purposes.

In general, we distinct two independent approaches where protein-DNA conjugates are generated according to either covalent coupling chemistry or non-covalent molecular assembly. Aiming DNA-protein conjugation procedure, several methods, which are not based on direct chemical bonding, are proposed. As example, we can benefit from metal-complexing properties of the nitrilotriacetic acid (NTA) and subsequent metal ion (*e.g.* Ni^{2+}) interaction with polyhistidine (*e.g.* His_6) molecular tail. Therefore NTA-modified DNA oligomers possibly complex nickel(II) ion and consequently interact with His_6-tagged protein in order to eventually form a stable DNA-protein architecture.[103] Another, more prevalent non-covalent strategy is established upon remarkably strong interaction between biotin molecule and homotetrameric proteins: avidin and streptavidin. Gentle procedures of biotinylation and therefore the availability of biomolecule-biotin derivates (*e.g.* DNA, antibody) make molecular assemblies based on STV-biotin couple useful for the on-chip functional construction.[20, 114, 138] An exemplary protocol introduces a streptavidin molecule covalently bridged to a short oligonucleotide as a first step of the molecular assembly[117] that constitutes a versatile platform for further conjugation to biotinylated molecules[139] such as IgG in living cell microarrays.[114] However, the construction of such molecular assembly requires stoichiometric control of DNA-protein conjugation and the tetrameric structure of streptavidin may thus become a barrier because it provides multiple potential interactions with biotin-modified species.

Alternative solutions are brought by using covalent coupling between well-defined functional groups pending on the biomolecules of interest. If precise reaction conditions are applied, an efficient linkage may be generated involving such moieties like primary amines or thiols naturally occurring (*e.g.* lysine or cysteine as protein building blocks) or

synthetically introduced to biomolecules (*e.g.* commercially available oligonucleotides modified by –NH$_2$ or –SH). One of imaginable strategies may imply activation of carboxylic function (*e.g.* by EDC) to enable its reaction with primary amine, thus forming a stable amide bond.[140] The example of such straightforward conjugation is however hardly found in the literature. It is because nearly all proteins contain both –NH$_2$ as well as –COOH functions and coupling strategy incurs a risk of protein auto-aggregation generating significant purification difficulties. Therefore, common routes for covalent coupling of oligonucleotide and proteins mainly rely on protocol composed of two separated steps and frequently involving bi-functional cross-linking agent. The cross-linker is introduced in the first step and bears either homo-[127, 132] or hetero-functionalities.[128, 134, 135, 141]

In the goal of DNA and protein (antibody in particular) coupling, commonly applied cross-linking agents are composed of two functional groups providing efficient amine-to-sulfhydryl conjugation such as amine-reactive ester (N-hydroxysuccinimide ester) and maleimide group (prone to react with thiols). On the one hand, formation of stable amide linkage is therefore enabled owing to nucleophilic character of the amino-groups that remain reactive towards high electrophilic carbon of NHS ester group (provided that well-defined pH conditions are respected). On the other hand, thioether bond is generated according to nucleophilic addition of thiol to an electron deficient α-carbon of the maleimide group. Many examples of DNA-protein conjugation published so far report on efficient reaction between a thiol-modified short oligonucleotide and a protein necessarily equipped with amino groups by the means of lysine residues.[117, 128, 130, 131, 138, 142, 143] Some other groups describe a reverse synthesis based on the NHS-maleimide cross-linker which alternatively involves an amino-modified DNA and a bioengineered protein tagged by cysteine residues, exposing –SH functions for coupling.[133, 134, 136] However, this approach can not be directly applied to conjugation of native antibody molecules where sulfhydryl groups are tethered in disulfide bonds. Following a reduction step, only fragments of immunoglobulin undergo the effective coupling.[144, 145] Another alternative strategy may benefit from the primary amine group pending on antibody which is chemically modified to either latent sulfhydryl group and conjugated to a DNA-NH$_2$[106] or disulfide bond eventually exchanged to another disulfide involving DNA-SH molecule.[135] Thioether bond is however more frequently deployed because of its higher stability over disulfides. All these strategies consist of two conjugation steps - the former one providing protein activation for coupling and the latter one affecting a modified oligonucleotide. In the present study we firstly attempt to use a homobifunctional linker but such approach does not result in satisfactory coupling, as it is discussed below. Therefore the final strategy providing conjugation of an antibody with short DNA oligomer is realized by using cross-linking agent of NHS-maleimide type.

2.3.2 Conjugation by using homobifunctional cross-linker

As a first approach to synthesize the hybrid molecule composed of an antibody linked with DNA strands, we opted to use a homobifunctional conjugation agent - disuccinimidyl suberate (DSS). This chemical linker is reported as a useful molecular tool in protein bioconjugation procedures since it contains NHS esters that, in defined pH conditions, are highly reactive to primary amines.[127, 132]
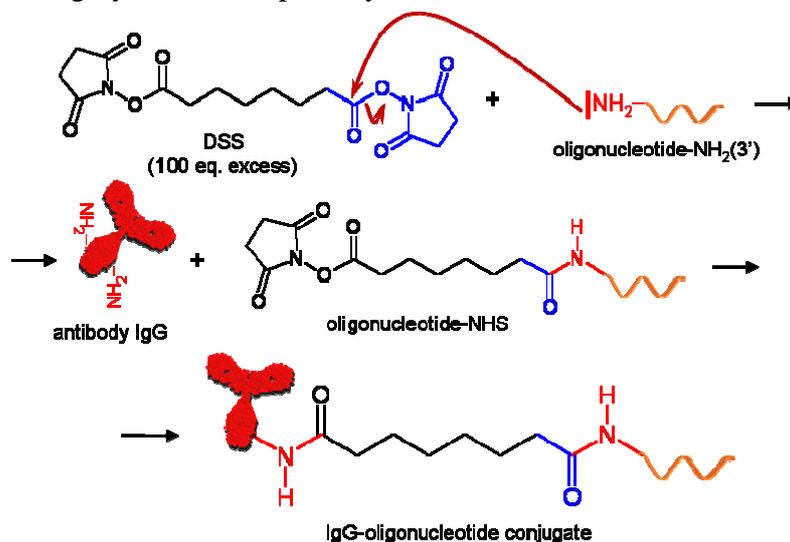
Figure 2.3 Antibody and DNA coupling reaction via DSS. At first, an oligonucleotide is coupled to the cross-linking agent which enables conjugation to an IgG molecule in the latter reaction step.

In the first step of the developed protocol, DSS molecule is coupled to an oligonucleotide strand modified by an alkylamine at 3' end (excess of the cross-linker is required to avoid DNA inter-linkage).[146] Reaction occurs rapidly (over barely few minutes) and after DSS excess removal, NHS-activated DNA undergoes subsequent coupling with an immunoglobulin G bearing primary amine functions throughout lysine moieties. (Fig.2.3) Purification of the final protein-DNA product is provided by size exclusion[132] or anion exchange chromatography.[127, 130] In the present study, the second purification method is chosen to separate the unreacted substrates (IgG and oligonucleotide) from the desired conjugation product (IgG–oligonucleotide). However, tests of coupling realized between IgG from rabbit serum (rab-IgG) and different amine-modified oligonucleotides (*Eco*RI*, *Nco*I* and *Pvu*II*) show that DSS-based strategy does not give acceptable results. It turns out that independently from the purification conditions and IgG/DNA coupling ratio, the conjugated product is hardly discerned by chromatographic purification (*cf.* Fig.2.4). It means that either DSS-driven conjugation does not take place or the coupling yield is very low. We speculate that the most probable reason explaining the observed conjugation failure is that the intermediate NHS-oligonucleotide degrades before being coupled to protein molecule. This conclusion is confirmed by mass spectrometry analysis kindly realized by C. Saint-Pierre from Nucleic Acid Lesions laboratory (LAN, CEA Grenoble). Namely, the MS results obtained for the intermediate *Eco*RI-NHS

evidence complete hydrolysis of the introduced succinimidyl ester (Appendix A). The efficient conjugation is neither revealed by modifying the intermediate step conditions (acid medium and low temperature) that are supposed to reduce further NH_2 reactivity and degradation of NHS.[147] Taking into account these findings, the coupling strategy based on DSS cross-linker is not longer retained in the present study. An alternative solution is proposed which as we will see hereafter, results in definitely higher coupling efficiency and this one is ultimately employed.
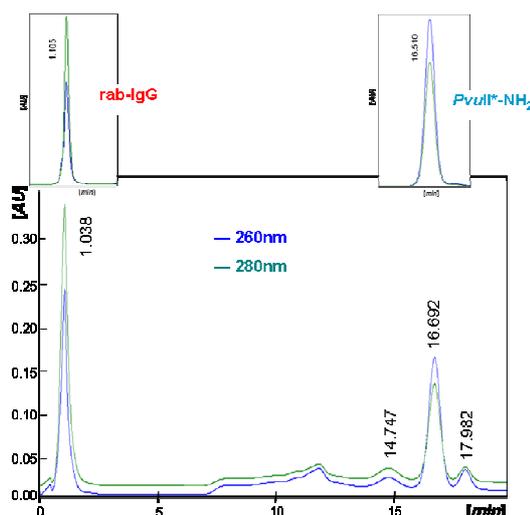
Figure 2.4 Chromatographic purification of products issued from the conjugation of rab-IgG and *Pvu*II*-NH$_2$ by using DSS coupling agent. HPLC profile evidences two main peaks corresponding to non-coupled substrates: rab-IgG (t_R = 1.038 min) and *Pvu*II* (t_R = 16.692 min) confirmed by independent purifications of native IgG and DNA sample (upper images). Elution conditions: 1 ml/min flow rate, NaCl gradient 137 mM – 1000 mM (pH 8.0). HPLC column: HiTrap^{TM} Q FF (GE Healthcare) 1 mL, 45-165 µm of bead size (6% highly cross-linked agarose modified by -N$^+$(CH$_3$)$_3$).

2.3.3   Efficient coupling by using a cross-linker of NHS-maleimide type

As a consequence of the above presented results, antibody-DNA coupling strategy is finally switched to another conjugation chemistry based on indirect amine linkage with thiol groups. As explained in the introduction to this section, cross-linkers of NHS-maleimide type are widely used in bioconjugation procedures since they enable proper coupling between primary amines (with help of N-succinimidyl-activated ester) and thiol functions (by maleimide group). Considering IgG and oligonucleotide chemical interconnection, two possible synthesis paths are conceivable: amine-modified DNA coupling to IgG molecule or DNA-thiol conjugation to native IgG (Fig.2.5). The first alternative is however less suitable since IgG thiol functions required for coupling are mainly incorporated in disulfide bonds. Their chemical reduction, even upon mild conditions,[144, 145] risks to destroy the functional structure of an IgG which is crucial for immunoassays and cell-based microarrays. Thus the second strategy is more rational since nearly all IgGs bear several NH_2 functionalities and thiol-modified oligonucleotides are commercially available.
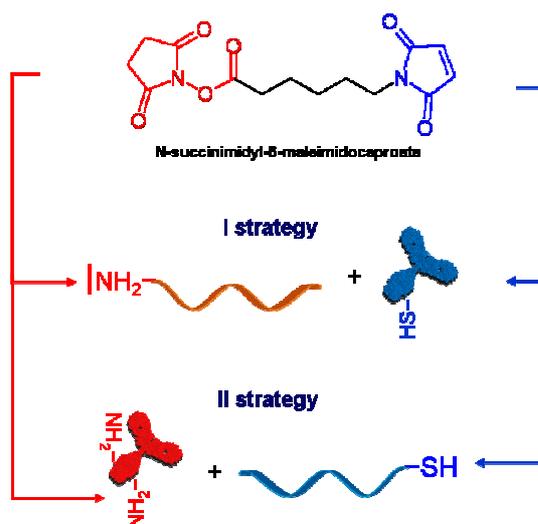
Figure 2.5 Strategies of IgG and DNA coupling by using a heterobifunctional cross-linker composed of maleimide group (prone to react with thiols) and N-hydroxysuccinimide ester (sensitive to nucleophilic substitution by primary amines).

According to the aforementioned statement, we decide to proceed in a two-step protocol, firstly involving antibody activation by means of the N-succinimidyl ester and subsequent coupling to 3' thiol-modified oligonucleotide through the maleimide-induced nucleophilic addition. [*cf.* Fig.2.6 a)]. To do so, a heterobifunctional cross-linker based on polyethylene glycol (PEG) structure is used (SM(PEG)$_{12}$ - succinimidyl-[(N-maleimidopropionamido)-dodecaethyleneglycol). Compared to other reagents containing purely hydrocarbon spacer arms,[128, 136, 143] linking reagents equipped with PEG chain are rather more convenient alternative.[140] The PEG presence improves water solubility and limits the risk of bioconjugate aggregation. It offers an increased flexibility of the bioconjugation reaction, resulting in reduced immunogenic response potentially provoked by the spacer itself. A hydrophilic character of the main structural chain ensures efficient water solvatation of the reagent and final conjugate molecule as well. Unlike PEG-based reagents, cross-linkers built out of hydrophobic spacer arm require application of organic solvents (*e.g.* DMSO) which may affect biomolecule stability and render purification step difficult. By using SM(PEG)$_{12}$, an efficient purification and conjugation steps are performed in aqueous solutions.
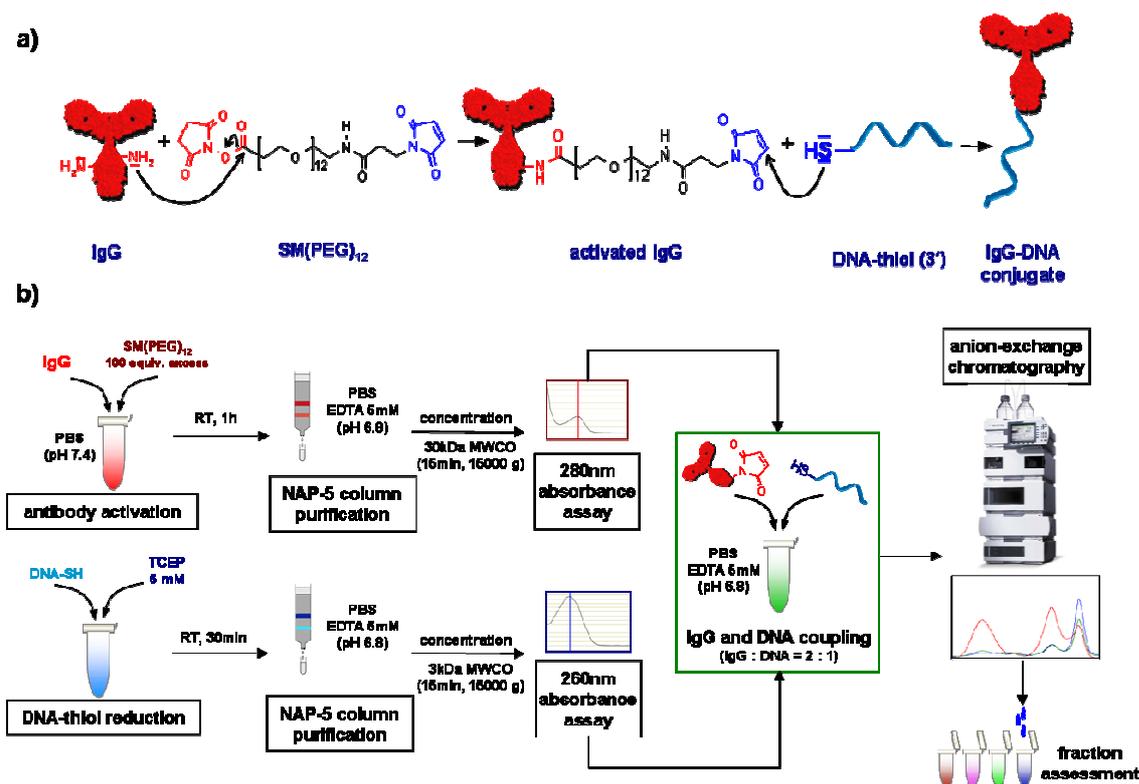
Figure 2.6 Conjugation of IgG and thiol-modified DNA by using SM(PEG)$_{12}$.
a) cross-linking reaction scheme; **b)** flowchart of the synthesis and purification protocol.

In the present work, several cell-directed antibody molecules are coupled to 3'-thiol modified oligonucleotides containing restriction sites (*Eco*RI*-SH, *Nco*I*-SH and *Pvu*II*-SH). However, an optimization step of the cross-linking reaction is performed by using a representative IgG antibody issued from rabbit serum (rab-IgG). Conjugation protocol and purification procedure are therefore adapted, and inspired from previously reported studies as well as from SM(PEG)$_{12}$ supplier recommendations.[148] The overall procedure of here developed IgG-to-DNA covalent linkage is schematically illustrated on Figure 2.6 b). Our goal is to obtain a conjugation product corresponding to one IgG molecule of interest synthetically bound to one oligonucleotide strand (monoconjugated hybrid molecule). For this purpose, the antibody loading with DNA is assessed by UV absorbance measurement executed on conjugation product fractions issued from final purification step.[117] The desired product is drawn apart by dint of anion exchange chromatography which enables a charge-depending separation of species. Therefore, polyanionic oligonucleotide fragments can be easily isolated from protein molecules provided that chromatographic purification conditions are closely related to IgG isoelectric point (pI) where its overall molecular charge is nearly zero. In the case of a human IgG, these conditions are estimated between 6.4 and 9.0 pH value and neighbor pH of neutral environment.[149] Accordingly, the protocol of chromatographic purification here applied puts in practice elution in a buffer of pH 8.0.
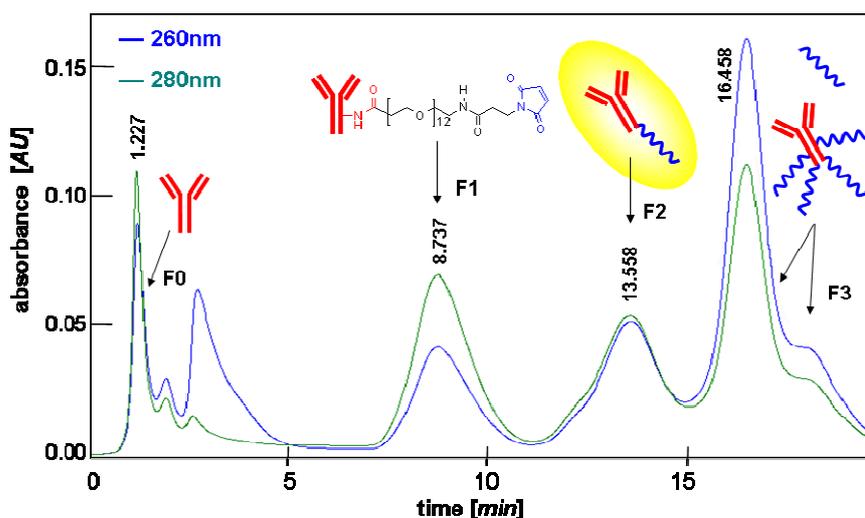
Figure 2.7 Purification of the IgG–DNA conjugation products by anion-exchange chromatography. Chromatographic profile evidences the following product fractions: F0 (native IgG), F1 (antibody modified by the cross-linking agent), F2 (the desired one-to-one conjugated molecule), F3 (multiconjugated product and/or free DNA oligomer). Elution conditions: 1 ml/min flow rate, NaCl gradient 137 mM – 784 mM (pH 8.0). HPLC column: HiTrap^{TM} Q FF (GE Healthcare) 1 mL, 45-165 µm of bead size (6% highly cross-linked agarose modified by -N$^+$(CH$_3$)$_3$).

2.3.4   Optimization of the IgG–DNA coupling reaction

In order to establish an efficient antibody-DNA coupling methodology several parameters have to be considered. A major issue of the reaction scheme is the stoichiometric control of the amount of DNA strands covalently linked to each protein molecule. Willing to obtain desired one-to-one bioconjugate, different substrate ratios are tested and antibody loading with DNA evaluated. The number of oligonucleotide fragments grafted on IgG molecules is assigned by chromatographic separation followed by absorbance measurements of the discriminated fractions.

The first step of the coupling procedure relies on IgG activation by SM(PEG)$_{12}$. In order to provide high reactivity of primary amines towards NHS ester, this stage has to be realized in delimited pH conditions – from 7.0 to 9.0 (PBS buffer of pH 7.4 in our case). Large excess of the cross-linking reagent is required to ensure proper conjugation of the N-succinimidyl-activated esters to primary amine functionalities pending on IgG molecules. Three values of the SM(PEG)$_{12}$ stoichiometric excess are tested (10, 50 and 100) and resulting chromatographic profiles investigated (Fig.2.8). Following the HPLC purification step, we discern three major product fractions: F1 corresponding to NHS-activated antibody, F2 which is the one-to-one conjugation product and finally F3 ascribed to free oligonucleotides and/or multiple-conjugated molecules (*cf.* Fig.2.7). Fraction assessment results from the absorbance measurements as well as immunofluorescence assay discussed in farther part of the present chapter.

59

From the registered HPLC profiles, we can conclude on the coupling efficiency obtained for the three tested SM(PEG)$_{12}$ ratios. As observed, F1 fraction is slightly shifted to higher retention times (t_R) if more of the cross-linker is employed. Knowing that the elution of native IgG (F0) occurs in the first minute after the injection to column (proving neutral net charge), we deduce that F1 corresponds to the maleimide-bearing antibody, interpreted as IgG molecules with modified net charge. Moreover, the maleimide groups are randomly introduced on the antibody molecule and higher cross-linker content results in a larger relevant peak.

Concerning the remaining part of the observed chromatographic profiles, one may notice that the F2- and F3- corresponding peaks are not perfectly resolved. These results demonstrate that the more of SM(PEG)$_{12}$ is employed for coupling, the more F2 and F3 peaks overlap. This can signify that an increased ratio of the linking reagent generates considerable level of derivative compounds built out of IgG linked to an undetermined number of DNA strands. Unfortunately, multiple coupling of DNA oligomers to single IgG molecule can not be completely circumvented. The F2 fraction can be however attributed to the desired monoconjugated product. It is because this fraction is characterized by an absorbance ratio (A_{260}/A_{280}) of around 1.0 which is consistent with previously reported findings.[117] The three given experiments are performed for the same molar quantity of protein and therefore the F2 peak magnitude may be approximated to coupling yield. Taking into account this fact, we consider 100 equivalent excess of SM(PEG)$_{12}$ cross-linker as suitable for efficient DNA and IgG conjugation. Higher excess is not attempted because an extensive charging of the IgG molecule is not desired regarding to the antibody functionality.
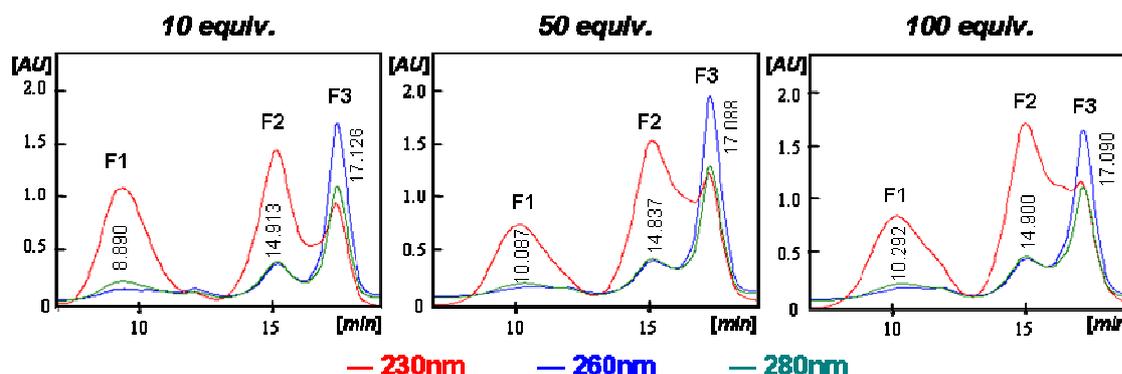
Figure 2.8 IgG–DNA coupling performed in different IgG : cross-linker ratios. Stoichiometric excess of SM(PEG)$_{12}$ is evaluated (10, 50 and 100) for the conjugation of rab-IgG and *Nco*I*-SH.

Once an IgG molecule is combined to the cross-linking agent and unreacted residues of SM(PEG)$_{12}$ removed by size exclusion chromatography, the maleimide-bearing antibody undergoes coupling to a thiol-modified oligonucleotide. As it makes up the latter step of the coupling strategy, such reaction involving maleimide functionality is more convenient compared to final linkage through N-hydroxysuccimide ester (*e.g.* DSS

strategy). It is because maleimide group is more stable in aqueous solution in contrast to NHS ester that rapidly sustains hydrolytic degradation. Maleimide stability and reactivity to sulfhydryls is however pH dependent as the group slowly hydrolyses at pH values greater than 7.5. Therefore the optimal conditions for the second stage of coupling reaction are placed between pH 6.5 and 7.5. In order to produce an efficient linkage by formation of thioether bond, the use of maleimide demands free sulfhydryl groups as binding partner. That is why thiol-modified oligonucleotides are submitted to chemical reduction prior to their conjugation to the activated IgG molecules.

In the fields of biochemistry and molecular biology, the most commonly used reduction agents are dithiothreitol (DTT) and 2-aminoethanthiol. Apart from their capacity to efficiently reduce disulfide bonds, as thiol-based compounds themselves, they may interfere in SH-involving reactions if they are not completely discarded. Thus, the protocol evaluated here relies on an alternative reducing conditions based on TCEP (tris(2-carboxyethyl)phosphine). This reagent is an advisable solution not only because of it physicochemical properties (odorless, non-volatile and resistant to oxidation in air) but mainly because of its capacity to selectively and completely reduce even the most stable water-soluble alkyl disulfides over a wide pH range. By using TCEP, the reduction side-product is a phosphine oxide which is non-reactive compound to other functional groups. After an oligonucleotide-SH is treated with TCEP, reduced sample is desalted on a size exclusion column (NAP[TM] 5) and subsequently recovered in EDTA-containing buffer. Presence of the chelating agent aims to hinder metal ions to induce disulfide bond regeneration before the DNA strand is coupled to antibody. The acidic-basic conditions (pH 6.8) ensure high reactivity of the maleimide functionalities pending on the IgG molecule towards thiol-modified oligonucleotides.

A key point of the cross-linking strategy here developed, is to provide appropriate stoichiometric conditions in order to obtain monoconjugated IgG–DNA product with considerable final yield. An important element is therefore to establish optimal coupling ratio between substrates involved in the ultimate step, *i.e.* maleimide-activated antibody and reduced DNA-thiol. Literature references frequently report on equimolar quantity of both biomolecular substrates which has been intuitively applied to the tests described above.[138, 143] (Fig. 2.8) However, IgG and DNA are biomolecules of distinct nature and contrasting structure mainly because of their size, charge distribution and accessibility of potentially reactive groups. IgG–maleimide molecules and DNA-thiol strands jointly suspended in solution may engender covalent linkage in a statistically random manner. Consequently, it is worth to optimize IgG/DNA ratio and evaluate the yield of desired conjugation.
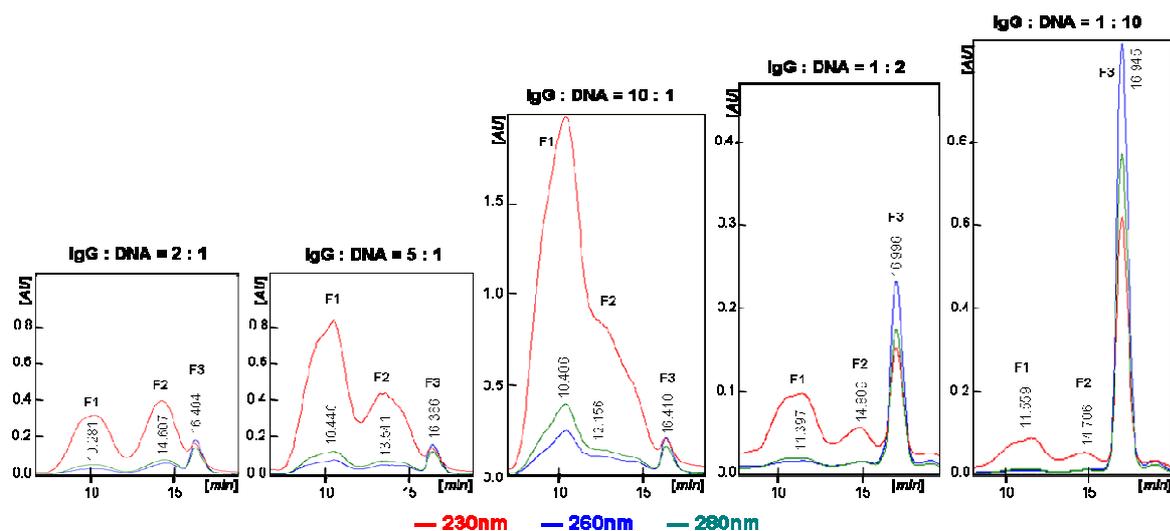
Figure 2.9 IgG/DNA conjugation by SM(PEG)$_{12}$ with different stoichiometric ratios of the substrates. Excess of the IgG (rab-IgG) and oligonucleotide (*Pvu*II*) is hereby evaluated.

Accordingly, the coupling reaction is performed by providing a greater molar content of the oligonucleotide-SH (1 and 10) or the activated IgG (2, 5 and 10) in order to examine the aforementioned concern. Following the incubation, reactive solutions are submitted to purification by anion exchange chromatography - the relevant chromatograms are represented on Figure 2.9. From the obtained results, we may clearly conclude that increased stoichiometric content of oligonucleotide used in the reaction does not generate higher rate of desirable IgG–DNA combined product, *a priori* represented by F2. Proportionally to the applied oligonucleotide excess, one may notice a magnification of F3 peak which retention time corresponds to the free DNA molecule. As to extension of the antibody molar contribution in the coupling reaction, proportional amplification of concerned peaks (F1 and F2) is similarly perceived. The mentioned peaks are not only higher but also less resolved on chromatographic profile if an important excess of the protein is used in the reaction. Considerable augmentation of the IgG/DNA ratio is able to produce an extension of derivative products and is therefore baseless. In such case, the registered absorbance signal reveals an elevated degree of non-coupled antibody as well (F1).

As observed on the obtained chromatographic profiles, IgG/DNA ratio equal to 2:1 yields a good resolution of F2 peak corresponding to monoconjugated product of our interest. This stoichiometric proportion is consequently proposed for the final coupling protocol which is applied to conceive the programmed antibody-oligonucleotide conjugates (Table 2.1). Although a considerable fraction of the antibody is still not coupled (~18% of starting IgG amount in recovered F2 fraction), the chosen protocol results in good yield of the monoconjugated IgG–DNA (14% – 29%). Further, confirmation of the efficient coupling is brought by absorbance measurements referred to theoretical values and described hereinafter. A proof for suitable antibody functionality is finally assessed by immunofluorescence assay and SPR imaging.

antibody	IgG–DNA conjugate	application	coupling yield
IgG from rabbit serum	rab-IgG–*Eco*RI*	conjugation reaction optimization, tests of biochip molecular assembly and enzymatic release	20%
	rab-IgG–*Pvu*II*		22%
	rab-IgG–*Nco*I*		16%
	rab-IgG–Zip2*	fraction assessment in immunofluorescence assay	19%
rat IgG anti-mouse CD19	CD19–*Eco*RI*	specific capture of B lymphocytes (CD19 membrane marker)	23%
rat IgG anti-mouse CD90	CD90–*Pvu*II*	specific capture of T lymphocytes (CD90 membrane marker)	29%
mouse IgG anti-HcB domain	HcB–*Nco*I*	negative control (non-relevant antibody)	14%

Table 2.1 Antibody-oligonucleotide conjugates synthesized within the framework of the present project. The coupling yield is expressed as ratio of the IgG amount in fraction corresponding to the monoconjugated product (F2) and starting quantity of the antibody employed in the reaction.

2.3.5 UV absorbance measurements

Consequently to the IgG and oligonucleotide coupling reaction, followed by purification on an anion-exchange chromatographic column, four main product fractions are discerned (F0, F1, F2 and F3). The relevant retention times observed on chromatograms give significant premises on the type of the obtained conjugation products (compared to t_R registered for native IgG or free DNA strand). The isolated fractions are however concentrated and their absorbance determined at 260 and 280 nm light wavelength. The measured absorbance ratios (A_{260}/A_{280}) are straightforwardly applied to evaluate the average number of DNA strands loaded on each antibody molecule (Appendix B).[117, 131] This is because the experimental values may be compared to the theoretical ones issued from Lambert-Beer absorbance law, knowing that absorbance maximum is placed at 260 nm for DNA and 280 nm for proteins.
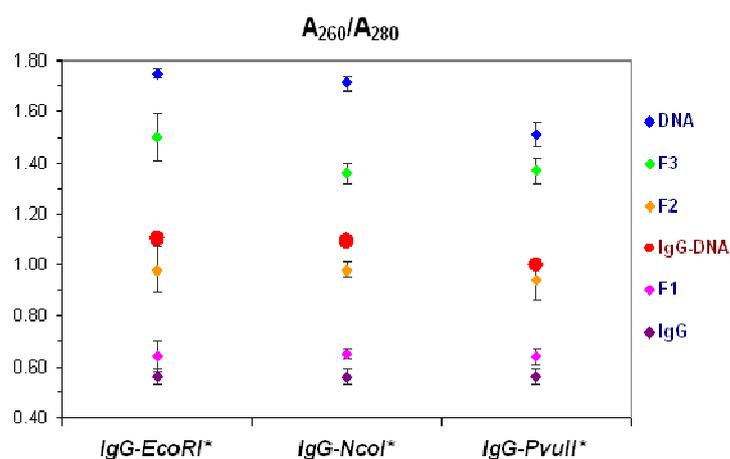
IgG–DNA	experimental A_{260}/A_{280}					calculated A_{260}/A_{280}
conjugate	F1	F2	F3	IgG	DNA	IgG–DNA
IgG–*Eco*RI*	0.64 (0.06)	0.98 (0.09)	1.50 (0.09)		1.75 (0.02)	1.10
IgG–*Pvu*II*	0.64 (0.03)	0.94 (0.08)	1.37 (0.05)	0.56 (0.03)	1.51 (0.05)	1.00
IgG–*Nco*I*	0.65 (0.02)	0.98 (0.03)	1.36 (0.04)		1.71 (0.03)	1.09

Figure 2.10 Estimation of the IgG loading by DNA molecules based on 260nm and 280nm absorbance measurements. Three fractions obtained from the conjugation reaction are considered (F1, F2 and F3). The experimental A_{260}/A_{280} values (in blue) are compared with the theoretical ones (in red) assigned to the monoconjugated IgG–DNA.

Figure 2.10 represents average absorbance ratios registered for fractions F1, F2 and F3 issued from conjugation of an IgG-type antibody with the relevant oligonucleotides. These empiric values are assembled with those observed for native IgG and DNA as well. A_{260}/A_{280} ratio is obtained from independent absorbance measurements and standard deviation is given. The experimental data are finally compared to the values theoretically assigned to the monoconjugated IgG–DNA. Determination of the theoretical value of absorbance ratio is based on Lambert-Beer formula taking into account the additivity of the absorbance law and assuming that the conjugation does not influence the extinction coefficients of DNA and protein. Comparison of 260nm/280nm absorbance ratios determined experimentally with their theoretical equivalents enables estimation of antibody loading level with DNA. Therefore, we affirm the presence of desired monoconjugated product in the fraction F2 which approximates the calculated value at most. Fraction F1 is thus identified as non-conjugated IgG, unlike the fraction F3 composed of multiconjugation products that can not be avoided (free oligonucleotide might be present as well). These conclusions are reflected by an additional examination realized on each of the recovered conjugation fractions and based on a fluorescence signal read-out.

2.3.6 Fraction assessment by immunofluorescence assay

Fluorescence microscopy is a robust detection technique deployed to identify DNA entities on microarrays due to its high sensitivity and multiplexing capabilities.[150] Therefore, an easy method for reliable assessment of the fractions collected from chromatographic separation of the bioconjugation products is to realize an on-chip immunoassay based on the fluorescence read-out. Such immunofluorescence test conducted on a DNA microarray enables validation of hybridizing capability of IgG–DNA conjugates and their coupling efficiency. Accordingly, this control is led on an oligonucleotide microarray functionalized with three probe sequences. (Fig.2.11.). In such configuration, Zip1 constitutes a positive control signal, Zip2 is devoted to fraction assay and Zip3 serves as a negative control. After incubation of each fraction issued from the rabbit-IgG conjugation to DNA (complementary Zip2*), a secondary immunorecognition antibody is introduced onto the biochip. The secondary anti-rabbit IgG conjugated with biotin enables interaction with streptavidin-R-phycoerythrin protein (STV-PE) based on high affinity of STV to biotin molecule (dissociation constant is around 10^{-15} M).[151] R-phycoerythrin is a versatile fluorescence label with strong light absorption (about 550 nm) and emission peak in green-yellowish light area (575 nm). Upon STV-PE binding, fluorescence signal may be directly observed.
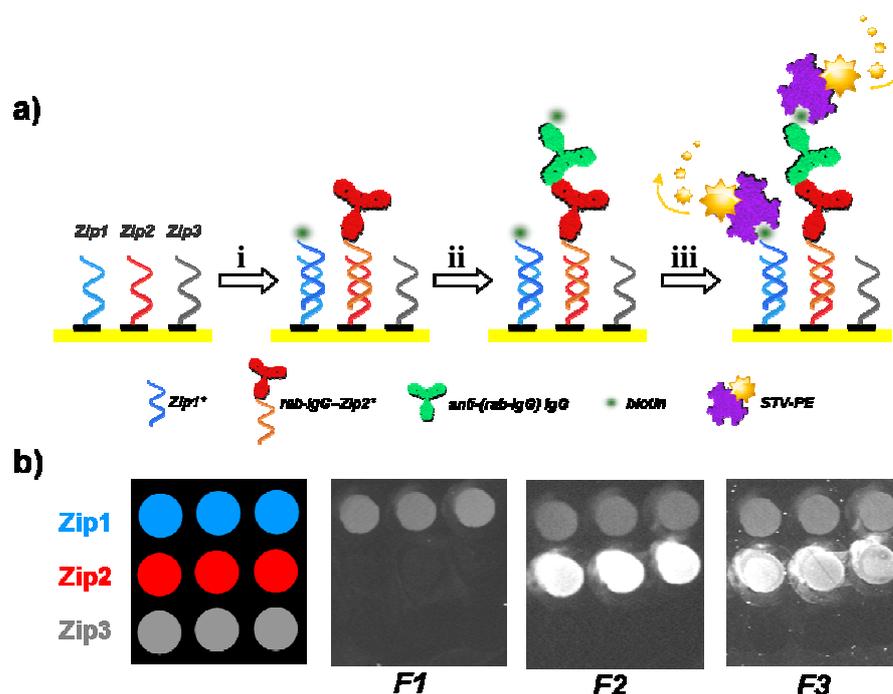
Figure 2.11 Immunofluorescence assay for assessment of the IgG–DNA conjugation products.
a) schematic representation of the experimental protocol: i - hybridization of the assayed fraction (rab-IgG–Zip2*) and positive control sequence (Zip1*-biotin), ii - incubation with biotinylated secondary antibody (anti-rab-IgG), iii - incubation with streptavidin-R-phycoerythrin (STV-PE) and fluorescence signal read-out;
b) revelation of the fluorescence signal in three independent tests of the fractions (F1, F2 and F3) issued from rab-IgG coupling to Zip2* oligomer.

In consequence of the test here described, fraction F1 does not show any fluorescence compared to Zip1 positive control. It confirms that the conjugation product is not involved in this fraction which may be attributed to the linker-activated IgG as it was proposed before. Regarding to F2 and F3 fractions, both hybridize properly on the given DNA-biochip resulting in strong signal from the Zip2 probe. We notice that Zip2 spots reveal enhanced fluorescence by comparison to the control complementary strand injected along each fraction (Zip1*-biotin). Unlike one biotin moiety on the control Zip1* sequence, numerous biotins pending on the secondary antibody (anti-rabbit IgG) are capable of multiple interactions with STV-PE, resulting in strong Zip2 fluorescence. Although fraction F2 appears as a single well resolved peak on the chromatogram, the F3 fraction is actually composed of multiple conjugation products (or free oligonucleotide), obviously due to possible covalent grafting of several oligonucleotides on the same IgG molecule. These findings are consistent with the aforementioned considerations based on the absorbance measurements at different wavelengths. Hence, it confirms the presence of the desired IgG/DNA monoconjugate in the fraction F2 that will be preferentially used in further experimentation to build the designed biochip assembly.

2.4 Real-time monitoring of the biochip molecular assembly

Molecular design of the biochip system here proposed, requires a versatile tool to follow construction of the assembly involving hybridization of short oligonucleotides and antibody-DNA conjugates as well as further detection of cellular targets in ensuing experimentation. To do so, the present work takes advantage from an optical method based on surface plasmon resonance (SPR) phenomenon. This analytical technique is widely used in the field of biosensors and deployed for various biological and chemical sensing applications.[39, 152] Small sample volume, real-time monitoring and possibility of parallelized detection makes SPR-based method a useful tool to investigate biomolecular interactions of different nature.[38, 153-155] More recently, it has been shown that particular technique of SPR imaging (SPRi) is also convenient for the label-free monitoring of living cells immobilized on a solid support.[40, 79] For these reasons, the SPR imaging has been chosen to track the biochip molecular build-up as well as cell capture/release events discussed in farther part of the manuscript. To understand the detection phenomenon, a general insight to SPR features is hereafter proposed and followed by description of the employed instrumental set-up.
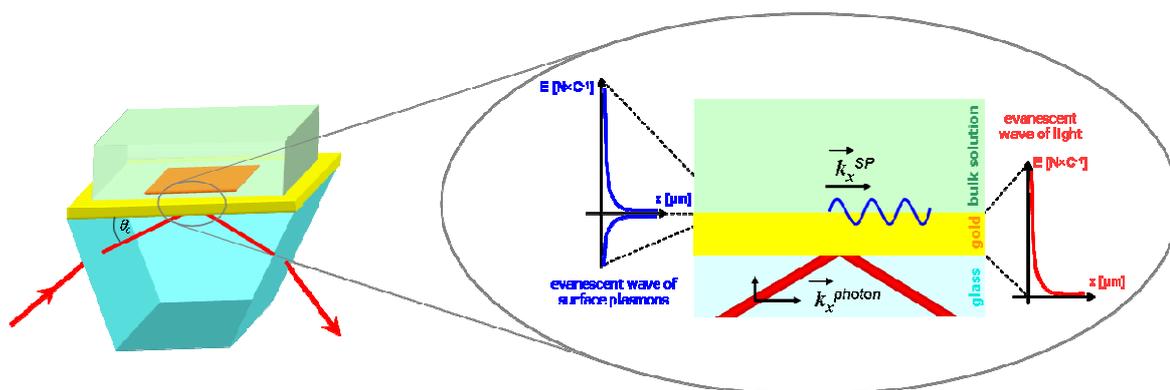
Figure 2.12 Surface plasmon resonance in Kretschmann's configuration. The gold layer SPs are excited by an incident light beam in total internal reflection conditions (TIR). The incoming photons are coupled to the free electron oscillations on the metal/dielectric interface, provided that the corresponding electric field components are parallel ($k_x^{photon} = k_x^{SP}$) which is proper to TM-polarization. The evanescent wave of surface plasmon penetrates into local medium at around 100 nm depth. The lateral resolution of the electric field decay is ~7 µm.

2.4.1 Surface plasmon resonance phenomenon

Surface plasmon resonance is an optical phenomenon that lays the foundation of particular biosensing systems.[156] SPR-based methods permit to follow variations of the refractive index in the neighborhood of a dielectric/metal interface and thus enable to observe specific biomolecular interactions. This feature is a result of the energy coupling that occurs between incoming photons (incident light) and free electron oscillations of the metal surface (surface plasmons - SP). The surface plasmon waves are produced upon

excitation by light wave and propagate along the interface (*cf.* Fig.2.12). Several conditions are required to obtain an efficient photon coupling to the electrons.

The developed biochip system based on the SPR detection employs a gold-coated glass prism (60° angle) according to configuration proposed by Kretschmann.[157] In such geometry, an incident beam of light strikes a thin gold layer (here ~50 nm) deposed on the prism in the conditions of total internal reflection (TIR). Willing to excite surface electron waves, the incoming light must be polarized in a transverse magnetic (TM) mode. This polarization ensures that the electric component of electromagnetic wave is normal to the interface and consequently parallel to the electric field vector of metal SPs.[158] Under a specific angle of incidence (*cf.* Fig.2.13), the incoming photons undergo a resonant coupling to the gold surface electron oscillations, which results in decrease of the reflected light intensity (resonance angle θ_R). Hence, the generated evanescent wave of surface plasmon remains sensitive to any refractive index changes induced in the neighborhood of the biochip surface. When working in fixed angular conditions (SPR imaging), the optical index changes produced by molecular adsorption phenomena are detected as a variation of the reflectivity depending on the occurring interaction. The SPRi instrumental set-up provides a real-time monitoring of a large biochip area (about one square centimeter) and allows simultaneous tracking of various biomolecular interactions specific to several immobilized probes.[123]
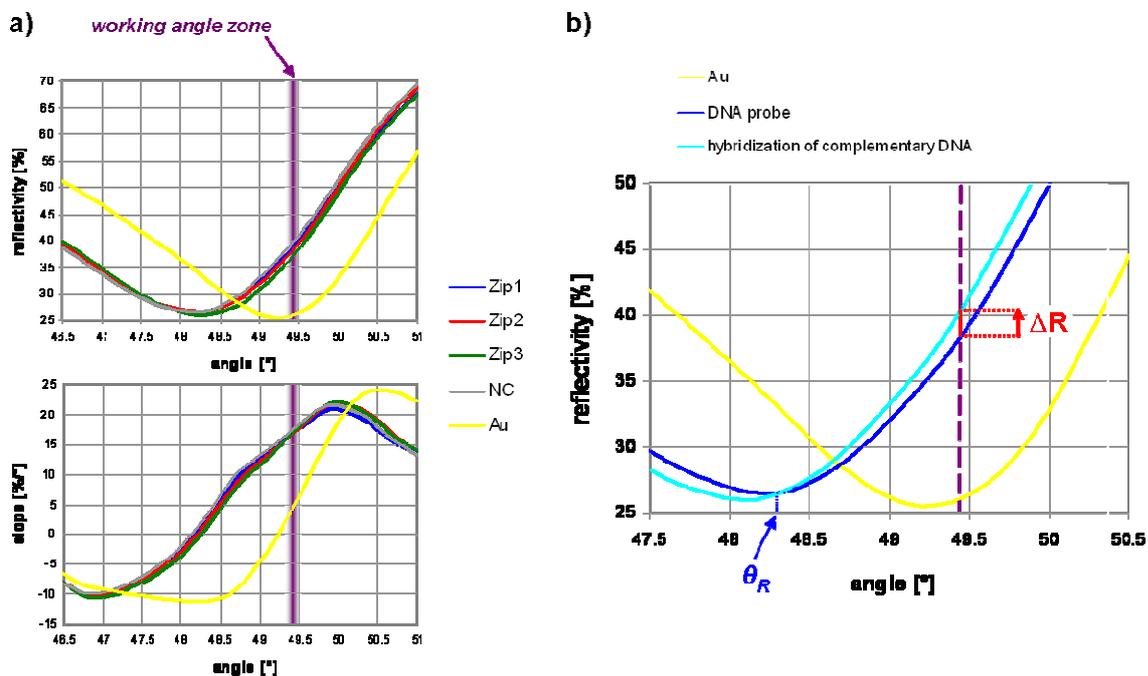
Figure 2.13 Plasmon curves on polypyrrole-based DNA spots and bare gold surface.
a) intensity of the reflected light (%) in function of the incident angle observed for grafted probes (Zip1, Zip2 and Zip3), control oligonucleotide (NC) and bare gold (Au); **b)** principle of the SPR imaging measurement upon complementary DNA hybridization. SPRi monitoring is performed at a fixed angle of incidence (working angle), biomolecular interactions are detected as the reflectivity shift. The reflectivity minimum is registered by CCD camera at θ_R corresponding to the angle of resonance.

2.4.2   SPR imaging instrumental set-up

The experiments demonstrated in the present work are based on SPR imaging set-up provided by *Horiba Scientific-GenOptics* (unless specified) and based on the Kretschmann's configuration (Fig.2.14) A DNA-functionalized biochip is placed in the optical detection system together with a flow cell (described in farther parts) and supplied with a running buffer by dint of proper microfluidics (syringe pump and injection valve). The experimental buffer is transported through a degassing system and delivered to the reaction chamber at a controlled flow rate. Samples are introduced in the liquid flow by using a 6-channel injection valve ensuring negligible dead volume. Biochip and flow cell set-up is housed in an incubator set at 37°C within a whole experiment.
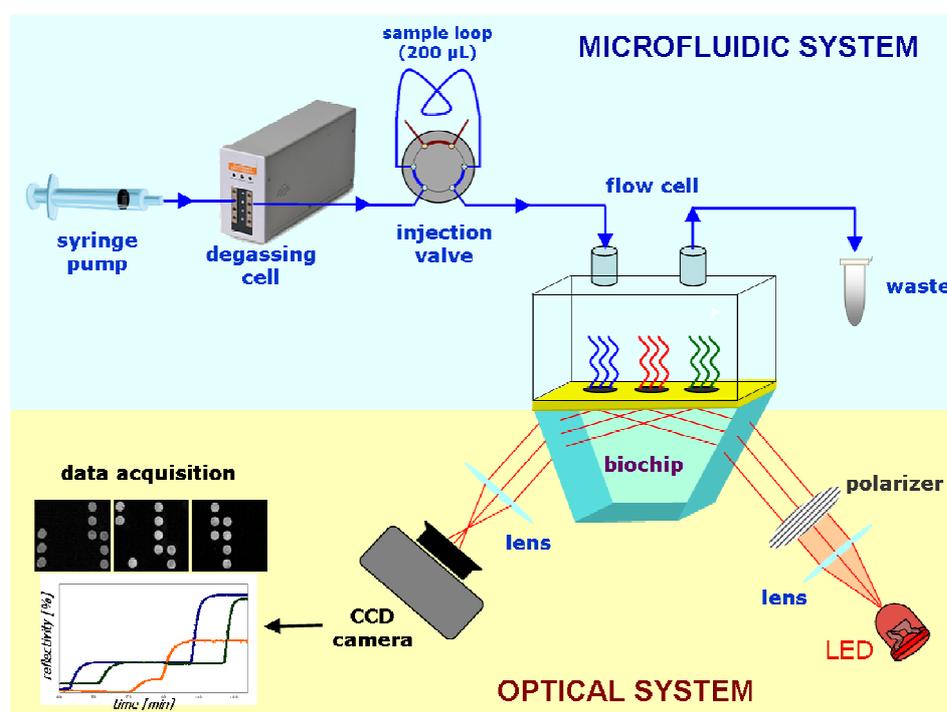
Figure 2.14 Surface Plasmon Resonance Imaging set-up. Samples are manually injected by a 6-channel injection valve and driven to the reaction chamber (flow cell) through a proper microfluidic system. The running buffer is delivered by remotely controlled syringe pump. The SPRi system (*Horiba Scientific-GenOptics*) is equipped with a LED ($\lambda = 660$ nm) and the reflectivity is registered by CCD camera connected to a computer and data acquisition is controlled by proper software. The optical system is incubated at 37°C within the experiment.

A heart of the SPRi detection system is composed of several elements of the optical nature. The incident light wave (660 nm) is generated by a light-emitting diode (LED) and collimated by a biconvex lens. Farther optical pathway is equipped with a rotating polarizer providing TM (SPR detection) or TE (total reflection used as reference) polarization mode. The incident light is reflected on the biochip surface and resulting light received by CCD camera (16-bit). An appropriate software provided by *Horiba Scientific-GenOptics* is used to monitor reflectivity variations observed at well-defined zones

corresponding to several assayed probes. Images are registered by the camera and processed data are represented on kinetics curves (% of reflectivity plotted in time).

2.4.3   SPRi monitoring of the DNA-based molecular assembly

As we have learnt, the SPR-based detection techniques offer great possibility to investigate large variety of biomolecular interactions. This is motivated by at least two major characteristics: label-free detection of any biomolecular target penetrating in the vicinity of a metal/dielectric interface (~100 nm) and real-time monitoring of target–probe interactions. Such approach gives the access to kinetic parameters, which usually can not be retrieved by conventional end-point analysis methods.[159] SPR imaging is hereby employed to assess functional assembly of the designed biochip, relying on IgG–DNA conjugate hybridization which enables consequent transformation of DNA microarray to an antibody pattern. Therefore three series of DNA features are arrayed on the gold surface according to the aforementioned electrospotting technique. Each probe is composed of a poly-T spacer arm on 5'-end followed by 24 base-long hybridizing sequence (*cf.* Table 6.1). The relevant probe sequences are of the same length and of similar thermodynamic properties. Besides, different base sequences disable cross-hybridization and enable probe-specific immobilization of designed targets. DNA-based addressing of antibodies is hereby demonstrated as preliminary step that evaluates the biochip functionality for further applications.

The set of immobilized oligonucleotides serves as a matrix to realize corresponding three-component molecular architectures which step-by-step erection is followed by SPRi (Fig.2.15). Each of the three grafted Zip probes is firstly hybridized with longer intermediate strand containing complementary Zip sequence on 3'-end and a restriction site on the 5'-end. Consequently, the relevant antibody-DNA conjugates are introduced on the biochip and immobilized according to the complementarity rules. Hence, the hybrid protein-DNA molecules composed of the restriction site-containing sequences combined with IgG are subsequently added to complete the molecular edifice. The specificity of successive hybridizations is confirmed by SPR imaging that generates proper reflectivity shifts consistent with the injections of each molecular building block. For the clarity of signal read-out, the background reflectivity of a control non-relevant probe (the NC probe) is subtracted from each SPR curve traced upon time (Appendix E).
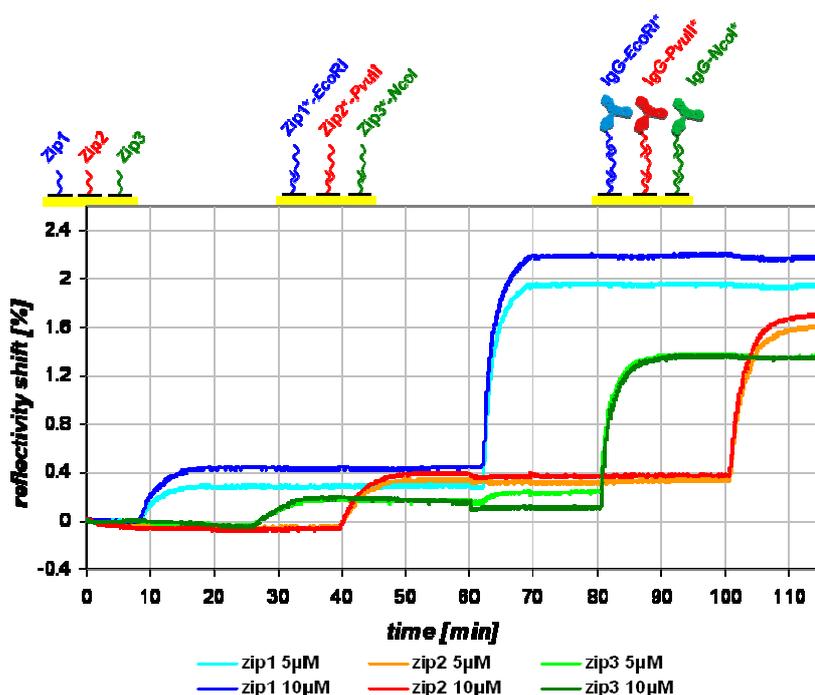
Figure 2.15 The biochip molecular assembly monitored by SPR imaging. In the first step, the complementary intermediate strands are introduced over the Zip sequence matrix (Zip1*-*Eco*RI, Zip2*-*Pvu*II and Zip3*-*Nco*I). 5µM and 10µM stand for the Zip concentration in the electrospotting solution. The molecular edifices are completed by successive hybridizations of the conjugation products composed of a rabbit IgG combined with the corresponding DNA oligomer (IgG–*Eco*RI*, IgG–*Pvu*II* and IgG–*Nco*I*). The experiment is incubated at 37°C and driven in the following running buffer: PBS, MgCl$_2$ 10mM, pH 7.4.

As we may interestingly observe, the addition of hybrid antibody-DNA conjugates triggers much higher reflectivity shifts compared to those registered for the underlying intermediate strands. This may be explained by the fact that reflectivity variation results from local modification of the refractive index, highly depending on the quantity of the adsorbed material. Therefore, the observed signal difference may be attributed to molecular weight of the immobilized species which is about 150 kDa for IgG molecules and only 15 kDa for the intermediate DNA strands. Since SPRi signal is proportional to the mass of captured molecules,[160] we opine that only one IgG–DNA conjugate is immobilized per each three to five complementary DNA strands. Target anchoring to all the available sites is hardly achieved probably due to steric hindrance effect related to the antibody molecule size. Nevertheless, the obtained results demonstrate that designed molecular assembly may be successfully build-up and followed under construction by SPRi detection technique. Moreover, thanks to the three component molecular architecture strategy, the DNA-microarray can be easily regenerated and original matrix eventually retrieved.[122] The recycled microarray can be thus used for several successive experiments without any significant signal loss provided that suitable storage conditions are respected (data not shown).

71

2.5 Conclusions: transformation of DNA biochip to functional antibody microarray

When designing biosensing surfaces, a key element is to enable efficient and specific binding of desired targets on a modified solid support. The findings described by the present chapter reported on the DNA-based microarray that can be easily turned into the antibody biochip. This feature is ensured by a molecular tool composed of an IgG molecule combined with an oligonucleotide strand. Accordingly, the antibody-DNA conjugation reaction was hereby proposed. The obtained product was consistent with the monoconjugation scheme (one-to-one hybrid molecule) which found confirmation in UV absorbance measurements. Furthermore, an independent immunofluorescence assay demonstrated the functionality of the IgG combined to short DNA and evidenced that the designed coupling protocol is not immunogenic. Additionally to this end-point analysis, the molecular assembly involving the antibody-oligonucleotide conjugate (fraction F2) was subsequently validated in real-time detection approach by using Surface Plasmon Resonance imaging.

In the developed chemical approach, DNA moieties are arbitrarily coupled to the IgG, owing to statistic distribution of many amine groups on an antibody molecule. This kind of molecular engineering does not certainly provide a non-modified antigen recognition site (Fab region). Unlike a biochip assembly ensuring antibody orientation (by using immunoglobulin-binding proteins expressed in bacteria and exhibiting specific interaction with Fc portion of an antibody molecule),[161-163] the synthetic IgG–DNA conjugate offers a random orientation of the IgG paratope to a desired target. Nevertheless, the DNA-Directed Immobilization remains a versatile strategy in construction of biosensing platforms capable of efficient addressing of different targets ranging from proteins[138] to whole living cells.[114] The designed molecular assembly is hereby applied to specifically immobilize several cell types which will be explored in the following chapters. Controlled release of the bound cells from the DNA-based biochip will be subsequently attempted, taking advantage from the presence of the restriction sites or thermosensible character of the DNA duplex. The feasibility of both cell sorting strategies will be demonstrated by using a label-free technique of SPR imaging. SPRi is therefore shown to follow in real time the biomolecular phenomena and the capture/release steps at cellular level as well.

Chapter 3

Specific release by enzymatic cleavage

3.1 Introduction

DNA molecule exemplifies a type of biopolymer that can be easily manipulated in a desirable manner in standard molecular biology protocols as well as for biosensing purposes. In the preceding chapter, we reported on design of the particular molecular assembly based on the oligonucleotide microarray that can be turned into an antibody pattern. We hereby exploit this molecular construction for further applications that aim to provide a versatile strategy of programmable release. We benefit from the intrinsic properties of the double stranded DNA and its susceptibility to enzymatic manipulation, in this particular case relying on digestion of oligonucleotide sequences.
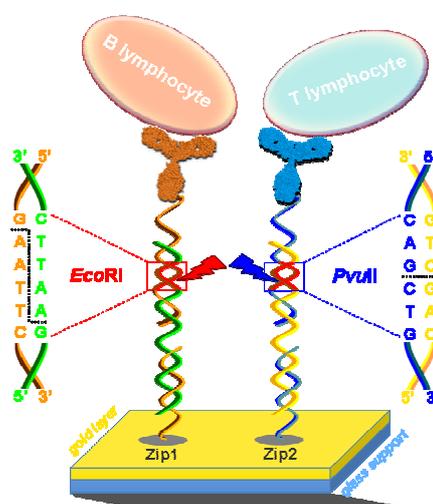
Figure 3.1 Schematic representation of cell release strategy driven by restriction endonucleases. *Eco*RI enzyme specifically recognizes Zip1-based construction (Zip1 + Zip1*-*Eco*RI + IgG–*Eco*RI*) and *Pvu*II cleaves Zip2-based assembly (Zip2 + Zip2*-*Pvu*II + IgG–*Pvu*II*). B- and T-type cells are captured by proper antibodies (anti-CD19 IgG and anti-CD90 IgG respectively).

The enzymatic cleavage of a nucleic acid substrate is reported as a specific and controllable reaction, thus desirable in development of new platforms for various biosensing goals.[164, 165] A particular example of biosensor concept is to realize selective and enzymatically driven removal of an analyte immobilized on a solid support.[105] An approach of this kind shall provide mere cleavage of DNA substrate[106, 166] or, more interestingly, trigger localized release of more sophisticated objects such as nanoparticles[167, 168] or living cells[75, 81] as well. Because cells are highly fragile and sensitive to any variation in their environment (salt concentration, pH, temperature, *etc.*), we propose a mild enzymatic cleavage process as a strategy for tunable cell sorting purposes. We make therefore use of restriction endonucleases capable of site-specific DNA digestion, ensuring fast reaction times and easy parallelization of target releasing events. The enzymatically driven desorption of cells from the microarray is enabled by

conjugation of cell-specific immunoglobulin G (IgG) to short oligonucleotides containing restriction sites. (Fig. 3.1) After full molecular build-up, the DNA-based sensor is indeed shown to efficiently capture living cells, whose orthogonal release is subsequently fired directly from the biochip.

When conducting the enzymatic digestion step, an advisable detection strategy is to enable real-time monitoring of enzymatic reaction exercised on DNA in order to get an insight into process kinetics. *In situ* assessment of cleavage phenomena may be for example performed by continuous measurement of fluorescence intensity[169] or an electrochemical signal.[170] In the present study, where target biomaterial is released from proper molecular architecture previously built on the microarray, we make use of label-free detection method based on surface plasmon resonance phenomenon as described in the previous chapter.
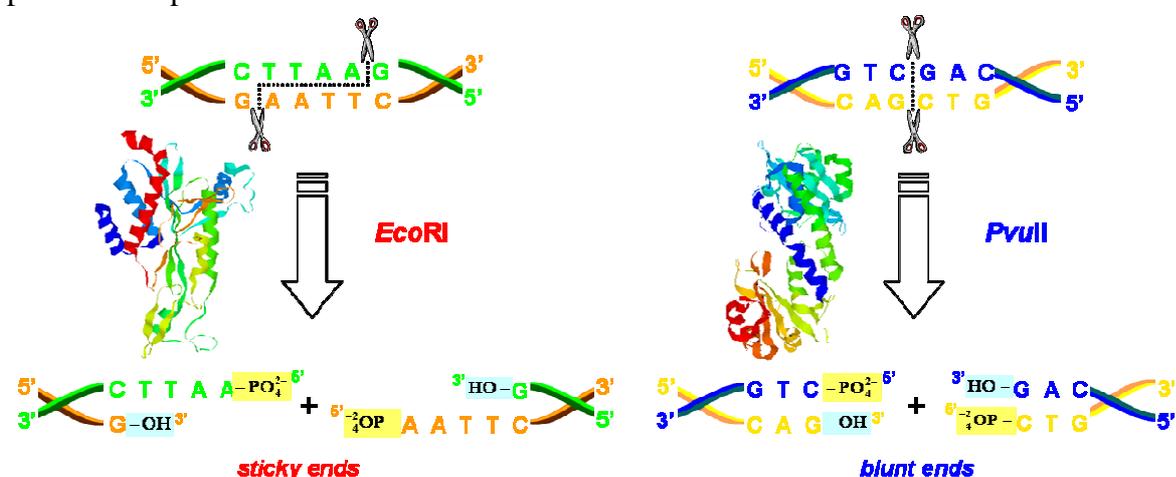
Figure 3.2 Enzymatic cleavage of double stranded DNA at well-defined restriction sites *Eco*RI and *Pvu*II. Upon enzymatic digestion, the relevant sequence is cut into two separate fragments characterized by sticky or blunt ends. Three-dimensional structures of endonucleases are represented according to Protein Data Bank (*Eco*RI is reported under PDB ID: 2OXV and *Pvu*II as 3KSK).[172]

Restriction enzymes employed for the need of the current work (*Eco*RI and *Pvu*II) are small homodimer proteins (MW ~70 kDa) capable of recognition and cleavage of short (4 – 8 bp) palindromic DNA sequences.[171] They are characterized by a high specificity to recognize well-defined restriction sites. To provide an enzymatic cleavage event, at first endonuclease molecule randomly binds to encountered dsDNA and is linearly diffused along the nucleic acid molecule. It is an efficient biochemical machinery that eventually locates its target sequence and produces hydrolysis of two opposite DNA backbones. Thus, enzymatic cleavage generates two separate DNA fragments (3'-hydroxyl and 5'-phosphate ends) equipped with so-called sticky (*Eco*RI) or blunt ends (*Pvu*II). (Fig. 3.2) Within this simplified mechanism concerning DNA substrate immobilized on a gold surface, we tend to realize target-specific release from biochip. Our attention is not in reality focused on exploring the enzymatic reaction kinetics but mainly on the final effect of precisely programmable desorption strategy which is hereafter discussed.

3.2 Enzymatic cleavage of microarrayed DNA strands

3.2.1 Optimization of the enzymatic digestion in biochip format

Restriction enzymes are proteins of fragile nature demanding proper handling and storage. In order to achieve the optimal digestion of nucleic acids, several key factors, such as buffer content, temperature, reaction time, solution volume and finally amount of enzyme, have to be considered and adapted in function of proper application. In standard enzymatic digestion protocols, the activity of restriction enzymes is executed on DNA material suspended in aqueous solution. However some groups report on the use of different proteins with hydrolase activity in the format of a microdevice where targeted molecules are immobilized on a solid support.[173, 174] The work here presented, benefits from oligonucleotides containing various restriction sites which are arrayed on a biochip surface and employed as molecular tools fin controlled capture and release purposes. Feasibility of the designed strategy needs therefore a detailed insight into several experimental conditions of the microsystem here developed.

Previously realized studies have shown that temperature is a crucial parameter to ensure high efficiency of enzyme-catalyzed cleavage driven in a biochip format.[146] The highest enzymatic activity was registered at 37°C maintained during whole digestion reaction time. Indeed, this is the optimal temperature recommended by the enzyme supplier for the given endonucleases. Here employed SPRi instrumental set-up is housed in an incubator that enables remote temperature control. Apart from the optical equipment, the main part of microfluidics system is therefore placed in the incubator set at 37°C within all experimentation steps. These conditions exactly correspond to further objectives, since they are compatible with cellular sample that will be loaded into the system in order to achieve the final goals. Even if the injection valve is installed externally to main experiment ambience, microfluidics system is based on small diameter tubing (ID of ~250 µm) and the incoming liquid phase is thus sufficiently conditioned at the right temperature prior to get in contact with the biosensing surface. Indeed, upon biochip positioning and a few minutes incubation, SPRi signal remains stable within hours (providing that any external perturbation comes about) at constant flow rate (up to 100µL/min). Another issue is however related to the material structuring the microfluidic system that has to be compatible with all injected biomaterials including enzyme molecules and living cells as well.

Proteins are generally very sensitive to their surrounding environment and readily sustain irreversible denaturation when getting into contact with solutions or surfaces that are not entirely biocompatible. Such contact might be risky for their functional structure and generate perturbation or complete depletion of biological task of an antibody or enzyme for instance. The biochip system here developed, requires therefore to use such

material for construction of injection and microfluidics equipment that is harmonious to protein samples. In very preliminary studies, we remarked denaturation effect upon enzyme injection into flow cell made of polytetrafluoroethylene (PTFE). The effect was observable as macroscopic white flocs of denatured protein on the surface of biochip removed from SPRi. PTFE commonly known as *Teflon®* is a highly hydrophobic material based on fluorocarbonic solid structure. Proteins neighboring a material of such properties incur risk of their structure and functionality alteration. That is why teflon-based modules and tubing should be avoided in enzyme bioassays. Henceforward, the present study benefits from microfluidics entirely built by using other polymer - polyether ether ketone (PEEK) which is reported as a biocompatible material employed in various biomolecular analysis methods (*e.g.* bioanalytical HPLC column)[175] and for medical applications as well.[176]

Apart from the aforementioned considerations of microfluidic material, such experimental parameters like pH or ionic strength have to be pointed out as important factors in enzymatic digestion strategies.[169] Willing to realize a successful cleavage in biochip format, the working conditions need to be adapted to ensure optimal activity of the restriction enzyme. Here, the composition of employed buffer is one of the essential issues related to functionality of an enzyme. According to the supplier (New England Biolabs), optimal conditions for commonly used endonucleases are brought by buffers characterized by pH ranging from 7.0 to 7.9 and salt molarity between 60 and 150 mM (*e.g.* sodium chloride, potassium acetate, Tris-HCl). A crucial component of enzyme-destined buffers is magnesium chloride.[169] Mg^{2+} ions are essential co-factor of the endonuclease reactivity and use of other metal ions is not suitable. The former study reports on the use of an enzymatic reaction buffer whose composition merely corresponds to one commercially available.[146] When several experimental steps are concerned, the success of SPRi-based assays relies on design of a well adapted running buffer applied in the course of a whole experiment. The project here reported, needs application of such reaction environment that is adapted not only to enzymatic cleavage but also ensures optimal DNA hybridization and biocompatibility with cellular sample. Within this study, any extended optimization of the enzymatic reaction buffer is however not attempted and proposed conditions might not be ideal for both of herein assayed enzymes (*Pvu*II, *Eco*RI). We consider that providing physiologically adequate environment is an essential concern of great importance in here developed microsystem finally applied to cell analysis. In this scope, the designed running buffer is based on PBS – a well known saline solution employed in biological research because of its isotonic to living cells character. The buffer is however supplemented with $MgCl_2$ (10 mM) which, as we will see, triggers specific DNA hybridization signals and yields a satisfactory restriction enzyme activity as well.

When considering enzymatic reaction of any kind, an important issue is to assign the amount of enzyme needed to catalyze the conversion of concrete quantity of DNA in optimal conditions. In the field of biochemistry, a functional parameter used to express the

enzymatic activity is number of enzyme units (U). In the particular case of a restriction enzyme, one unit is determined as the amount of the enzyme required to digest 1 µg of λ bacteriophage DNA in one hour, in total reaction volume of 50 µl and at 37°C. Therefore, protocols established to digest other DNA substrates need to be adjusted by taking into account the amount of target substrate and number of enzyme-specific sites.[177] Accordingly, minimal number of units that should be provided, in relation to quantity of oligonucleotide material immobilized on gold surface (estimated to 2 pmoles), is approximated to barely few units. (Appendix D) The previously reported work states that 250 U of the restriction enzyme is the optimal value to achieve fair cleavage in a biochip format.[146] However, those results concern digestion of microarrayed DNA realized in static bulk solution merely placed on the biochip surface. SPRi optical technique combined with proper microfluidics system provides proper dynamic flow conditions. This is characterized by different mass transfer phenomena compared to static experiments based on end-point analysis (*e.g.* fluorescence read-out) where enzyme is generally incubated within 1-2 hours.[75] Therefore, the kinetics of enzymatic reaction observed in both cases is different and can not be directly referred.

The flow cell used in SPRi experiments is of small volume (~15 µL) and a sample introduced to bulk solution sustains particular mass transfer conditions strongly depending on the running buffer flow rate. A crucial element of digestion driven by restriction endonucleases is their binding to DNA polymer and linear diffusion along it, until target restriction DNA sequence is reached. Such mechanism implies spontaneous enzyme association with substrate, followed by DNA molecule scanning and enzyme dissociation which frequency depends on the applied flow parameters. In fact, when imposing low flow rate, we increase the probability of enzyme interaction with several dsDNA, as opposed to a higher flow rate that generates faster protein washing away from the biosensing surface. Indeed, when loading the enzyme sample (even up to 200 U) at a flow rate applied during injections of the molecular specimens (20 µL/min), SPRi signal remains unchanged after the enzymatic solution is washed off the reactor. This means that the protein molecules can not efficiently act on DNA strands and thus the enzymatic digestion does not take place. Satisfactory result may be registered not until running flow is decreased enough, allowing enzyme molecules to sufficiently interact with the immobilized substrate. Cleavage efficiency is therefore conditioned by dynamic flow parameters and also, as we will see below, by the amount of enzyme entities introduced into the bulk solution.
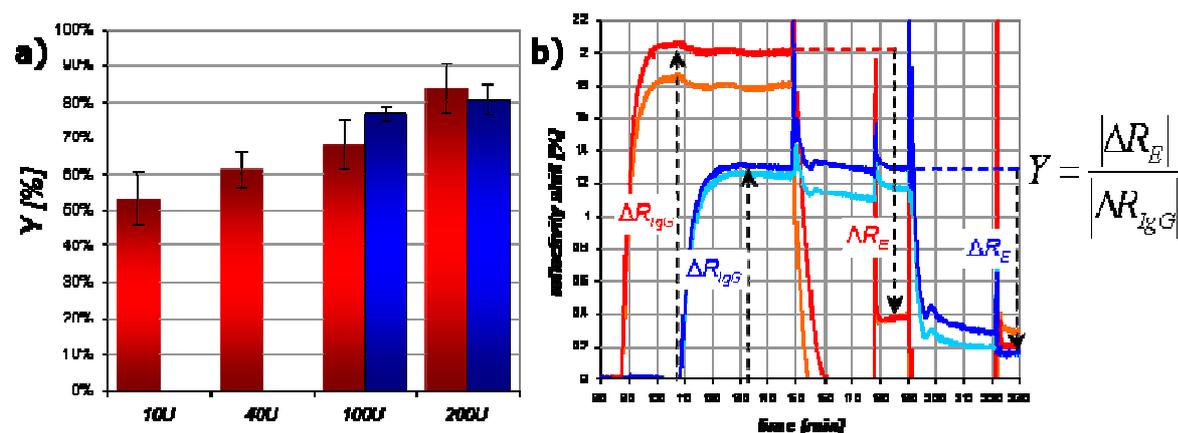
Figure 3.3 Enzymatic reaction efficiency in the biochip format. **a)** enzymatic cleavage yield (Y) observed for different enzyme content (*Eco*RI in red, *Pvu*II in blue); **b)** estimation of cleavage efficiency as ratio of SPRi signal triggered by enzyme loading (ΔR_E) to reflectivity shift upon IgG–DNA hybridization (ΔR_{IgG}). Enzyme injections are performed at 7 µL/min flow rate.

To execute enzymatically driven release of molecular targets, we inject *Eco*RI or *Pvu*II sample at decelerated flow of 7-10 µL/min, thus providing 20-30 min of reaction time. Figure 3.3 demonstrates a comparative study of the enzymatic cleavage efficiency depending on a number of the enzymatic units loaded to the biochip system. These data evidence cleavage yields corresponding to different amount of the injected restriction enzyme ranging from 10 to 200 U. The yields are represented as percentage of the relative reflectivity signal lost upon enzymatic digestion in comparison to the reflectivity shift previously triggered by the relevant IgG–DNA hybridization. As we may note, cleavage efficiency increases with number of enzymatic units used in the experiment and the highest yield is observed at 200 U (up to even 93%). This value is significantly higher compared to one suggested by theoretical calculations which mention only few enzyme units required to digest the given amount of DNA substrate. It is probably because the designed biochip molecular assembly relies on antibody addressing to DNA substrate (via IgG–DNA conjugate) which may induce certain level of steric hindrance and possibly reduce the probability of enzyme interaction with the target oligonucleotide strand. Even if cleavage is not complete, we consider the yield of 80-85 % as a satisfactory result and consequently opt to apply the evaluated enzyme content in digestion sample (200 U). Taking into account further application of the developed system, such solution additionally seems correct, since DNA/antibody surface-density will not be the only parameter regarding to enzyme accessibility to the substrate. Indeed, incubation of cellular targets may additionally reduce direct access to underlying restriction sites because of the cell size and probable physicochemical interactions with the enzyme. Need for high enzymatic content may be furthermore explained by the fact that conditions of the designed experiment are not exactly corresponding to enzyme supplier recommendations in terms of reaction time (20 min instead of 1 h), bulk solution volume (barely few microlitres, hydrodynamic flow) and optimal buffer composition (PBS + MgCl$_2$).

3.2.2 Real time monitoring of enzymatically driven release

The aforementioned considerations are taken into account in order to realize successful cleavage of different target DNA strands immobilized on gold surface by polypyrrole chemistry. As we learnt before, SPR imaging technique is a versatile tool to observe in real time the construction of probe-specific assembly on the biochip. It allows us not only to follow step-by-step generation of molecular architectures but also their programmable degradation produced over enzymatic digestions. Molecular target release may be straightforwardly registered by relevant reflectivity signal decreases and cleavage efficiency therefore properly assigned. In the case of the present study, three particular molecular assemblies are built in order to achieve enzyme specific release of two antibody-DNA targets in two separate steps. Consequently, this experimentation scheme will be extended to programmable desorption of cellular samples captured on appropriate biochip molecular build-up.

Analogously to the previously reported on-chip assembly, we herein make use of DNA-biochip arrayed with four oligonucleotide probes devoid of cross-hybridization possibility: Zip1, Zip2 and Zip3 as well as a non-relevant negative control probe (NC). Experiment is entirely carried out at 37°C and in PBS (pH 7.4) supplemented with 10 mM of $MgCl_2$. The running buffer is delivered at 20 µL/min flow rate during molecular assembly construction and 7-10 µL/min when restriction enzyme is injected. Prior to target injections, biochip is incubated with PBS solution of 1 % BSA within 15 min, formerly reported in enzyme-based assays realized in a DNA biochip format.[122] It seems to be a good blocking solution regarding to restriction enzymes used in the present study if we take into account the values of their isoelectric points (pI). This parameter may be easily found with help of an online calculation tool[178] based on primary structure of desired enzyme or protein that can be, as to it, retrieved from Protein Data Bank website.[172] Thus, *Eco*RI enzyme results in pI ~ 6.2 and *Pvu*II one is approximated to ~ 6.5. It means that in the condition of running buffer pH, injected enzyme molecules are characterized by negative total charge similarly to the adsorbed on gold BSA (pI=4.7) and we may expect their repulsion from surface.
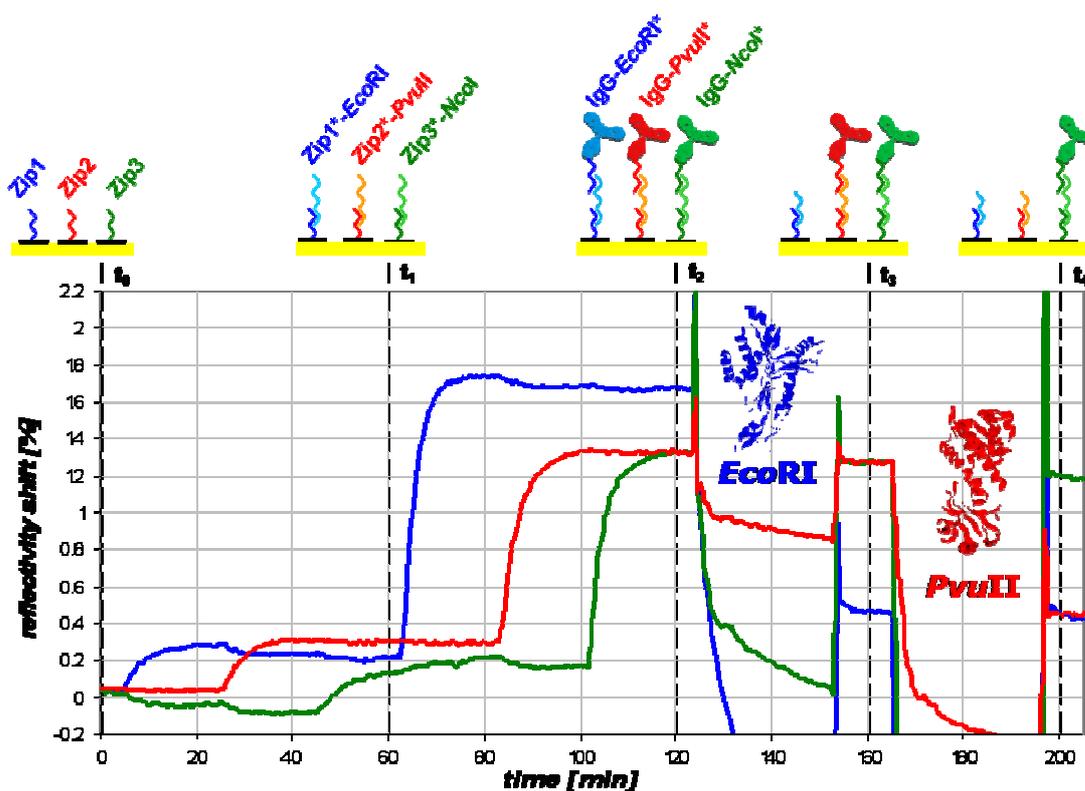
Figure 3.4 Enzymatic cleavage of the biochip molecular assembly monitored by SPRi. (t_0) Zip1, Zip2 and Zip3 probes grafted on the gold surface; (t_1) intermediate strand hybridizations (Zip1*–EcoRI, Zip2*–PvuII, Zip*3–NcoI); (t_2) immobilization of IgG–DNA conjugates (rab-IgG–EcoRI*, rab-IgG–PvuII*, rab-IgG–NcoI*); (t_3) EcoRI enzymatic cleavage; (t_4) PvuII enzymatic cleavage. All SPRi signals are rectified by a subtraction of NC signal (negative control probe).

As previously described, the first step of the three-component molecular assembly is given by hybridization of an intermediate strand complementary to Zip sequences and the final one by injection of an IgG–oligonucleotide conjugate. (Fig 3.4) The independent molecular assemblies are equipped with three different restriction sites corresponding to different enzymes EcoRI, PvuII and NcoI, where the last one is actually not used in the enzymatic release strategy and serves as control. Subsequently to successive hybridizations and complete molecular build-up, the enzymatic cleavage is fired by consecutive injections of two endonucleases (EcoRI and PvuII enzymes, 200 U each). Incubation with EcoRI enzyme results in reflectivity signal drop observed for Zip1 probe which correctly corresponds to EcoRI restriction sequence. SPRi responses simultaneously confirm the integrity of Zip2 and Zip3 molecular assemblies based on PvuII and NcoI sequences, respectively. The latter step of the enzymatically driven release is performed by injection of the second restriction enzyme PvuII in analogous experimental conditions. Once again, control NcoI-containing hybrid architecture remains intact (Zip3) whereas PvuII-based signal probe (Zip2) exhibits similar negative SPR response as Zip1 probe formerly concerned by cleavage. We may thus state that the developed biochip conditions provide target-specific enzymatic cleavage amenable to being applied in tunable strategies.

Kinetics of enzymatic reaction is a parameter that, in the case of here proposed biochip system, can not be properly studied. This is because injection of enzyme solution generates global refractive index change observed by SPR imaging as an abrupt reflectivity rise. (Appendix E) Such effect results from abundant composition of the enzymatic sample (protein, up to 5% of glycerol) which strongly affects optical properties of the reaction medium neighboring the biomolecular features immobilized on the surface. Consequently, subtraction of the negative control (NC signal) results in over-correction of the SPRi signal mainly due to the lack of its linearity in the conditions of considerable refractive index change (SPRi signal saturation). Thus, a straightforward interpretation is disabled during the enzymatic incubations and enzyme functionality can not be assigned as long as it is not washed off the reactor. Nevertheless, the cleavage specificity is unanimously proven by differential images issued from SPRi monitoring. (Fig. 3.5) Together with ΔR signals, they confirm high level of enzymatically driven release that is estimated to about 85 %. These findings are conclusive when considering programmable target release which will be consequently explored in living cell assays.
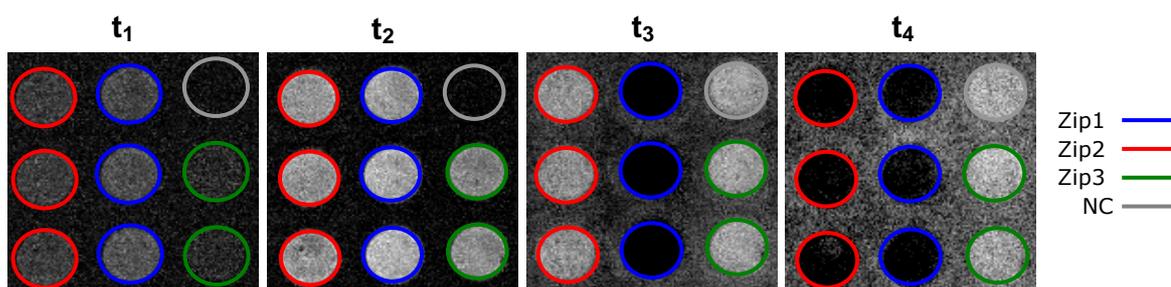
Figure 3.5 Differential SPR images registered upon molecular assembly and enzymatic release steps. (t_1) hybridization of intermediate strands on Zip1, Zip2 and Zip3 probes; (t_2) complete molecular build-up involving IgG-DNA conjugates (rab-IgG–*Eco*RI*, rab-IgG–*Pvu*II*, rab-IgG–*Nco*I); (t_3) *Eco*RI enzymatic digestion directed to Zip1 substrate; (t_4) *Pvu*II enzymatic cleavage executed on Zip2 molecular assembly. The observed spots are of 800 µm in diameter.

3.3 Specific capture and controlled release of living cells followed by SPR imaging

3.3.1 Cellular samples

The designed biochip capture–release strategy is finally applied to live cells – lymphocytes essentially, involved in immune response phenomena. Such approach provides an important development in the matter of novel research tools employed in the field of immunology and hereby fulfill the objectives brought by the present PhD thesis. At first, we conduct a proof-of-concept study with well-defined cells issued from established cell lines. Consequently, we make use of the enzymatically driven release strategy to primary cells directly issued from a living organism.

The initial study is realized with B- and T-type lymphocytes originating from regular cell lines: 3A9 and LS-102.9, kindly provided by P. Marche from Institut Albert Bonniot (IAB) in La Tronche (France). The first cellular type corresponds to T cell hybridomas whereas the latter one is represented by B lymphocyte hybridomas. Hybrid cell lines, so-called hybridomas, are bioengineered cells produced by fusion of a specific cell of interest (*e.g.* antibody-producing B lymphocyte or activated T cell) with parent tumor cells (*e.g.* myeloma or thymoma cells). This technology was originally developed to produce high amount of monoclonal antibodies from stable and rapidly dividing cell lines. Indeed, hybridomas have the capacity to grow spontaneously in standard culture conditions devoid of stimulating components and are therefore interesting tool for biological research. Hybrid cells are featured by their intrinsic properties established from the original cell and may, for instance, secrete a specific antibody or cytokine. Here employed 3A9 and LS-102.9 cell lines are characterized in terms of membranar marker expression and demonstrate high-level expression of CD19 marker on LS-102.9 (CD19+ CD90-) and CD90 by 3A9 (CD90+ CD19-). These phenotypes enable to realize controlled addressing of living cells on microarray by using cell-specific antibodies.[79]

Excepting lymphocytes issued from cell lines, we subsequently assay the developed biochip system on primary cells retrieved from mouse spleen. In a living organism, this organ plays an important role in active immune responses. Apart from red blood cells, spleen is built out of lymphoid tissue aggregates, composed of a large variety of B and T lymphocytes and other accessory cells (monocytes, dendritic cells). Here used splenocytes are a mixture of B and T lymphocytes (with large majority of B type cells) that is collected from C57Bl/6 adult mice and directly provided from IAB. Manipulation of primary cells issued from a living organism is more demanding compared to well-established cell lines because of their fragility and culture requirements. Indeed, splenocytes freshly isolated from mouse spleen need to be cultured in enriched culture medium in order to stimulate

specific marker expression and ensure efficient cell proliferation. Therefore, prior to use in the biochip assay, the mixture of primary B and T lymphocytes is incubated for 24 – 48 hours in complete culture medium at 37°C (*cf.* section 6.2.7). The incubation solution is supplemented with antibiotics and concanavalin A – a mitogenic agent particularly increasing T cell division.[179] Even if working with cell lines seems to be a more practical solution, studies on primary cells constitute an important advance. In this case, cells originate from a physiologically independent organism and are not obtained from biotechnological manipulation. Such approach gives therefore the opportunity to precise determination of immunological response in relation to a specific biological subject (*e.g.* patient).

3.3.2   Adaptation of the experimental conditions to living cells

When working with living cells, an important concern is to ensure that the experimental conditions are compatible with the biological sample. The parameters formerly optimized for enzymatic digestion purpose fit fairly well with the prerequisites of a biochip system where cell injection and incubation are performed. Namely, microfluidic set-up is built by using biocompatible PEEK material, highly adapted to cell-based microsystems. Besides, experimental protocol enabling efficient enzymatic release from the biochip surface is designed to maintain bulk solution temperature at 37°C and anticipates use of PBS-based running buffer – conditions closely related to physiological environment. Biocompatibility of PBS buffer supplemented with 10 mM of $MgCl_2$ is assessed empirically. Indeed, primary lymphocytes, *a priori* more susceptible to unfavorable environmental conditions in comparison to stable cell lines, demonstrate high level of viability when incubated in the proposed running buffer within a few hours. (Fig 3.6) Noteworthy is the fact that commercially available buffers optimized for enzymatic reaction are hardly adapted to cell-based assays. Some of commercial buffers might contain a particular supplementation providing enzyme stability and activity. Such formulation which may also influence cellular physiology and reduce viability of cells (*e.g.* surfactant Triton X-100 added to *Eco*RI buffer). Application of PBS buffer supplemented with magnesium ions providing efficient enzymatic digestion is therefore a well-grounded solution. Therefore, PBS + 10 mM $MgCl_2$ formulation is implemented as a running buffer all along the experiment, *i.e.* molecular assembly construction, lymphocyte capture and incubation, and finally enzymatic cleavage step.
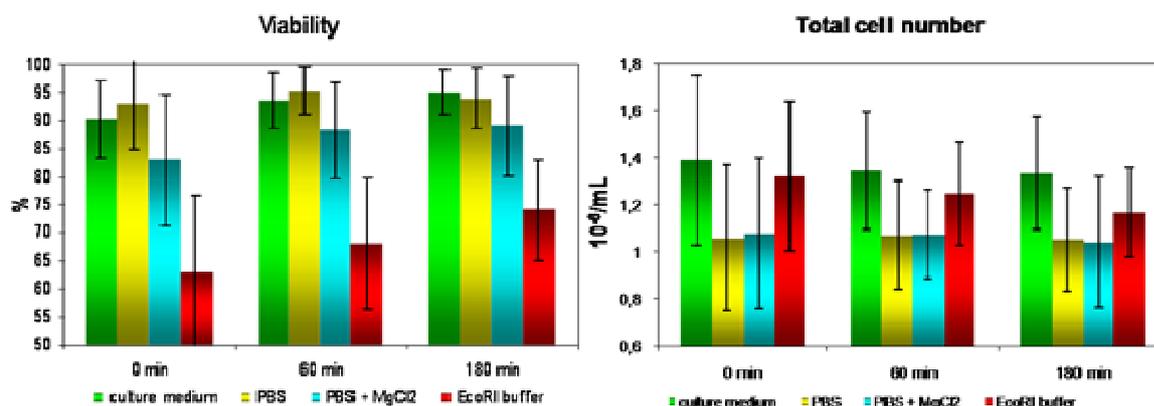
Figure 3.6 Monitoring of splenocyte viability in different incubation media. Cells are incubated within 3 hours at 37°C in the conditions of 95% humidity and 5% CO_2. The assayed buffers are: RPMI culture medium (supplemented with 10% FBS, 50 U/mL penicillin and 50 µg/mL streptomycin), PBS (pH 7.4), PBS + $MgCl_2$ (10 mM), *Eco*RI commercial buffer (50 mM NaCl, 100 mM Tris-HCl, 10 mM $MgCl_2$, 0.025 % Triton X-100, pH 7.5). Considerable loss of viability is observed in the *Eco*RI buffer unlike the other solutions. The increase of viability in time results from eradication of dead cells.

a) Surface blocking optimization

Introduction of a cell suspension on the biosensing surface implies an important optimization step aiming to establish an adequate state of surfaces of contact. Alike the aforementioned enzymes, there exists an important need to provide proper treatment of the biochip surface in order to reduce non-specific adsorption of cells which may occur independently from the hydrodynamic conditions. Namely, living cells are decorated by a large variety of biomolecules (lipids, proteins and sugars) and can thus interact with their surrounding environment (*e.g.* biochip surface) by the means of physicochemical interactions of different nature: electrostatic, hydrophobic, dispersion (*e.g.* Van der Waals interaction), by hydrogen bonds, *etc.* From the cell micropattern point of view, surface modification is therefore a key requisite in order to ensure proper cell immobilization assisted by the absence of any non-specific interactions.

In this matter, many approaches are based on poly(ethylene glycol) self-assembled monolayers (PEG-SAM) that are stable in time and shown to efficiently inhibit protein adsorption.[180, 181] Chemically modified PEGs are characterized by more hydrophilic properties and thus increased cell-repellent ability.[182, 183] Good results are observed as well with PEG chains covalently linked to surface in the form of microgels capped with an adequate protein. Therefore, PEG-microgels capped by BSA exhibit an efficient resistance to cell adhesion in contrast to bovine fibrinogen-capped coatings.[184]

Apart from PEG chemistry, high-molecular-mass organosilane compounds equipped with perfluoroalkyl groups are proposed as an alternative solution for protein- and cell-repellent surface modifications.[185, 186] However, these are examples that mainly require precise surface engineering provided by microfabrication methods in combination with molecular assembly techniques. It makes object of an extensive review by D.

Falconnet *et al.*[187] In our approach we do not benefit from such advanced techniques to elaborate biosensing surface which is based on polypyrrole chemistry. That is why for the need of our study, we will use a simple alkane-thiol blocking (1-dodecanethiol) combined with protein backfilling. Application of this protocol, as we will see, results in a satisfactory effect.

The present work relies on biochip fabrication that is founded upon electrochemical deposition of probes over hydrophobic gold surface generated by former incubation with 1-dodecanethiol solution. In order to produce a cell-repulsing layer, common strategies involve surface backfilling with proteins. For cell-based assays, one of the solutions is to realize surface passivation by using running buffer (or even culture medium) supplemented with fetal bovine serum (FBS). FBS is prenatally collected from calf and contains a large variety of proteins (mainly BSA). It is frequently used as component of the culture medium employed for *in vitro* cell cultures. In a protocol proposed by S. Milgram (CREAB), blocking solution consists of RPMI medium supplemented with 10 % of FBS and is applied prior to introduction of cell samples on the microarray surface.[30]

Preliminary tests realized within the framework of the present study show that the protocol cited above may not be suitable. Namely, upon incubation with 10 % FBS in PBS, considerable decrease of hybridization signals is observed. We speculate that this may be due to phenomenon of surface over-loading or even degradation of DNA probes. However, this can not be certainly concluded because FBS-based solution was attempted point-wise and no regular studies confirm the unfavorable conditions. Consequently, we decide to switch to blocking solutions based on bovine serum albumin previously employed in the enzymatic cleavage experiments.

Several tests with BSA-containing solutions realized under microscopic observations evidence that a longer incubation (45 – 60 min) with blocking buffer exhibits lack of the non-specific cell adsorption (images non-available). Optimal effect is observed with PBS-based solution containing 10 µM of BSA and supplemented with cytochrome *c* at 5 µM of final concentration. In practice, these two proteins have different physicochemical properties. Namely, BSA is a 69.3 kDa commonly used protein with an isoelectric point of 4.7 whereas cytochrome *c* is a smaller protein (12.4 kDa) with more basic isoelectric point of about 10. It means that in the conditions of the running buffer pH (7.4), the two proteins demonstrate divergent values of net molecular charge: BSA is negatively and cytochrome *c* positively charged. Regarding to these characteristics, we may consider that these two components differently interact with biosensor surface and thus provide higher backfilling of out-of-spot surface. That is why, the BSA/cytochrome *c* blocking solution will be preferentially used in the cell-based assays.

b) Microfluidic parameters in regard to cellular sample injection

The complexity of cellular samples leads us to consider not only physicochemical concerns as buffer content or blocking strategy. Lymphocytes introduced into the biochip system are of microscopic size (~ 10 µm in diameter) and therefore submitted to mechanical constraints when channeled through the microsystem. Owing to their volumetric properties, cell diffusion in a microfluidic system is particularly conditioned by mass transfer parameters such as the running buffer viscosity, microfluidic tube cross-section, flow rate and presence of counter ions. Adapted microfluidic system should be based on tubes of sufficient internal diameter in order to reduce risk of shear forces possibly exercised on the injected cells. For the sake of the present study, the cell-destined tubing is characterized by ID of about 760 µm unlike 250 µm ID of microfluidic tubes providing molecular sample flow through (building blocks of the biochip molecular assembly and restriction enzymes). To do so, the system is additionally equipped with a switchable 200 µL secondary loop devoted to injections of lymphocyte samples. Cell injection loop is installed directly over the flow cell (so incubated at 37°C during whole experiment) and separated from bulk solution by a small dead volume (less than 10 µL). (Fig 3.7) Injected cells promptly arrive over functionalized surface and are not retained in tubing for a long time (sample loop is loaded just before the injection to reactor). Such approach enables moreover to physically isolate two steps of the experiment: specific cell immobilization and enzymatically driven cell release from the surface.
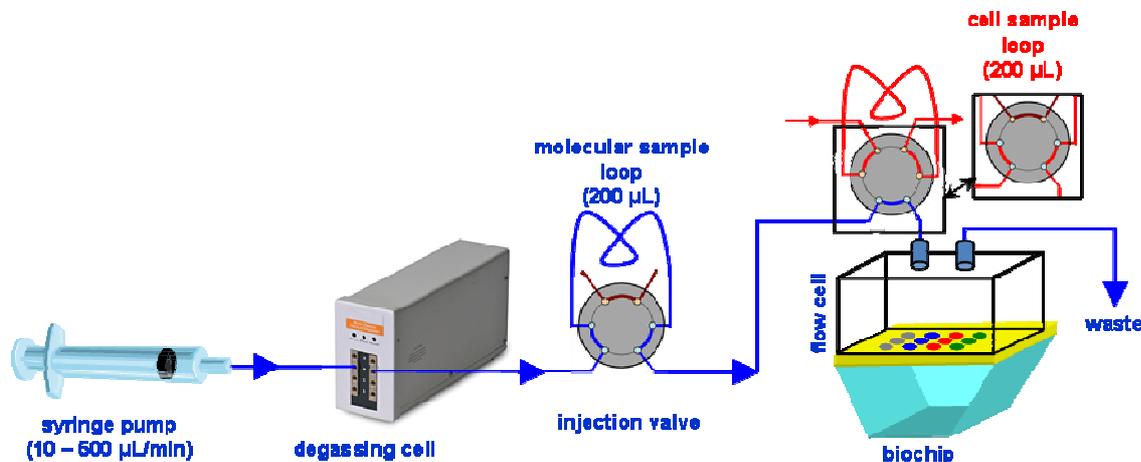
Figure 3.7 Microfluidic set-up with two separate injection valves. Secondary injection loop is engaged in the flow exclusively during cellular sample injections.

Apart from the employed microtubing, flow cell is other essential element of fluidic system set-up. Design of a flow cell module (*i.e.* volume, shape) imposes proper hydrodynamic constrains that are responsible for mass transfer in the liquid environment directly surrounding the biosensing surface. Reaction chamber construction conditions the diffusion profile of ions and small molecules, and particularly influences bigger entities like biomolecules and living cells. We observe that lymphocytes introduced to bulk solution exhibit different behaviors depending on flow module dimensions conditioning

bioreactor volume and cell distance from specifically functionalized interface. Use of deep reaction chamber (600 – 1000 µm in depth) requires employment of low flow rates (10 µL/min) in order to ensure sufficient sedimentation of cell entities in the neighborhood of specific antibodies situated over DNA biochip matrix. However, such approach hardly enables to control specific addressing of cells on surface and mainly incites their non-specific adsorption registered by SPRi (Fig. 3.8). That is why, a suitable solution is to implement reaction chamber module of smaller volume that allows driving cells closer to their recognition site and makes cell capture from dynamic flow easier.
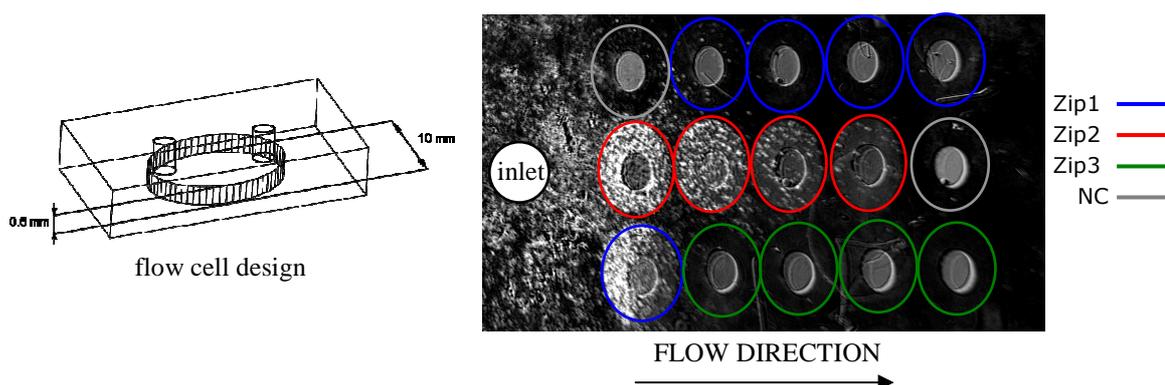
Figure 3.8 Non-specific adsorption of lymphocyte hybridomas in non-adequate flow conditions. Applied flow rate is too slow (10 µL/min) and flow cell too deep (here 600 µm) which correspond to a very weak linear velocity (0.03 mm/s at the central cross-section). Cells are mainly adsorbed near the inlet of the reactor. Observed halo effect results from insufficient adjustment of micro-pipette tip to the gold surface during electrospotting process (proper spot diameter is 400 µm).

In the present experimentation, two PEEK-made flow cells are employed ensuring reaction chamber of an approximate volume of 15 µL and 100 µm in depth. (*cf.* Fig. 3.9 and Appendix F) In these conditions, we opine to have laminar flow with a cone-shaped streamline by taking into account aqueous character of the running buffer, the small cross-section and relatively low flow rate. This feature may be indicated by non-specific adsorption of injected cells depending on flow conditions. Indeed, at certain value of flow rate, hybridomas have tendency to non-specifically adsorb in lateral zones of the flow cell whereas central biochip reveals specific on-spot immobilization of the introduced cells. From this example, we see that velocity of running buffer stream is a crucial element and has to be individually adapted to each injected cell type.
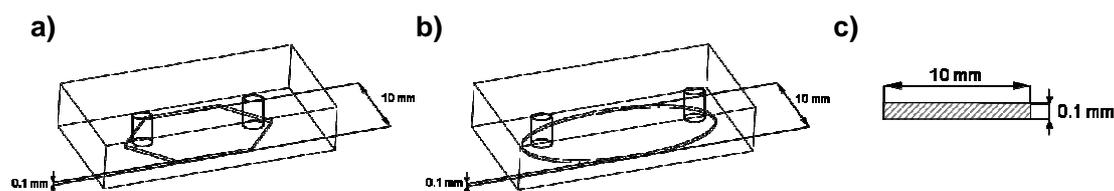
Figure 3.9 Schematic design of the PEEK-made flow cells applied in the study.
a) hexagon-shaped flow cell used for the experiments with hybridomas; **b)** oval flow cell employed in assays with hybridomas and primary cells; **c)** central cross-section of the reaction chamber *lumen*. In order to enable efficient immobilization of lymphocytes, flow cells work at linear flow rates of 0.33-1.67 mm/s (observed at the central cross-section), depending on the injected cell type.

Generally, optimal flow rate needs to be sufficiently high to minimize non-specific adsorption of cells on surface and low enough to ensure cell interactions with specifically binding antibodies. In practice, during injections of the cellular samples a compromised flow rate is applied in order to generate a volumetric mass transport adequate to injected cell sample. We remark higher values for hybridoma samples (50 – 100 µL/min) than for primary cells (20 – 60 µL/min), which may be explained by different levels of surface-marker expression determining the probability of lymphocyte capture. An average linear flow rate observed at central cross-section of the 100 µm deep bioreactor is estimated to 1.25 mm/s for hybridomas and 0.67 mm/s for primary lymphocytes. Alternative solution to aforementioned type of flow cell may be exemplified by serpentine-type PEEK module where injected samples are directly flown over functionalized spots.(Fig. 3.10) In the case of hybridoma injection, such system exhibits specific capture of lymphocytes devoid of side-adsorption at low running buffer flow rate (down to 10 µL/min which corresponds to 0.83 mm/s of flow velocity).
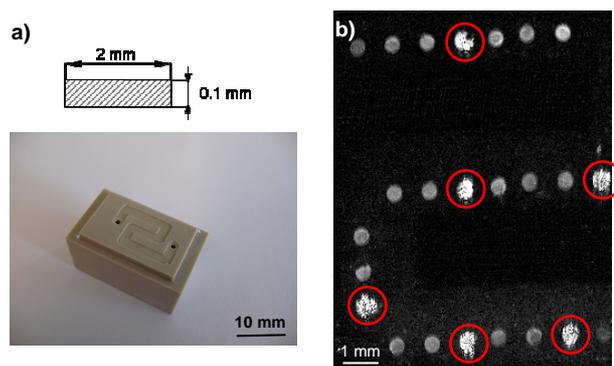
Figure 3.10 Serpentine-type flow cell potentially used in the cell capture experiment.
 a) Photograph of PEEK module with serpentine shape flow (upper caption details the dimensions of the flow channel *lumen*); **b)** SPR differential image upon injection of T lymphocyte hybridomas (3A9) at 10 µL/min; cell are specifically immobilised on Zip2 spots (on red) without significant side-adsorption.

3.3.3 Specific immobilization of murine cell lines and their subsequent enzymatic desorption

The study here described is carried out with B- and T-type hybridomas (murine cell lines) that are specifically addressed to biochip surface by dint of specific antibodies (IgG anti-CD19 and IgG anti-CD90). Once 3A9 and LS-102.9 lymphocytes are captured, we proceed to their sequential release through an enzymatic digestion protocol. The test realized on cells issued from well-established cell lines is interpreted as a proof-of-concept approach that defines necessary experimental step before the biochip strategy is finally applied to primary lymphocytes. For this purpose, a DNA-microarray with electrochemically generated Zip spots is placed in SPRi configuration and turned into cell capturing antibody microarray in the course of the experiment. Accordingly, following antibodies are introduced onto the biochip: anti-CD19 IgG covalently coupled to *Eco*RI* sequence and having great immunoaffinity to B cell (LS-102.9)[188] as well as anti-CD90 IgG combined with *Pvu*II* oligomer which corresponds to T-cell (3A9) recognition (*cf.* Fig.3.1).[189] On-spot cell immobilization phenomena are registered by proper reflectivity shifts observed on Zip1 and Zip2 signals which correspond to specific capture of B and T lymphocytes respectively. (Fig 3.11) It is demonstrated that the injected cells are not recognized by non-relevant antibody tethered on control Zip3 spots. Furthermore, we can notice that SPRi signals triggered upon the injections of lymphocytes hardly attain a *plateau*. We suppose that this may be the effect of cell on-spot flattening, generated by membranar marker recruitment near the site of their specific recognition. Condensation of the plasma membrane at the site of lymphocyte activation[190] is driven by the intrinsic dynamics of the bilipidic layer which enables diffusion and organization of transmembranar domains.[191]
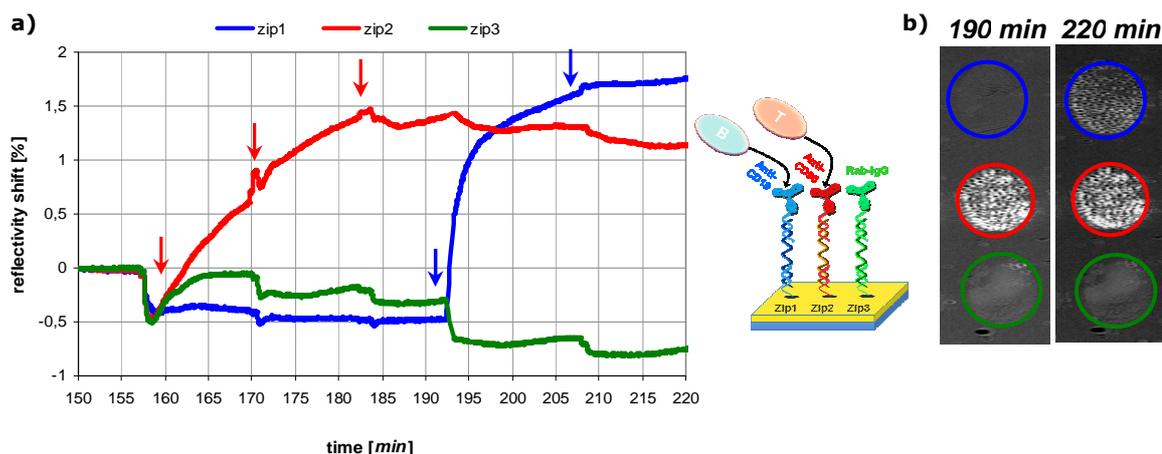
Figure 3.11 SPRi monitoring of specific immobilization of B and T hybridomas.
a) SPR signals observed upon injections of T cell hybridomas 3A9 (red arrows) and B cell hybridomas LS-102.9 (blue arrows); **b)** differential images registered after each cell capture step (800 µm of spot diameter). T lymphocytes are captured on Zip2 probe and B cells on Zip1 probe thanks to specific molecular assembly (anti-CD90 IgG and anti-CD19 IgG respectively), whereas no cell is observed on control Zip3 probe.

As a consequence of stepwise injections of cellular samples, we however observe slight decreases of SPRi signals that are not concerned by factual cell incubation. Declining reflectivity results from subtraction of the negative control probe signal (NC) which is probably more affected by refractive index variations of the background solution. We speculate that hybridoma samples may contain residues of culture medium that are susceptible to interact with spots equipped with bare DNA strands. Nevertheless, B and T lymphocytes are correctly trapped on corresponding spots which is confirmed on differential images obtained from the SPR imaging apparatus. Apart from accurate construction of the biomolecular assembly, we may thus clearly identify zones of specific lymphocyte recognition. Observations of differential images evidence efficient addressing of hybridoma cells on appropriate molecular architectures which furthermore confirm the high expression of membrane markers: CD19 on LS-102.9 and CD90 on 3A9.

Interestingly, specific capture of B- and T-type lymphocytes takes place even at very low density of grafted DNA probe and consequently immobilized antibody. High level of immunorecognition is proven by many cell attachment events observed on spots grafted with barely 0.2 µM solution of oligonucleotide or even registered on characteristic "comet tail" resulting from inappropriate rinsing step (realized directly after the electrospotting process). (Fig. 3.12) It is noteworthy to point out that immobilization of living cells on a microarray, in reality depends on density of antibodies grafted throughout DNA matrix. In the present study, DNA matrix obtained with low spotting concentration (oligonucleotide probe at 0.2 – 1 µM) results in satisfactory capture of hybridoma. As we will see later on, grafting density needs to be increased in case of primary cells that express less cell-specific markers in comparison to well established hybridoma.
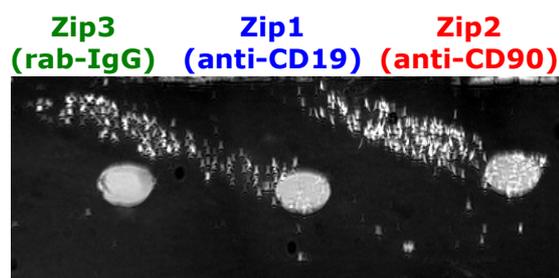
Figure 3.12 Immobilisation of B and T lymphocyte hybridomas on spots exhibiting "comet tail". Comet effect is evidenced by SPRi and caused by inappropriate rinsing step following the electrospotting process. Interestingly, cells are captured on comet tail as well, which may prove high expression level of specific membrane markers. Spots have a 400 µm diameter.

In order to complete biochip system performance, once lymphocytes are specifically trapped on the microarray, subsequent enzymatic digestions are fired and followed in real time by SPRi. Restriction endonucleases are introduced into reactor in separate steps by using the primary injection valve and not the one accessorily installed and devoted to cellular samples. (Fig. 3.7) Therefore, properly loaded enzyme arrives to

the reaction chamber in about 1 min and flow rate is then decreased to the desired value of 7-10 µL/min. Such proceeding provides sufficient incubation time to ensure efficient biomaterial release. Even if during this time SPRi signal can not be directly interpreted, once enzyme is washed off from the bulk solution, desorption events are evidenced (Fig. 3.13)
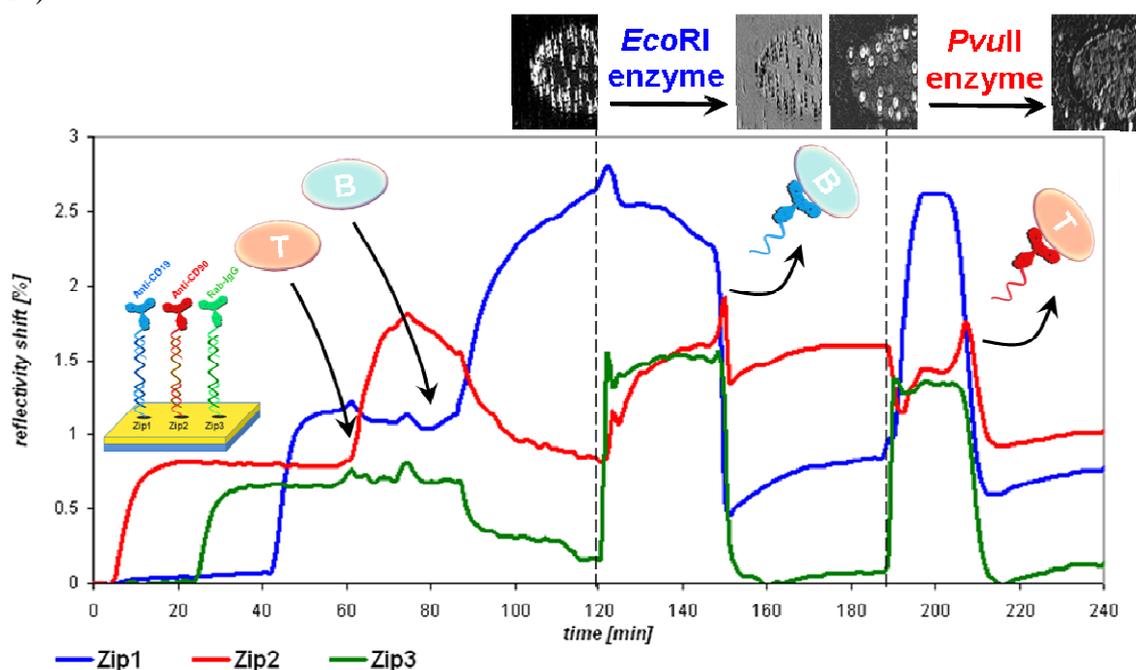
Figure 3.13 Real-time monitoring of subsequent release of B and T lymphocyte hybridomas specifically immobilized on the antibody-DNA matrix. 0–60 min: hybridization of IgG-DNA conjugates (anti-CD19–*Eco*RI*, anti-CD90–*Pvu*II*, rab-IgG–*Nco*I*); 60min: injection of 3A9 hybridomas; 75min: injection of LS-102.9 hybridomas; 120–150min: digestion by *Eco*RI enzyme; 190–215min: digestion by *Pvu*II enzyme. Differential image captions represent Zip1 and Zip2 spot (800µm of diameter) before and after the enzymatic cleavage steps by *Eco*RI and *Pvu*II, respectively. All SPRi signals are rectified by subtraction of NC signal (negative control probe).

Indeed, *Eco*RI-specific signal drop is observed on Zip1 and followed by a negative reflectivity variation registered on Zip2 upon *Pvu*II enzyme injection. Responses induced by enzymatic cleavage steps are however not precisely consistent with those triggered upon cell capture. We may thus think that cell release is not complete or even that the released lymphocytes are non-specifically retained near biochip surface in the conditions of decreased flow. Confirmation of specific cell release is however brought by analysis of SPR differential images registered after the enzymatic cleavage steps. Indeed, we can clearly remark localized desorption of biological objects as soon as the accelerated flow washes out the enzymatic sample. Differential images prove individual lymphocyte detachment events that are referred to microscopic cell-prints, observed after the relevant digestion steps. B-type hybridomas are shown to be desorbed in *Eco*RI step as opposed to T-type hybridoma release by *Pvu*II driven digestion. The obtained results meet the requirements of proof-of-concept approach and consequently allow us to execute this programmable release strategy on more fragile cell samples, such as splenocytes.

3.3.4 Capture/release strategy employed to primary cell assay

Application of the designed capture–release biochip system to primary cells is a challenging approach. Cells used in the present study are retrieved from the spleen of a wild-type mouse (C57Bl/6) and defined as a mixture of various B- and T- type lymphocytes in different ratio. In contrast to well established cell lines, splenocytes are less regular regarding to expression of the specific marker and more troublesome in culture because they do not divide spontaneously unless stimulation protocol is applied. Non-stimulated primary cells are small and, as experience shows, hardly observable when introduced to SPRi-based biochip. We speculate that freshly isolated from spleen cells are resting lymphocytes characterized by low level of cellular metabolism. Possible features of such state are reduced cytoplasmatic volume as well as low exposition of membrane domains which disable efficient on-chip capture and SPRi detection. In order to disrupt this kind of "stand-by" physiology, the splenocytes must be activated prior to injection. This is realized by incubation in complete culture medium supplemented with concanavalin A (ConA). ConA is a growth factor particularly inducing proliferation of T lymphocytes[179] which fraction is minor in the assayed cellular sample. Cells are incubated in controlled atmosphere (37°C, 95% humidity, 5% CO_2) for 24 - 48 h and their accurate stimulation assigned by classical microscopy observations – activated lymphocytes appear bigger and form aggregates. Prior to injection into biochip system, cultured splenocytes are recovered in the cell-compatible running buffer (PBS + 10 mM $MgCl_2$).

Analogously to the study realized on hybridoma cells, step-by-step process of the multi-spot building-up as well as cell capture events are monitored in real time by using SPR imaging. (Fig. 3.14) The ability of designed microarray to specifically immobilize primary cells is therefore investigated. To do so, we execute DNA-directed immobilization of antibodies specific towards membranar markers expressed by different immune cell populations: anti-CD19 IgG targeting immune B lymphocytes and anti-CD90 IgG directed to T lymphocytes. Three-component architectures are built, containing anti-CD19 or anti-CD90 on Zip1 and Zip2 probe, respectively. Alike to previous tests, Zip3 probe is deployed as a negative control to both enzymatic cleavage (*Nco*I restriction site) and immobilization of living cells. In the present study, Zip3 probe is indirectly assembled with IgG–*Nco*I* conjugate obtained for a non-relevant monoclonal antibody. Namely, anti-HcB mouse IgG, kindly provided by L. Bellanger from CEA/IBEB (Marcoule, France), is directed to a non-relevant HcB domain. The use of the non-specific monoclonal antibody instead of a classical polyclonal IgG is required to avoid improper cell binding. In fact, a polyclonal IgG (*e.g.* isolated from rabbit serum) is not advisable because of its unknown affinity to cells originated from a wild-type organism.
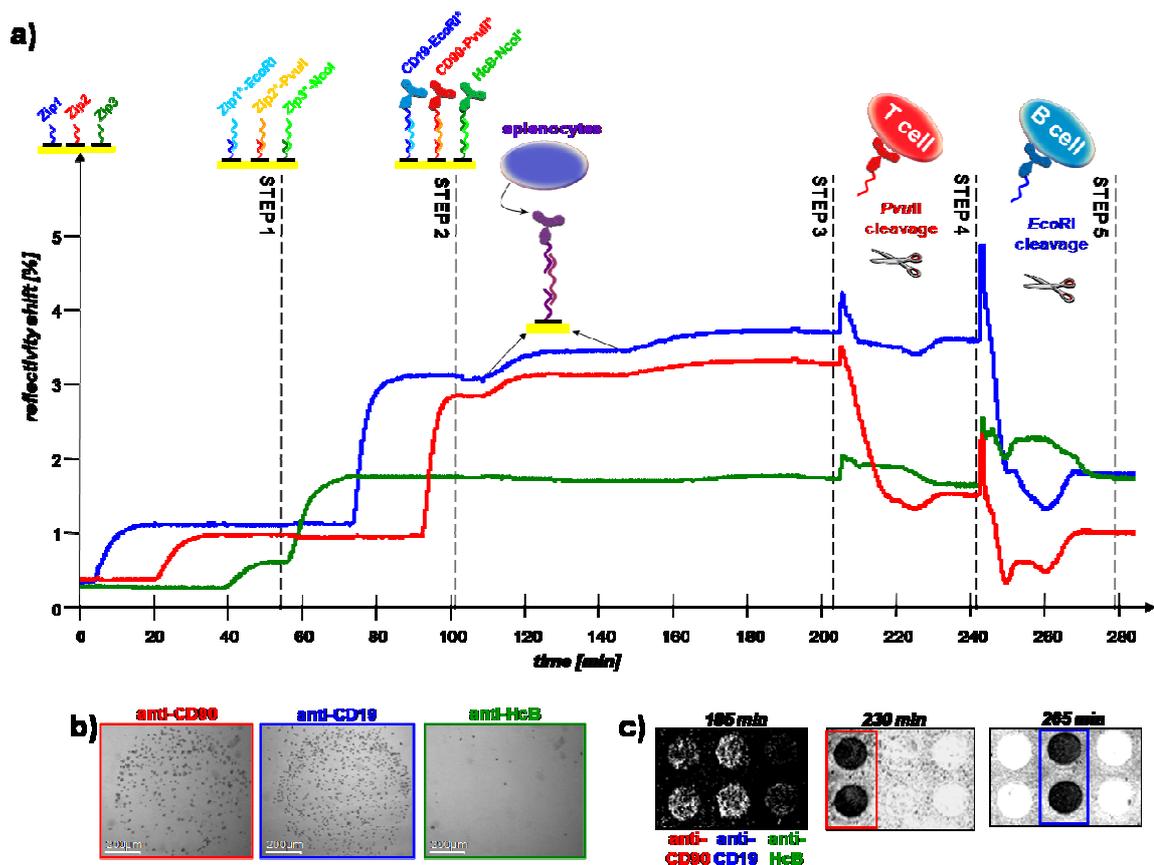
Figure 3.14 B and T lymphocyte capture and sequential release by enzymatic cleavage
a) SPRi monitoring curves: Step 1 - intermediate DNA strand hybridization (Zip1*–*Eco*RI, Zip2*–*Pvu*II, Zip*3–*Nco*I); Step 2 - IgG–DNA conjugate immobilization (anti-CD19–*Eco*RI*, anti-CD90–*Pvu*II*, anti-HcB–*Nco*I*); Step 3 - injections of splenocytes (containing both B and T lymphocytes); Step 4 - lymphocyte T specific release within *Pvu*II enzymatic cleavage; Step 5 - lymphocyte B specific release within *Eco*RI enzymatic cleavage. All SPRi signals are rectified by subtraction of NC signal (negative control probe). **b)** microscope images (×4) of the captured cells. **c)** SPRi differential images registered at the end of step 3 to 5 (reference images are taken at the beginning of each step in order to highlight the capture/cleavage specificity).

Consequently to correct molecular on-chip erection, splenocytes are introduced onto the microarray. In this case B and T cells are jointly injected and signal generated by lymphocyte immobilization may be solely differentiated from Zip3 negative control. The stepwise loading of the cellular sample surprisingly results in only slight increase of reflectivity signal which contrasts to signals observed for B- and T-type hybridoma. We attempt however to explain this finding by the fact that splenocytes expose probably fewer specific markers compared to the cell lines. The observed SPRi signal is weak since a small amount of primary cells is captured but also because only minor fraction of cellular volume penetrates within the detection layer (resulting from 100 nm evanescent wave). Nevertheless, specific on-biochip capture of the injected lymphocytes is confirmed by SPR images and microscopic observations realized in an independent assay. Analogously to previously reported detection of hybridoma, primary lymphocytes are clearly visualized as discrete objects confined to anti-CD19 and anti-CD90 spots. (Fig. 3.15)

95

Specifically immobilized B and T lymphocytes are eventually submitted to orthogonal release from the biochip surface, performed by incubations with *Pvu*II and *Eco*RI endonucleases. Similarly to former findings, reflectivity variations confirm fast and specific cleavage precisely restrained to spots equipped with the relevant restriction sites. Once again, important drops of reflectivity are registered on the Zip1 and Zip2 signals, and specificity of the enzymatic digestion is proven by the integrity of non-concerned Zip3 control signal. Even if the reflectivity variations are mainly related to loss of molecular assembly, withdrawal of the individual cells from the microarray is clearly monitored by zooming in on the individual spot features (Fig. 3.15). We may thus identify well resolved cellular entities and validate their prompt detachment (over barely few minutes) in the enzymatically driven release step. This experiment shows that specific capture of primary cells can be followed by their programmable orthogonal release in the format of the proposed biochip system.
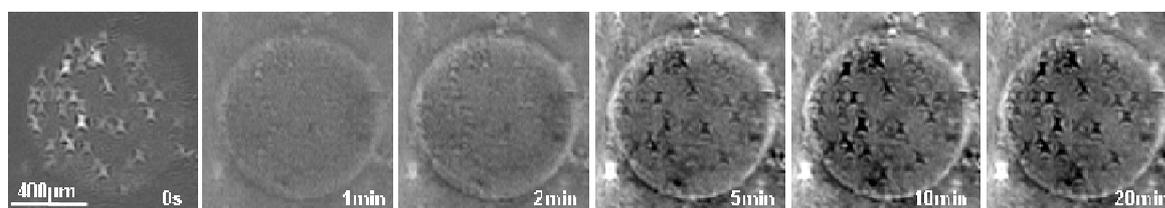
Figure 3.15 Magnified views of a single Zip1 spot during *Eco*RI enzyme incubation. Image sequence shows spot evolution in time (0s image is the reference). Release of the individual cells is evidenced by dark imprints on the differential images. The star–like shape of the individual cells observed on SPR images is due to optical aberrations of the experimental set–up (see Appendix G). Image treatment is performed in ImageJ *(Wayne Rasband, National Institutes of Health, USA).*

3.3.5   Cell recovery upon the enzymatic release steps

An important feature of cell sorting system is not only to provide programmable selective fractionation of cell populations but also efficient recovery of the discriminated fractions. The biochip here designed biochip relies on DNA-directed immobilization of cells on the microarray, thus providing their sorting into distinct spatial locations and guided by cognate antibody-oligonucleotide assembly. It is therefore an example of versatile platform for multiplexed sorting purposes.[59] Successive enzymatic cleavage steps enable the controlled release of proper cell populations from well-defined biochip locations with the help of restriction endonucleases highly specific to the corresponding DNA sequences. Recovery of lymphocyte fractions desorbed in step-by-step process of the enzymatic digestion is subsequently attempted.

Efficient collection of individual cellular fractions forming a part of more complex biological sample (*e.g.* blood) offers a priceless possibility for downstream analysis of specifically recovered cell types. Moreover, demonstration of functionality and viability of sequentially released cells is of great importance in the development of cell sorting strategies. That is why the released lymphocytes are collected in fractions desorbed in two separated enzymatic digestion steps. Accordingly, cells are retrieved directly from the

96

outlet of microfluidics and in total volume of about 300 µL. Taking into account fair content of B and T lymphocytes in the released sample, it is extremely difficult to detect the eluted cells in such important sample volume. Indeed, visualizations of concentrated fractions reveal poor quantity of the recovered cells (only four cells were identified within three independent trials, *cf.* Fig. 3.16 b). This remains an important issue for downstream characterization.
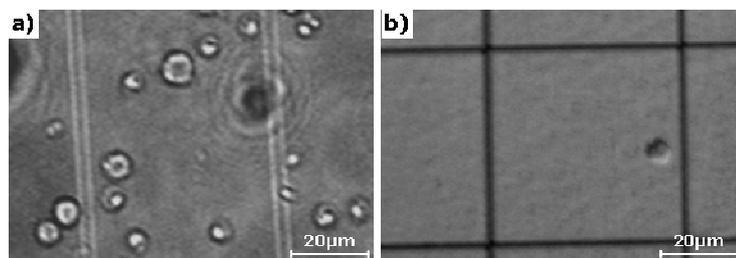
Figure 3.16 Lymphocytes observed over microscope. **a)** Surplus of injected to biochip splenocytes observed in sample retrieved from the outlet of microfluidics during injection; **b)** individual cell detected in a sample recovered upon enzymatic cleavage.

In regard to encountered difficulties to perform an easy detection of cellular entities issued from designed cell sorting experiment, further work should be carried out in this matter. As imaginable solution to increase the probability of cell disclosing in desorbed sample, we may imagine to extend the range of specific cell micropatterning or adapt microfluidics system to generate small sample volumes.[192] An example of integrated set-up could enable on-line identification of released biological cells directly in the flow by guiding the sample through a narrow channel where the read-out of cell-specific signal can be done (*e.g.* by optical or electrical means[193]).

Putting aside so sophisticated developments, we may nevertheless summarize that the overall findings reported in the present section give sufficient premises to suppose viability of lymphocytes introduced in the developed biochip configuration. Namely, we state the biocompatibility of running buffer and show that hydrodynamic flow conditions are harmonious with cellular sample which can be observed after being flown throughout microfluidics set-up (Fig. 3.16 a). Living cells specifically captured on biochip are additionally detected as discrete objects on SPR images and their morphological integrity may be furthermore confirmed by observations under classical microscopy. Moreover, lymphocytes trapped by interaction with specific antibody and incubated within several hours on a microarray surface demonstrate proper functionality registered for example as high level of secretion activity.[29, 30] Here developed biochip strategy of "cell catch and release" may be hence considered as a promising approach for cell sorting purposes realized on complex biological samples.

3.4 Application of the controlled capture-release strategy to bacterial sample analysis

3.4.1 Biosensors devoted to microbiological assay

Previous sections have shown that sequential enzymatic cleavage of DNA substrates immobilized on solid support may be turned to programmable procedure providing selective release of several cell populations captured on a DNA microarray. In the scope of applying such strategy to analyze various cellular samples, we evaluate the designed biochip system on cells other than lymphocytes and potentially devoted to other research areas.

Development of micro-systems capable of multiparametric, rapid and precise analysis of bacterial samples is of great interest for both health and food safety issues. Standard protocols employed nowadays in this field are mainly laborious and require long preparations. That is why micro- and nanotechnologies emerge as desirable solution for novel research and diagnostic tools.[194] Apart from many studies reporting on eukaryotic cells assayed in micro-devices (neurons, tumor cells, blood cells *etc.*), bacteria may be also introduced to similar systems of miniaturized format thus providing parallelized and high-throughput screening of the sample of interest. One of the rapidly growing trends in the field of microarray technology is focused on development of microbial whole-cell arrays where bioengineered bacteria are patterned on a solid support and exploited as functional biosensing layers.[195-197] Usefulness of similar systems is oriented to biotechnological applications (*e.g.* gene expression analysis) or to environmental specimen characterization (*e.g.* contamination monitoring or toxicity testing). On the other hand, microarray technologies are explored as sensitive platforms to realize fast and quantitative detection of bacterial strains, mainly for food safety purposes. DNA- or antibody-based biochips are employed to identify characteristic bacterial pathogens[198-200] or accurately detect bacteria of a specified type.[201, 202] Among others, SPR is reported as a label-free method for real-time and qualitative assaying of bacterial sample.[203] In the present work we combine SPR-based technique and IgG–DNA conjugate chemistry to provide efficient detection and release of bacterial cells of interest. This approach is therefore an example of biosensing system potentially devoted to analyze samples of microbiological nature.

3.4.2 Bacteria capture and desorption from DNA-based biochip

In the present assay of cell capture and release, we use the bacterial strain *Streptococcus pneumoniae* (R6) provided thanks to collaboration with T. Vernet from the Institut de Biologie Structurale (IBS) in Grenoble (France). This bacterium is reported to be an important source of invasive infections in human and responsible for several diseases such as pneumonia or meningitis.[204] Choline-binding protein E (CbpE) is one of the proteins from the Cbp family exposed on *S.pneumoniae* surface. CbpE is shown to be a virulence factor playing a major role in host/pathogen interactions.[205, 206] This bacterium may be therefore recognized and trapped on a biosensing surface with the help of a CbpE-specific antibody. In the present experimentation, we use the anti-CbpE immunoglobulin obtained at the IBS, kindly purified and characterized by S. Bouguelia (CREAB). We realize efficient addressing of bacterial cells on a DNA microarray by the means of IgG–oligonucleotide driven assembly. On-chip capture of the injected cells and their subsequent desorption from surface by enzymatic digestion are followed by using real-time SPRi technique. (Fig. 3.17)
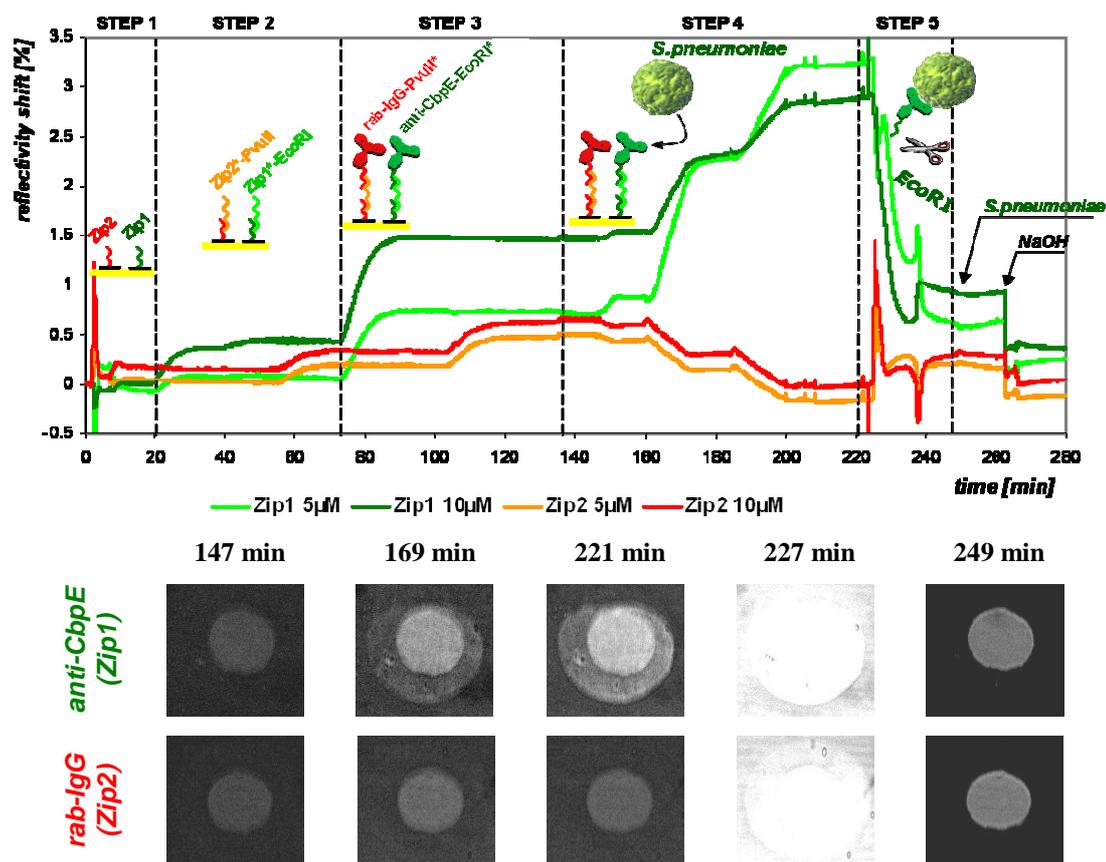
Figure 3.17 SPR monitoring of *S.pneumoniae* capture and subsequent release. Step 1: intermediate DNA strand hybridization (Zip1*–*Eco*RI, Zip2*–*Pvu*II); Step 2: IgG–DNA conjugate immobilization (anti-CbpE IgG–*Eco*RI*, rab-IgG–*Pvu*II*); Step 3: injections of bacteria suspended in PBS; Step 4: enzymatic release of *S.pneumoniae* by *Eco*RI cleavage; A repeated injection of bacterial sample (250 min) confirm that anti-CbpE IgG is efficiently removed. Eventually, the DNA biochip is regenerated by NaOH washing (260 min). All SPRi signals are rectified by subtraction of NC signal (negative control probe).

The provided antibody (IgG anti-CpbE) is covalently conjugated to *Eco*RI* oligonucleotide sequence according to synthetic approach described in the Chapter 2. The obtained product assigned to monoconjugated IgG–DNA is employed to realize proper molecular assembly capable of *S.pneumoniae* capture on biochip. Prior to use, DNA functionalized gold surface (Zip1, Zip2 and Zip3) is saturated with PBS solution of 10 µM BSA/5 µM cyt *c*. The whole experiment is driven in PBS buffer (pH 7.4) and incubated at 37°C. Stepwise on-chip construction is monitored by SPRi and evidences correct signals triggered by molecular build-up steps. Following specific immobilization of anti-CbpE–*Eco*RI* conjugate, bacterial sample (10^9 cells per mL) is consequently loaded in the bioreactor by using the secondary injection valve (200 µL). Two successive incubations of appreciatively 20 min result in positive variation of reflectivity observed for Zip1 probe which is ascribed to *S.pneumoniae*-responding antibody. Bacteria can not be however discerned as discrete objects on concerned spots visualized by SPRi, as it was the case of lymphocytes, because single bacterium size (~1 µm) is smaller than the optical system resolution. Nevertheless, specific capture events are confirmed by comparison of Zip1 signal to control Zip2 probe equipped with non-relevant IgG and characterized by insignificant reflectivity shift (interpreted as global change of background solution refractive index). Phenomenon of proper on-chip capture of *S.pneumoniae* bacteria is additionally confirmed by microscopic observations realized in an independent test (*cf.* Fig. 3.18).
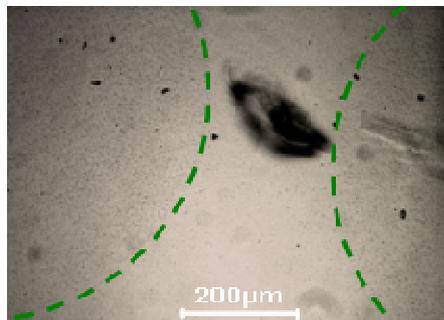
Figure 3.18 Specific capture of *S.pneumoniae* bacteria on Zip1 probe (anti-CbpE IgG) visualised under microscope.

Once bacteria are immobilized on the biosensor surface, the desorption step is realized by injection of *Eco*RI enzyme specifically directed against DNA substrate underlying *S.pneumoniae* cells. As expected, it results in specific decrease of Zip1 reflectivity signal confirmed by images issued from SPRi. After enzymatic digestion step, sample is recovered at final point of microfluidics and evidences considerable number of isolated micrometric objects that may be ascribed to the released bacteria (microscopic images not available). Apart from that, accurate biomaterial desorption from proper biochip locations may be additionally confirmed by a repeated injection of bacteria, realized by the end of the described experiment. Lack of specific interaction represented by absence of SPR signal related to this injection proves that antibody layer and consequently

bacteria have been efficiently removed. These findings illustrate once again a proof-of-concept study, showing that the developed strategy of programmable biochip system may be successfully applied to bacterial specimens. In the future, such approach may enable multiplexed sample analysis from the angle of its microbiological content, leading to identification of characteristic bacterial strain present in sample of various provenances.

3.5   Conclusions and perspectives

The findings presented in this chapter illustrate the example of programmable strategy that may be potentially employed to characterization of cellular samples. This approach relies on highly biocompatible processes of controlled release from the biochip generated with help of specific endonucleases. Surface functionalization and proper molecular assembly are the key elements of the methodology here proposed. As demonstrated, DNA-based biochips can be easily turned into cell capturing microarrays by the means of cell-specific antibody combined with short oligonucleotide sequence. The biosensing interface is in consequence able to specifically address living cells of different types to well-defined locations on the microarray. Using SPRi label-free detection technique, we provide the opportunity to assay native cells originating from a crude biological sample. Since no cell labeling is required, such biochip system is therefore a promising tool to realize universal characterization of cells issued from complex mixtures. Therefore, the designed methodology can find an application to sort different type of cells (*e.g.* lymphocytes and bacteria) providing that accurate immunorecognition is ensured.

As we have evidenced, once living cells are specifically captured on the microarray, they can be subsequently released by site-specific enzymatic digestion. The approach of enzymatic cleavage has been herein explored in the microdevice format, giving concluding results at molecular and eventually cellular level. The designed biochip system based on DNA matrix may be furthermore upscaled and accommodate many different oligonucleotide sequences bearing various restriction sites. We could therefore benefit from a large repertoire of corresponding restriction endonucleases that are commercially available and easily handled in microarray applications. Such approach would extend the range of possible cellular targets that can be addressed on surface and specifically released by successive enzymatic digestions. The suggested possibility of multiplexed analysis could consequently drive to realization of cell sorting task on complex biological samples.

Chapter 4

Local heating by the photothermal effect as a tool for controlled release

4.1 Introduction

4.1.1 The photothermal phenomenon and its applications

This study explores an original approach to achieve the controlled release of molecular and biological targets previously fixed on a biochip surface. The developed strategy is based on the physical desorption by local heating generated with the use of laser beam. Before we examine this particular approach more closely, let us learn more about the photothermal effect which lays a foundation for the here proposed methodology. By the present introduction, we will thus get familiar with this phenomenon from the angle of its multiple interesting applications in modern biotechnologies.
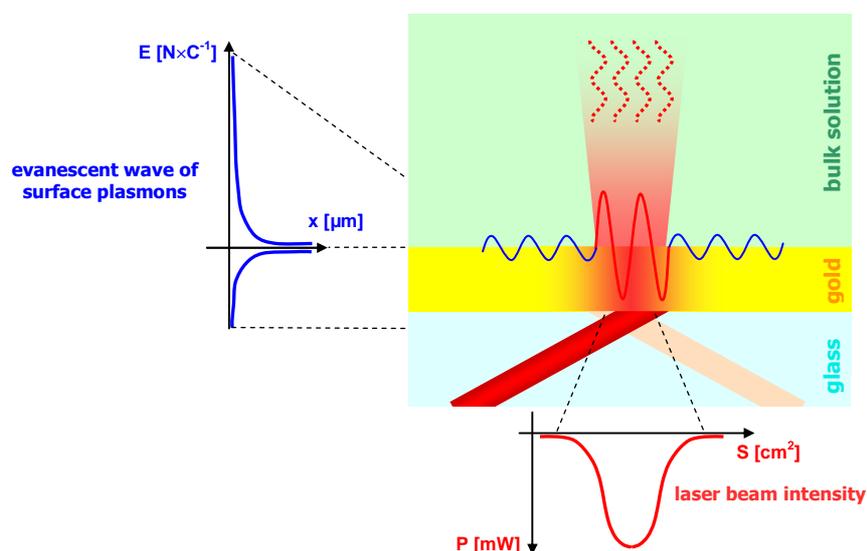
Figure 4.1 Schematic representation of laser-induced photothermal effect assisted by gold surface plasmons (in Kretschmann configuration).[207] The energy of incoming photons is absorbed by surface electron oscillations and converted into heat which is dissipated to local medium. Local confinement of thermal energy generation is due to the laser beam focalization.

In scientific literature, one finds various examples of similar processes that are jointly associated with the photothermal phenomenon.[99, 208-210] Generally, the term *photothermal effect* is applied to particular events when an electromagnetic wave induces photoexcitation of a material thus generating thermal energy, *i.e.* heat. In the specific case of a metal surface exposed to a laser beam placed under a certain angular incidence, the heating phenomenon can be enhanced owing to the presence of surface plasmons. Heat generation arises from the energy transfer between the incident light photons and the electron oscillations occurring on gold or other noble metal surfaces. This happens only in the conditions of surface plasmon resonance when the electric field vector of the incident light wave is parallel to the vector of surface plasmons generated on a metal surface.[158]

Hence, a major fraction of the enhanced surface plasmon energy is converted into heat by the means of a non-radiative relaxation to a neighboring medium (Fig. 4.1).[211-213]

The laser-induced thermal effect assisted by surface plasmon resonance has been considered in detail by X. Xiao *et al.*[214] Authors report on a phenomenon of temperature increase in the bulk medium in regard to possible error for SPR measurements assisted by a laser. Indeed, considerable elevation of temperature is evidenced when metal surface is exposed to laser illumination within a certain time (provided that surface plasmon resonance conditions are established).[215, 216] This effect is therefore interpreted as conversion of the energy from the surface excited state to heat and a subsequent dissipation of the following to the surrounding medium. The level of thermal energy dissipation at the metal-solution interface depends on a few factors such as hydrodynamic parameters (*e.g.* solution flow rate), compactness of the adsorbed layer or power of the laser beam. Noteworthy is to underline the fact that in the case of plane surfaces, temperature increase occurs in a very small area where the laser beam is momentarily focused. Beyond significant influence on SPR measurements, thus generated thermal effect may in some cases become useful and intentionally produced. Indeed, it turns out that the surface plasmon-assisted photothermal effect can find some very interesting applications which have been particularly explored in the field of nanobiotechnology and nanomedicine. That is why I decided to make a short overview of the various potential applications of this particular phenomenon, in order to underline its pertinence in development of modern technologies.

The photothermal effect has been widely studied in the case of optically excited gold nanoparticles (NPs) due to their great interest for modern biotechnology and therapeutics. Richardson and Govorov stated that the heating efficiency is particularly strong under surface plasmon resonance conditions and described it in the study of metal nanoheaters capable of ice melting[217] and water local heating.[216] The ability of nanoparticles to produce laser-induced local temperature increase has paved the way to their multiple potential applications, such as drug delivery,[218-220] gene regulation,[209] reaction catalysis,[215, 221] microfluidics,[222] material processing[223] or even non-invasive cancer therapy[224] and biological imaging.[225] Since the photothermal effect is assisted by the surface plasmons, design of nanoparticles may offer selection of surface plasmon conditions (*e.g.* laser wavelength). It thus give an opportunity for facile tunability of such system in function of the NP composition, size and geometry.[226] Therefore, modified nanoparticles may be applied to remote release of molecules[208, 227] and development of such tools is extremely attractive for therapeutic purposes. The introduction of similar system *in vivo* may avoid a radical temperature rise since the heating is confined to few nanometer distance, thus keeping neighboring biomolecules or tissue intact.

A recent review of S.E. Lee and L.P. Lee focuses on the photothermal effect generated on DNA functionalized nanoparticles that can be exploited for gene regulation purposes.[209] The authors mention two different manners for laser-induced genetic material

release: photothermal dehybridization by using continuous–wave illumination and photothermal melting realized with a pulsed illumination source. In the second case, DNA modified nanocarriers undergo melting into spheres resulting in complete destabilization of DNA-gold binding and efficient liberation of DNA material (ssDNA or plasmid). Unlike to this process that remains definitive, the other approach is reversible since the released DNA may re-hybridize out of the laser beam, once the thermodynamic equilibrium has been reached again. Reismann *et al.* demonstrate similar concept of the remote release by giving the example of gold nanoparticle disassembly/reassembly system.[226] Therefore, this study proves the intactness of DNA structural integrity. Functionality of a DNA material released from nanorods by the laser irradiation is also evidenced by Yamada *et al.*[228] They report on DNA material released by laser induced photothermal effect, further amplified by PCR and finally analyzed on gel electrophoresis where none of structural damages are evidenced.

As we can see, the photothermal effect induced on NP surface plasmons is a useful phenomenon that has been broadly explored so far and opens up to a multitude of potential applications (*e.g.* cancer treatment). That it why, the laser-induced thermal effect assisted by surface plasmons has been particularly well described in the last decade by widespread studies of nanoparticles. In this introduction, a particular focus was ascribed to application of this interesting phenomenon to remote DNA release which high attractiveness is brought by its local character and reversibility of such process. Hence, controlled DNA release induced by the local heating constitutes a base of the strategy making object of the present chapter.

4.1.2   DNA-driven release from gold surface

In order to develop an alternative strategy of target release from a chemically modified biochip surface, we propose a controlled liberation generated by means of thermal stimuli brought by a localized laser illumination. As we have learnt above, the laser-induced photothermal effect is particularly observable when it is assisted by excitation of metal surface plasmons. Thus, here developed methodology takes advantage from surface plasmons possibly occurring on the gold surface and originally exploited in our configuration for the real-time detection of biomolecular interactions (SPRi). The use of thermal energy in terms of controlled release requires conception of a thermo-sensitive molecular construction ensuring specific immobilization of several targets of different nature (from proteins to whole living cells and bacteria).

The previous chapters have evidenced that a DNA biochip can be readily transformed into a functional antibody micropattern by using the antibody-DNA conjugate chemistry. Therefore, such molecular assembly enables several biological targets to be captured on individual features by the means of highly specific recognition. In this study of

novel approach to capture/release biochip system, we use the analogous biomolecular construction erected on the gold-coated prism. Concerning target release step, it takes advantage from the physicochemical properties of short oligonucleotide sequences immobilized on the biochip surface. Thermodynamic stability of DNA duplexes assembled in such biochip format has been widely explored in a previous work carried out in CREAB laboratory by J.B. Fiche and J.Fuchs.[122, 229] By using the SPRi methodology, it was demonstrated that stability of DNA duplex immobilized on the biochip surface depends on the environment salinity, presence of denaturing agents and finally temperature. Therefore, in our concept of selective and controlled release provided by local heating, we benefit from the intrinsic properties of double stranded DNA and its natural behavior regarding to temperature increase induced in the neighborhood of the nucleic acid substrate.
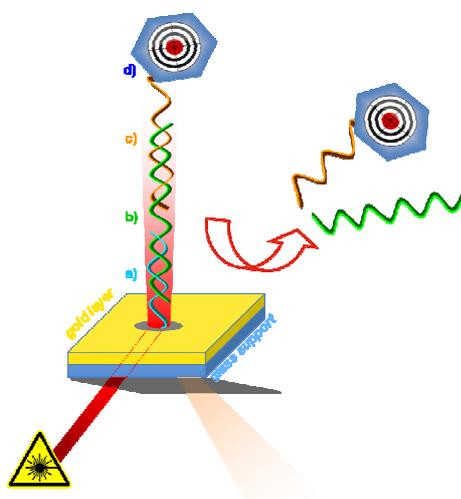
Figure 4.2 Schematic representation of target release strategy based on a local heating by the photothermal effect. a) probe oligonucleotide grafted on the gold surface; b) intermediate DNA strand; c) protein-DNA conjugate (antibody-DNA in particular); d) molecular or cellular target immobilized through specific interactions.

A phenomenon of DNA duplex dissociation may occur if sufficiently high temperature is attained (above DNA melting temperature)[230] without even minor damages of DNA primary structure[228] (providing that the temperature rise does not exceed 100°C). Thermal energy delivered to DNA duplex breaks up hydrogen bonds between nucleic acid strands which are in consequence released one from each other. The susceptibility of the double strand to dissociate upon a heat stimulus is expressed by melting temperature (T_m) and strongly depends on the nucleic acid primary sequence (G-C base-pairing is generally stronger than A-T couple). In thermodynamics, melting point is interpreted as situation when statistically half of available DNA remains as double-helical strand while the rest is dissociated to a random coil state.[231] The inherent thermo-sensitive nature of dsDNA is therefore employed in the biochip strategy here proposed.

Release of biological object of interest immobilized on the biochip relies on a separation of the complementary strands by mere temperature increase. Clue point of the presented strategy is that thermal events are produced in a locally confined way. In the

introduction to this chapter we have learnt that the energy of photons delivered by a laser beam is absorbed by electron oscillations of the gold surface and subsequently transformed into heat. In the case of nanoparticles, the local character of the energy conversion is related to their nanometric size. As to planar gold surface, the laser beam is focalized on the gold layer and thus generation of thermal energy dissipating into surrounding medium takes place in an extremely localized way. It provides a temporal and spatial control of immobilized target release based on DNA double strand dissociation. Moreover, the DNA chemistry enables the reversibility of such process and further target addressing may be produced.

Hence, the present study describes a photothermally driven desorption of various target elements ranging from proteins to living cells (*cf.* Fig.4.2). Targeted species are immobilized on the gold surface according to DNA complementarity rules and via protein-DNA or - in particular - antibody-DNA conjugates. The photothermal effect is generated by an external laser source that requires elaboration of a necessary instrumental set-up. Okano's group also reports on DNA targets efficiently removed from a metal-coated surface by thermal denaturation.[99] In the cited study, an infrared laser beam irradiates a small chip area perpendicularly to its surface and detection of the concerned events is enabled by fluorescence microscopy. In contrast to this end-point analysis our approach takes advantage of a real-time detection that is realized on a gold-coated prism in the configuration of Surface Plasmon Resonance imaging. Indeed, SPRi enables spatial and temporal monitoring of specific capture and controlled release steps. The SPRi apparatus is furthermore coupled to a laser source in an instrumental assembly revealed in detail by the following section.

4.2   Instrumental set-up

The instrumental set-up used for the study of laser-driven photothermal desorption is based on the previously described SPR configuration proposed by Kretschmann.[207] The gold-coated prism, functionalized by DNA probes in the electrochemically driven deposition, is therefore assembled with a flow cell module ensuring contact with biological medium. Surface plasmons are excited by a light beam under well-defined angle of incidence and the reflected signal is recovered by camera, thus enabling detection of the specific interactions. As we have learnt from the introduction to this chapter, if a light bundle of high intensity is delivered in the SPR configuration, locally confined heating may occur. Therefore, for the sake of our study the surface plasmon-assisted photothermal effect is generated irradiation with a red-light laser. The optical configuration combining all mentioned elements has been developed in our laboratory by L.Leroy. Thus, a home-made system joints the possibility of real-time detection by SPRi, generation of the laser-induced photothermal effect and visualizations by classical microscopy. This section specifies all features of the conceived optical set-up as well as needful microfluidic system. The described device is subsequently used to study spatially and temporally controlled capture-release steps realized on biomolecules and micro-objects, including living cells.

4.2.1   Microfluidics

The experiment is driven in a dynamic flow, provided by a syringe pump working in 10 to 500 µL/min flow range. An appropriate buffer is delivered by PEEK and polyethylene tubes (ID of 760 µm) through a degassing system and injection valve to a transparent flow cell. (Fig. 4.3) The flow cell is put together with the gold coated prism with help of two vices positioned on the opposite extremities of the prism. These elements are accurately assembled in order to avoid any external leaks of liquid. The overall assembly is housed on an aluminium support placed between LED and camera, and under a microscope objective. The elements of optical nature are detailed in the following section.
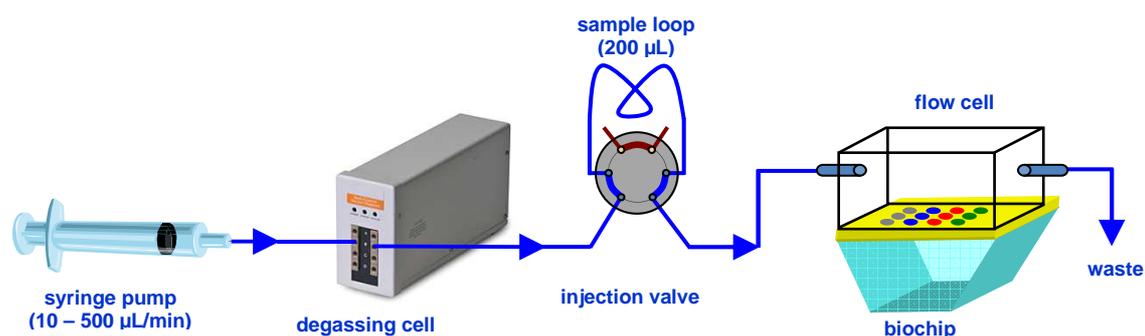
Figure 4.3 Microfluidic set-up scheme. The buffer is constantly delivered by a 50mL-syringe pump and directed through PEEK or polyethylene tubes to the bioreactor. The flow system is equipped with a degassing module and a 6-channel injection valve.

In this work, two types of flow cells are used depending on the experiment application. The preliminary studies realized at the molecular level make use of a fluidic module fabricated in silicon-based organic polymer PDMS (polydimethylsiloxane) and equipped with reaction chamber of 1 mm in depth. (Fig. 4.4) However, tests on capture-release of micro-objects are realized with another type of the flow module providing a smaller reaction chamber volume. As we have seen before, hydrodynamic conditions are crucial parameters when considering efficient capture and release of micro-objects, including cells. The present study needs therefore to design an experimental reactor of a weak volume. By using PDMS flow cell of similarly small depth, we might however experience some difficulties. It is because the material elasticity incurs a risk of probe matrix damage when assembled together with biochip prism. To overcome this obstacle, one solution is proposed to use a thin PDMS film attached to rigid *Plexiglass*® fragment fit out with fluidics inlet and outlet. A flow cell is thus formed by an oval opening carved in the PDMS film of 150-200 µm thickness. The flow module of such type remains transparent and enables microscopic observations which are essentially used in the experiments on biological micro-objects.

111
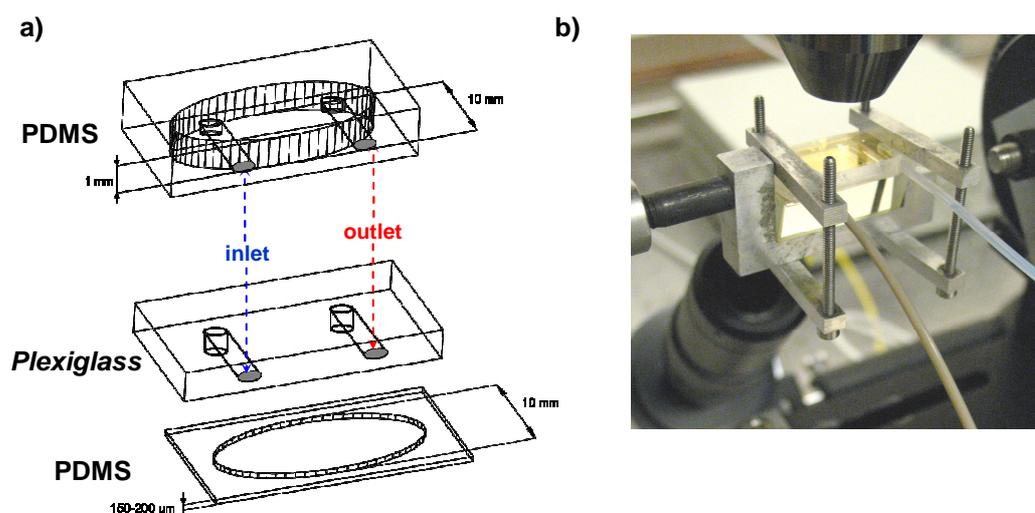
Figure 4.4 Flow cells employed in the experiment of photothermally driven desorption.
a) schematic design of two microfluidic modules: PDMS module with a reaction chamber of 1 mm in depth (upper figure); set of *Plexiglass* and carved PDMS film providing an experimental reactor of 150-200 µm in depth (bottom image); **b)** Photograph of the biochip assembled with the flow cell and placed into the experimental set-up.

4.2.2   Optical configuration

The assembly of different optical elements is a key part of the instrumentation explored in the present study. It consists of a home-made instrumental set-up erected on an optical table housed in a dark experimental room. The basic elements are assembled in analogous way to the commercial SPRi apparatus (*Horiba-Genoptics*) used in the previous studies. It thus comprises a light emitting diode (λ = 660 nm) equipped with focusing lens/polarizer set and a 16-bit CCD camera (Pike F-145B by *Allied Vision Technologies GmbH*), both installed from the opposite sides of the prism [Fig. 4.5 a)]. The LED-polarizer system is integrated with a goniometer which position is operated by an external motor. This precise control enables to set up the light beam at correct angle of incidence under which detection of reflectivity variations is optimal (working angle). The reflected light is registered by the camera and observed in real time thanks to software interface developed in the LabView programming platform.

a) SPR imaging mode
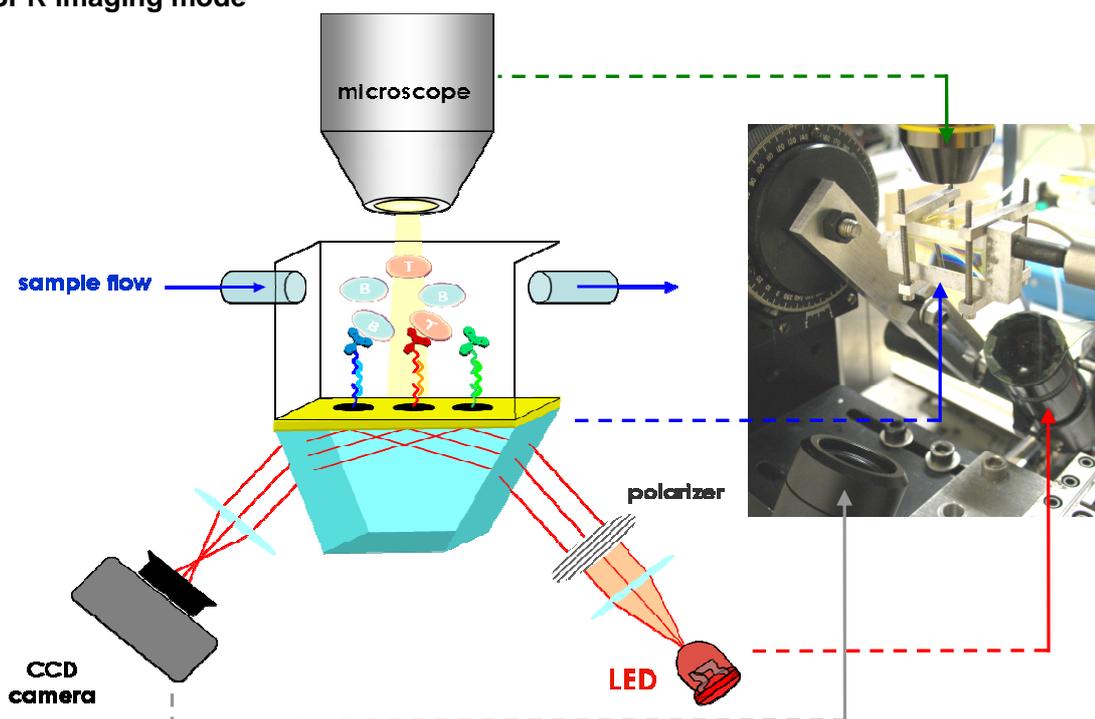
b) lasing mode
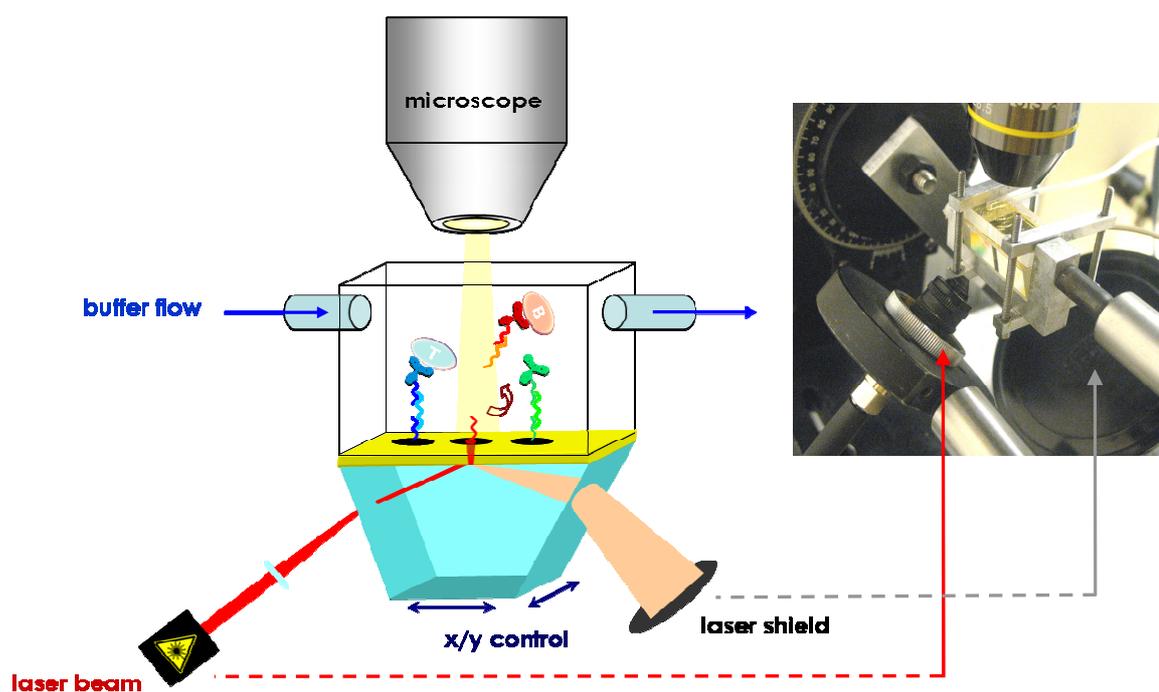
Figure 4.5 General scheme of the instrumental set-up used in the experiments of laser-induced desorption.
a) Surface Plasmon Resonance Imaging mode: real-time monitoring of biochip molecular assembly construction and cell capture/release steps **b)** Lasing mode: photothermal desorption of species induced by a laser beam.

Apart from the SPR imaging mode, the here developed instrumental set-up may work in parallel in a second mode enabling photothermally driven desorption of the material immobilized on the biochip. When required, a red-light laser beam is introduced from one side of the prism [Fig. 4.5 b)]. In our studies two laser sources working in continuous-wave illumination are used: diode laser of a small intensity ($\lambda = 665$ nm) and more intense fiber-integrated diode laser ($\lambda = 653$ nm). The principle parameters of here used lasers are given in Figure 4.6 (more detailed features are included in the Appendix H). In order to produce the photothermal effect, a TM polarized laser beam strikes the gold surface under conditions of surface plasmon resonance defined by the incidence angle. The proper angle is adjusted manually until well-defined black strip is observed on the reflected light spot – a phenomenon identified as absorption of laser energy by surface plasmons. The starting position of the laser spot is set up with two micrometer screws steering the laser support. All the initial settings are done at a weak light intensity. Proper experiment is driven at maximally available current and accompanied by remotely directed displacements of the laser spot in *x/y* directions on the microarray surface. Relative position of the focalized laser is commanded by external motors (step motor controller by *Oriel*) which provide motions of prism-LED-camera set-up with the reference to location of the laser spot. Therefore, laser tracing may be precisely executed on each probe family of spots or one spot in particular.

Parameter	Diode laser	Fiber-integrated diode laser
wavelength	665 nm	653 nm
P_{in}	73 mW	220 mW
P_{out}	25 mW	72 mW
P_{SP}	15 mW	63 mW
focalised spot diameter	50 – 150 µm	~ 550 µm
effective surface power [a]	~ 1.9 µW/µm^2	~ 0.3 µW/µm^2

[a] effective fraction of laser intensity consumed in coupling to surface plasmons (P_{SP}) referred to gold surface unit
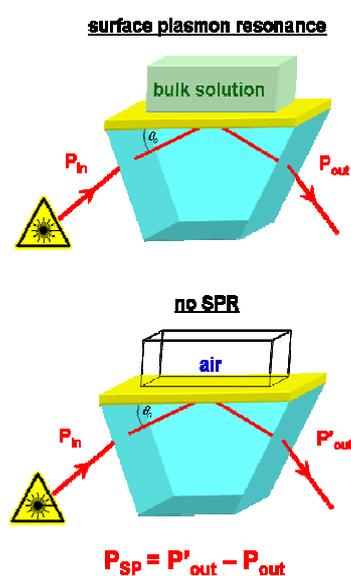
Figure 4.6 Parameters of the laser sources used in the study. The right image depicts power measurements performed on the incoming and reflected light in the conditions with/without surface plasmon resonance. Measurement uncertainty is estimated to 5 %.

The instrumental configuration developed for the purpose of the present study is additionally enriched by another element of the optical nature. In order to enable direct observations of capture-release steps realized with micro-objects (*e.g.* living cells), a microscope objective is placed over the biochip. The optic microscope (*Olympus Optical*) is powered by a halogen lamp and observations are realized in the reflection mode by using $\times$ 4 and $\times$ 10 objectives. Direct visualizations of microscopic object immobilization and desorption from the functionalized gold surface are enabled through transparent flow cell pressed onto the surface as explained above. Images are acquired by a 8-bit color camera (Infinity2-3C by *Lumenera*) and registered by using a proper software. This element of instrumentation is introduced as a complementary tool to enable validation of immobilization and desorption events related to micrometric objects that can not be integrally registered by SPR imaging.

4.3 Use of the photothermal effect for physical desorption at the molecular level

In this section, we explore the laser-induced photothermal release of molecular targets in the SPR configuration, by using the instrumental set-up previously described. We discuss some essential elements of the experimental conditions in order to validate the strategy of physical desorption before we move to tests on micro-objects. For this purpose, we use the molecular on-chip assembly analogous to one used in the previous studies on enzymatically driven release. Such approach provides a certain level of standardization in terms of biochip functional assembly. The described herein experiments are carried out in the home-made SPR imaging set-up and on a DNA functionalized gold prism. The photothermal desorption is executed by a diode-laser of small intensity (P_{in} = 73 mW). Therefore, we show an efficient laser-induced release of several molecular targets, carried out under spatial and temporal control. The specificity of here developed desorption strategy is confirmed by relevant data issued from SPR imaging and mass spectrometry analysis. Consequently, the present section makes the reader acquainted with all indispensable elements that are required to confirm the feasibility of the developed methodology.
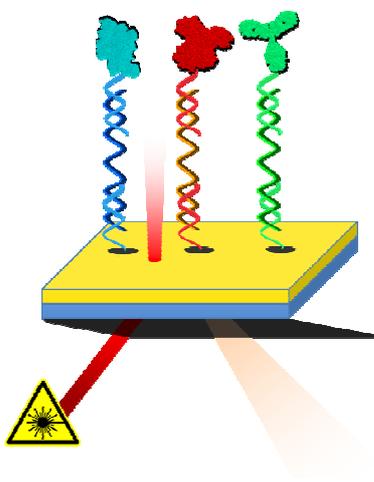
Figure 4.7 Schematic representation of laser-induced desorption of various protein targets. Several proteins are immobilized on Zip sequence-based matrix through corresponding intermediate strands and protein-DNA conjugates.

4.3.1   Protein release from DNA biochip

As demonstrated by Okano's group, DNA material immobilized on a metal support can be subjected to a localized by a laser beam.[99] The phenomenon is based on dsDNA denaturation which results from the laser-assisted photothermal effect. One of the main advantages of such approach is the fact that DNA chemistry enables reversibility of dissociation process and once target strand has been released, new hybridization may come about according to the complementarity rules. Moreover, DNA sequence recovered from photothermal release remains functional and can be thus amplified by PCR method for further assays. Therefore, the strategy proposed by Okano *et al.* has the potential application in the field of genomics and can serve as a powerful tool for gene expression studies.

In our approach, we provide an example of study that extends the application of photothermally driven desorption beyond the DNA level. Even if the controlled release is substantially based upon dissociation of double stranded DNA, an extended molecular assembly enables more sophisticated purposes (Fig. 4.7). Typically, the use of protein-DNA or more particular antibody-DNA conjugates can be thus applied to so-called "ligand fishing" from complex mixtures and in more advanced applications to realize cell sorting task as well. In development of such elaborated systems based on the photothermal effect, an essential prerequisite is to ensure optimal conditions for controlled release by preliminary studies at the molecular level.

The experimentation here discussed makes use of the biochip molecular construction based on a DNA matrix consisting of several Zip1, Zip2 and/or Zip3 spots obtained according to the electropolymerization protocol. Each probe is subsequently assembled with the corresponding intermediate strand and eventually completed by the protein-DNA conjugate. Few protein-DNA hybrid molecules have been elaborated according to the previously developed conjugation chemistry (*cf.* section 2.3). Taking into account the designed 3-component on-chip construction, conjugation reaction has been realized on the same DNA oligomers as previously exploited for enzymatic cleavage purpose (*Eco*RI*, *Nco*I* and *Pvu*II*). Apart from rab-IgG, the oligonucleotide sequences have also been conjugated to an other protein – human creatine kinase (CK). The selection of this protein was driven by the possibility of its fairly easy detection by mass spectrometry which is the method of choice for the validation of the molecular targets released in the photothermal approach. In this scope, the experiments with CK-DNA conjugates are hereby demonstrated and exemplify feasibility of the developed strategy.

Creatine kinase (CK), otherwise known as creatine phosphokinase (CPK) is a human enzyme involved in the cellular processes of energy conversion.[232] The protein is responsible for phosphate group transfer from ATP (adenosine triphosphate) to creatine molecule (and reversibly). This enzyme plays a major role in tissues characterized by high consumption of energy. In particular, cytoplasmic CK can be found in muscle, heart and brain cells. CK is composed of two possible subunits that can be of B type (brain) or M

type (muscle). Therefore, three different isoenzymes can be listed: CKBB, CKMM and less abundant in the human body CKMB. Each subunit is of about 43 kDa MW and very precise mass spectrometry assays attribute 42 970 Da to M fraction and 42 512 Da to B fraction of the creatine kinase.[233] That is why CKMM-*Pvu*II* and CKBB-*Eco*RI* conjugates have been conceived in order to provide their clear identification by MS facility. They are addressed on surface by DNA hybridization and subsequently released by the photothermal effect. Separately recovered samples are consequently transferred to mass spectrometry analysis which is kindly realized by M. Jaquinod from Proteomic Analysis Laboratory EdYP (CEA Grenoble, IRTSV). The ultimate goal of such proceeding is to verify the specificity of molecular target controlled release.

4.3.2   "Ligand fishing" approach

As we know, Surface Plasmon Resonance is a powerful technique capable of label-free monitoring whole range of biomolecular interactions in order to detect DNA, proteins, sugars, viruses or even cell. In the case of complex biological samples of unknown content, SPR may be combined with other detection instruments to enable more advanced analysis. In a particular example, SPR technique is coupled to amass spectrometry device in order to perform rapid and versatile sample identification. Such experiment conceptualizes so-called "ligand fishing" approach which is widely explored in proteomics and mainly by using *Biacore*® SPR systems.

A number of studies is thus reported to detect small amounts of protein in a biological extract or even identify new ligands of unknown affinity to receptors.[234-238] In a typical ligand fishing experiment, the analyzed sample is loaded onto the recognition surface where species are captured and then recovered for further identification. Bound elements are eluted in a one-shot operation based on salinity[237] or pH[238] variation. In SPR-MS integrated device, the recovered sample is straightforwardly driven through LC column if desalting needed. Following ionization step (ESI or MALDI), the sample is analyzed on-line by mass spectrometer. Several studies report that mass spectrometry may be successfully applied to specifically identify interacting proteins down to femtomolar level. In the present work, we thus decide to use the MS technique to realize downstream detection of proteins released from the surface. Subsequently to laser-induced release, the recovered samples are adequately prepared and transferred to mass spectrometer where protein profile is investigated. It is not performed in an integrated SPR-MS device as our study constitutes a proof-of-concept for photothermally assisted desorption strategy. In such approach, MS aims to give us additional information that confirms specificity of the developed methodology.

a) Experimental protocol

Some introductory elements concerning this study have already been mentioned in the previous sections. Indeed, we have learnt how the photothermal effect may act on DNA-based molecular assembly and in which instrumental set-up is explored to attain the assumed objectives. Our goal is to demonstrate not only the specific addressing of targets on a microarray surface but also their controlled desorption from the solid support and further identification. The original experiment reported her, is assisted by combination of two detection techniques (Surface Plasmon Resonance and Mass Spectrometry) and may be therefore ascribed to a "ligand fishing" strategy. This particular approach is discussed in the following lines in the light of the relevant findings. We thus treat of given proteins that are specifically recognized by DNA matrix (thanks to protein-DNA conjugates), subsequently removed by photothermal desorption and possibly identified in the recovered sample by MS analysis (Fig. 4.8). Let us now see if the relevant concept proves correct in practice.
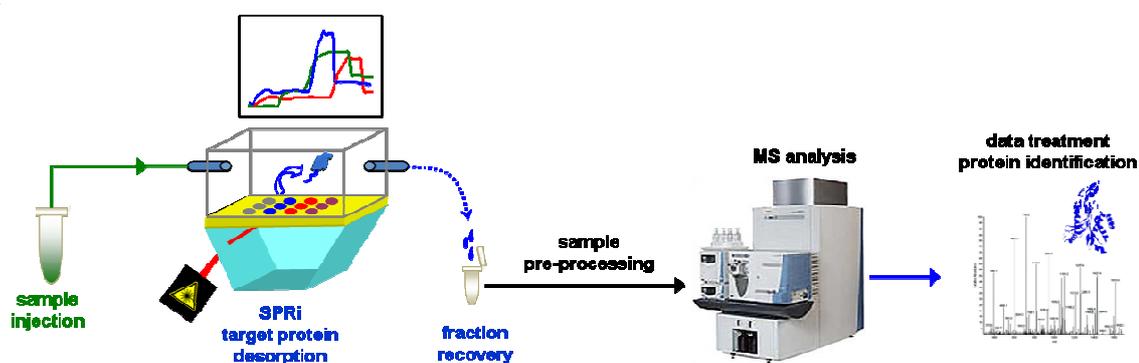
Figure 4.8 Run diagram of the proposed "ligand-fishing" approach. Sample is injected to the reactor chamber where analytes are specifically immobilized and subsequently desorbed by the local heating. Recovered fraction is pre-processed (protein digestion by trypsin, purification by Nano-LC) and analyzed in mass spectrometer. Target protein is identified by using proper software and protein library.

According to the previously depicted instrumental approach, the experiment of photothermally directed target desorption is driven in the SPRi configuration. A DNA functionalized prism is therefore assembled with the PDMS flow cell (1 mm in depth in this particular case). The instrumental set-up allows all steps of molecular construction and material desorption to be monitored by dint of SPR imaging. Relevant targets are sequentially injected to the microfluidic system and flowed over the DNA matrix where they are specifically hybridized. Once the on-chip immobilization of protein-oligonucleotide molecules is accomplished, their photothermal release is achieved by using a diode-laser at 665 nm. Because its position can be precisely directed in two axes, laser tracing is performed for each spot family in separate steps. In parallel to this, corresponding sample is recovered from the outlet of microfluidics. Collected fractions are subsequently submitted to protein assessment by mass spectrometry, being the last step of experimentation enabled within the framework of the collaboration with M. Jaquinod from EdyP laboratory. This group is renowned in the field of applied proteomics owing to a high

level expertise and technologically advanced equipment. Taking into account the final examination method, experimental conditions should be submitted to optimization from the point of view of the further analysis by mass spectrometry. Adaption of the overall method of operation is therefore desired.

b) Keratins – an important issue for MS analysis

In the scope of MS investigation, a basic and most important concern is the quality of final sample intended for analysis. The illustrated before approach appoints the need for meticulous proceeding in the preparation of samples devoted to downstream investigations. Substantially, we have to consider a few requirements aiming to avoid contaminations coming from the experimental environment which are mainly represented by keratins. These species are fibrous structural proteins abundantly existing in the surrounding medium. Indeed, a typical laboratory environment is in reality an important source of contamination by keratins transported by dust and principally coming from skin, hair and clothing. Their presence highly pollutes MS signal and disturbs efficient protein identification especially in case of low content of the target material. In order to reduce the risk of contamination, particular precautions should be undertaken, assuming that everything in the environment is a potential source of keratins. In the case of here developed experimentation, all used material is thus thoroughly cleaned and micro-tubing washed with detergent and sterile miliQ quality water before the experiment. Injected samples and buffers are also prepared in an accurate way by using sterile materials and chemicals. Finally, sample recovery is performed at the exit of possibly well separated and closed fluidic circuit. These steps have to be absolutely undertaken especially if small quantity of recovered protein is expected, which is actually the case in our approach. Although the precautions are taken, the realized experiment consists of many hand-operated steps and it is extremely difficult to establish completely keratin-free conditions. As it will be discussed later on, this is a significant issue and appears problematic for the MS analysis of recovered samples. Nevertheless, the obtained results will enable us to draw pertinent conclusions and confirm target-specific out-of-biochip desorption.

c) Optimization of the experimental buffer regarding MS assay

Regarding downstream MS analysis of samples coming from specific target release experiment, the use of compatible buffer is an important concern. In such proceeding, mass spectrometer involves sample ionization step and thus the experimental buffer should not contain salt at considerable concentration. Typically, samples recovered in PBS buffer can not be directly put to examinations because ions provided by NaCl or KCl could interfere with formation of target ions and thus influence correct identification of species. In case of MS involving procedures, a commonly used basis for sample preparation is ammonium bicarbonate salt, otherwise ammonium hydrogen carbonate (NH_4HCO_3).[239, 240] This reagent

provides a volatile aqueous solution that readily releases ammonia and CO_2 (pH 7.8 at 25°C). This property makes ammonium bicarbonate a good buffer for the applications associated to sample preparation by lyophilization. Lyophilization procedure of NH_4HCO_3-based sample enables to obtain a material devoid of any salt residues which is highly applicable to MS ionization approach by MALDI or electrospray techniques. Therefore, here reported study makes use of ammonium bicarbonate solution as running buffer applied along the experiment.

Although the aforementioned buffer is compatible with MS detection, the key point of here developed experimental approach is expressed by target addressing/release based on DNA chemistry. That is why, we have to take into account the fact that NH_4HCO_3 dissolved in water is not typical a saline solution used in DNA studies.

The electrostatic interactions play an essential role in double DNA helix formation. Deoxyribonucleic acid molecule is negatively charged owing to many phosphate moieties integrated in DNA backbone primary structure. Therefore, the hybridization process of complementary strands has to be assisted by an environment of sufficient salinity that ensures the presence of ions providing negative charge screening. Stabilization of the double strand is mainly generated by monovalent ions distributed in the surrounding medium. In NH_4CO_3 solution, the ion equilibrium is driven by ammonia-ammonium couple and carbonate chemistry that involves HCO_3^- to CO_3^{-2} transformation assisted by carbamate formation.[241] None of particular studies treating of dsDNA stability in NH_4HCO_3 buffer are proposed in the literature.

Thus, we here report on initial experiments realized in the ammonium bicarbonate buffer. This is to examine hybridization of DNA and protein-DNA molecules on the biochip surface in such unusual conditions. Obtained hereby SPRi signals show good responses in 200 and 300 mM solutions of NH_4HCO_3 (*cf.* Fig. 4.9). These results are consistent with those observed in standard saline solutions containing NaCl (*e.g.* PBS). We have thus decided to introduce 200 mM ammonium bicarbonate solution as a running buffer in protocol of the present capture-release experiment.
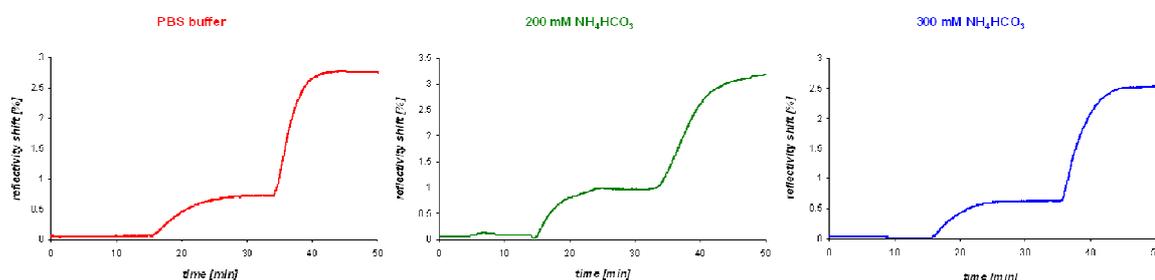
Figure 4.9 SPRi monitoring of DNA hybridization realized in buffers of different salinity. The former reflectivity shift (~15 min) corresponds to hybridization of Zip2*-*Pvu*II on Zip2 probe. The latter one is consistent with immobilization of rab-IgG-*Pvu*II* conjugate.

4.3.3   Thermodynamic stability of the DNA substrate

The key element of the following study is not only to provide an efficient target addressing by DNA hybridization, but above all, to enable an effective target release based on DNA dissociation induced by the photothermal effect. The preliminary tests realized with available DNA oligomers and protein-DNA conjugates did not result in desired desorption of immobilized material. None of expected desorption events was observed, even at the highest laser intensity practicable in our set-up. We may thus speculate that the employed optical configuration and laser powers are not qualified to generate a sufficient temperature increase, required for the experiment. The use of more powerful light source would be probably a good solution but such instrumentation is not available for the present project. We must however take into account that more efficient heating could generate inadvisable secondary effects such as perturbation of biomolecular stability or creation of vapor bubble. Further, if we assume the final application of the biochip system to living cells, such phenomena could be a significant factor of physiological stress and should be thus avoided. To overcome the problem of the insufficient laser power, we need to make deeper insight into thermodynamic stability of the DNA strands employed in the present work.

In order to estimate thermal conditions required to produce efficient target release from the biochip surface, it is useful to characterize melting temperature of the oligonucleotides used in the molecular constructs. To do so, we make use of a computational method for nucleic acid thermodynamics, available on-line.[242] This simulation tool is based on two-state melting model of DNA (double strand and random coil) and enables approximation of T_m which can be safely applied to short oligonucleotide sequences.[243] The thermodynamic parameters characterizing melting process of dsDNA are determined by using the nearest-neighbor method and as it was demonstrated by SantaLucia fit well the experimental data.[231] These calculations concern however DNA melting and hybridization observed in solution but are fairly accurate to evaluate short duplex thermodynamics in the microarray format.

double strand	T_m
Zip1-Zip1*	68.2°C
Zip2-Zip2*	67.3°C
Zip3-Zip3*	69.0°C
*Eco*RI-*Eco*RI*	62.7°C
*Pvu*II-*Pvu*II*	62.1°C
*Nco*I-*Nco*I*	64.1°C

Table 4.1 Melting temperature predictions for the oligonucleotides employed in biochip molecular assembly. Theoretical T_m values are calculated by using *The DINAMelt Web Server*[242] and obtained for the relevant hybridization conditions: 0.25 µM of DNA, 25°C, PBS buffer.

According to the aforementioned numerical simulation, melting temperatures are estimated for Zip and restriction site-containing sequences deployed in the biochip molecular assembly (*cf.* Table 4.1) The values hereby established provide information on the thermal energy that should be delivered to realize dissociation of the oligonucleotides – a phenomenon that lays a foundation of here explored photothermal release of molecular targets from the microarray surface. Willing to achieve this final goal, it is actually not necessary to attain the melting point which essentially serves to determine conditions where statistically half of available nucleic acid strands still remains as double helices. We expect that thermal energy represented by lower temperatures, sufficiently influences DNA dissociation constant (K_{off}) and may produce individual dehybridization events. One may observe that T_m values approximated for the oligonucleotides in question are however quite high and may thus explain the lack of satisfactory results in the preliminarily realized tests. Indeed, we deduce that the optical configuration originally conceived probably does not provide sufficient level of heating and dissociation kinetics is still very slow. That is why a useful solution is to provide supplementary destabilization of DNA thermodynamic equilibrium regardless to lasing conditions available in the present study.

In literature, thermodynamic stability of DNA duplex is widely studied in terms of various factors: salt concentration,[244] temperature,[245] base pair mismatches[246] or presence of organic compounds.[247] Non-equilibrium DNA state can considerably decrease DNA melting temperature and thus facilitate double strand dissociation. To do so, among different solutions, we can mention for instance destabilization of dsDNA by introducing point mutations into base pair sequence or by modifying the surrounding medium with denaturing agents. The second alternative seems more straightforward and is applied for the need of the study here reported.

Among DNA denaturing agents, we can enumerate several chemical compounds like for example formamide,[247] urea and its derivatives,[248] guanidinium hydrochloride[249] and other chaotropic salts. According to J. Fuchs (CREAB), a buffer supplemented with 20 % of formamide (v/v) enables hybridization of oligonucleotides on microarray and noticeably decreases the DNA melting temperature.[122] In the present study, it is decided to make use of N,N-dimethylformamide (DMF) also reported to influence DNA duplex stability and to induce measurable drop of melting temperature while introduced to a solution.[250] We thus apply the analogous 20 % DMF content which seems to be correct since formamide and N,N-dimethylformamide are closely related chemical compounds and act on the dsDNA stability in a similar way.[251] Therefore, we may consider further J. Fuchs's statement assuming that every percent of formamide added to the buffer induces ~0.6°C decrease of T_m. Taking into account the presence of the denaturing agent, the consequent melting temperature ascribed to our experimental conditions may be approximated to about 55°C. However, we hopefully think that local heating generated by the photothermal effect in our configuration does not rich this melting temperature level since it would certainly perturb the condition of biomolecular or/and cellular entities.

Detailed insight into thermal effects generated in the employed optical strategy does not in fact make object of the present PhD thesis and none of measurable temperature is given. Nevertheless, we speculate that employment of the buffer supplemented by DMF provides an ample shift of thermodynamic equilibrium to single stranded DNA and thus ensures efficient target release which is demonstrated by the following findings.

4.3.4   Photothermally driven protein release from the DNA-based matrix

After the necessary optimization elements have been discussed, we may now proceed to demonstrate a case study of photothermally driven release observed for independent molecular targets. For this purpose, a DNA functionalized biochip (Zip1 and Zip2) is shown to specifically address two molecular targets: CKBB-*Eco*RI* and CKMM-*Pvu*II* by means of the corresponding intermediate strands. All building blocks of the molecular architecture are introduced in the flow cell in 200 mM ammonium bicarbonate buffer, supplemented with 20 % of DMF (v/v). SPR imaging allows monitoring of the on-chip construction steps in real time and in the absence of labeling (Fig. 4.10). From the obtained results, we notice that registered reflectivity shift is higher for the complementary DNA than for the protein-DNA conjugate. This result might be explained by the fact that creatine kinase is a smaller protein in comparison to an IgG for example. Here addressed targets are probably composed of chemically modified CK subunits (brain or muscle fraction of nearly 40 kDa), which gives almost fourfold difference of the molecular weight comparing to the IgG molecule (150 kDa). Moreover, as it was evidenced before, the corresponding partners at intermediate (*i.e.* Zip1-*Eco*RI) and final level of the molecular construction (*i.e.* rab-IgG–*Eco*RI*) do not hybridize in equivalent proportion. SPR data revealed previously that one protein-DNA molecule hybridizes to one of about 4 complementary strands available. The unequal hybridization ration is probably the case in here demonstrated experiment.
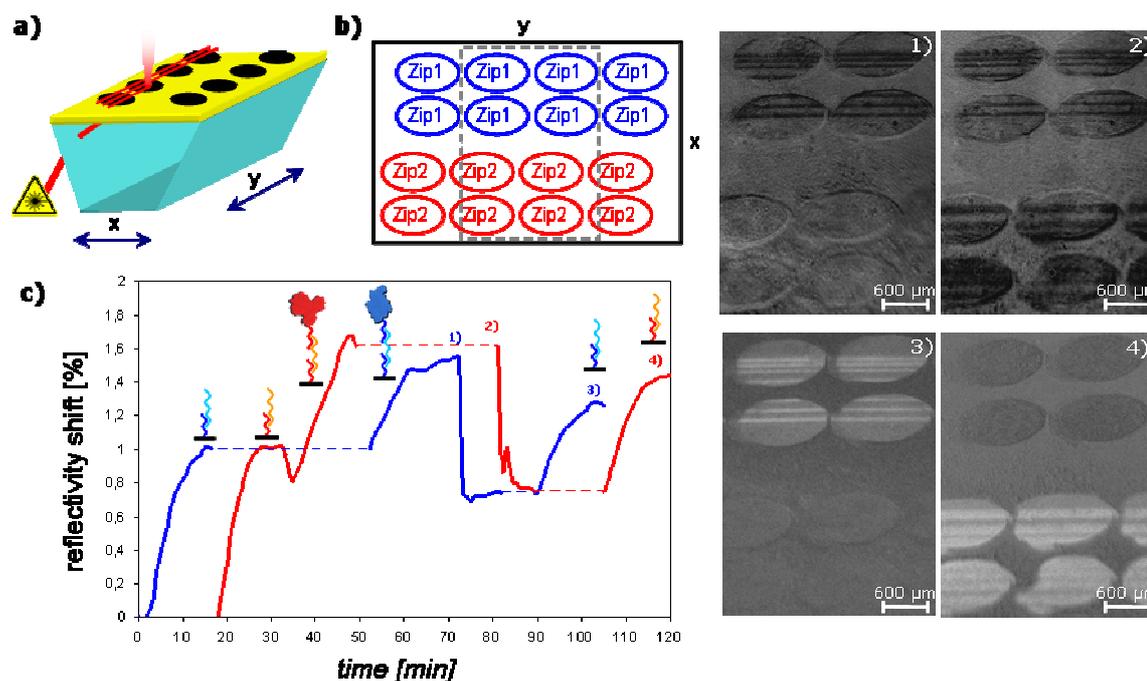
Figure 4.10 Photothermally driven release of CKBB and CKMM proteins immobilized on the DNA matrix **a)** schematic representation of laser tracing on a gold prism; **b)** DNA matrix composed of Zip1 and Zip2 spots (1.2 mm in diameter); **c)** SPR monitoring of the experimental steps: molecular assembly (Zip1 + Zip1*–*Eco*RI + CKBB–*Eco*RI* and Zip2 + Zip2*–*Pvu*II + CKMM–*Pvu*II*), controlled release from Zip1 then Zip2, re-hybridization (Zip1*–*Eco*RI and Zip2*–*Pvu*II) [Δ]; SPRi difference image captions: **1)** laser tracing on the Zip1 family of spots, **2)** laser tracing on the Zip2 family of spots, **3)** re-hybridization of Zip1*–*Eco*RI, **4)** re-hybridization of Zip2*-*Pvu*II.
[Δ] registered Zip1 and Zip2 signals are relative one to each other because no reference probe signal is present and considerable refractive index are generated in the bulk solution.

Subsequently to the immobilization of proteins, we perform their photothermally induced desorption. Local heating provided by the laser beam is realized in two separate steps. To do so, laser tracing is performed in parallel lines along the *y* axis as depicted on the Figure 4.10 a). The DNA matrix is conceived in such manner that desorption of target material is sequentially executed for each family of spots. Probes are grafted on the biochip in several copies of large spots (~1.2 mm in diameter) in order to increase the amount of eventually desorbed proteins which is almost at the MS detection limit. At first, laser tracing is executed on Zip1 family of spots situated on the left side of the prism (in the *y* direction) and then on the second Zip2 probe placed on the right side. After each probe-specific desorption, the SPR signal is registered in order to visualize the relevant reflectivity shifts.

Processed data evidence specific release of the concerned targets. Following each laser tracing step, we can indeed observe negative reflectivity shifts corresponding to the following probes: Zip1 in the first step and Zip2 afterwards. As clearly seen, the registered signal drops do not completely attain starting level (before construction of the molecular assembly) and represent about a half of the original signal. This fact can have one simple explanation. Namely, the monitored reflectivity signals are for each probe averaged over

all pixels on the corresponding spot surface image. From the other hand, these spots are not integrally covered by desorption effect and thus the signal drops are not total. Indeed, the SPR differential images expose the exact zones from which the material has been removed. We can thus clearly identify the lasing lines that are revealed by a lower level of the grayscale [*cf.* Fig.4.10 1)-2)]. We can also notice some difference in thickness of the observed lines that reflect the size of the laser spot. It is because in reality, when displacing the laser in the x direction, its on-surface focalization is slightly changed and therefore the laser spot size modified. In the here presented configuration, it may vary from about 50 to 150 µm which corresponds to an approximate value of laser intensity of about 1.9 µW/µm^2 (*cf.* Fig. 4.6).

The reported experiment involves laser tracing at a controlled displacement rate which provides instantaneous heating confined to the local environment where thermal energy is consequently dissipated. As a result, we produce local DNA dissociation and specific target liberation, keeping primary DNA probe intact. It is confirmed by the last step of the experiment monitored by SPRi [Fig 4.10 3)-4)] where complementary strands are re-introduced on the biochip surface. An efficient step-by-step re-hybridization is thus registered specifically for Zip1 and then for Zip2 probe. This finding is unequivocally confirmed by the associated differential images where the reflectivity signal is retrieved exactly in the same zone from where the material has been previously desorbed. It means that the applied conditions of local heating do not destroy the original probes that remain functional. Noteworthy is the fact that we are able not only to realize a localized desorption of the immobilized targets but also to restore the molecular architecture. Therefore, one advantage of using DNA matrix is that it can be completely regenerated once the experiment is finished. Regeneration is provided by a short washing with 100 mM solution of NaOH. Rinsed in miliQ water and dried under argon stream, such DNA biochip may be used for further experiments within a few months if properly stored.

4.3.5   Mass spectrometry assay of the recovered samples

Taking into account the obtained data represented by images issued from SPRi as well as the SPR kinetics signal, we have thus demonstrated the efficient method for target-specific and localized removal of biological materials previously immobilized on a solid support. In order to confirm the results obtained from SPRi, samples recovered from the experiment were assayed by mass spectrometry to investigate presence of the released proteins (CKBB or CKMM). Therefore three consequent fractions were collected from the outlet of fluidics: "0" as blank sample before laser desorption, "1" during Zip1 probe laser tracing and "2" when desorption was performed on the Zip2 spot family. All three samples were given to M. Jaquinod for protein assay on OrbiTRAP mass spectrometer.

The MS analysis has unfortunately revealed an important amount of impurities in the given samples. Though necessary precautions were undertaken, a certain level of

contamination was possible taking into account the manual character of several steps. Therefore, the MS signal has confirmed considerable pollution by keratins and other non-relevant proteins in all three samples. Tests "0" and "1" have not evidenced any trace of proteins corresponding to the experiment. Nevertheless, thorough analysis of "2" sample has resulted positively in the presence of the creatine kinase M fraction. Although, the amount of the indentified protein was minor and covered by many other signals, the test has approved the existence of right protein in its specific sample. Effectively, CKMM (or more exactly CKMM-*Pvu*II*) was desorbed from Zip2-based spots and subsequently recovered in the "2" sample. The quantity of the released protein has been estimated to about 100 fmol which makes it extremely challenging to detect especially if impurities are present. Although the amount of protein material was weak and efficient analysis hampered by polluting proteins, we may consider these partial results as concluding. We deduce that desorption from specific spots in reality happens and does not come about spontaneously. If it was the case, CKMM (and also CKBB) would be found in other samples since they were injected to fluidics in more important quantities than effectively immobilized on spots.

4.3.6   Conclusions

We hereby demonstrated a simplified example of the ligand fishing approach (SPRi detection + MS analysis) which may be potentially applied complex protein mixtures. Instrumental improvement shall become an object for future system development in order to conceive high-performance automated operation. The great advantage of such device, comparing to the original ligand fishing approach, would be the possibility to "fish" several targets through specific biomolecular interactions in one single experiment. We demonstrate that protein-DNA chemistry provides high specific target addressing (DNA hybridization, specific antibodies) followed by spatially controlled desorption of at least two different targets. The present biochip system may be thus potentially employed to investigate complex biological mixtures with high throughput and for advanced applications in proteomics.

4.4   Application of the photothermal effect to the micro-object release

Having the proof of controlled release at a molecular lever by using the photothermal effect in the SPR configuration, we may proceed to explore the efficiency of such strategy on more developed on-chip assemblies amenable to capturing objects of a micrometric size. The essential objective behind that is to realize a specific immobilization of living cells followed by their subsequent release from the surface by local heating. But before starting to work with living biological objects, an important development step intends to realize preliminary studies in order to validate the system functionality on less vulnerable targets. Indeed, living cells are of complex nature that makes them susceptible to even slight variation of external parameters in the surrounding medium (temperature, electric field intensity, buffer content). Therefore, this section investigates the laser-induced desorption executed on proper molecular assembly capable of the immobilization of synthetic microbeads. Polystyrene (PS) microspheres are used as target objects that imitate cell specific capture based on a membranar marker and its specific interaction with an antibody (Fig. 4.11).
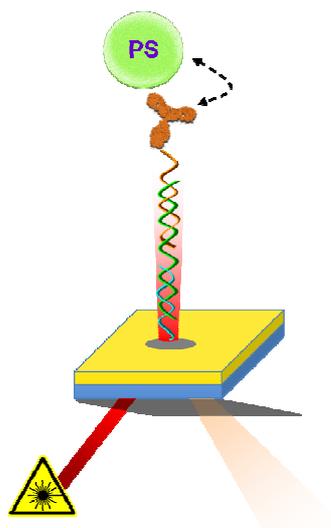
Figure 4.11 Schematic representation of the laser-induced release of polystyrene μbeads from the biochip surface.

4.4.1   Photothermally driven release from the IgG–DNA based construction

As a preliminary study to micro-object release assays, we realize an experiment of the laser-induced desorption on IgG–DNA constructs, analogously to the tests with protein-DNA conjugates described before. For this purpose, rab-IgG–*Pvu*II* and rab-IgG–*Eco*RI* are introduced on the corresponding Zip1 and Zip2 probes (via intermediate strands) and subsequently released by the laser irradiation. This approach constitutes the first step to more sophisticated applications based on cell-directed antibodies and leading

to controlled release of specific cell fractions. For this purpose, we show efficient desorption of rabbit antibody from DNA-based biochip which relies on double strand dissociation provided by the local heating. SPRi kinetics proves accurate addressing of a rab-IgG–DNA target realized in PBS buffer supplemented with 20 % of DMF (Fig. 4.12). These results are consistent with the former ones obtained in the enzymatic cleavage approach. Target capture is therefore specific to the corresponding probes and triggers analogous responses as previously observed: the IgG–DNA signals are 3 to 5 times higher than those of the intermediate oligomers. This confirms that hybridization is correct despite the presence of the denaturing agent. Moreover, the laser-induced desorption proves to be probe-specific and reveals accurate reflectivity drops that can be eventually retrieved if the relevant building blocks are injected again. Hence, the biochip system validates the concept of the photothermally driven antibody release from a DNA microarray and gives thus an opportunity of extension to more advanced applications. If antibodies directed to specific target are used, this approach may be furthermore explored in terms of micro-object release which makes the object of the following sections.
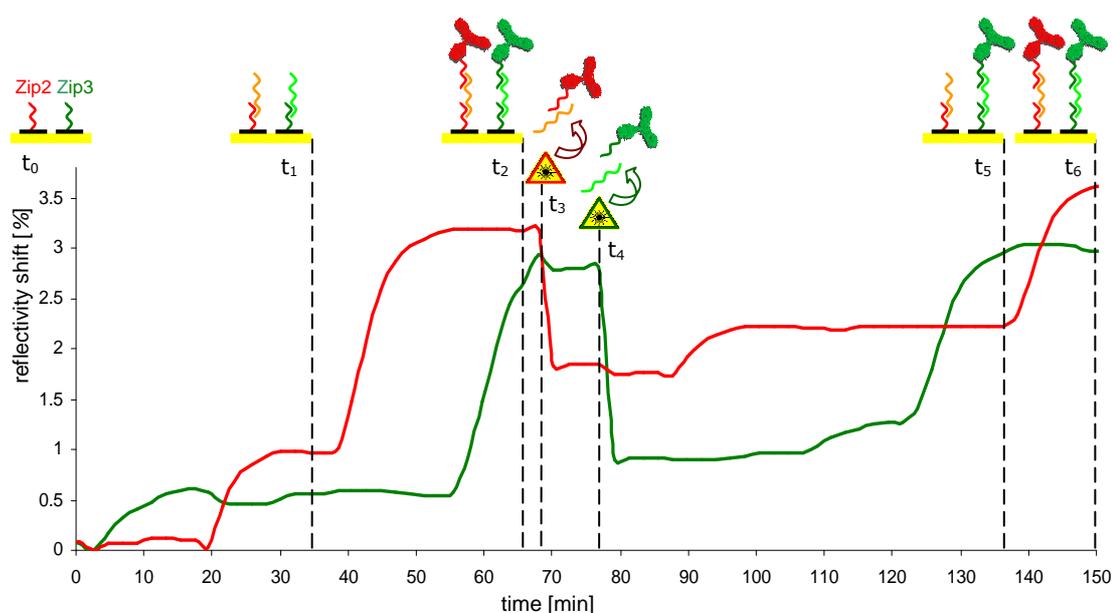
Figure 4.12 Surface Plasmon Resonance (SPR) monitoring of the biochip molecular construction and the photothermal desorption induced by laser beam. (t_0) Zip2 and Zip3 probes grafted on the gold surface; (t_1) intermediate strand hybridizations (Zip2*–*Pvu*II and Zip3*–*Nco*I); (t_2) immobilization of IgG–DNA conjugates (rab-IgG–*Pvu*II* and rab-IgG–*Nco*I*); (t_3) laser tracing on Zip2; (t_4) laser tracing on Zip3; (t_5), (t_6) reconstruction of molecular assembly. Zip2 and Zip3 signals are averaged and rectified by subtraction of NC signal (reference probe).

4.4.2   Molecular assembly capable of microbead immobilization

The present experimentation employs streptavidin-coated polystyrene (PS) microspheres. Polystyrene-based microparticles exemplify an easy to functionalize material which can be deployed for many applications. Chemical engineering of this polymer enables efficient conjugation with various biomolecules (DNA,[252] protein[253]) and generation of functional conjugates as potential tool for biosensing[254, 255] or development of immunoassay techniques.[253, 256] Wilson *et al.* report on the use of streptavidin-coated microspheres as a primitive model of cell or bacterium system. Interaction between streptavidin (STV) and biotin-modified target is thus supposed to mimic an interaction with the cell surface. In such case, it is a much simplified model of cell surface marker and antibody interaction since any antibody-antigen interaction is involved. Nevertheless, the STV-biotin, as having the highest dissociation constant among naturally occurring biological complexes, is a desirable couple for molecular biology assays. Therefore, streptavidin-coated polystyrene microbeads are chosen as target destined to test the developed capture-release strategy.
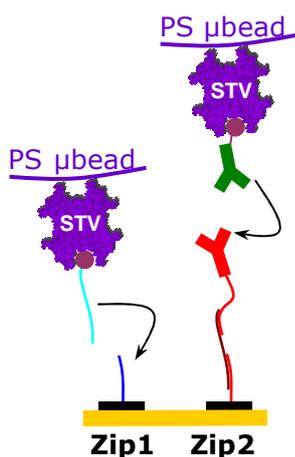
Figure 4.13 Schematic representation of molecular assemblies on Zip1 (Zip1*-biotin + STV-µbead) and Zip2 (Zip2*-*Pvu*II + rab-IgG-*Pvu*II* + IgG-anti-(rab-IgG)IgG-biotin + STV-µbead).

Because the photothermally driven target desorption from the gold surface is based on dsDNA dissociation, the on-chip immobilization of STV-PS microbeads has to involve hybridization process on DNA-based biochip. From the other hand, primary amine-modified oligonucleotides or antibodies can be easily coupled to biotin via biotin-NHS. Therefore, two molecular assemblies are employed for specific capture of the microspheres provided by STV-to-biotin affinity (Fig. 4.13). The former one is based on direct hybridization of a complementary biotin-modified oligonucleotide (Zip1). As to the latter one, microbead capture involves the interaction between an immobilized antibody (via antibody-DNA conjugate) and a biotin-conjugated secondary antibody assembled on the PS microbead (Zip2). The second case closely reproduces the molecular assembly which is here deployed as cell capturing construction. In this study, we use commercially available streptavidin-coated microspheres made of polystyrene and of 6 µm in diameter. SPR

imaging system enables detection of phenomena at a molecular level occurring on the gold surface. The microbead capture and desorption steps are evidenced by direct visualization under microscopy.

4.4.3 PS µsphere immobilization and release followed in SPRi and microscopy

As explained above, microbeads are captured on the gold surface functionalized with Zip1 and Zip2 probes, and according to two different molecular architectures. Thus, microbeads conjugated to Zip1*-biotin are immobilized on the Zip1 spots, while the Zip2 spots, previously assembled with intermediate Zip2*-*Pvu*II strand and rab-IgG–*Pvu*II* conjugate, are designed to capture microbeads coupled to biotinylated anti-(rab-IgG) antibody. The phenomena of target microbead immobilization and photothermally driven release are directly observed thanks to a transparent flow cell (*cf.* 4.2.1). As it turns out, the hydrodynamic conditions are crucial for the efficient capture and release of micro-objects. Significant non-specific (out-of-spot) adsorption of microspheres on gold surface is observed if the flow rate is too slow during injections. Therefore, when flow cell depth is quite big (*e.g.* PDMS flow cell of 1 mm depth), the buffer flux has to be decelerated to enable microbead sedimentation which results in a considerable side adsorption [*cf.* Fig. 4.14 c)]. Once the µbeads have been non-specifically adsorbed on the gold surface, they can not be removed even by a flow rate instantly increased (up to 500 µL/min which actually corresponds to a weak linear flow of 0.83 mm/s).
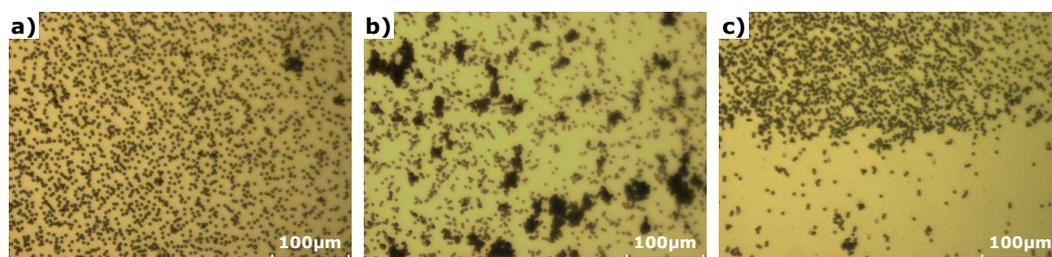
Figure 4.14 Polystyrene microsphere immobilization on the DNA-based biochip according to proper molecular assemblies. **a)** Zip1 spot centre; **b)** Zip2 spot centre; **c)** Zip1 spot boundary. PS µbeads are injected at 0.3 % (w/v) in PBS supplemented with 0.5 % of BSA. Self-aggregation is observed in the case of µbeads conjugated to biotinylated IgG (Zip2-based assembly). Tests are realized by using 1 mm PDMS flow cell.

Concentration of microbeads in the injected sample is also an important concern. Indeed, more than 0.3 % (w/v) of PS microbeads in the injection preparation favors out-of-spot µsphere immobilization despite surface blocking by 1% solution of BSA. Thus, higher content of PS microsphere should be avoided even if it facilitates direct observations of immobilization events - biochip spots are visible to the naked eye. Moreover, in the case of PS-STV microbeads conjugated to the biotinylated IgG (secondary anti-rab-IgG), high concentration of this antibody induces µsphere self-aggregation [*cf.* Fig. 4.14 b)]. Nevertheless, this phenomenon can not be entirely suppressed because several biotin moieties are potentially available to interact with their affinity sites placed on streptavidin

molecules and belonging to different µbeads. Taking into account all these concerns, optimal parameters are worked out in order to guarantee a specific on-chip µbead immobilization and restrain non-specific interactions.
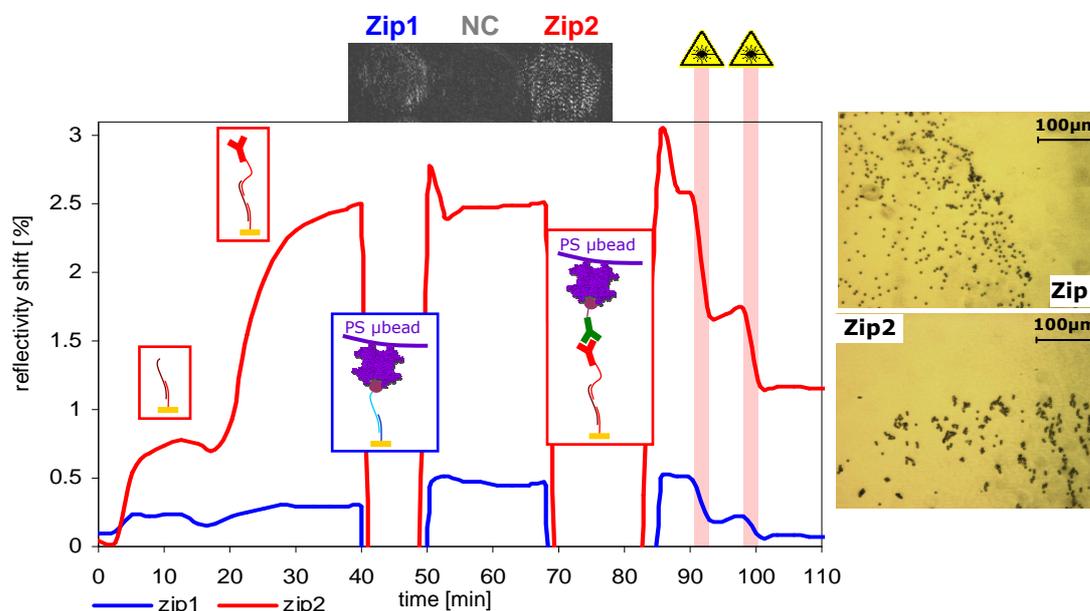
Figure 4.15 SPR monitoring of PS microbead capture and release. The following experimental steps are observed: Zip2*-*Pvu*II hybridization (3 min), rab-IgG-*Pvu*II* injection (18 min), loading of PS-µbead assembled with Zip1*-biotin (40 min), injection of PS µbead assembled with IgG-anti-(rab-IgG)-biotin (68 min), laser tracing on Zip1 and Zip2 (90 min, 98 min). Zip1 and Zip2 signals are averaged and rectified by subtraction of NC signal (reference probe). Inset images evidence specific microbead immobilization on Zip1 and Zip2 spots.

In order to drive the experiment in the optimal conditions, a flow cell of 150 µm in thickness is used in order to provide sufficient control of PS microbead immobilization on corresponding spots and limit non-specific interactions. The transparent flow cell is placed over DNA-functionalized gold surface in the SPRi configuration previously described. The biochip is prepared according to the electropolymerization method and provides DNA probe spots of 1.2 mm in diameter: Zip1, Zip2 and reference NC probe for background signal correction. As it was evidenced before, the running buffer has to be supplemented with the denaturing agent in order to facilitate DNA dissociation. Therefore PBS with 20 % of DMF (v/v) is flowed over the biochip at 15-25 µL/min during sample injection steps (linear flow of 0.17-0.28 mm/s) and accelerated to 250 µL/min during laser tracing (2.78 mm/s). The on-chip assembly is monitored under construction by SPR imaging system (Fig 4.15). Observations of kinetics result in an adequate signal as to DNA and IgG–DNA conjugate hybridization (Zip2) but registers only slight reflectivity shifts when microbead conjugates are captured (observed on both Zip1 and Zip2). In this case, the minor signal is probably due to microbead size which is not suitable for efficient detection in such SPRi configuration. It is because the SPRi detection is practically provided by the evanescent

wave penetrating into contact medium up to about 100 nm of depth and thus can not attain micrometric objects. Nevertheless, SPR differential images issued over microbead injections, show correct response on Zip1 and Zip2, unlike the reference probe signal (NC) that remains negative. Microbead capture, even if barely detected, is therefore specific and additionally confirmed by direct microscopic observations. Indeed, registered images evidence proper PS-µbead immobilization where no significant side adsorption is observed. We notice the presence of auto-aggregated µbeads on the Zip2 spot but, as it was said, it can not be avoided since multivalent interactions between PS-STV microbead and multi-biotinylated antibody are possible. Following target capture step, one may proceed to test the efficiency of the photothermally driven controlled release.

In the 4.3 section, we examined the first approach to the laser-induced photothermal desorption and confirmed the process specificity at molecular level. Subsequently, we use the analogous instrumental set-up to induce micro-object release by the local heating. A laser-diode of similar intensity range is thus deployed and PS µbead liberation evidenced by direct visualizations under a microscope objective. Subjected to plasmon resonance conditions, the laser beam is focalized on the biochip zone corresponding to immobilized target microbeads. Direct images are recorded by a camera along with laser displacement at 10 µm/s. In the demonstrated experiment (Fig. 4.15), the laser tracing is performed in two steps evidenced by SPR signal decreases registered on the both probes. The corresponding reflectivity shifts are mainly resulting from desorption of molecular entities. Therefore, it explains more significant decrease of Zip2 signal related to its more developed molecular architecture (involving IgG–DNA conjugate). Surprisingly, microscope visualizations reveal that microbead release does not take place on Zip1 spots at all and only in the slight extent in the case of Zip2 spots. In fact, a minor fraction of polystyrene microspheres immobilized on Zip2-based assembly is desorbed (Fig. 4.16). The observed phenomenon is instantaneous, being probably assisted by hydrodynamic forces provided by accelerated buffer flow (up to 500µL/min). The release efficiency has been estimated to less than 10 % within a few essays. Moreover, increase of DNA destabilizing agent content (DMF) to 40 % (v/v) does not generate more efficient microbead release. An extended irradiation by diode-laser (up to a few minutes) does not produce new microbead release events, neither.
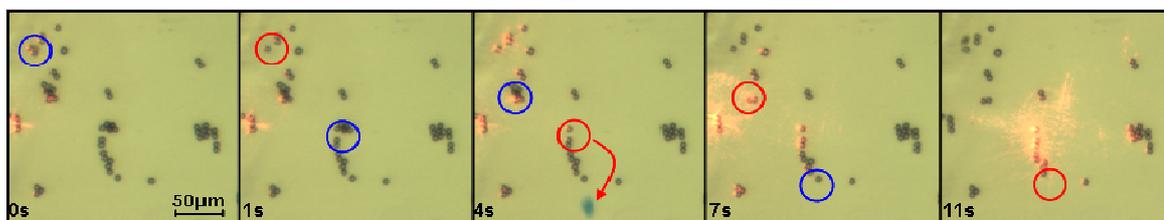
Figure 4.16 Sequences of images registered during laser-induced desorption of PS µbeads immobilized on Zip2 spot. Circles evidence zones of µbead release (before desorption in blue and after desorption in red). None of µbeads are desorbed from Zip1-based construction.

To explain different results observed on Zip1- and Zip2-based constructions as well as the low efficiency of the microbead release, we may consider this as an effect of different thermodynamic equilibrium attributed to the corresponding sequences. It is however difficult to point out an important contrast in the T_m values between Zip1-Zip1* and Zip2-Zip2* (or even *Pvu*II-*Pvu*II*) which can be estimated to less than 5°C. We must additionally take into account the fact that the microbeads are not directly attached to the support by simple DNA duplex. Therefore, in order to understand why the laser-induced microsphere release is not complete, we should look closer at molecular arrangement on the surface and consider contribution of more developed micro-object attachment than by simple double strand.

4.4.4 Multivalent interactions

In principle, microbead immobilization on the functionalized gold surface is enabled by the interaction between streptavidin and biotinylated intermediate molecules (oligonucleotide or antibody). As we know, the biotin molecule has a remarkably strong interaction with a homotetrameric protein STV which is characterized by an extremely high dissociation constant of ~10^{-15} M.[151] This biomolecular interaction represents the strongest ligand-receptor couple currently known. One streptavidin protein has four subunits with identical recognition sites for biotin molecule. Taking into account the strong affinity of biotin to STV and quadruple possibility of such interaction, more realistic model of on-chip assembly with PS µbeads should be considered (Fig. 4.17). Therefore the micro-objects may be anchored on the surface by multiple interactions. Probably, one microsphere is engaged within several STV-biotin bridges and with a few DNA duplexes. In order to obtain an efficient liberation event, all of the anchoring double strands should dissociate in the same time. However, locally increased temperature produces DNA melting phenomena in a fairly statistic way. That is why, an individually dissociated oligonucleotide is staying close to the surface and may eventually find a new complementary strand before all other neighboring DNA duplexes participating in µbead anchoring will dissociate. Hence, the probability of an instantaneous multiple dsDNA dissociation leading to microbead liberation is weak.

The aforementioned phenomenon finds reflection in DNA hybridization studies realized on a microarray and carried out with SPRi device equipped with temperature scan facility.[122] In the cited work, J. Fuchs demonstrates that DNA amplification by biotinylated oligomer conjugated to streptavidin (or STV-coated gold NPs) results in increase of the melting temperature. Considerable difference in T_m is revealed and attains about 15°C in the particular example of short oligonucleotides (15 bp). This study confirms the difficulty to perform an efficient detachment of PS microbead by local heating in the case when target is bound by multiple STV-biotin interactions. Perhaps, incorporation of more

powerful laser source (*e.g.* fiber laser) would be more efficient but it is not tested in the present approach.
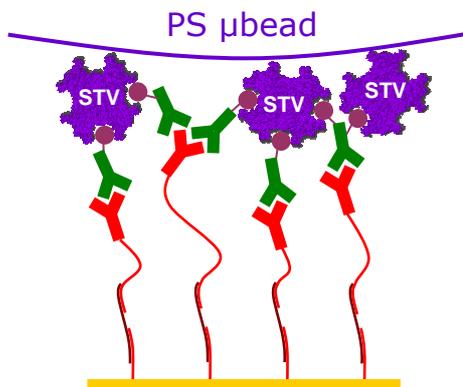
Figure 4.17 Realistic model of PS-µbead multiple binding. Each microsphere is equipped with several STVs, having four sites of specific interaction with biotin. Multivalent binding may be also explained by the presence of several biotin moieties on anti-(rab-IgG) antibody molecules (µbead self-aggregation).

Further tests could be carried out in the scope of enhancing micro-object release by the local heating. Improvement solutions could be mainly focused on limiting the multiple interactions: by using engineered streptavidin with only one binding site or by partially blocking the available sites for biotin recognition. It could reduce the potential multi-interaction of target microsphere with the immobilized probe and drive to more oriented on-chip capture. However, this development is not of real significance here, since PS microbeads are supposed to imitate the cell interaction with antibody where biomolecular recognition is directed by the abundant presence of cell membrane domains. This study demonstrates that photothermally induced release of microspheres is possible by using the proper on-chip assembly. In the particular case of Zip2-based construction the microbead immobilization relies on the antibody-antigen recognition (rab-IgG immunorecognition by anti-(rab-IgG) IgG) which may be ascribed to interactions occurring between cell membranar markers and specific antibodies. Although it remains only a very approximate model of cell capture on the surface, in the following section we will make use of the experience here acquired and realize controlled release of living cells by the means of laser-induced local heating.

4.5   Specific capture and controlled release of living cells

The photothermally induced release of living objects such as blood cells is the culmination part of the study described in the present chapter. We have learnt from the previous experiments that the local heating generated on the metal surface plasmons by laser irradiation may produce a controlled release of the molecular components or polystyrene microbeads. Desorption events are generated in a localized way and thus may concern targets of interest specifically immobilized on the biochip surface. In the present section, we indeed report on an efficient addressing of lymphocytes onto the biochip surface and their sequential release by laser illuminations. In addition to the results obtained in the restriction enzyme-based strategy (chapter 3), we demonstrate specific capture of splenocytes by means of microscopic observations. The controlled release of cells founded upon dsDNA dissociation by local heating is then evidenced.
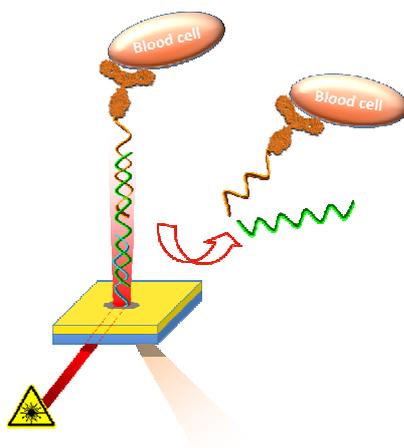
Figure 4.18 Schematic representation of lymphocyte release from the biochip surface induced by the photothermal effect. The cell is captured through specific antibody tethered on DNA-based assembly.

4.5.1   The experimental conditions

For the sake of the present work, we dispose of mouse splenocytes characterized by diameter of about 10 µm, which enables their direct observation in microscopy. Therefore, we benefit from the developed instrumental configuration where the biochip assembled with transparent flow cell is placed under a microscope objective (the configuration previously exploited by the occasion of PS microbead experiment). This set-up provides the possibility of real-time visualizations and follow cell capture and release happenings. Compared to microspheres, living cells are of more complex nature and various possible physicochemical interactions may be thus considered. As we have learnt before, an important issue is to create optimal conditions of the hydrodynamic flow in order to ensure

correct immobilization of cells on the specific spots and to reduce their non-specific adsorption on the surface.

The previously reported experiments driven with cells (the enzymatic release strategy) or microspheres evidenced that using a flow cell of an important thickness (1 mm) demands application of low flow rates which provide the micro-object sedimentation (weak volume flow rate) and important non-specific immobilization. The injection of lymphocytes in such microfluidic conditions implies more or less uniform distribution of the cellular sample over the gold surface. In this situation, specific spots can not be accurately determined. As previously evidenced, an efficient on-spot capture may be enabled by imposing sufficient flow rate and using smaller reaction chamber volume. However, as experience shows, by using too thin flow cell (*e.g.* 50 µm) none of cell immobilization events are observed by microscopy (even at a very slow flow rate).We speculate that in this particular fluidic conditions cells are submitted to considerable shear forces which disable their efficient on-chip capture.[70] Too small reaction chambers should be therefore avoided. In consequence, it is decided to use a flow cell of 200 µm thickness as described in section 4.2.1 and apply a flow rate of 30 µL/min at least. Linear velocity is therefore estimated to at least 0.25 mm/s at central cross-section of the reaction chamber.

4.5.2 Buffer biocompatibility

One of the major issues when working with living cells is to ensure biocompatibility of the experimental buffers. In this particular study, proper conditions need to be provided in order to trigger effective DNA dissociation and realize successful target desorption (live cell in our case). The former evaluation of the experimental parameters points out that the running buffer needs to be enriched with a denaturing agent (here 20 % of N,N-dimethylformamide) to enable sufficient destabilization of the DNA substrate. DMF is however an organic solvent which is not a standard component of cell culture media. Its polar nature may induce possible interactions with the cell surface and alter physicochemical properties of the cell membrane, *e.g.* microviscosity. DMF has been mainly considered in the terms of its toxicity in humans and animals but is not classifiable as a carcinogen by the International Agency for Research on Cancer (IARC).[257] Some studies driven on cancer cell cultures report on DMF-induced inhibition of cell culture growth (within many hours of incubation) and induction of cell morphological changes (*e.g.* flattening, low density cells or cytoplasmatic extensions).[258-260] In particular cases, loss of tumorigenicity or cells of more mature phenotype are observed. Nevertheless, all these effects are demonstrated to be reversible if DMF is removed from the cell culture medium.

Regarding to lymphocytes, DMF action has not been widely explored. It is however evidenced that DMF does not have mutagenic influence on human lymphocytes[261] and induces inhibition of lymphocyte proliferation during a long-time incubation.[262] Since the denaturing agent is crucial element of here used buffer that cells will get in contact with, it

has been decided to perform preliminary tests of splenocyte incubation in the presence of this reagent (*cf.* Fig. 4.19). It turns out that cell viability is sustained over 95 % within up to three hours of incubation in PBS supplemented with 20 % of DMF (v/v), independently if splenocyte growth is stimulated with ConA or not. In the particular case of our study, lymphocytes are suspended in the running buffer for a short time (lees than one hour). They get in contact with DMF only when injected to microfluidics and till laser-induced release. Once cells are released from the biosensor, they might be resuspended in a buffer devoid of DMF. Although DMF may alter cell morphology or growth, the effect is reversible as demonstrated by previous works. Such system may be thus successfully applied to cell sorting purposes.
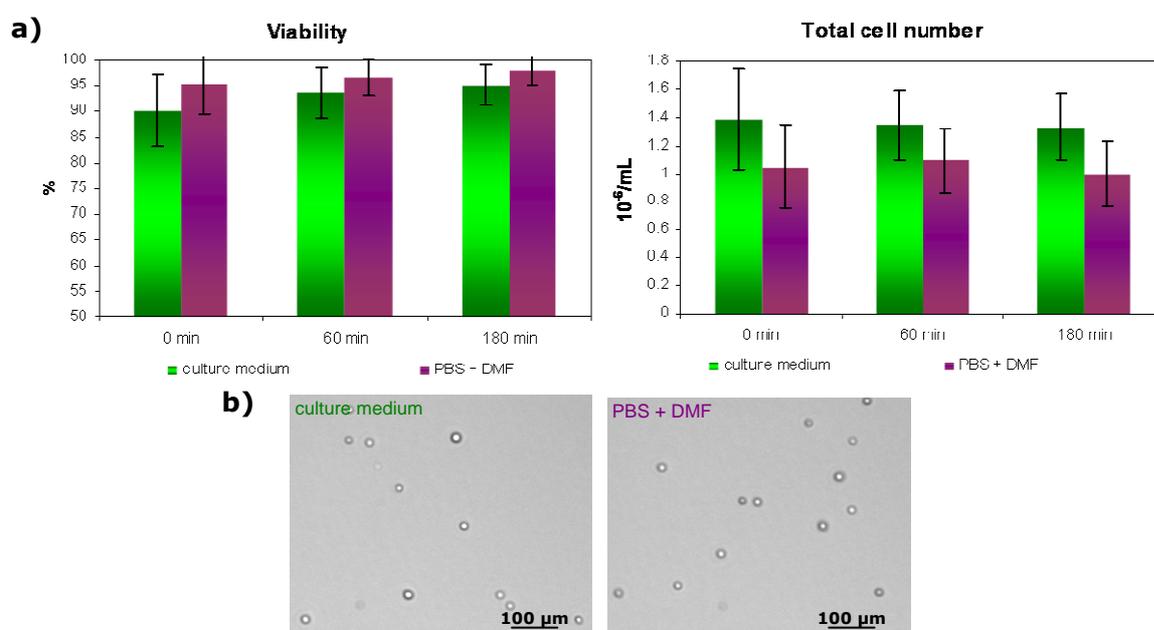
Figure 4.19 Incubation of the splenocyte sample in PBS supplemented with 20 % DMF (v/v). **a)** monitoring of cell viability within 3 hours of culture in PBS/DMF solution compared to standard RPMI medium. **b)** visualisation of cellular sample upon 48 h of incubation. Cell cultures are incubated at 37°C in the conditions of 95% humidity and 5% CO_2. DMF content do not reveals particular influence on lymphocyte viability and morphological appearance.

4.5.3   Specific lymphocyte capture revealed by microscopic visualizations

The developed strategy aspires to ensure controlled capture and photothermal release of primary lymphocytes, by basing on analogous molecular assembly as it was demonstrated for the enzymatically driven desorption. For this purpose, we use the previously exploited on-chip assembly relying on 3-component architectures. As mentioned above, the experiment is driven in PBS + 20 % DMF (v/v) and by using 200 μm flow cell assembled with DNA-biochip in the configuration of the home-made SPRi. A mixture of B- and T-type cells stimulated in 48 hour-incubation with ConA, is introduced and immobilized on the biosensor surface thanks to the specific immunorecognition. Therefore, B lymphocytes are directed to Zip1 spots assembled with anti-CD19 antibody whereas T lymphocytes are recognized on Zip2 spots where anti-CD90 antibody is tethered (both antibodies are immobilized through the relevant intermediate DNA strands and IgG–DNA conjugates). Zip3 probe serves as negative control since it undergoes hybridization with non-relevant IgG–DNA conjugate (anti-HcB-*Nco*I* and through Zip3*-*Nco*I). The step-by-step molecular construction is controlled in real time by SPRi which triggers analogous reflectivity shifts as those previously obtained with rab-IgG–DNA conjugates.

In addition to SPRi data, cell immobilization is monitored by direct observations under the microscope (Fig. 4.20). Following the injection of splenocytes, we notice their specific addressing on the corresponding spots (*i.e.* Zip1 and Zip2) and do not observe any of binding events on the negative spots (*i.e.* Zip3). Confined on-spot cell trapping and absence of significant non-specific adsorption validate the applied blocking protocol (BSA/cytochrome *c*) and the established hydrodynamic conditions. Moreover, under sufficient magnification we can clearly observe morphological differences between the immobilized cells which might confirm specific on-chip immobilization of the lymphocytes. Microscopic examinations of the splenocytes captured on the biochip surface reveal indeed a considerable size contrast between cells observed on Zip1 spots (*a priori* B lymphocytes) and Zip2 spots (deduced as T lymphocytes). We tend to explain this result by the fact that prior to experiment, the splenocytes are cultured in the presence of concanavalin A (ConA) reported as T cell stimulation factor.
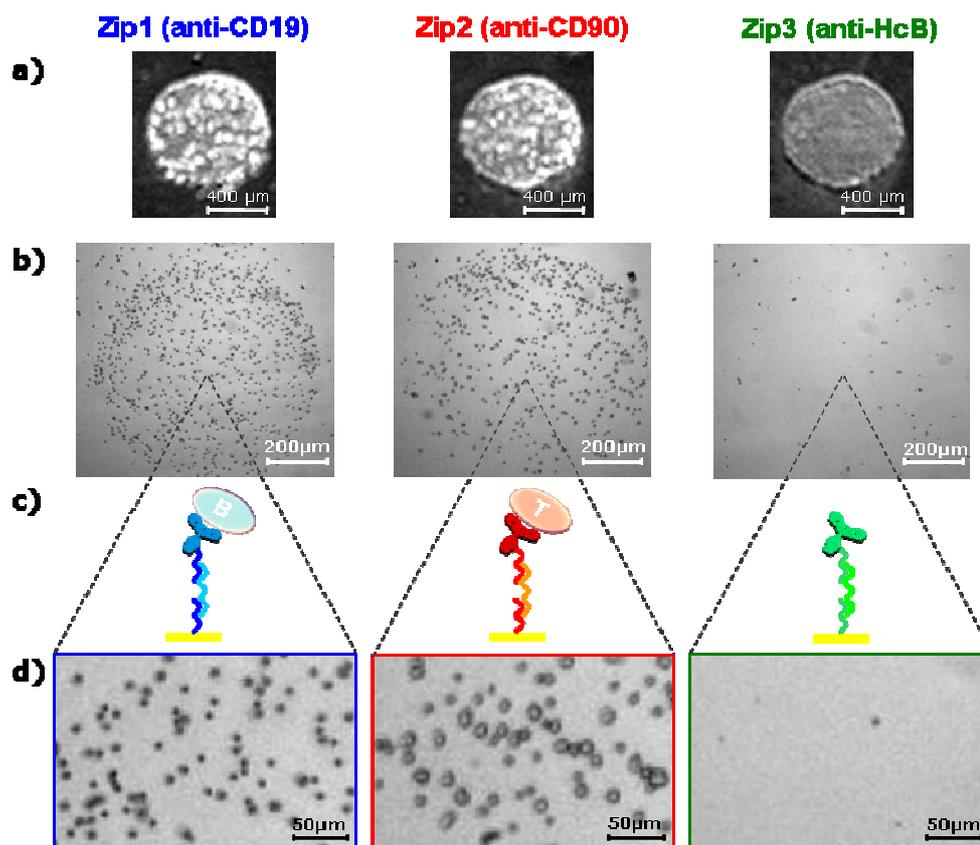
Figure 4.20 Specific capture of B- and T-lymphocytes on the DNA functionalized biochip and via cell directed antibody-DNA conjugates. B-cells are captured on Zip1 probe by anti-CD19 IgG and T-cells on Zip2 probe – by anti-CD90 IgG. Zip3 probe is used as negative probe and assembled with non-relevant anti-HcB IgG. **a)** SPRi images of Zip1, Zip2 and Zip3 spots; **b)** microscopic visualizations of the relevant spots under × 10 magnification; **c)** schematic representation of the on-spot molecular assemblies and resulting cell capture; **d)** numerical magnification on the relevant spot areas.

Concanavalin A is a homotetrameric lectin recognized as a mitogenic agent that provides preferential activation of large number of T-cells.[179] It binds with high affinity to D-mannose and D-glucose sugar residues being a part of glycolipidic and glycoproteic structures of cell surface.[263] Therefore, ConA presence in culture medium gives rise to cell agglutination which is also the case of the splenocyte culture here studied (a great number of floating cellular aggregates is observed starting from 24 hours of incubation). Concanavalin A induces proliferation of T-cells and enhances their energy metabolism by boosting ATP turnover.[264] Upon stimulation by the mitogenic agent, T lymphocytes constantly divide from lymphoblasts grouped in the agglutinated cell aggregates.[265] According to Abbas *et al.*, lymphoblasts are considered as large activated lymphocytes characterized by more important number of organelles and increased cellular metabolism reflecting a greater cytoplasmatic volume.[10] Incubation of mouse lymphocytes in the presence of ConA reveals in fact ~2 µm cell diameter growth within 48 hours of culture. (Fig. 4.21) Since the influence of concanavalin A on stimulation of murine B-type cells has not been evidenced, we can speculate that increased cell size is mainly due to T-lymphocyte growth. It seems to explain size differences observed for the lymphocytes

captured on the biochip and thus may testify a successful immobilization of B-cells on Zip1 spots and T-cells on Zip2. However, an independent test based on cell immunostaining by using fluorescence markers could be additionally envisaged in order to unequivocally confirm the specific cell capture.
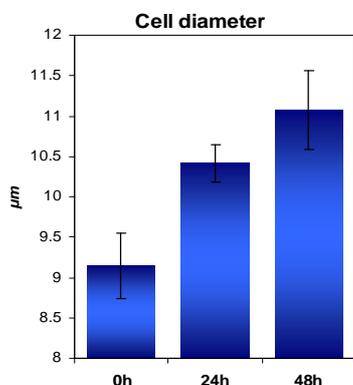
Figure 4.21 Lymphocyte diameter increase observed within 48h culture in the presence of ConA. Data retrieved from *Cell Viability Analyser Vi-Cell* (*Beckman Coulter*).

4.5.4 Lymphocyte desorption by the local heating

As we know, living cells are physiologically independent entities which equilibrium is prone to be destabilized in the presence of different environmental stimuli. Laser illumination is thus a potential source of cellular stress depending on its wavelength and intensity, optical focalization, irradiation time, *etc*. The beam of high-energetic photons may induce variations of thermal (temperature increase), electric or mechanical (*e.g.* cavitation bubble) parameters in the cell environment. The results of such modification can be harmful for the cell physiological condition. However, some studies show that laser-induced stress wave does not necessarily produce fatal-to-cell effects. Maezawa *et al.* elucidate similar influence on differentiation of cells when detached from a surface by laser-induced stress or by trypsin treatment.[266] Some lasers have also been safely used in the field of photothermal therapy. Near-infrared laser generating photothermal effect on gold NPs is shown to be marginally absorbed by biological tissues.[227, 267] Regarding to the single cell level, a red light laser is reported to produce some morphological changes[268] and enhance lymphocyte proliferation.[269] In these examples, laser biocompatibility is mainly discussed in terms of direct cell exposure to a laser beam. In the case of our study, cells are however introduced in the environment devoid of direct laser radiation (only small part of the laser energy is reflected on the glass-gold interface). Namely, the photothermal effect induced on the gold surface plasmons generates a non-radiative dissipation of the energy to the cell surrounding medium by means of the electric field enhancement and the temperature increase. These two parameters should be in reality considered as potential source of cell stress. However, as we will see, the obtained results seem to prove biocompatibility of the developed strategy.

The following experiments employ the optical configuration combined with the diode laser integrated with an optical fiber (P_{in} = 220 mW). Once the lymphocytes are specifically captured on the DNA-based molecular assembly, we proceed to their

sequential liberation by the laser irradiation. The photothermally driven release is executed locally on each relevant spot and followed in real time by microscopic visualizations (Fig. 4.22). The registered optical images evidence that surface lasing step induces the localized detachment of cells which occurs instantaneously. Since the laser tracing is remotely controlled, B- and T-type lymphocytes immobilized on the relevant spots (Zip1 and Zip2 respectively) are subsequently released in independent spot-specific steps.
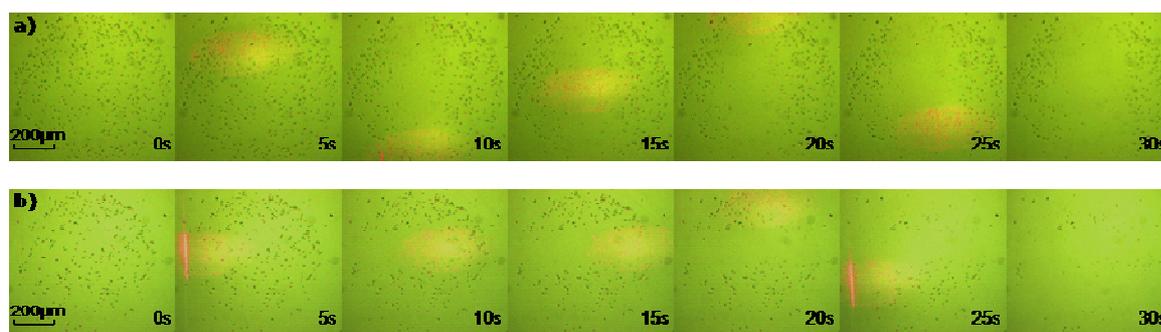
Figure 4.22 Sequential release of B- and T-type cells by laser beam: **a)** laser tracing on Zip1 spot and release of B lymphocytes captured via anti CD19– *Eco*RI*; **b)** laser tracing on Zip2 spot and release of T lymphocytes captured via anti CD90–*Pvu*II*. All images are obtained upon × 4 magnification.

Willing to realize photothermally driven cell sorting from the biochip surface, an important concern is also to evidence the reusability of such system. As it was previously demonstrated at the molecular level, oligonucleotide probes retain their integrity over lasing step and proper biochip assembly may be restored. In addition to this, we hereby prove that cells introduced to reconstructed microarray are still specifically captured on the spots where material was previously removed (Fig. 4.23).
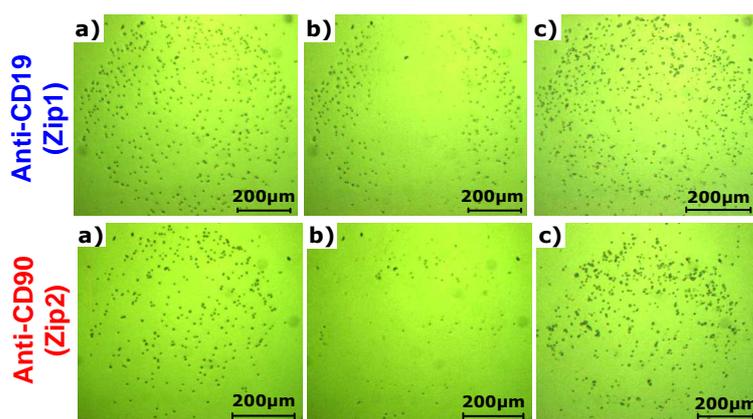
Figure 4.23 Reusability of the developed biochip system. **a)** B- and T-type lymphocytes immobilized by proper antibodies tethered on Zip1 and Zip2 spot, respectively; **b)** cell detachment by local heating; **c)** successful capture of splenocytes upon reconstruction of the relevant molecular assembly (Zip1*-*Eco*RI + anti-CD19–*Eco*RI* on Zip1 spot and Zip2*-*Pvu*II + antii-CD90–*Pvu*II* on Zip2 spot). All images are obtained upon × 4 magnification.

When performing microscopic observations during desorption step, the laser localization is identified as reddish spot barely observable because only inconsiderable percentage of the radiation is reflected (probably on the gold-glass interface defects) and may be directly observed. It confirms that a great part of the energy is involved in coupling with the surface plasmons and further transformation to the local heating. Considering single cell release events, we speculate that after the laser-induced DNA dissociation occurs, a liberated lymphocyte is orthogonally repulsed by convection currents and carried away in hydrodynamic buffer flow.

In reality, the laser spot specific to the fiber-diode laser is bigger that the one obtained for simple diode laser previously employed (laser spot diameter of ~550 µm and ~100 µm, respectively). This certainly results in better distribution of thermal energy to the local medium. Even if the level of energy consumed per surface unit is lower than for the diode-laser (0.3 compared to 1.9 µW/µm^2), we opine that the observed here micro-object desorption is mainly enabled by more efficient distribution of the locally produced heat. Namely, the laser spot of greater size generates larger profile of the heat diffusion which covers more of the surrounding solution volume. Although the measurement of local temperature increase is not done and comparative study is disabled, an efficient release of the immobilized cells induced by the fiber-diode laser is here demonstrated. More detailed characterization of the thermal conditions generated by the photothermal effect near the surface need further investigations and will be the object of a future work.

4.5.5 Laser-induced release observable at single cell level

In another approach, we attempt to demonstrate the photothermally driven release by observations at the level of the individual lymphocytes. Namely, we use a DNA-biochip functionalized by microcantilever technique which enables to obtain probe spots of a few micrometer size. This polypyrrole-based spotting technology has been developed in LAAS-CNRS laboratory from Toulouse (France) and offers the possibility of biomaterial deposition in form of miniaturized spots.[270-272] (Fig. 4.24) In a previous work, such high-density matrix is reported to realize an organization of lymphocytes by dint of specific antibodies grafted on the surface.[273] By using the relevant molecular assembly including IgG–oligonucleotide conjugates, DNA matrix is consequently transformed to the cell-specific antibody microarray capable of capturing one cell per each microspot of ~7 µm in diameter. Although totality of microspot matrix is not occupied by properly immobilized lymphocytes, we do not observe any cell binding on negative spots (polypyrrole in this case) and thus consider cell recognition as specific.

143
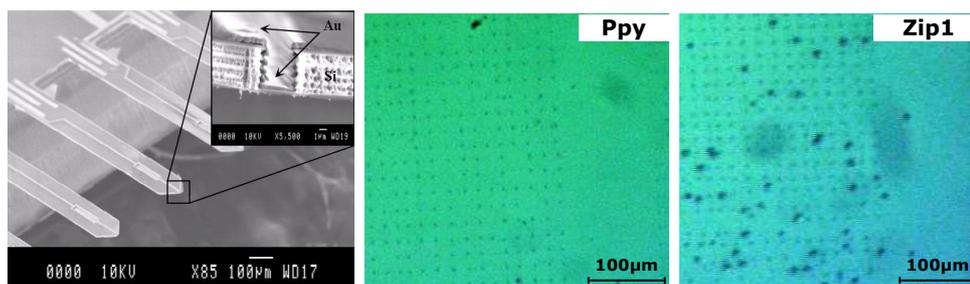
Figure 4.24 Lymphocyte immobilization on the DNA-based biochip functionalized by microcantilever (left image) electrospotting technique. The obtained microspots have about 7 µm in diameter and enable to resolve cell immobilization to each individual spot. Specific capture of the splenocytes is realized on the molecular assembly based on the IgG–DNA architectures.

One advantage when using the biochip of dense matrix composed of microspots is that we may focus on a smaller area of the local heating and observe release phenomena on the individual lymphocytes (Fig. 4.25). Cell liberation is in reality instantaneous and evidenced for single cells – optical magnification provides real time observation of individual lymphocytes released in the laser illumination spot and its subsequent carrying away in the buffer flow. From the registered images it is possible to conclude that lymphocytes keep their integrity since they are demonstrated as well-defined discrete objects withdrawn from the biochip surface by hydrodynamic flow. Although, any regular studies of morphological cell modification possibly produced in the photothermal effect are not carried out, we may consider the demonstrated results as sufficient to prove that such strategy may find an application to cell sorting purposes.
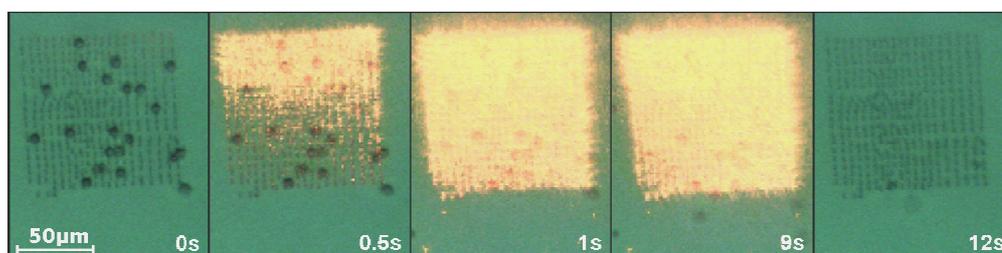
Figure 4.25 Focus on release phenomena of B-type cells by laser-induced local heating. Primary lymphocytes are immobilized on Zip1 microspot matrix via an antibody-oligonucleotide conjugate (anti-CD19–*Eco*RI*) and instantaneously desorbed by photothermal effect.

144

4.6 Conclusions

Recapitulating the presented findings, we must underline that photothermal effect assisted by surface plasmons can efficiently release material immobilized on a biochip surface. The developed instrumentation enables to realize locally defined desorption of molecular targets, synthetic microbeads and biological cells as well. Further improvement of the experimental set-up can be however foreseen. The proposed configuration requires certain level of manual manipulations - mainly between each step of laser-induced desorption, when the laser source is momentarily removed and SPRi signal retrieved. Better solution would be therefore to employ a pulsed laser permanently installed with SPR imaging set-up where a remotely controlled shutter could cut the signal registration for short intervals during the lasing step. This would enable simultaneous detection of reflectivity variations accompanied by photothermally induced desorption.

Further development may be also proposed in the matter of flow cell used in this study. Conception of new microfluidic modules may be foreseen in order to provide an oriented flow of micro-objects and to make their on-chip distribution more uniform. Pertinent solutions are given by advanced fabrication techniques based on lithography in polymers.[274] Cyclic olefin copolymer (COC) is an example of transparent and resistant polymer which is of great interest for new applications. Its excellent properties make it a high-tech material for micro- and nanodevice development.[275] The preliminary tests with COC-made microfluidic modules are currently carried out in the CREAB laboratory (L. Leroy, Y. Roupioz) and mainly focused on application to biochip systems based on living cells or bacteria.

The presented in this study approach may open up to new perspectives founded upon controlled release of species from a DNA microarray. The strategy benefits from the intrinsic thermodynamic properties of DNA double strand which can undergo dissociation if local heating applied. The advantage of the proposed approach is that the experiment is driven in the absence of markers, *i.e.* on native cells, and followed in real time by SPR imaging and microscopic examination. Moreover, the particular on-chip assembly enables regeneration of the original matrix that can be employed for further biosensing investigations. Since the biochip is based on DNA chemistry, a future development may rely on the conception of tunable system by introducing DNA building blocks of a different thermodynamic equilibrium (*e.g.* by point mutations or various DNA length) on the same sensor surface. It could thus produce abrupt dissociation events at well-defined temperatures giving birth to more sophisticated release strategies. Since a DNA matrix may be easily transformed to cell specific micropattern (thanks to antibody-DNA conjugates), an efficient cell sorting from complex biological extracts could be thus enabled.

Apart characterization of cellular suspensions, the developed methodology may find also other applications. As it has been demonstrated in our study, samples issued from

the experiment are assayed by mass spectrometry technique in terms of specific protein identification. In this particular case, such proceeding is a kind of proof-of-concept that confirms target-specificity of the developed release strategy. Nevertheless, the present methodology may become a powerful tool to analyze complex biological samples (*e.g.* plasma, cell culture supernatants), if further improvements are introduced. Integration of DNA biochips and protein-DNA conjugate chemistry into Surface Plasmon Resonance technique combined to MS analysis may give solid bases for construction of novel versatile device potentially explored in the field of proteomics. Automation of sample identification process, reduction of recovered sample volume[192] and enabling investigation from weak quantities of analyte would thus open various applications for the ligand fishing from diverse biological materials.[234]

Chapter 5

Conclusions and perspectives

Concluding the present PhD thesis, I would like to recapitulate the overall findings here reported and put forward some perspectives that the developed biochip can open up to. By this work, we have shown the example of biochip performing in selective capture of several molecular and cellular targets as well as their subsequent release under spatio-temporal control. DNA-based matrix has been therefore proposed as a miniaturized molecular platform, easy to fabricate and handle, making it a versatile tool for biosensing strategies. It was demonstrated that a DNA microarray can be readily turned into an antibody pattern with help of proper antibody-oligonucleotide conjugates. The developed synthetic approach permitted to obtain a monoconjugated IgG–DNA product with satisfactory yield and proven functionality in the three-component biochip assembly. Further, the proposed conjugation protocol might be applied to create a set of IgGs combined with exclusive DNA oligomers in order to realize multiplexed capture of several targets. By using antibodies directed to specific antigens (*e.g.* proteins, cells, bacteria), they can be properly addressed on the biochip surface and thus open up an opportunity of efficient "ligand fishing" or cell sorting from a heterogeneous mixture. Indeed, the reported study has evidenced a controlled sorting of B and T lymphocytes to well-defined spatial locations, characterized by cell-specific molecular assemblies.

The main goal of the present project was to enable a specific sorting of cellular samples into individual fractions of cells. According to the announced objectives, we have demonstrated a DNA-based microarray performing selective capture and subsequent release of B and T lymphocytes characterized by specific phenotypes (CD19 and CD90, respectively). Living cells were addressed on the biochip with help of corresponding surface functionalization, resulting in great affinity to the defined cell type (anti-CD19 and anti-CD90 IgGs). Proper molecular assemblies allowed efficient immobilization of the lymphocyte subsets onto spatially confined areas: large spots (several hundreds of cellular entities per spot) or microspots (one cell per spot). Subsequently to the realized on-chip capture, cells were shown to be released by dint of two independent strategies.

The former approach of cell release was provided by the enzymatic cleavage performed with help of endonucleases yielding a specific digestion of well-defined DNA sequences (restriction sites). The latter methodology relied on direct dissociation of dsDNA substrates enabled by local heating generated in the photothermal phenomenon. The main features of the both proposed strategies are grouped in Table 5.1. By the present work, we have demonstrated the performance of the proposed strategies by realizing a programmable sorting of two types of lymphocytes. Both developed approaches can be potentially extended to more multiplexed system, ensuring specific release of several cellular targets. On the one hand, it can be achieved by using different commercially available restriction enzymes which are prone to perform precise cleavage at different oligonucleotide sequences. On the other hand, laser-induced dissociation of double-stranded DNA offers a possibility to use thermodynamically different substrates which

denaturation is achieved at a distinct level of the local heating (*e.g.* point mutations).[122] In the first case, using several restriction enzymes in a single experiment incurs however a risk of star activity (relaxation or alternation of enzyme specificity) and considerably increases the cost of cell sorting strategy. The method based on photothermal desorption seems to be more straightforward and does not involve the use of costly reagents. The main issue of the second strategy is employment of sophisticated instrumentation which involves integration of optical elements (SPRi system, laser beam) and precise mechanical control system (positioning of the laser spot). Nevertheless, the both proposed capture-release systems benefit from a real-time and label-free detection by SPRi. Unlike FACS- or MACS-based methods, the developed approaches enable to conduct an assay on crude biological samples devoid of particular pre-processing step (*i.e.* labeling). Moreover, a great advantage of the DNA-based biochip is that it can be regenerated and the original matrix recovered, once an individual test has been accomplished. In the future, it could thus provide an opportunity for high-throughput studies of complex cellular samples in the scope of human immunology or for biomedical investigations.

	ENZYMATIC CLEAVAGE	LASER DRIVEN DESORPTION
principle of cell release	enzymatic digestion of DNA substrate	dissociation of dsDNA by local heating
desorption time span	several minutes	over seconds
source of multiplexed analysis	multitude of restriction sites	large variety of synthetic oligomers (different sequence lengths, point mutations)
weakness of cell sorting strategy	consumption of additional reagents (enzymes)	sophisticated instrumental set-up (SPRi combined with precisely controlled laser source)
potential improvements	- recovery of cell fraction - simultaneous microscopic observations	- new flow cell design - introduction of a pulsed laser for simultaneous SPRi detection and laser desorption - recovery of released samples (cell sorting, *ligand fishing)*
required conditions for successful release	- temperature 37°C - buffer (Mg^{2+} content)	- powerful laser source - destabilizing conditions (addition of DMF)
advantages	- highly-specific cell capture based on immunorecognition - robust biochip molecular assembly (DNA matrix, IgG–DNA monoconjugation) - reusability (regeneration of the original matrix) - label-free method (no sample pre-processing needed) - simultaneous monitoring of molecular and cellular events	

Table 5.1 Comparative table of both developed strategies of cell sorting

The hereby developed biochip system emerges therefore as a potential cell sorting tool prone to find an application in advanced studies on blood cells. The reported findings describe selective release of B and T lymphocytes from a functionalized surface into separate fractions that can be imaginably devoted to downstream analysis at different level (whole-cell functional assays, transcriptomics and proteomics). Thus, the established study provides an attractive element in the field of research on the undiscovered aspects of the human immunology. Indeed, thorough studies on a precise lymphocyte family could pave the way to better understanding of defense mechanisms against pathogenic infections, malignancies or particular reactions of auto- and allo-immunity. Apart from answering many questions of the immunological nature, profound examination of individual lymphocyte populations could drive to formulation of novel strategies to cure various diseases with immune foundations. Indeed, numerous infectious disorders still do not have an efficient treatment (*e.g.* HIV) and evaluation of new vaccines and biological drugs is of great interest. Bioassays carried out on specific lymphocyte units might provide a detailed screening of immune cell responses upon contact with antigen and thus enable essential information in the design of novel pharmaceutics. A special focus in the development of new vaccines is ascribed to cancer immunology. Currently employed methods examine lymphocytes on a large scale and thus only offer statistically meaningful results. Investigation of discriminated populations of the immune cells is a valuable approach that shall give a larger insight into immune responses involved in cancer. Further, comprehensive examination of individual subsets of lymphocytes is highly advantageous when assaying immunological responses against effectors originating from the same or foreign host organism. It could open up to rational treatment of autoimmunity disorders and rapid diagnostics in the field of clinical transplantation.
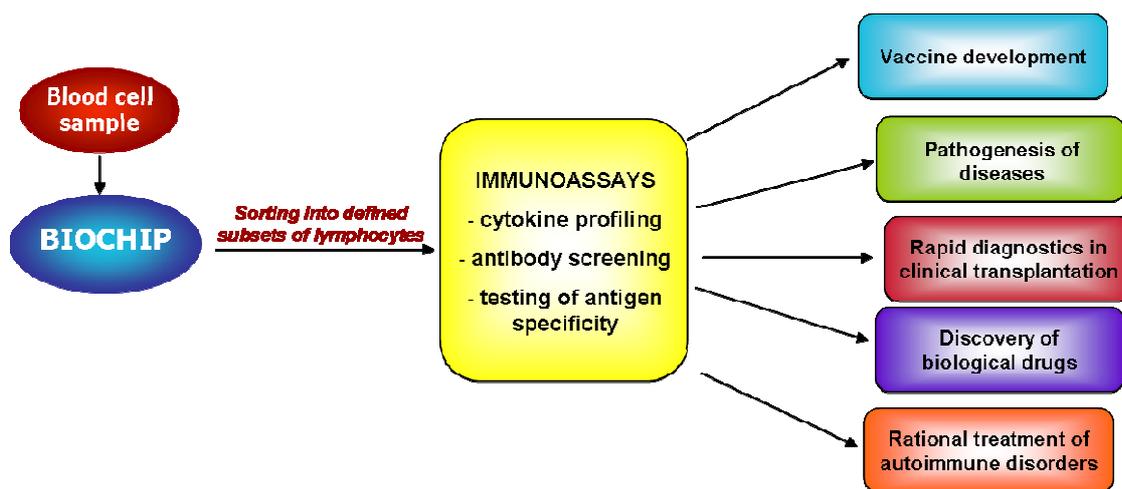
Figure 5.1 Potential applications of the developed biochip in studies on several aspects of the human immunology.

152

In the matter of cell-based biosensors for research goals, an extremely challenging approach is to provide the design of such miniaturized systems that are capable of working at single cell level. Strategies of that kind are extremely attractive for various research purposes because they offer a great potential to discover particular features of a cell type of interest in terms of its proper functionality and physiology.[276] Such approach is also interesting in regard to studies based on immune cells, aiming to reveal complex mechanisms of immunological responses.[277]

Using the molecular tool developed in this work, an intriguing study is currently carried out on development of an original biosensor that may be potentially employed to explore lymphocytes at a single cell level. As a fruit of collaboration with J. Liu (CREAB), we demonstrated a specific trapping of individual immune cells inside pores of micrometric size (*cf.* Fig. 5.2). The inner wall of such micropore was originally functionalized by Zip sequences (using CLEF process)[278] and a single lymphocyte was captured by dint of the cell-specific antibody combined with a corresponding DNA strand. Therefore, this study exemplifies the development of a single-cell biosensor that may give the opportunity of thorough studies driven on various cellular samples from the angle of individual cell metabolism (*e.g.* secretory activity), morphological changes, pathologic behavior, *etc.* In the field of assays at single-cell level, an extremely interesting approach is to give the insight into functionality of an exclusive immune cell unit (a lymphocyte characterized by a well-defined phenotype)[33, 34] and further development will be continued in this direction.

Figure 5.2 T lymphocyte captured inside a micropore. Inner wall of the µpore is functionalized by Zip2 and the cell is trapped by dint of adequate molecular assembly (Zip2*-*Pvu*II + anti-CD90–*Pvu*II*).

Isolation of well-defined cell samples emerges not only as a breakthrough in the fundamental research but in biomedical field as well. Even if the proposed microsystem is far from a real "point-of-care" device, such cell sorting methodology could be foreseen as a potential tool in medical diagnostics. It could therefore enable a rapid and label-free assessment of parameters based on blood cell sampling (*e.g.* cancer biomarkers, viral antibodies). Biomedical application demands however that a potential test fulfills several important criteria like precision of measurement, linearity and reproducibility of the generated data. Every diagnostic tool needs to answer to these requirements for a standardized performance before it really finds the application at the site of patient care. We consider the present work as development of a building block of potential diagnostic device that in the future may find the light of day.

Chapter 6

Experimental section

This chapter introduces all necessary elements concerning the experiments which results have been discussed in the previous parts of the present manuscript. At the beginning, an exhaustive list of the used materials is presented where following items are listed: chemical reagents, synthetic oligonucleotides, biomolecules (antibodies, proteins) and finally cells assayed within the framework of hereby reported studies. Subsequently, detailed protocols of the concerned experiments are described. A step-by-step description of these proceedings gives thus thorough insight into the developed experimentation and if needed may help to reproduce it in the future.

6.1 Experimental supplies

Chemicals

→ NaCl, KCl, Dithiothreitol (DTT), NaOH, H_2SO_4 96%, H_2O_2, Dimethyl sulfoxide (DMSO), Sodium dodecyl sulfate (SDS), Tris(2-carboxyethyl) phosphine hydrochloride (TCEP), 1-dodecanethiol, Phosphate Buffer Saline (PBS), Ethylenediaminetetraacetic acid (EDTA), salmon DNA (10mg/mL), Denhart 50x, acetonitrile, RPMI-1640 culture medium, Sodium pyruvate, 2-Mercaptoethanol, Penicilin-Streptomicin stabilized solution, , $MgCl_2$ (*Sigma-Aldrich, France*)

→ NH_4HCO_3, $LiClO_4$, N,N-Dimethylformamide (DMF), Tween20 (*Fluka, France*)

→ Ethanol (96.2% and 99.9%) (*Carlo Erba reagents*)

→ Tris-HCl (Tris(hydroxymethyl) aminomethane) (*Interchim, France*)

→ Pyrrole (*Tokyo Casei, Japan*)

→ Streptavidin conjugated polystyrene microspheres 6µm (*Polysciences Europe GmbH, Germany*)

→ SM(PEG)$_{12}$ (succinimidyl-[(N-maleimidopropionamido)-dodecaethyleneglycol), Succinimidyl-6-(biotinamido)-6-hexanamido hexanoate (biotin-NHS) (*Thermo Fischer Scientific, France*)

Materials

→ Glass prism (angle 60°) top-coated by double metallic layer: titanium 5nm and gold 45nm of thickness (*Horiba Scientific-GenOptics, France*)

→ Glass slide for microscopy coated by double layer: chromium (2nm) and gold (55nm) (*Schott Swiss SA, Switzerland*)

→ HPLC column: HiTrap^{TM} Q FF 1mL (*GE Healthcare, UK*)

→ Spin filter membranes (500µL) 3kDa, 30kDa and 50 kDa MWCO (*VivaScience, France*)

→ NAP^{TM} 5 columns, Sephadex^{TM} G-25 (*GE Healthcare, UK*)

Oligonucleotides

The oligonucleotide sequences were all purchased from *Eurogentec (France)*. Probe sequences (oligonucleotide-NH_2(3')) were coupled to Py-NHS as previously described.[279] Zip1*-NH_2(3') was conjugated to biotin-NHS as follows: biotin-NHS was added in 20 molar excess to ~30 µM solution of the oligonucleotide (in PBS, pH 7.4) and reaction was maintained during 60 min in room temperature; the conjugation product was purified on NAP^TM 5 column (elution with deionized water) and final concentration assigned by 260 nm absorbance measurement. This and all further absorbance measurements were realized by using ND-1000 Spectrophotometer Nanodrop (*Labtech International*).

Table 6.1 Oligonucleotide sequences employed in the present work.

Name	Sequence (5′→3′)
	Probes
Zip1	pyrrole-(T_{10})-GACCGGTATGCGACCTGGTATGCG
Zip2	pyrrole-(T_{10})-GACCATCGTGCGGGTAGGTAGACC
Zip3	pyrrole-(T_{10})-TGCGATCGCAGCGGTAACCTGACC
NC	pyrrole-(T_{10})-TGGAGCTGCTGGCGT
	Intermediate strands
Zip1*–*Eco*RI	TACCTTCG-**GAATTC**-ACTCGCACCGCATACCAGGTCGCATACCGGTC
Zip2*–*Pvu*II	GACAAGGT-**CAGCTG**-TAGGCAAGGGTCTACCTACCCGCACGATGGTC
Zip3*–*Nco*I	CACTCACT-**CCATGG**-GCACTTGCGGTCAGGTTACCGCTGCGATCGCA
	Targets
*Eco*RI*	GTGCGAGT-**GAATTC**-CGAAGGTA-(T_{10})-SH
*Pvu*II*	CTTGCCTA-**CAGCTG**-ACCTTGTC-(T_{10})-SH
*Nco*I*	GCAAGTGC-**CCATGG**-AGTGAGTG-(T_{10})-SH
Zip2*	HS-(T_{10})-GGTCTACCTACCCGCACGATGGTC
Zip1*–biotin	biotin-(T_{10})-CGCATACCAGGTCGCATACCGGTC

Complementary target strands are pointed out by an asterisk (*).
Restriction sites are expressed in **bold type**.

Antibodies

$\rightarrow$ IgG from rabbit serum (Sigma-Aldrich, France)

$\rightarrow$ Biotin-modified anti-rabbit IgG (whole molecule) antibody produced in goat (Sigma-Aldrich, France)

$\rightarrow$ Monoclonal rat anti-mouse CD19 (clone: 1D3) (BD Biosciences, France)

$\rightarrow$ Monoclonal rat anti-mouse CD90 (clone: G7) (BD Biosciences, France)

$\rightarrow$ Monoclonal mouse IgG anti-HcB domain kindly provided by L. Bellanger (CEA/IBEB, France)

$\rightarrow$ Rabbit anti-CbpE IgG was provided from the *Institut de Biologie Structurale* (Grenoble, France)

Proteins

$\rightarrow$ Streptavidin-R-phycoerythrin (STV-PE) (*Invitrogen, France*)

$\rightarrow$ Concanavalin A (ConA) (*Sigma-Aldrich, France*)

$\rightarrow$ Creatine kinase brain and muscle fractions, human (CKBB and CKMM) (*VWR, France*).

$\rightarrow$ Bovine serum albumin (BSA) (*Sigma-Aldrich, France*)

$\rightarrow$ Foetal bovine serum (FBS) (*Sigma-Aldrich, France*)

$\rightarrow$ *Eco*RI enzyme 20,000U/mL (*New England Biolabs, UK*)

$\rightarrow$ *Pvu*II enzyme 10,000U/mL (*New Englands Biolabs, UK*)

Buffers

$\rightarrow$ Hybridization buffer H: NaCl 537mM, K_2HPO_4 10mM, KCl 2.7mM, Tween20 0.1%, Denhart 50x 2%, Salmon DNA (10mg/ml) 0.1%, pH 7.4

$\rightarrow$ Rinsing buffer R: NaCl 537mM, K_2HPO_4 10mM, KCl 2.7mM, Tween20 0.1%

$\rightarrow$ Buffer GDALi: $LiClO_4$ 100mM, glycerol 1% (v/v), acetonitrile 30% (v/v), DMSO 20% (v/v), prepared in 25mL of deionized water (18.2 MΩ.cm)

$\rightarrow$ PBE buffer: PBS, EDTA 5mM, pH 6.8 (IgG–DNA coupling reaction)

$\rightarrow$ Blocking solutions: 1% BSA (w/v) in PBS; 2µM cytochrome *c* in PBS; 10µM BSA + 5µM cytochrome *c* in PBS

$\rightarrow$ Running buffer 1: PBS, $MgCl_2$ 10mM, pH 7.4 (enzymatically driven release assay)

$\rightarrow$ Running buffer 2A: PBS, DMF 20% (v/v), pH 7.4 (laser-induced desorption of microbeads and cells)

$\rightarrow$ Running buffer 2B: NH_4HCO_3 200mM, DMF 20% (v/v), pH 7.8 (laser-induced desorption of proteins for downstream MS analysis)

→ Buffer A: NaCl 137mM, Tris-HCl 20mM, pH 8.0 (HPLC purification)

→ Buffer B: NaCl 1M, Tris-HCl 20mM, pH 8.0 (HPLC purification)

Culture media

→ RPMI-1640 culture medium (*Sigma-Aldrich, France*)

→ DMEM culture medium (*Invitrogen, France*)

→ TH liquid broth (*BD Biosciences, France*)

Cells and bacteria

→ LS-102.9 (B cell hybridoma) and 3A9 (T cell hybridoma), collaboration with P. Marche from *Institut Albert Bonniot (IAB)* in La Tronche (France).

→ Mouse splenocytes (C57Bl/6), collaboration with *IAB* (La Tronche, France)

→ *Streptococcus pneumoniae* bacteria (R6 strain), collaboration with T. Vernet from the *Institut de Biologie Structurale (IBS)* in Grenoble (France).

6.2 Experimental procedures

6.2.1   DNA biochip fabrication by electrospotting

DNA chips were prepared either on a gold-coated glass prism (SPRi experiments) or on a glass slide (fluorescence immunoassay). Prior to functionalization, the gold layer was cleaned from potentially adsorbed impurities by a piranha solution (2:1 H_2SO_4/H_2O_2 mixture; Caution: piranha solution is exothermic and strongly reacts with organics). An alternative solution was to use physical cleaning by oxygen/argon (75%/25%) plasma stream (plasma cleaner by Electronic Diener GmbH, Germany) but this protocol was not regularly employed. The cleaned gold surface was then immersed in 20 mM solution of 1-dodecanethiol (in 99.9 % ethanol) for ~30 min at room temperature. By means of SAMs, a hydrophobic layer was formed in order to enable better confinement of probe spots and avoid inter-spot contamination during the electrospotting process. After the hydrophobic treatment accomplished, the surface was rinsed through successive washes with ethanol (96.2 %) and deionised water (18.2 MΩ.cm). The DNA probe grafting was subsequently realized upon electropolymerization method by using a home-made spotting device as previously described.[121, 122]

Solutions of several oligonucleotide probes (*cf.* Table 6.1) were prepared in GDALi buffer and could be stored up to 24h before use (4°C). Each spotting sample contained 20mM of pyrrole monomer and pyrrole-modified probe at 0.2 µM, 1 µM, 5 µM or 10 µM depending on the experiment. Subsequent concentrations of DNA oligomer were prepared by dilution in series with 20 mM pyrrole solution (in GDALi). Electrochemically directed copolymerization steps were achieved by using a micropipette tip (10 µL) with an opening diameter (ϕ) of around 400 µm, 800 µm or 1200 µm, equilibrated with the 20 mM pyrrole solution prior to use. The counter electrode (platinum wire inside the tip) and the working electrode (gold surface) were connected to an external potentiostat (SP-200, Bio-Logic Science Instruments or PGSTAT30, Autolab). The pipette tip was filled-up with a relevant probe sample and placed over gold by using a motor control device (ESP300, Newport). Probe-bearing Ppy spots were synthesized by 2V electric pulse of 100 ms (100 µA of current range). Size of thus obtained spots was reflected in a charge recorded during the deposition step: ~1.5 µC (ϕ = 400µm), ~2.8 µC (ϕ = 800 µm) and ~8.8 µC (ϕ = 1200µm). The registered charge values testified nanometric thickness of the grafted Ppy film which is crucial for SPRi detection sensitivity.[123] Density of thus deposited oligonucleotide probe was estimated to around 10 pmol/cm^2.

Successive polymerizations were carried out upon the same process with different oligonucleotide probes. Between consecutive tip loadings, the microcell was abundantly

washed with 20 mM Py in GDALi buffer in order to reduce the cross-contamination risk. Zip probes as well as NC (negative control) were deposited in multiplets to control the reproducibility (3-10 spots per probe). In a special case of biochip devoted to the photothermal protein desorption and further MS analysis, large and more numerous spots were grafted (over a dozen of 1200µm in diameter). As soon as the deposition of DNA matrix has been accomplished, the prism (or slide) was disconnected from the system, rinsed abundantly with deionised water and after drying under an argon stream, stored at 4˚C. Washing step was performed by dipping upside-down in a big volume of water in order to avoid "comet tail" effect (*cf.* Fig.3.12). Such biochip was used within a few days but yielded a good hybridization signal when used after several months of proper storage. Removal of the polypyrrole and complete regeneration of the gold surface could be achieved by incubation overnight with 10% solution of commercial bleach.

6.2.2   DNA biochip fabrication using microcantilever system

Willing to reduce the probe spot size, electropolymerization was performed by using microcantilever system developed at the LAAS-CNRS laboratory (Toulouse, France).[280] This system based on electrochemically driven deposition of Ppy film, permits to obtain up to 250,000 spots per cm^2 and of ~7 µm in diameter. Analogously to previously described method, spotting solutions used in the experiment (1: Zip1-Py 10 µM + Py 20 mM; 2: Py 20 mM) were prepared in GDALi buffer (supplemented with 25% (v/v) of glycerol to avoid excessive evaporation). Successive electro-polymerization steps were done by using microcantilever set-up[272] providing precise control of the cantilever position by an external step motor. Analogously to the electrospotting process described above, cantilevers were filled up with the relevant spotting solution and placed over the gold layer. A 2 V potential difference was then applied (100 ms) between gold surface (WE) and the gold canal of the silicon cantilever (CE). The microarray was produced by successive "touch and go" steps giving rise to a matrix composed of Zip1 probe spots (5 µm or 15 µm of lateral interval) and negative control Ppy spots (15 µm of lateral distribution).

6.2.3 DNA and IgG coupling reaction

An antibody coupling with a short DNA oligomer (thiolated target oligonucleotide) was performed by using the hetero-bifunctional cross-linker SM(PEG)$_{12}$ according to the protocol represented on Fig.2.6 b). In the first step, an IgG molecule underwent covalent coupling with the cross-linking agent. An appropriate IgG was suspended at 10-20 µM in pH 7.4 PBS buffer, then 100 molar excess of the SM(PEG)$_{12}$ (stock solution at 100 mM in DMSO) was added and the obtained solution gently stirred. The IgG activation reaction was carried out for 1 h at room temperature. The reactive sample was consequently purified on a NAP^{TM} 5 column previously equilibrated with PBE buffer (triple washing) in order to remove the excess of the cross-linker. Purification eluate was therefore concentrated by using 30 kDa MWCO spin filter membrane (15 min, 15000 g; single washing with PBE) and suspended in PBE at ~25 µM. The concentration of the activated antibody-maleimide was determined by 280 nm absorbance measurement (ε_{280} = 210000 M^{-1}.cm^{-1}).

In parallel to the antibody activation, a DNA oligomer suspended in deionised water (80-95 µM) was mixed with TCEP (5 mM of final concentration) and the solution was homogenized. The reductive agent was added to eradicate disulfide bonds possibly formed between thiolated DNA oligomers, prior to further coupling. The reduction reaction was run for 30 min at room temperature, followed by purification on a NAP^{TM} 5 column (elution with PBE). The obtained eluate was concentrated by using 3 kDa MWCO membranes (15 min, 15000 g; double washing with PBE). The final concentration in PBE was assayed by 260 nm absorbance measurement.

The final conjugation was subsequently realized. For this purpose, solutions of reduced DNA oligomer and maleimide activated IgG were put into reaction. A 2-fold molar excess of the antibody was combined with the DNA strand, gently stirred by micropipetting and allowed to react overnight at room temperature. The reaction sample was then concentrated to less than 100 µL by using 30 kDa MWCO spin filter (15 min, 15000 g). During the concentration, buffer was exchanged to PBS pH 7.4 and sample was consequently purified on anion exchange chromatography.

The coupling protocol and purification method detailed below, were analogously used to conjugate creatine kinase with corresponding DNA oligomers used in the study (*cf.* 4.4). Protein activated by the cross-linker (CKBB or CKMM) and reduced oligonucleotide (*Eco*RI*-SH or *Pvu*II*-SH, respectively) were combined at 1 : 1.5 stoichiometric ratio (kinase : DNA). Estimated yield of the obtained monoconjugated products were ~25 % and further optimization was not done.

6.2.4 Purification of protein-DNA conjugate by anion exchange chromatography

Chromatographic purification of the IgG–DNA conjugation sample was realized on HPLC system Agilent 1200 Infinity Series LC (Agilent Technologies, France). The employed apparatus comprised the following modules: a manual injector equipped with a 200µL injection loop, a 4-channel vacuum degasser, a quaternary pump, a multiple wavelength detector (UV-Vis) and an automatic fraction collector. Effective separation of the unreacted substrates as well as the conjugation products were provided by an anion exchange column HiTrap^{TM} Q FF (1mL) characterized by 45-165µm of bead size (6% highly cross-linked agarose modified by $-N^+(CH_3)_3$). The described system was alimented with buffers A and B meticulously prepared (filtration at 0.22µm membrane) and properly stored (4°C, up to one month).

Prior to injections, the HPLC system was purged with deionised water (3ml/min flow, at least 10 min), washed with 100% of buffer B for 3-5min and then equilibrated with the starting buffer A (at least 5 column volumes). The analyzed sample was consequently injected to sample loop in 80-100 µL of total volume (partial loop filling avoided the sample loss in laminar flow). Species were eluted from the column in adequate conditions: 1ml/min flow rate, working pressure of around 20 bar and NaCl gradient from 137 mM (t_R = 5 min) to 784 mM (t_R = 30 min). In reality a two-step gradient was applied: 1) 5-10 min, ~60 mM NaCl/min (up to 35% of buffer B) and 2) 10-30 min, ~17 mM NaCl/min (35% to 75% of buffer B). The second slower gradient was employed in order to obtain better resolution of peaks corresponding to fractions F2 (monoconjugated IgG–DNA) and F3 (multiconjugated products and/or free oligonucleotides). Purification products were followed by simultaneous absorbance measurements at 230 nm, 260 nm and 280 nm.

Fractions corresponding to peaks registered on a chromatographic profile were collected, concentrated on 30 kDa MWCO spin filter membranes (15 min, 15000 g) and suspended in pH 7.4 PBS. Collected fractions were subsequently assayed by UV absorbance measurements at 260 nm and 280 nm. The IgG loading by DNA oligomers as well as concentration of the monoconjugated IgG–DNA were assessed by using the obtained 260 nm and 280 nm absorbance values.[117]

6.2.5   Immunofluorescence assay

The immunofluorescence test was realized to assess fractions F1, F2 and F3 obtained upon purification of products issued from the conjugation reaction of rabbit IgG and Zip2*-SH (rab-IgG–Zip2*). For this study, a gold-covered glass slide was functionalized with Zip1, Zip2 and NC sequences (in triplets) according to the electrospotting protocol. Such DNA biochip was firstly incubated with blocking solution of 1% BSA in PBS (room temperature, 10 min). In three independent assays, the probe matrix was incubated for 15 min (45°C) with a hybridization sample containing one of the relevant fractions (F1, F2 or F3) suspended in the hybridization buffer H. Each solution was supplemented with 0.1µM Zip1*–biotin for positive control. After hybridization, the biochip surface was abundantly washed with rinsing buffer R and incubated with biotin-conjugated anti-rabbit IgG (1/1000 dilution in PBS) during 30 min at 37°C. The biochip was then washed with PBS and treated by 5% STV-PE (v/v) in PBS for 10 min in the dark (room temperature). After abundant rinsing with PBS, fluorescence signal read-out was directly observed by using optical microscope (BX60F-3 furnished by *Olympus Optical*) equipped with × 4 microscope objective WIG filter. Images were registered by 8-bit CCD camera (*Hamamatsu*) and proper software *Image ProPlus* (*Media Cybernetics*). Between each fraction assay, the biochip was regenerated with 0.1M NaOH (2-3 min incubation) and equilibrated with the R buffer prior to subsequent hybridizations.

6.2.6   PS microbead sample preparation

Streptavidin-coated polystyrene microbeads were combined with biotinylated species (anti-(rab-IgG) IgG-biotin or Zip1*-biot) prior to injection. 150 µL of microbead-STV at 1.38 % (w/v) was submitted to triple washing in 0.5% BSA solution in PBS (6 min, 10000 g) and re-suspended in the same volume (in PBS with 0.5% BSA). 100 µL of washed microbeads were mixed with 10 µL of Zip1*-biotin (at 100 µM). 50 µL of microbead solution was combined with 20 µL of ant-rabbit IgG-biotin (1/1000 dilution in PBS + 0.5% BSA). Both solutions were incubated at 4°C during 30-40 min. After the incubation, samples were washed three times (6 min, 10000 g) and functionalized microbeads were re-suspended in PBS + 0.5% BSA solution to the following final concentrations: µbead-STV-biotin-Zip1* at 0.07 % (w/v) and µbead-STV-biotin-IgG at 0.14 % (w/v). Loss of the microbeads during washing steps was neglected.

6.2.7 Preparation of cell sample

Hybridoma cell lines LS-102.9 (B cells) and 3A9 (T cells) were kindly provided by P. Marche from *Institut Albert Bonniot (IAB)* in La Tronche (France). Frozen (-70°C) cell suspensions were thawed and incubated in standard conditions for mammalian cell culture (37°C, 95% humidity, 5% CO_2). Hybridoma cells were grown in DMEM culture medium supplemented with 10% FBS, non-essential amino acids (0.1 mM), sodium pyruvate (1 mM), 2-mercaptoethanol (50 µM), penicillin (50 U/mL) and streptomycin (50 µg/mL). Culture was driven during a few weeks and cells were regularly splitted to a fresh medium. Prior to use in the experiment (capture and release by enzymatic cleavage), LS-102.9 and 3A9 were centrifuged (5 min, 300 g) and suspended in the PBS buffer supplemented with 10 mM of $MgCl_2$ (running buffer 1) at 0.5 - 1.0×10^6 cells per mL. Number of cells in a sample was estimated on *Cell Viability Analyser Vi-Cell (Beckman Coulter)*.

Primary splenocytes were collected from an adult C57Bl/6 mouse (female). Directly after removal of the spleen, cells were separated on a grid mesh and suspended in cell culture medium (RPMI). The cellular suspension was then centrifuged (5 min, 300 g) and incubated with a lysis buffer (8.3 g/L NH_4Cl, 0.8 g/L $NaHCO_3$, 0.04 g/L EDTA) during 5 min in order to eliminate red blood cells. B and T lymphocyte mixture was washed in PBS and centrifuged again (5 min, 300 g). Cell pellet was subsequently re-suspended in a complete medium: RPMI supplemented with 10 % FBS, penicillin (50 U/mL) and streptomycin (50 µg/mL). Concanavalin A was added (at 2 µg/mL of final concentration) in order to stimulate T lymphocyte proliferation. Cells were cultured for 24 to 72 h at 37 °C in the environment of 95% humidity and 5% CO_2 (*Forma Steri-Cycle CO_2 Incubator, Thermo Scientific*). Prior to injection into the SPRi microfluidics, mouse splenocytes were centrifuged (5 min, 300 g) and suspended in the adequate experimental buffer at 3.0 - 5.0×10^6 cells per mL. In the enzymatic cleavage experiment, cells were injected in running buffer 1. For the photothermal desorption test, lymphocytes were suspended in running buffer 2A or the complete culture medium.

Streptococcus pneumoniae (R6 strain) used for the bacterial study was a non-encapsulated derivative of strain R36A (gift from the *Rockefeller University, New York, USA*). Bacterial culture was kindly performed by S. Bouguelia (CREAB), in TH liquid broth (composed of bacteriological peptone, heart infusion, dextrose, $NaCO_3$, NaCl and Na_2CO_3). For the SPRi experiment, bacteria were retrieved from mid-exponentially grown cultures (OD_{600nm} = 0.4). The given optical density (OD) corresponded to 10^8 colony forming unit per milliliter (cfu/ml), calculated by counting the colonies grown on solid support. Prior to injection, *S.pneumoniae* culture was extensively washed in PBS by two consecutive centrifugations (20 min, 1500 g). The bacterial pellet was eventually re-suspended in running buffer 1 at final 10^9 cfu/mL concentration.

6.2.8 Target release from the biochip by enzymatic cleavage

The molecular phenomena (hybridization and enzymatic cleavage) as well as cell-involving events (capture and release from biochip surface) were monitored by a commercial SPRi apparatus (*Horiba Scientific-GenOptics*). The optical set-up was equipped with a 660nm LED and a 16-bit CCD camera (Pike F-145B or Dolphin F-145B by *Allied Vision Technologies GmbH*) as well as a TM/TE polarizer, a rotary mirror and a set of biconvex lenses. Adapted microfluidics was composed of a syringe pump (1 or 2.5 mL Cavro XLP 6000 Pump by *Tecan Systems, Inc*), a degassing system (Elite™ Degassing System by *Alltech*) and a 6-channel injection valve. The main tubing (250 µm or 760 µm of ID) as well as the flow cells (~15µL of reaction chamber volume) employed here, were integrally made of PEEK. In a particular case of cellular sample injections, a transparent polyethylene-based tubing (760 µm of ID) was used (Fig.3.7). The running buffer 1 (PBS + 10 mM MgCl$_2$) was delivered at a flow rate depending on the experimental step: 20 µL/min during biochip molecular assembly (intermediate DNA strands and IgG–DNA conjugates), 7-10 µL/min within the enzymatic digestion step, 15-20 µL/min during bacteria injections and higher values when lymphocytes were injected (50-100 µL/min for hybridomas and 20-60 µL/min for splenocytes).

A functionalized DNA biochip (Zip1, Zip2, Zip3 and NC) was set up with a flow cell and housed in an incubator (IPP400, *Memmert*) at 37°C during the whole experiment. Prior to assay, the biochip surface was submitted to ultrasonication (1-2 min) and then incubated with blocking solution: 1% BSA in PBS (~15 min) or a mixture of 10 µM BSA and 5 µM cytochrome *c* in PBS (45-60 min) which was preferential for cell-based assays. The main experiment was followed in real time by SPRi (reflectivity signal monitoring), once the initial adjustments had been accomplished (equilibration with buffer, choice of the working angle). Molecular as well as bacterial and cellular samples prepared in the running buffer 1 were manually injected by using 200µL injection loops. Firstly, the intermediate DNA oligomers were independently introduced to the bioreactor (150 nM). Subsequently to that, injections of corresponding IgG–DNA monoconjugates at 50-60 nM (as calculated concentration of the relevant antibody) were performed. Following the molecular construction, lymphocytes or bacteria were loaded on the biochip within 2-3 repeated injections at an adequate concentration detailed above. After cell-specific capture has been done, the restriction enzymes were injected in two subsequent digestion steps (200 U each). *Eco*RI and *Pvu*II enzyme samples were prepared directly before the injection and remained for 20-30 min in the reaction chamber (total duration of the enzyme injection). During the enzymatic cleavage steps, fractions were recovered from the outlet of microfluidics directly into a 1.5 mL *eppendorf* tube and could be devoted to further characterization.

The employed biochip was regenerated by 0.1 M NaOH solution (2-3 min), washed by water and dried under an argon stream. Such prism was stored at 4°C and could be

potentially used in subsequent experimentation. After the experiment, the microfluidic system was cleaned by 2% solution of the commercial bleach (at least 30min), then washed by 1% solution of SDS and finally deionised water. Registered SPRi data (proper software by *Genoptics*) were subsequently treated as described in the Appendices.

6.2.9   Controlled target desorption by photothermal effect

The experiments of photothermally induced desorption of biomolecules and micro-objects were realized on a home-made system detailed in Chapter 4. Running buffer 2A or 2B was delivered by a 50 mL syringe pump (A-99, *Razel Scientific Instruments Inc.)* at 20 µL/min within whole assay (unless specified) and through PEEK/polyethylene tubing (ID = 760 µm). DNA biochips were prepared according to the electrochemical deposition process resulting in probe matrix composed of spots of diameter depending on the experiment: 7 µm or 800 µm for cell-based assay and 1200 µm in µbead and protein assay (in order to enable high level of material immobilization which is eventually desorbed for downstream MS analysis).

Prior to the assay, a DNA biochip was cleaned in an ultrasonic bath (1-2 min) followed by incubation in a blocking solution depending on the experiment: 15 min with 2µM cytochrome *c* (in PBS) for assay at molecular level, 15 min with 1% BSA (in PBS) for PS-µbead assay and 45-60 min with a mixture of 10µM BSA and 5µM cytochrome *c* (in PBS) for cell capture-release experiment. Once the biochip assembled with an adequate flow cell (detailed by the occasion of each experiment) has been placed into the optical system and the initial settings have been accomplished (manual adjustment of the working angle), injections of relevant specimens could start.

Molecular samples were prepared in buffer 2A for microbead- and cell-based experiment, and in buffer 2B in protein assay for further MS analysis. They were manually injected by using an injection valve equipped with 200 µL or 500 µL (exclusively for the assay of "ligand fishing" type) injection loop. A dead volume between the injector and the biochip was estimated to around 30 µL and injections arrived into the reaction chamber in less then 2 min. Firstly, the complementary DNA strands were introduced at an appropriate concentration: 200 nM (cell-based experiment), 250 nM (µbead capture-release) or 300-400 nM (protein assay). Hybridization of the intermediate strands was followed by injections of protein-DNA conjugates (exceptionally IgG–DNA) at 50-60 nM, 70 nM or 150 nM, respectively. Subsequently to the molecular construction, functionalized microbead or cell sample (both detailed above) were loaded into reactor by injections at 15-25 µL/min (microbeads) or 30-50 µL/min (splenocytes) flow rate. Specific capture of the micro-objects was followed by a microscope under × 4 or × 10 magnification (*Olympus Optical*) and registered by a proper camera (Infinity2-3C, *Lumenera*).

Consequently to the target capture on the functionalized biochip surface, controlled desorption was realized in independent lasing steps specific to each probe. Initial settings as well as the laser tracing phase were detailed in Chapter 4. In the proposed configuration, laser source was manually introduced between camera and prism (*cf.* Fig. 4.5). Therefore, the laser source was momentarily removed between each step of the photothermal desorption and SPRi signal retrieved. In this case, prism-LED-camera set-up could be slightly perturbed and the initial SPRi position restored manually (with the help of supplementary micrometric screws). During similar adjustments, SPRi signal remained unsettled and was not taken into consideration.

An important issue when realizing out-of-support release by laser beam is the level of energy consumed to generate photothermal effect. As it was stressed out before, the dimension of local heating produced by the photothermal effect strongly depends on the irradiation time and the incoming laser intensity.[214, 215] Okano's group showed that local heating generated on a metal surface may induce partial destruction of solid support if the laser intensity is high enough.[99] Characterization of the optical configuration used in our study has evidenced moderate level of surface energy generated on gold covered prism. However, if longer irradiation was realized (more than 5 min) thermal energy was accumulated in time and we could effectively observe some damages on the gold layer (black spot of probably carbonized material deposited on surface). Nevertheless, the experiments here reported, provided instantaneous contact of focused laser beam on surface (laser spot was displaced at 10-200 µm/s rate) which excluded material destruction phenomena.

In the course of the experiment of the laser-induced desorption of creatine kinases (CKMM and CKBB), three fractions were recovered in the outlet of microfluidics (*cf.* 4.3):"0" as blank sample before the lasing step, "1" and "2" samples within laser-assisted desorption on Zip1 and Zip2 spot family, respectively. The samples meticulously recovered into low-adsorption tubes (500-1000 µL) were then frozen and assigned to MS analysis. Cell or microbead recovery was not attempted in this experimentation. Biochip was regenerated and microfluidic system cleaned according to the protocol detailed in section 6.2.8.

The developed instrumentation is an example of home-made experimental set-up. Entire system is a free-standing device placed in a dark room. Therefore, the whole experiment temperature control was disabled and could not be precisely regulated. Room temperature was thus considered as working condition, although it could be higher in the reality because most of the experiments have been carried out in summer (over 30°C). SPRi signal remained stable within many hours of experiment while only buffer was flowed through the system. Influence of the external temperature on detected signal may be therefore neglected. Although regular temperature measurements were not done, we speculate that heating of bulk solution generated by the photothermal effect may be disregarded as well. This statement is founded upon a few reasons such as local

confinement of the photothermal phenomenon, laser tracing accomplished in several minutes and finally considerable flow rate during desorption step.

6.2.10 Mass Spectrometry analysis

Samples recovered from the protein photothermal desorption experiment (samples "0", "1" and "2") were assayed by mass spectrometry kindly realized by M. Jaquinod (IRTSV, CEA Grenoble). The tested solutions were firstly dried under speed vacuum to evaporate ammonium bicarbonate. They were subsequently re-dissolved in 100 µL of 10% (v/v) acetonitrile (in 100 mM NH_4HCO_3, pH 7.9) and incubated at room temperature for 15 min. Samples were then submitted to reductive conditions by addition of 2 µL of 500 mM TCEP and incubation during 30 min (RT). In further step of sample pre-processing, alkylation of cysteine residues was performed by addition of 10 µL of 100 mM iodoacetamide and followed by incubation for 30 min (RT). Samples consequently underwent protein digestion induced by trypsin (*Promega Corp*) – 0.5 µg was added and followed by incubation for 4 h at 37°C. The digestion solutions were then dried under speed vacuum and the obtained peptide mixtures re-suspended in 25 µl of chromatographic purification liquid phase: H2O/acetonitrile 95%/5% (v/v) containing 0.2 % of formic acid (FA). The trypsin-digested samples were finally submitted to LC-MS/MS analysis. The samples were firstly separated on a nano-LC system, subsequently coupled to an OrbiTRAP mass spectrometer (*ThermoFinnigan*). The chromatographic analysis was enabled on 300 µm × 5 mm PepMap C18 pre-column and 75 µm × 150 mm C18 column (Gemini C18 phase). The employed method consisted in a 60-minute gradient flow (300 nL/min) based on two buffers: I (5% acetonitrile and 0.2% formic acid in water) and II (80% acetonitrile and 0.08% formic acid in water). MS/MS data were acquired using *Xcalibur (Thermo Fischer Scientific)* and processed automatically using *Mascot Daemon* software (*Matrix Science*).

Appendices

Appendix A: MS analysis of the sample recovered upon *Eco*RI*-NH$_2$ conjugation with DSS

*Eco*RI*-NH$_2$ was coupled to DSS (100 molar equivalent) according to the protocol previously reported.[146] After purification on NAP[TM] 5 column (elution with water), the sample was lyophilized and transferred to MS analysis kindly realized by C. Saint-Pierre from LAN laboratory (CEA Grenoble).
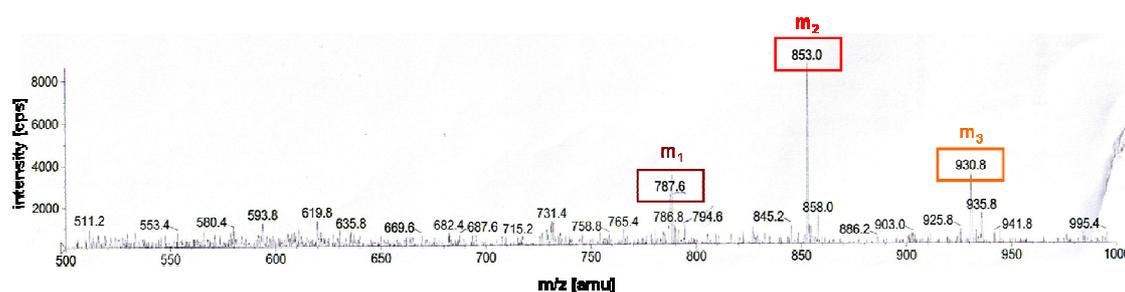
	m/z	charge	mass
m1	786.8	13	10251.8
m2	853.0	12	10248.0
m3	930.8	11	10249.8

calculated mass:
10249.9 Da (1.9 Da)
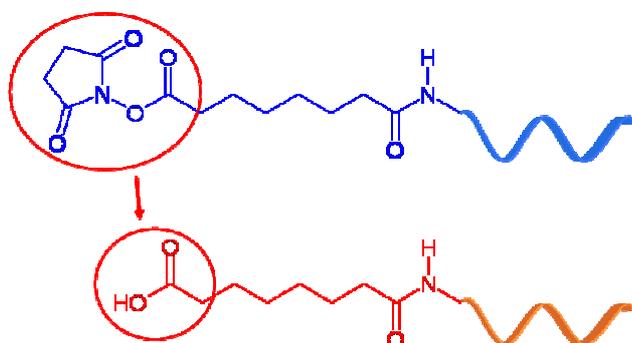
expected oligonucleotide activated by NHS
*Eco*RI-NHS
MW = 10350 Da

hydrolyzed oligonucleotide
*Eco*RI-COOH
MW = 10250 Da

The obtained results confirmed presence of hydrolyzed products in the analyzed sample (*Eco*RI*-COOH). The activated DNA-NHS was not evidenced which may indicate that NHS ester is susceptible to destruction before subsequent step of the conjugation protocol.

Appendix B: Calculations of the IgG loading with DNA

Willing to estimate the number of DNA strands coupled with a single IgG molecule, we make use of the absorbance law. Considering the absorbance of the conjugated product, we benefit from additivity of the Lambert-Beer law of absorbance. By assuming that conjugation of IgG and DNA does not influence their ε values, we have:

$$A_{260} = l \times \left(\varepsilon_{260}^{DNA} \times n^{DNA} + \varepsilon_{260}^{IgG} \times n^{IgG} \right)$$

$$A_{280} = l \times \left(\varepsilon_{280}^{DNA} \times n^{DNA} + \varepsilon_{280}^{IgG} \times n^{IgG} \right)$$

where: A_{260} and A_{280} – absorbance values measured on the IgG–DNA conjugate at 260 nm and 280 nm;

l – length of optical pathway [cm];

ε_{260} and ε_{280} – extinction coefficients at 260 nm and 280 nm [$M^{-1}cm^{-1}$];

n – number of moles in a given volume [M].

For the product fractions obtained upon conjugation of an IgG with an oligonucleotide, the measured absorbances (A_{260} and A_{280}) permit to estimate **Z:**

$$Z = \frac{\varepsilon_{280}^{IgG}}{\varepsilon_{260}^{DNA}} \times \frac{\left[R_{IgG} - A_{260_{280}} \right]}{\left[\dfrac{A_{260_{280}}}{R_{DNA}} - 1 \right]}$$

where: **Z** – theoretical number of DNA strands conjugated with single IgG molecule;

R – ratio of extinction coefficients ($\varepsilon_{260}/\varepsilon_{280}$)

$A_{260/280}$ – ratio of the measured absorbance values

Estimation of antibody loading with DNA molecules is therefore enabled and accordingly assigned to the fractions issued from antibody coupling to three independent DNA sequences (*Eco*RI*, *Pvu*II* and *Nco*I*):

	EcoRI	PvuII	NcoI			IgG
ε_{260}^{DNA} [$M^{-1}cm^{-1}$]	306180	271620	301590		ε_{280}^{IgG} [$M^{-1}cm^{-1}$]	210000
$R_{DNA} = \dfrac{\varepsilon_{260}^{DNA}}{\varepsilon_{280}^{DNA}}$	1.79	1.57	1.74		$R_{IgG} = \dfrac{\varepsilon_{260}^{IgG}}{\varepsilon_{280}^{IgG}}$	0.61

fraction	IgG–*Eco*RI*		IgG–*Pvu*II*		IgG–*Nco*I*	
	A_{260}/A_{280}	Z	A_{260}/A_{280}	Z	A_{260}/A_{280}	Z
F1	0.64	0.0	0.64	0.0	0.65	0.0
F2	0.98	0.6	0.94	0.6	0.98	0.6
F3	1.5	3.8	1.37	4.7	1.36	2.4

Appendix C: Assessment of IgG–DNA concentration in the fraction of monoconjugated product

Fractions obtained upon chromatographic purification are concentrated, re-suspended in PBS (pH 7.4) and their absorbance is measured (example of rab-IgG coupling to *Eco*RI*-SH):
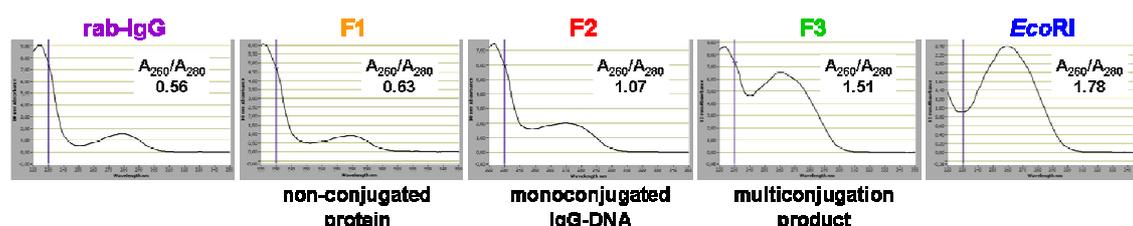
$$C_{IgG} = \frac{R_{DNA} \times A_{280} - A_{260}}{(R_{DNA} - R_{IgG}) \times \varepsilon_{280}^{IgG}}$$

Appendix D: Theoretical value of restriction enzyme units (U) needed to digest the microarrayed DNA

This appendix serves to establish an approximate theoretical value of U (restriction enzyme units) which is optimal to perform digestion of immobilized DNA substrate. Following calculations were done for *Eco*RI enzyme according to data taken from Fuchs *et al.*[177]

DNA Substrate	Base Pairs	Picomoles in 1µg*	Cut Sites (*Eco*RI)	Picomoles Cut Sites	Units Needed
Unit definition (lambda)	48502	0.0317	5	0.1585	1
plasmid	3000	0.5	1	0.5	3**
PCR fragment	700	2.2	1	2.2	14
oligonucleotide (Zip1*-*Eco*RI)	46	33	1	33	208

*Based on 650 Daltons per base pair of DNA.
**Enzymes differ in their ability to digest supercoiled vs. linear substrates.

In the present study, DNA duplexes assembled on the biochip surface are of 46 bp length (*e.g.* Zip1*-*Eco*RI). According to the illustrated above table, each microgram of such substrate (33 pmol) needs 208 U of the restriction enzyme. When considering a DNA matrix composed of ~40 spots of 800 µm in diameter, we obtain 0.2 cm^2 of surface coverage by probe-modified Ppy. It corresponds to around 2 pmoles of the immobilized oligonucleotide (10 pmol/cm^2 according to previous studies),[123] finally giving 12.6 U of *Eco*RI which approximates the optimal quantity of enzyme required to digest the adequate amount of the substrate.

175

Appendix E: SPRi data treatment

The SPRi data were acquired using proper software furnished by *Horiba Scientific-GenOptics* (*SPRiViewlt*). It permitted to follow changes in reflectivity on the available biochip area through defined zones (so-called masks) corresponding to the spots of interest. Registered spot-specific reflectivity signals (R) were normalized to the luminosity observed in conditions devoid of SPR phenomenon (TE mode) and expressed in %. The SPRi system automatically subtracted background noise registered at the beginning of each experiment. Recording of the reflectivity signal was enabled by a 16-bit camera and plotted upon time during the whole assay (reflectivity kinetics curves).

The obtained raw data were pre-processed in order to improve the clarity of their presentation. In the first step of the data treatment, all recovered signals (generally 35% - 45% of R) were zeroed to the baseline, by subtraction of the average reflectivity registered for each spot at the beginning of the experiment or just before the injection. Further, the obtained curves corresponding to the same species were averaged and traced in time (starting injection of the blocking solution was omitted).
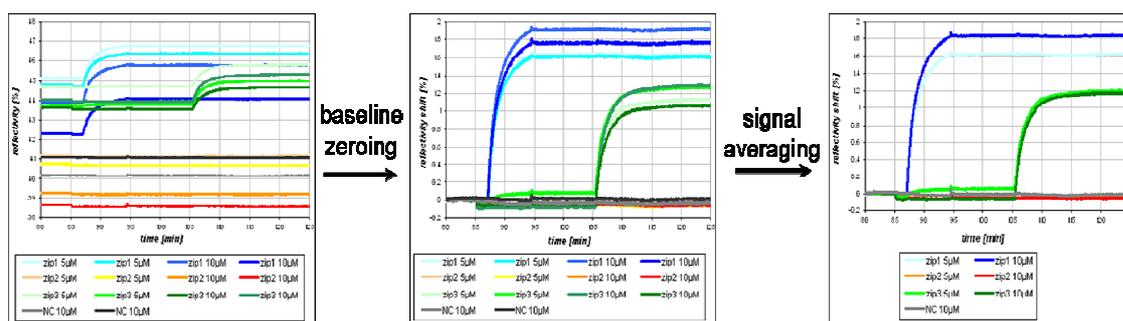
As the final operation, the averaged reflectivity signals were corrected by a negative control (signal observed for NC probe). Subtraction of the NC signal aimed to eliminate the background reflectivity changes generated by global variations of the bulk solution refractive index. Such proceeding was particularly required during injections of enzymatic and cellular samples. The definitive curves were therefore plotted as relative reflectivity shift in function of time.
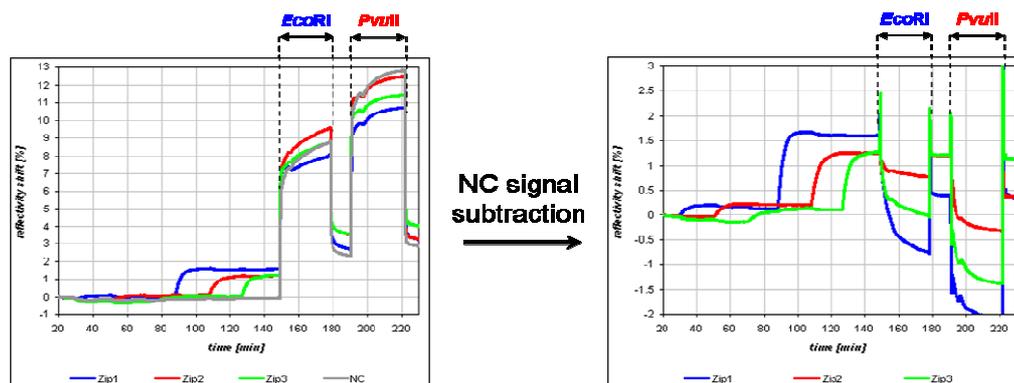
In fact, kinetics of enzymatic reaction was a parameter that, in the case of here proposed biochip system, could not be properly studied. It was because injection of enzyme solution generated global refractive index change observed by SPR imaging as an abrupt reflectivity rise (*cf.* figure above). Such effect was induced by introduction to the reaction chamber of high protein content in abundant buffer. Indeed, injected enzyme samples were based on commercially available solutions stored at -20°C. Such storage conditions required presence of glycerol at high levels (30-50 %) in order to keep the proteins properly folded. Samples of *Eco*RI and *Pvu*II enzymes were prepared directly before injection and eventually contained up to 5% of glycerol. Similar preparation loaded to biochip system, strongly affected optical properties of the reaction medium and produced momentary variation of global reflectivity. Subtraction of the negative control (NC signal) resulted in SPRi signal over-correction mainly due to the lack of linearity of the reflectivity signal in the conditions of considerable refractive index change (signal saturation). Thus, a straightforward interpretation was disabled during the enzymatic incubations and enzyme functionality could not be assigned as long as it was not washed off the reactor.

Simultaneously to the real-time monitoring of reflectivity signal proper to each of the defined spots, *GenOptics* program acquired images of the whole biochip area along the experiment (~2 images per minute). Thus, a useful tool to follow the biomolecular and cellular phenomena was to observe SPR differential images. A differential image resulted from subtraction of the reference image to the currently acquired one. Reference images were often taken at the beginning of an injection in order to highlight each step of the experiment (hybridization of DNA or IgG–DNA, cell immobilization, specific release). However during cellular and enzymatic injections, global variation of the refractive index influenced the registered differential images resulting in their poor contrast. In these cases, SPR images were processed by using image treatment software (ImageJ v1.43u, *National Institutes of Health, USA*) where final contrast was improved and proper phenomena revealed.

image registered by SPRi camera
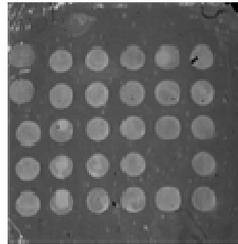
differential images observed during the experiment
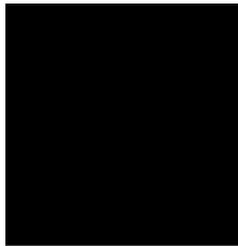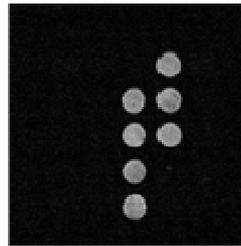
reference image   hybridization steps   enzymatic cleavage
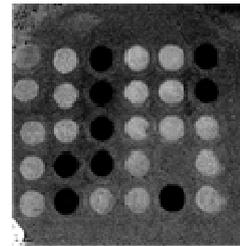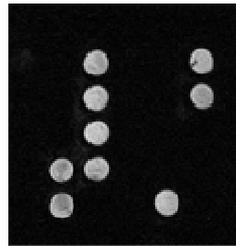
Appendix F: PEEK-made flow cells used in the experiments

Hexagon-shaped flow cell

Oval flow cell

Serpentine-type flow cell
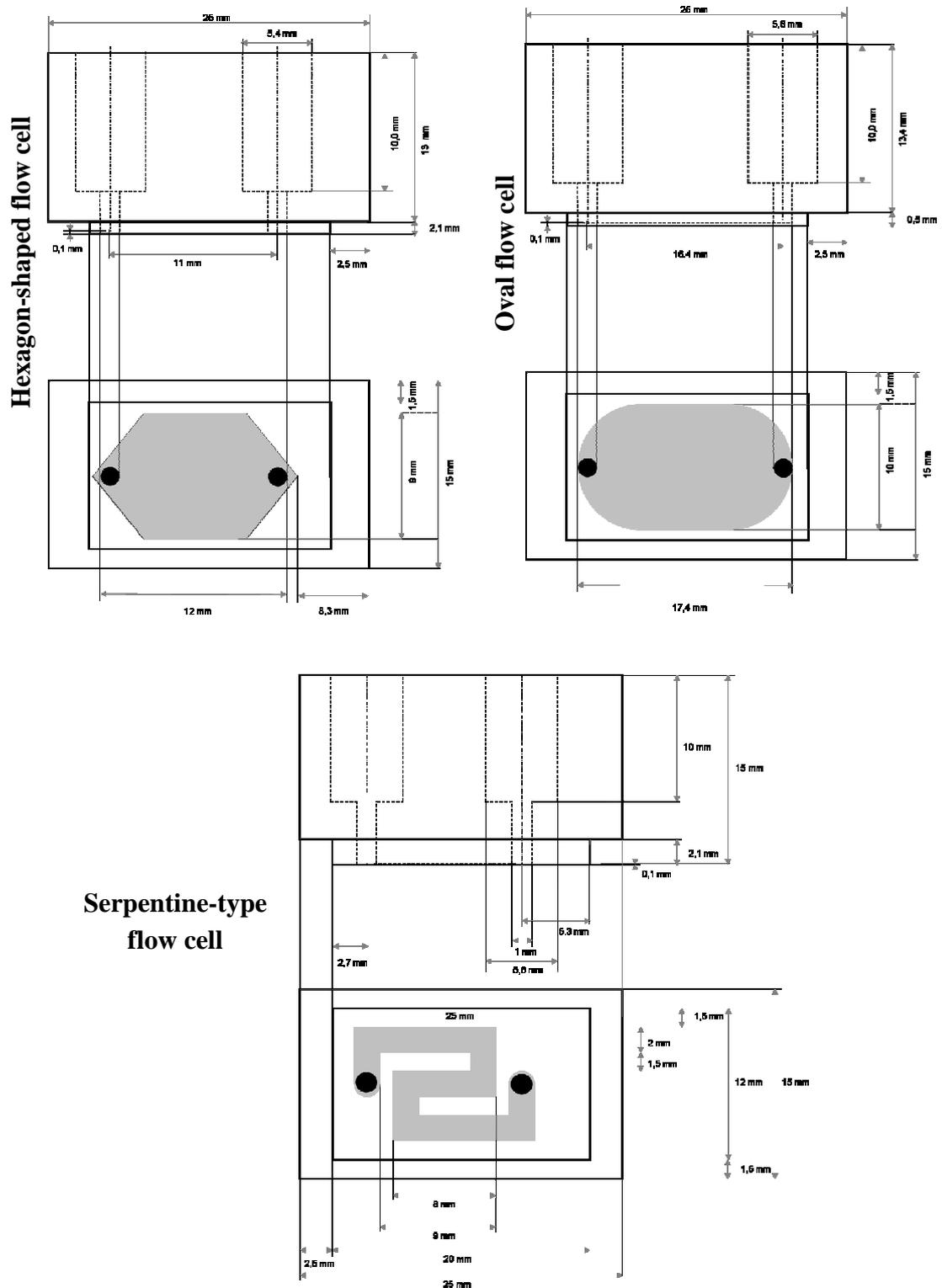
Appendix G: Visualizations of splenocytes in SPR imaging
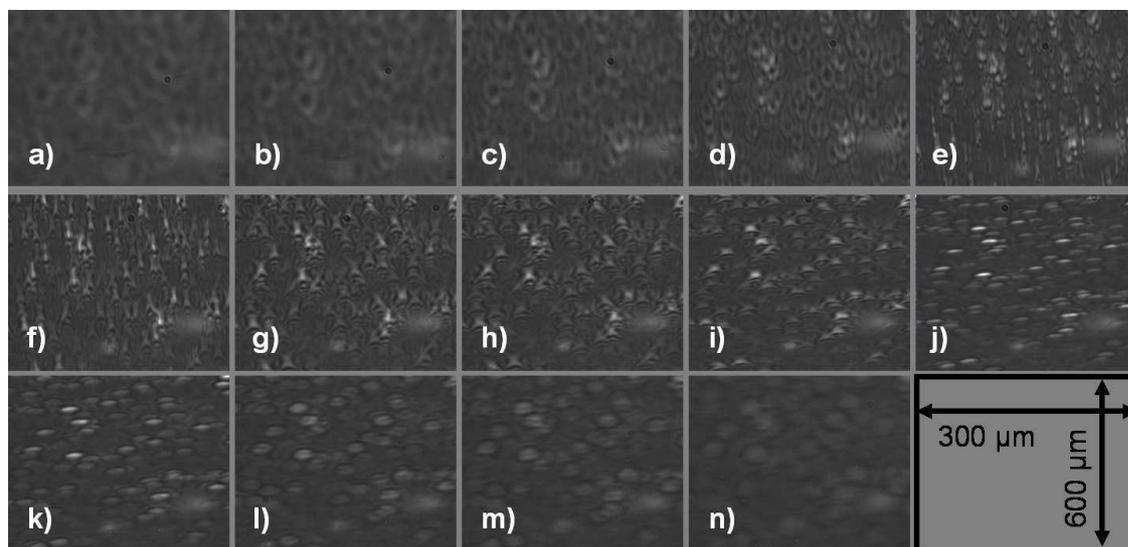
Primary lymphocytes from mouse spleen (C57Bl/6) were straightforwardly loaded onto the gold surface devoid of particular treatment and functionalization. SPR images were sequentially registered at different focalization distances (from a) to n) ~1.5 mm of focalization distance shift). In function of the focalization, cells were visualized as oval to star-shaped discrete objects.

Appendix H: Characteristics of the laser configurations
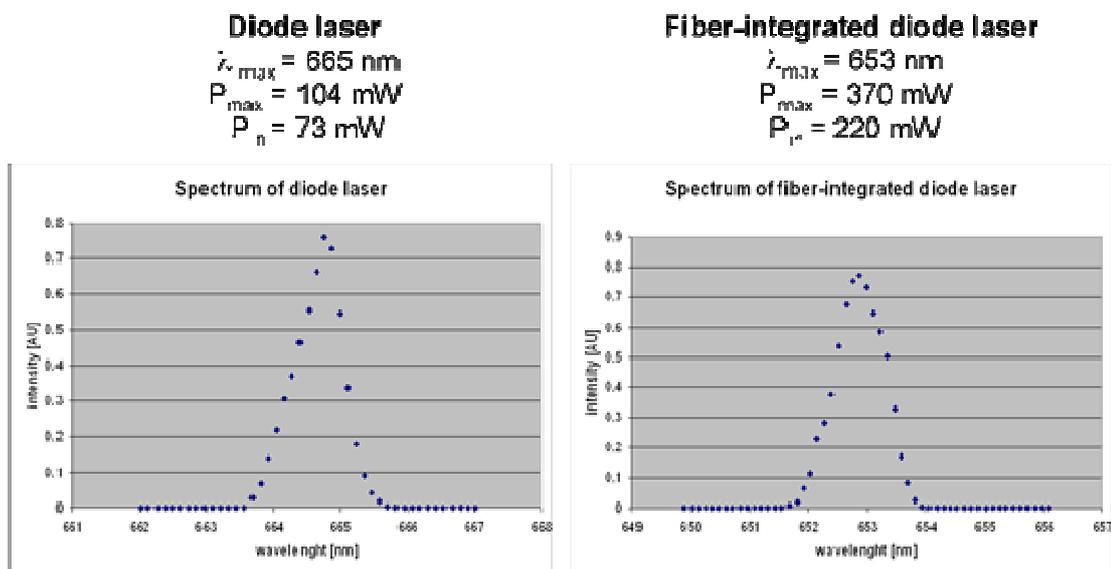
Diode laser
λ_{max} = 665 nm
P_{max} = 104 mW
P_n = 73 mW

Fiber-integrated diode laser
λ_{max} = 653 nm
P_{max} = 370 mW
P_{i} = 220 mW

Angular distribution of the laser intensity
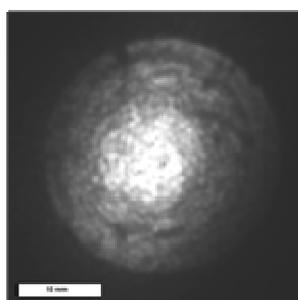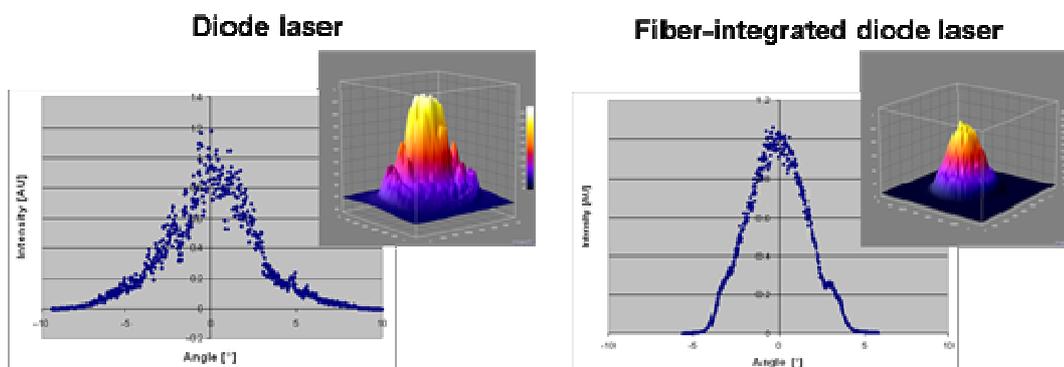
Image of the laser beam at 10 cm from the focal distance
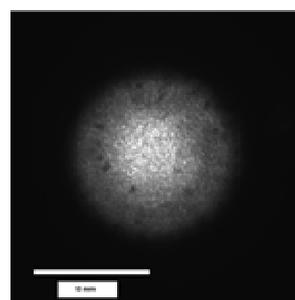
Laser light spectra were registered with help of CCS100 Compact Fiber Spectrometer (*Thorlabs GmbH, Germany*). Measurements of the laser intensity were provided by a portable laser power meter *LaserCheck* (*Coherent, France*).

Appendix I: Capture of single lymphocyte inside a micropore

The present appendix describes the study realized in collaboration with J. Liu (CREAB), where we have demonstrated the specific capture of primary B and T lymphocytes inside micropores. For this purpose, we used a set of 9 pores of 15 µm in diameter etched in a silicon substrate and thermally covered by 4 µm-thick silica. The micropores were functionalized with DNA according to the CLEF technique previously described.[278] Briefly, probes of interest (Zip1 and Zip2) were introduced to each micropore by electrochemically driven deposition of a polypyrrole film. As result of the electropolymerization, the generated oligonucleotide-bearing polypyrrole film was regularly distributed on the inner wall of a single micropore and demonstrated high level of attachment.
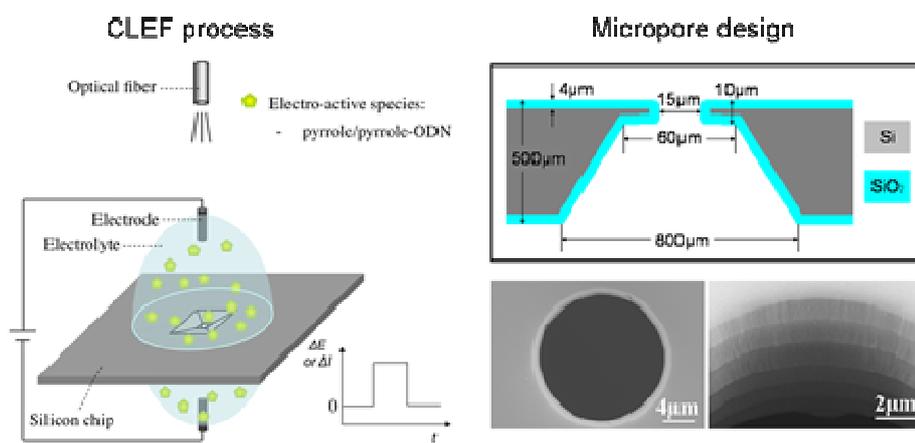
Subsequently to the functionalization, the obtained chip was assigned to an experiment with mouse splenocytes. Within whole assay, the system was housed in a home-made support and integrally immersed in buffer volume (firstly hybridization buffer H and then pH 7.4 PBS). Prior to incubation with target samples, the biochip was saturated with 1% solution of BSA (in PBS). Stepwise hybridizations were consequently performed in order to provide three-component molecular assembly capable of specific cell capture. Namely, Zip1-based micropores were assembled with complementary Zip1*-*Eco*RI strand and eventually functionalized by anti-CD19–*Eco*RI* whereas Zip2 sequence hybridized with anti-CD90–*Pvu*II* through the intermediate Zip2*-*Pvu*II oligonucleotide. Following the molecular construction, the hybridization buffer H was exchanged to PBS and the cellular sample was then introduced to the biosensor.

Lymphocyte capture inside DNA-funtionalized micropores

A suspension of B- and T-type primary lymphocytes issued from mouse spleen was loaded on the biochip and cells were directly observed under microscope. Over a few minutes upon the deposition of the cellular sample allowing cell sedimentation in the buffer volume, lymphocytes could be observed when approaching to micropore locations. Most of cell units rolled over membrane and adsorbed non-specifically before reaching the micropore *lumen*. Several lymphocytes attained bottom of the membrane pyramidal openings and penetrated inside a micropore. Therefore, two different phenomena were registered: a single cell was translocated through the encountered micrometric hole or trapped inside the pore if specific interactions were ensured. The introduced lymphocytes became tethered in biochip locations decorated with anti-CD19 (Zip1 µpore) and anti-CD90 (Zip2 µpore) antibodies in contrast to negative Ppy micropores where no cell capture was observed. Nevertheless, an efficient immobilization of splenocytes rarely took place since in reality, only a small fraction of the cellular sample got into contact with the functionalized surfaces. Furthermore, despite reliable functional coverage of micropore inner wall, lymphocyte immobilization was not a long-lasting event, probably due to characteristic hydrodynamic constraints. Indeed, once the buffer solution was actuated by rinsing in fresh PBS or even by a simple chip displacement, trapped lymphocytes were washed off from the micropores. We speculated that living cells remaining in such small diameter of the order of cell size, incurred considerable shear forces generated by surrounding liquid flow conditions. This conclusion was confirmed by the fact that once cells approached a single micropore border, they were rapidly translocated through the hole probably by a rapid liquid stream. It additionally explained why the quantity of effectively captured lymphocytes was so poor.

specific lymphocyte capture inside micropore (Zip2)

translocation of non-recognized cell through micropore (Zip2)
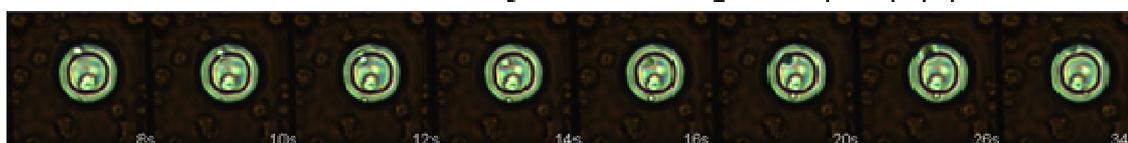
Despite the aforementioned difficulties and low rate of cell immobilization inside micropores, the realized study may be considered as promising approach to a single-cell level biosensor. The reported above experiment demonstrated phenomena of individual cell capture in well-defined biochip locations. Precise immobilization of lymphocytes loaded onto biochip in a mixed population of immune cells was ascribed to their specific recognition by molecular assembly based on antibody-DNA conjugates. Further studies will be carried out in order to improve the performance of the proposed single-cell assay. In this matter, the DNA involving molecular architecture may be potentially exploited to enzymatically driven release of an individual cell for its downstream examination. An important development would be to design more sophisticated microfluidic set-up to eventually meet the requirements of a lab-on-a-chip system. Rheological parameters inside a micropore should be therefore considered to ensure proper environment devoid of excessive shear stress regarding to cellular sample. An example of such microdevice should provide well guided flow of cell-containing solution to precise biosensing locations represented by functionalized micropore positions.

References

1.   Anderson, N. L.; Anderson, N. G., The human plasma proteome: history, character, and diagnostic prospects. *Mol Cell Proteomics* **2002,** 1, (11), 845-67.

2.   Toner, M.; Irimia, D., Blood-on-a-chip. *Annu Rev Biomed Eng* **2005,** 7, 77-103.

3.   Petrik, J.; Robb, J. S., Microarray and Blood Diagnostics. In *Bioarrays: from basics to diagnostics*, Appasani, K., Ed. Totowa, NJ (USA), 2007.

4.   Kotz, K. T.; Irimia, D.; Tompkins, R. G.; Toner, M., Immunoaffinity Capture of Cells from Whole Blood. In *Methods in Bioengineering, Microdevices in Biology and Medicine*, Nahmias, Y.; Bhatia, S. N., Eds. Artech House: 2009; pp 1-24.

5.   Kim, D. S.; Lee, S. H.; Ahn, C. H.; Lee, J. Y.; Kwon, T. H., Disposable integrated microfluidic biochip for blood typing by plastic microinjection moulding. *Lab Chip* **2006,** 6, (6), 794-802.

6.   Fan, R.; Vermesh, O.; Srivastava, A.; Yen, B. K.; Qin, L.; Ahmad, H.; Kwong, G. A.; Liu, C. C.; Gould, J.; Hood, L.; Heath, J. R., Integrated barcode chips for rapid, multiplexed analysis of proteins in microliter quantities of blood. *Nat Biotechnol* **2008,** 26, (12), 1373-8.

7.   Dimov, I. K.; Basabe-Desmonts, L.; Garcia-Cordero, J. L.; Ross, B. M.; Ricco, A. J.; Lee, L. P., Stand-alone self-powered integrated microfluidic blood analysis system (SIMBAS). *Lab Chip* **2011,** 11, (5), 845-50.

8.   Browne, A. W.; Ramasamy, L.; Cripe, T. P.; Ahn, C. H., A lab-on-a-chip for rapid blood separation and quantification of hematocrit and serum analytes. *Lab Chip* 11, (14), 2440-6.

9.   Sollier, E. Microsystèmes pour la préparation d'échantillons sanguins. PhD thesis, Université Joseph Fourier - Grenoble I, Grenoble, 2009.

10.   Abbas, A. K.; Lichtman, A. H.; Pillai, S., *Cellular and molecular immunology*. Saunders Elsevier: 2007.

11.   Janeway, C. A., *Immunobiology*. Garland Publishing: 2001.

12.   Hackett, C. J.; Rotrosen, D.; Auchincloss, H.; Fauci, A. S., Immunology research: challenges and opportunities in a time of budgetary constraint. *Nat Immunol* **2007,** 8, (2), 114-7.

13.   Funding the future in UK science. *Nat Immunol* **2011,** 12, (1), 1.

14.   Cao, X., Immunology in China: the past, present and future. *Nat Immunol* **2008,** 9, (4), 339-42.

15.   *Estimates of Funding for Various Research, Condition, and Disease Categories (RCDC). Annual report of the National Institutes of Health*; 14.02.2011.

16.   Hernandez-Fuentes, M. P.; Warrens, A. N.; Lechler, R. I., Immunologic monitoring. *Immunol Rev* **2003,** 196, 247-64.

17.   Whiteside, T. L.; Gulley, J. L.; Clay, T. M.; Tsang, K. Y., Immunologic monitoring of cellular immune responses in cancer vaccine therapy. *J Biomed Biotechnol* **2011,** 2011, 370374.

18.   Robins, H. S.; Campregher, P. V.; Srivastava, S. K.; Wacher, A.; Turtle, C. J.; Kahsai, O.; Riddell, S. R.; Warren, E. H.; Carlson, C. S., Comprehensive assessment of T-cell receptor beta-chain diversity in alphabeta T cells. *Blood* **2009,** 114, (19), 4099-107.

19.   Obenauer-Kutner, L. J.; Jacobs, S. J.; Kolz, K.; Tobias, L. M.; Bordens, R. W., A highly sensitive electrochemiluminescence immunoassay for interferon alfa-2b in human serum. *J Immunol Methods* **1997,** 206, (1-2), 25-33.

20.   Niemeyer, C. M.; Adler, M.; Wacker, R., Detecting antigens by quantitative immuno-PCR. *Nat Protoc* **2007,** 2, (8), 1918-30.

21.   Adler, M.; Schulz, S.; Spengler, M. *Cytokine quantification in drug development: a comparison of sensitive immunoassay platforms*; Chimera Biotec (Case study): 2010.

22.   Czerkinsky, C. C.; Nilsson, L. A.; Nygren, H.; Ouchterlony, O.; Tarkowski, A., A solid-phase enzyme-linked immunospot (ELISPOT) assay for enumeration of specific antibody-secreting cells. *J Immunol Methods* **1983,** 65, (1-2), 109-21.

23.   Janetzki, S.; Schaed, S.; Blachere, N. E.; Ben-Porat, L.; Houghton, A. N.; Panageas, K. S., Evaluation of Elispot assays: influence of method and operator on variability of results. *J Immunol Methods* **2004,** 291, (1-2), 175-83.

24.   Papagno, L.; Almeida, J. R.; Nemes, E.; Autran, B.; Appay, V., Cell permeabilization for the assessment of T lymphocyte polyfunctional capacity. *J Immunol Methods* **2007,** 328, (1-2), 182-8.

25.   Prussin, C.; Metcalfe, D. D., Detection of intracytoplasmic cytokine using flow cytometry and directly conjugated anti-cytokine antibodies. *J Immunol Methods* **1995,** 188, (1), 117-28.

26.   Hsueh, R. C.; Roach, T.; Lin, K.-M.; O'Connell, T. D.; Han, H.; Yan, Z., Purification and characterization of mouse splenic B lymphocytes. *Alliance for Cellular Signaling Laboratories Research Reports* **2002,** 1, 1-11.

27.   Manz, R.; Assenmacher, M.; Pfluger, E.; Miltenyi, S.; Radbruch, A., Analysis and sorting of live cells according to secreted molecules, relocated to a cell-surface affinity matrix. *Proc Natl Acad Sci U S A* **1995,** 92, (6), 1921-5.

28.   Zhu, H.; Macal, M.; Jones, C. N.; George, M. D.; Dandekar, S.; Revzin, A., A miniature cytometry platform for capture and characterization of T-lymphocytes from human blood. *Anal Chim Acta* **2008,** 608, (2), 186-96.

29.   Zhu, H.; Stybayeva, G.; Macal, M.; Ramanculov, E.; George, M. D.; Dandekar, S.; Revzin, A., A microdevice for multiplexed detection of T-cell-secreted cytokines. *Lab Chip* **2008,** 8, (12), 2197-205.

30.   Milgram, S.; Cortes, S.; Villiers, M. B.; Marche, P.; Buhot, A.; Livache, T.; Roupioz, Y., On chip real time monitoring of B-cells hybridoma secretion of immunoglobulin. *Biosens Bioelectron* **2011**, (26), 2728-2732.

31.   Stybayeva, G.; Kairova, M.; Ramanculov, E.; Simonian, A. L.; Revzin, A., Detecting interferon-gamma release from human CD4 T-cells using surface plasmon resonance. *Colloids Surf B Biointerfaces* **2010,** 80, (2), 251-5.

32.   Ma, C.; Fan, R.; Ahmad, H.; Shi, Q.; Comin-Anduix, B.; Chodon, T.; Koya, R. C.; Liu, C. C.; Kwong, G. A.; Radu, C. G.; Ribas, A.; Heath, J. R., A clinical microchip for evaluation of single immune cells reveals high functional heterogeneity in phenotypically similar T cells. *Nat Med* **2011,** 17, (6), 738-43.

33.   Love, J. C.; Ronan, J. L.; Grotenbreg, G. M.; van der Veen, A. G.; Ploegh, H. L., A microengraving method for rapid selection of single cells producing antigen-specific antibodies. *Nat Biotechnol* **2006,** 24, (6), 703-7.

34.   Ogunniyi, A. O.; Story, C. M.; Papa, E.; Guillen, E.; Love, J. C., Screening individual hybridomas by microengraving to discover monoclonal antibodies. *Nat Protoc* **2009,** 4, (5), 767-82.

35.   Zhu, H.; Stybayeva, G.; Silangcruz, J.; Yan, J.; Ramanculov, E.; Dandekar, S.; George, M. D.; Revzin, A., Detecting cytokine release from single T-cells. *Anal Chem* **2009,** 81, (19), 8150-6.

36.   Tokimitsu, Y.; Kishi, H.; Kondo, S.; Honda, R.; Tajiri, K.; Motoki, K.; Ozawa, T.; Kadowaki, S.; Obata, T.; Fujiki, S.; Tateno, C.; Takaishi, H.; Chayama, K.; Yoshizato, K.; Tamiya, E.; Sugiyama, T.; Muraguchi, A., Single lymphocyte analysis with a microwell array chip. *Cytometry A* **2007,** 71, (12), 1003-10.

37.   Reddy, S. T.; Georgiou, G., Systems analysis of adaptive immunity by utilization of high-throughput technologies. *Curr Opin Biotechnol* **2011,** 22, (4), 584-9.

38.   Piliarik, M.; Bockova, M.; Homola, J., Surface plasmon resonance biosensor for parallelized detection of protein biomarkers in diluted blood plasma. *Biosens Bioelectron* 26, (4), 1656-61.

39.   Englebienne, P.; Van Hoonacker, A.; Verhas, M., Surface plasmon resonance: principles, methods and applications in biomedical sciences. *Spectroscopy* **2003,** 17, 255-273.

40.   Chabot, V.; Cuerrier, C. M.; Escher, E.; Aimez, V.; Grandbois, M.; Charette, P. G., Biosensing based on surface plasmon resonance and living cells. *Biosens Bioelectron* **2009,** 24, (6), 1667-73.

41.   Bienvenu, J.; Monneret, G.; Fabien, N.; Revillard, J. P., The clinical usefulness of the measurement of cytokines. *Clin Chem Lab Med* **2000,** 38, (4), 267-85.

42.   Mattanovich, D.; Borth, N., Applications of cell sorting in biotechnology. *Microb Cell Fact* **2006,** 5, 12.

43.   El-Ali, J.; Sorger, P. K.; Jensen, K. F., Cells on chips. *Nature* **2006,** 442, (7101), 403-11.

44.   Andersson, E.; Van den Berg, A., Microfluidic devices for cellomics. A general overview of the field. In *Lab-on-Chips for cellomics*, Springer: 2007; pp 1-22.

45.   Salieb-Beugelaar, G. B.; Simone, G.; Arora, A.; Philippi, A.; Manz, A., Latest developments in microfluidic cell biology and analysis systems. *Analytical Chemistry* **2010,** 82, (12), 4848-64.

46.   Manbachi, A.; Shrivastava, S.; Cioffi, M.; Chung, B. G.; Moretti, M.; Demirci, U.; Yliperttula, M.; Khademhosseini, A., Microcirculation within grooved substrates regulates cell positioning and cell docking inside microfluidic channels. *Lab Chip* **2008,** 8, (5), 747-54.

47.   Horsman, K. M.; Barker, S. L.; Ferrance, J. P.; Forrest, K. A.; Koen, K. A.; Landers, J. P., Separation of sperm and epithelial cells in a microfabricated device: potential application to forensic analysis of sexual assault evidence. *Anal Chem* **2005,** 77, (3), 742-9.

48.   Kim, S. M.; Lee, S. H.; Suh, K. Y., Cell research with physically modified microfluidic channels: a review. *Lab Chip* **2008,** 8, (7), 1015-23.

49.   Johann, R.; Renaud, P., A simple mechanism for reliable particle sorting in a microdevice with combined electroosmotic and pressure-driven flow. *Electrophoresis* **2004,** 25, (21-22), 3720-9.

50.   Chou, H.-P.; Spence, C.; Fu, A.; Scherer, A.; Quake, S., Disposable microdevices for dna analysis and cell sorting. *Proceedings in Solid-State Sensor and Actuator Workshop* **1998**, 11-14.

51.   Taff, B. M.; Voldman, J., A scalable addressable positive-dielectrophoretic cell-sorting array. *Anal Chem* **2005,** 77, (24), 7976-83.

52.   Fuchs, A. B.; Romani, A.; Freida, D.; Medoro, G.; Abonnenc, M.; Altomare, L.; Chartier, I.; Guergour, D.; Villiers, C.; Marche, P. N.; Tartagni, M.; Guerrieri, R.; Chatelain, F.; Manaresi, N., Electronic sorting and recovery of single live cells from microlitre sized samples. *Lab Chip* **2006,** 6, (1), 121-6.

53.   Adams, J. D.; Kim, U.; Soh, H. T., Multitarget magnetic activated cell sorter. *Proceedings of the National Academy of Sciences of the United States of America* **2008,** 105, (47), 18165-18170.

54.   Saliba, A. E.; Saias, L.; Psychari, E.; Minc, N.; Simon, D.; Bidard, F. C.; Mathiot, C.; Pierga, J. Y.; Fraisier, V.; Salamero, J.; Saada, V.; Farace, F.; Vielh, P.; Malaquin, L.; Viovy, J. L., Microfluidic sorting and multimodal typing of cancer cells in self-assembled magnetic arrays. *Proc Natl Acad Sci U S A* **2010,** 107, (33), 14524-9.

55.   Werner, M.; Merenda, F.; Piguet, J.; Salathe, R. P.; Vogel, H., Microfluidic array cytometer based on refractive optical tweezers for parallel trapping, imaging and sorting of individual cells. *Lab Chip* **2011,** 11, (14), 2432-9.

56.   Cho, S. H.; Chen, C. H.; Tsai, F. S.; Godin, J. M.; Lo, Y. H., Human mammalian cell sorting using a highly integrated micro-fabricated fluorescence-activated cell sorter (microFACS). *Lab Chip* **2010,** 10, (12), 1567-73.

57.   Revzin, A.; Sekine, K.; Sin, A.; Tompkins, R. G.; Toner, M., Development of a microfabricated cytometry platform for characterization and sorting of individual leukocytes. *Lab Chip* **2005,** 5, (1), 30-7.

58.   Plouffe, B. D.; Brown, M. A.; Iyer, R. K.; Radisic, M.; Murthy, S. K., Controlled capture and release of cardiac fibroblasts using peptide-functionalized alginate gels in microfluidic channels. *Lab Chip* **2009,** 9, (11), 1507-10.

59.   Bailey, R. C.; Kwong, G. A.; Radu, C. G.; Witte, O. N.; Heath, J. R., DNA-encoded antibody libraries: A unified platform for multiplexed cell sorting and detection of genes and proteins. *Journal of the American Chemical Society* **2007,** 129, (7), 1959-1967.

60.   Nagrath, S.; Sequist, L. V.; Maheswaran, S.; Bell, D. W.; Irimia, D.; Ulkus, L.; Smith, M. R.; Kwak, E. L.; Digumarthy, S.; Muzikansky, A.; Ryan, P.; Balis, U. J.; Tompkins, R. G.; Haber,

D. A.; Toner, M., Isolation of rare circulating tumour cells in cancer patients by microchip technology. *Nature* **2007,** 450, (7173), 1235-9.

61.   Xia, N.; Hunt, T. P.; Mayers, B. T.; Alsberg, E.; Whitesides, G. M.; Westervelt, R. M.; Ingber, D. E., Combined microfluidic-micromagnetic separation of living cells in continuous flow. *Biomed Microdevices* **2006,** 8, (4), 299-308.

62.   Kose, A. R.; Fischer, B.; Mao, L.; Koser, H., Label-free cellular manipulation and sorting via biocompatible ferrofluids. *Proc Natl Acad Sci U S A* **2009,** 106, (51), 21478-83.

63.   Estes, M. D.; Ouyang, B.; Ho, S.-M.; Ahn, C. H., Isolation of prostate cancer cell subpopulations of functional interest by use of an on-chip magnetic bead-based cell separator. *Journal of Micromechanics and Microengineering* **2009,** 19, 1-8.

64.   Zborowski, M.; Chalmers, J. J., Rare Cell Separation and Analysis by Magnetic Sorting. *Analytical Chemistry* **2011**.

65.   Kim, D. H.; Haake, A.; Sun, Y.; Neild, A. P.; Ihm, J. E.; Dual, J.; Hubbell, J. A.; Ju, B. K.; Nelson, B. J., High-throughput cell manipulation using ultrasound fields. *Conf Proc IEEE Eng Med Biol Soc* **2004,** 4, 2571-4.

66.   Johansson, L.; Nikolajeff, F.; Johansson, S.; Thorslund, S., On-chip fluorescence-activated cell sorting by an integrated miniaturized ultrasonic transducer. *Anal Chem* **2009,** 81, (13), 5188-96.

67.   Jonas, A.; Zemanek, P., Light at work: the use of optical forces for particle manipulation, sorting, and analysis. *Electrophoresis* **2008,** 29, (24), 4813-51.

68.   Wang, M. M.; Tu, E.; Raymond, D. E.; Yang, J. M.; Zhang, H.; Hagen, N.; Dees, B.; Mercer, E. M.; Forster, A. H.; Kariv, I.; Marchand, P. J.; Butler, W. F., Microfluidic sorting of mammalian cells by optical force switching. *Nat Biotechnol* **2005,** 23, (1), 83-7.

69.   Fu, A. Y.; Spence, C.; Scherer, A.; Arnold, F. H.; Quake, S. R., A microfabricated fluorescence-activated cell sorter. *Nat Biotechnol* **1999,** 17, (11), 1109-11.

70.   Didar, T. F.; Tabrizian, M., Adhesion based detection, sorting and enrichment of cells in microfluidic Lab-on-Chip devices. *Lab Chip* **2010,** 10, (22), 3043-53.

71.   Wysocki, L. J.; Sato, V. L., "Panning" for lymphocytes: a method for cell selection. *Proc Natl Acad Sci U S A* **1978,** 75, (6), 2844-8.

72.   Anglin, E. J.; Salisbury, C.; Bailey, S.; Hor, M.; Macardle, P.; Fenech, M.; Thissen, H.; Voelcker, N. H., Sorted cell microarrays as platforms for high-content informational bioassays. *Lab Chip* **2010,** 10, (24), 3413-21.

73.   Plouffe, B. D.; Radisic, M.; Murthy, S. K., Microfluidic depletion of endothelial cells, smooth muscle cells, and fibroblasts from heterogeneous suspensions. *Lab Chip* **2008,** 8, (3), 462-72.

74.   Xu, Y.; Phillips, J. A.; Yan, J.; Li, Q.; Fan, Z. H.; Tan, W., Aptamer-based microfluidic device for enrichment, sorting, and detection of multiple cancer cells. *Anal Chem* **2009,** 81, (17), 7436-42.

75.   Kwong, G. A.; Radu, C. G.; Hwang, K.; Shu, C. J. Y.; Ma, C.; Koya, R. C.; Comin-Anduix, B.; Hadrup, S. R.; Bailey, R. C.; Witte, O. N.; Schumacher, T. N.; Ribas, A.; Heath, J. R., Modular Nucleic Acid Assembled p/MHC Microarrays for Multiplexed Sorting of Antigen-Specific T Cells. *Journal of the American Chemical Society* **2009,** 131, (28), 9695-9703.

76.   Adams, A. A.; Okagbare, P. I.; Feng, J.; Hupert, M. L.; Patterson, D.; Gottert, J.; McCarley, R. L.; Nikitopoulos, D.; Murphy, M. C.; Soper, S. A., Highly efficient circulating tumor cell isolation from whole blood and label-free enumeration using polymer-based microfluidics with an integrated conductivity sensor. *J Am Chem Soc* **2008,** 130, (27), 8633-41.

77.   Kaji, H.; Tsukidate, K.; Hashimoto, M.; Matsue, T.; Nishizawa, M., Patterning the surface cytophobicity of an albumin-physisorbed substrate by electrochemical means. *Langmuir* **2005,** 21, (15), 6966-6969.

78.   Hattori, K.; Sugiura, S.; Kanamori, T., On-chip cell culture on a microarray of extracellular matrix with surface modification of poly(dimethylsiloxane). *Biotechnol J* **2010,** 5, (5), 463-9.

79.   Suraniti, E.; Sollier, E.; Calemczuk, R.; Livache, T.; Marche, P. N.; Villiers, M. B.; Roupioz, Y., Real-time detection of lymphocytes binding on an antibody chip using SPR imaging. *Lab Chip* **2007,** 7, (9), 1206-8.

80.   Schroeder, H.; Ellinger, B.; Becker, C. F.; Waldmann, H.; Niemeyer, C. M., Generation of live-cell microarrays by means of DNA-Directed immobilization of specific cell-surface ligands. *Angew Chem Int Ed Engl* **2007,** 46, (22), 4180-3.

81.   Chen, L.; Liu, X.; Su, B.; Li, J.; Jiang, L.; Han, D.; Wang, S., Aptamer-Mediated Efficient Capture and Release of T Lymphocytes on Nanostructured Surfaces. *Adv Mater* **2011**.

82.   Chandra, R. A.; Douglas, E. S.; Mathies, R. A.; Bertozzi, C. R.; Francis, M. B., Programmable cell adhesion encoded by DNA hybridization. *Angew Chem Int Ed Engl* **2006,** 45, (6), 896-901.

83.   Douglas, E. S.; Chandra, R. A.; Bertozzi, C. R.; Mathies, R. A.; Francis, M. B., Self-assembled cellular microarrays patterned using DNA barcodes. *Lab Chip* **2007,** 7, (11), 1442-8.

84.   Kovac, J. R.; Voldman, J., Intuitive, image-based cell sorting using optofluidic cell sorting. *Anal Chem* **2007,** 79, (24), 9321-30.

85.   Wang, Y.; Phillips, C.; Xu, W.; Pai, J. H.; Dhopeshwarkar, R.; Sims, C. E.; Allbritton, N., Micromolded arrays for separation of adherent cells. *Lab Chip* **2010,** 10, (21), 2917-24.

86.   Mulvaney, S. P.; Cole, C. L.; Kniller, M. D.; Malito, M.; Tamanaha, C. R.; Rife, J. C.; Stanton, M. W.; Whitman, L. J., Rapid, femtomolar bioassays in complex matrices combining microfluidics and magnetoelectronics. *Biosens Bioelectron* **2007,** 23, (2), 191-200.

87.   Wankhede, S. P.; Du, Z.; Berg, J. M.; Vaughn, M. W.; Dallas, T.; Cheng, K. H.; Gollahon, L., Cell detachment model for an antibody-based microfluidic cancer screening system. *Biotechnol Prog* **2006,** 22, (5), 1426-33.

88.   Mendes, P. M., Stimuli-responsive surfaces for bio-applications. *Chem Soc Rev* **2008,** 37, (11), 2512-29.

89.   Robertus, J.; Browne, W. R.; Feringa, B. L., Dynamic control over cell adhesive properties using molecular-based surface engineering strategies. *Chem Soc Rev* **2010,** 39, (1), 354-78.

90.   Zhu, H.; Yan, J.; Revzin, A., Catch and release cell sorting: electrochemical desorption of T-cells from antibody-modified microelectrodes. *Colloids Surf B Biointerfaces* **2008,** 64, (2), 260-8.

91.   Choi, S.; Chae, J., Reusable biosensors via in situ electrochemical surface regeneration in microfluidic applications. *Biosensors & Bioelectronics* **2009,** 25, (2), 527-531.

92.   Chan, E. W. L.; Park, S.; Yousaf, M. N., An electroactive catalytic dynamic substrate that immobilizes and releases patterned ligands, proteins, and cells. *Angewandte Chemie-International Edition* **2008,** 47, (33), 6267-6271.

93.   Yeo, W. S.; Yousaf, M. N.; Mrksich, M., Dynamic interfaces between cells and surfaces: electroactive substrates that sequentially release and attach cells. *J Am Chem Soc* **2003,** 125, (49), 14994-5.

94.   Yeo, W. S.; Hodneland, C. D.; Mrksich, M., Electroactive monolayer substrates that selectively release adherent cells. *Chembiochem* **2001,** 2, (7-8), 590-3.

95.   Dubacheva, G. V.; Galibert, M.; Coche-Guerente, L.; Dumy, P.; Boturyn, D.; Labbe, P., Redox strategy for reversible attachment of biomolecules using bifunctional linkers. *Chem Commun (Camb)* **2011,** 47, (12), 3565-7.

96.   Yeo, W. S.; Mrksich, M., Electroactive self-assembled monolayers that permit orthogonal control over the adhesion of cells to patterned substrates. *Langmuir* **2006,** 22, (25), 10816-20.

97.   Derfus, A. M.; von Maltzahn, G.; Harris, T. J.; Duza, T.; Vecchio, K. S.; Ruoslahti, E.; Bhatia, S. N., Remotely triggered release from magnetic nanoparticles. *Advanced Materials* **2007,** 19, (22), 3932-+.

98.   Hatakeyama, H.; Kikuchi, A.; Yamato, M.; Okano, T., Patterned biofunctional designs of thermoresponsive surfaces for spatiotemporally controlled cell adhesion, growth, and thermally induced detachment. *Biomaterials* **2007,** 28, (25), 3632-3643.

99.   Okano, K.; Yasuda, K.; Ishiwata, S., Position-specific release of DNA from a chip by using photothermal denaturation. *Sensors and Actuators B-Chemical* **2000,** 64, (1-3), 88-94.

100.   Cheng, X. H.; Wang, Y. B.; Hanein, Y.; Bohringer, K. F.; Ratner, B. D., Novel cell patterning using microheater-controlled thermoresponsive plasma films. *Journal of Biomedical Materials Research Part A* **2004,** 70A, (2), 159-168.

101.   Higuchi, A.; Hamamura, A.; Shindo, Y.; Kitamura, H.; Yoon, B. O.; Mori, T.; Uyama, T.; Umezawa, A., Photon-modulated changes of cell attachments on poly(spiropyran-co-methyl methacrylate) membranes. *Biomacromolecules* **2004,** 5, (5), 1770-1774.

102.   Angelos, S.; Yang, Y. W.; Patel, K.; Stoddart, J. F.; Zink, J. I., pH-responsive supramolecular nanovalves based on cucurbit[6]uril pseudorotaxanes. *Angew Chem Int Ed Engl* **2008,** 47, (12), 2222-6.

103. Goodman, R. P.; Erben, C. M.; Malo, J.; Ho, W. M.; McKee, M. L.; Kapanidis, A. N.; Turberfield, A. J., A facile method for reversibly linking a recombinant protein to DNA. *Chembiochem* **2009,** 10, (9), 1551-7.

104. Fernandes, R.; Zuniga, M.; Sassine, F. R.; Karakoy, M.; Gracias, D. H., Enabling cargo-carrying bacteria via surface attachment and triggered release. *Small* **2011,** 7, (5), 588-92.

105. Van Beuningen, M. G. J. Novel high density arrays and methods for analyte analysis, United States Patent Application Publication (US 2005/0202433 A1). 2005.

106. Fischer, A.; von Eiff, C.; Kuczius, T.; Omoe, K.; Peters, G.; Becker, K., A quantitative real-time immuno-PCR approach for detection of staphylococcal enterotoxins. *J Mol Med (Berl)* **2007,** 85, (5), 461-9.

107. Palmer, E., Cell-based microarrays: overview. *Methods Mol Biol* **2011,** 706, 1-12.

108. Ziauddin, J.; Sabatini, D. M., Microarrays of cells expressing defined cDNAs. *Nature* **2001,** 411, (6833), 107-10.

109. Zhu, H.; Snyder, M., Protein chip technology. *Curr Opin Chem Biol* **2003,** 7, (1), 55-63.

110. Belov, L.; de la Vega, O.; dos Remedios, C. G.; Mulligan, S. P.; Christopherson, R. I., Immunophenotyping of leukemias using a cluster of differentiation antibody microarray. *Cancer Res* **2001,** 61, (11), 4483-9.

111. Lal, S. P.; Christopherson, R. I.; dos Remedios, C. G., Antibody arrays: an embryonic but rapidly growing technology. *Drug Discov Today* **2002,** 7, (18 Suppl), S143-9.

112. Rivas, L. A.; Garcia-Villadangos, M.; Moreno-Paz, M.; Cruz-Gil, P.; Gomez-Elvira, J.; Parro, V., A 200-antibody microarray biochip for environmental monitoring: searching for universal microbial biomarkers through immunoprofiling. *Anal Chem* **2008,** 80, (21), 7970-9.

113. Douglas, E. S.; Hsiao, S. C.; Onoe, H.; Bertozzi, C. R.; Francis, M. B.; Mathies, R. A., DNA-barcode directed capture and electrochemical metabolic analysis of single mammalian cells on a microelectrode array. *Lab Chip* **2009,** 9, (14), 2010-5.

114. Reisewitz, S.; Schroeder, H.; Tort, N.; Edwards, K. A.; Baeumner, A. J.; Niemeyer, C. M., Capture and Culturing of Living Cells on Microstructured DNA Substrates. *Small* **2010,** 6, (19), 2162-2168.

115. Bovin, N. V.; Gilliver, L. G.; Henry, S. M.; Korchagina, E. Y. Synthetic molecule constructs. New Zealand Patent (550705). 2011.

116. Wacker, R.; Schroder, H.; Niemeyer, C. M., Performance of antibody microarrays fabricated by either DNA-directed immobilization, direct spotting, or streptavidin-biotin attachment: a comparative study. *Analytical Biochemistry* **2004,** 330, (2), 281-287.

117. Niemeyer, C. M.; Sano, T.; Smith, C. L.; Cantor, C. R., Oligonucleotide-Directed Self-Assembly of Proteins - Semisynthetic DNA Streptavidin Hybrid Molecules as Connectors for the Generation of Macroscopic Arrays and the Construction of Supramolecular Bioconjugates. *Nucleic Acids Research* **1994,** 22, (25), 5530-5539.

118.	Kang, D. J.; Kim, D. C., Molecular Recognition and Specific Interactions for Biosensing Applications. *Sensors* **2008,** 8, (10), 6605-6641.

119.	Sarkar, A.; Samanta, D., Immobilization of bio-macromolecules on self-assembled monolayers: methods and sensor applications. *Chemical Society Reviews* **2011,** 40, (5), 2567-2592.

120.	Garnier, F.; Bouabdallaoui, B.; Srivastava, P.; Mandrand, B.; Chaix, C., Conjugated polymer-based DNA chip with real time access and femtomol detection threshold. *Sensors and Actuators B-Chemical* **2007,** 123, (1), 13-20.

121.	Livache, T.; Roget, A.; Dejean, E.; Barthet, C.; Bidan, G.; Teoule, R., Preparation of a DNA Matrix Via an Electrochemically Directed Copolymerization of Pyrrole and Oligonucleotides Bearing a Pyrrole Group. *Nucleic Acids Research* **1994,** 22, (15), 2915-2921.

122.	Fuchs, J. Physicochemical study of DNA biochips. DNA duplex stability, point mutation detection and beyond. PhD thesis, Université Joseph Fourier - Grenoble I, Grenoble, 2008.

123.	Guedon, P.; Livache, T.; Martin, F.; Lesbre, F.; Roget, A.; Bidan, G.; Levy, Y., Characterization and optimization of a real-time, parallel, label-free, polypyrrole-based DNA sensor by surface plasmon resonance imaging. *Anal Chem* **2000,** 72, (24), 6003-9.

124.	Singh, Y.; Murat, P.; Defrancq, E., Recent developments in oligonucleotide conjugation. *Chem Soc Rev* **2010,** 39, (6), 2054-70.

125.	Niemeyer, C. M., Semisynthetic DNA-Protein Conjugates for Biosensing and Nanofabrication. *Angewandte Chemie-International Edition* **2010,** 49, (7), 1200-1216.

126.	Niemeyer, C. M., The developments of semisynthetic DNA-protein conjugates. *Trends in Biotechnology* **2002,** 20, (9), 395-401.

127.	Jablonski, E.; Moomaw, E. W.; Tullis, R. H.; Ruth, J. L., Preparation of oligodeoxynucleotide-alkaline phosphatase conjugates and their use as hybridization probes. *Nucleic Acids Res* **1986,** 14, (15), 6115-28.

128.	Ghosh, S. S.; Kao, P. M.; McCue, A. W.; Chappelle, H. L., Use of maleimide-thiol coupling chemistry for efficient syntheses of oligonucleotide-enzyme conjugate hybridization probes. *Bioconjug Chem* **1990,** 1, (1), 71-6.

129.	Kynclova, E.; Hartig, A.; Schalkhammer, T., Oligonucleotide labelled lipase as a new sensitive hybridization probe and its use in bio-assays and biosensors. *Journal of Molecular Recognition* **1995,** 8, (1-2), 139-145.

130.	Fruk, L.; Muller, J.; Weber, G.; Narvaez, A.; Dominguez, E.; Niemeyer, C. M., DNA-Directed immobilization of horseradish peroxidase-DNA conjugates on microelectrode arrays: Towards electrochemical screening of enzyme libraries. *Chemistry-a European Journal* **2007,** 13, (18), 5223-5231.

131.	Kuijpers, W. H. A.; Bos, E. S.; Kaspersen, F. M.; Veeneman, G. H.; Vanboeckel, C. A. A., Specific Recognition of Antibody Oligonucleotide Conjugates by Radiolabeled Antisense Nucleotides - a Novel-Approach for 2-Step Radioimmunotherapy of Cancer. *Bioconjugate Chemistry* **1993,** 4, (1), 94-102.

132. Goussu, C.; Vasseur, J. J.; Bazin, H.; Trinquet, E.; Maurin, F.; Morvan, F., Optimized synthesis of functionalized fluorescent oligodeoxynucleotides for protein labeling. *Bioconjug Chem* **2005,** 16, (2), 465-70.

133. Jung, Y.; Lee, J. M.; Jung, H.; Chung, B. H., Self-directed and self-oriented immobilization of antibody by protein G-DNA conjugate. *Analytical Chemistry* **2007,** 79, (17), 6534-6541.

134. Lapiene, V.; Kukolka, F.; Kiko, K.; Arndt, A.; Niemeyer, C. M., Conjugation of fluorescent proteins with DNA oligonucleotides. *Bioconjug Chem* **2010,** 21, (5), 921-7.

135. Rajur, S. B.; Roth, C. M.; Morgan, J. R.; Yarmush, M. L., Covalent protein-oligonucleotide conjugates for efficient delivery of antisense molecules. *Bioconjugate Chemistry* **1997,** 8, (6), 935-940.

136. Kukolka, F.; Niemeyer, C. M., Synthesis of fluorescent oligonucleotide-EYFP conjugate: Towards supramolecular construction of semisynthetic biomolecular antennae. *Organic & Biomolecular Chemistry* **2004,** 2, (15), 2203-2206.

137. Sano, T.; Smith, C. L.; Cantor, C. R., Immuno-PCR: very sensitive antigen detection by means of specific antibody-DNA conjugates. *Science* **1992,** 258, (5079), 120-2.

138. Ladd, J.; Boozer, C.; Yu, Q. M.; Chen, S. F.; Homola, J.; Jiang, S., DNA-directed protein immobilization on mixed self-assembled monolayers via a Streptavidin bridge. *Langmuir* **2004,** 20, (19), 8090-8095.

139. Niemeyer, C. M.; Ceyhan, B.; Blohm, D., Functionalization of covalent DNA-streptavidin conjugates by means of biotinylated modulator components. *Bioconjugate Chemistry* **1999,** 10, (5), 708-719.

140. Hermanson, G. T., *Bioconjugate techniques*. Elsevier Inc.: 2008.

141. Ladd, J.; Taylor, A. D.; Piliarik, M.; Homola, J.; Jiang, S., Hybrid surface platform for the simultaneous detection of proteins and DNAs using a surface plasmon resonance imaging sensor. *Anal Chem* **2008,** 80, (11), 4231-6.

142. Kukolka, F.; Lovrinovic, M.; Wacker, R.; Niemeyer, C. M., Covalent coupling of DNA oligonucleotides and streptavidin. In *Methods in molecular biology, vol.283: Bioconjugation protocols: strategies and methods*, Humana Press Onc., Totowa, NJ.

143. Boozer, C.; Ladd, J.; Chen, S. F.; Yu, Q.; Homola, J.; Jiang, S. Y., DNA directed protein immobilization on mixed ssDNA/oligo(ethylene glycol) self-assembled monolayers for sensitive biosensors. *Analytical Chemistry* **2004,** 76, (23), 6967-6972.

144. Chaudri, Z. N.; Bartlet-Jones, M.; Panayotou, G.; Klonisch, T.; Roitt, I. M.; Lund, T.; Delves, P. J., Dual specificity antibodies using a double-stranded oligonucleotide bridge. *Febs Letters* **1999,** 450, (1-2), 23-26.

145. Kawabata, T.; Watanabe, M.; Nakamura, K.; Satomura, S., Liquid-phase binding assay of alpha-fetoprotein using DNA-coupled antibody and capillary chip electrophoresis. *Anal Chem* **2005,** 77, (17), 5579-82.

146. Bombera, R. Biochips development for biological applications: restriction enzyme exploration and antibody-DNA conjugate chemistry for reversible cell capture. Master thesis, Gdansk University of Technology/Joseph Fourier University in Grenoble, Gdansk, 2008.

147. Ruth, J. L., Protocols for oligonucleotide conjugates. In *Methods in molecular biology*, Vol. 26, pp 170-177.

148. Boozer, C.; Ladd, J.; Chen, S. F.; Jiang, S. T., DNA-directed protein immobilization for simultaneous detection of multiple analytes by surface plasmon resonance biosensor. *Analytical Chemistry* **2006,** 78, (5), 1515-1519.

149. Li, G.; Stewart, R.; Conlan, B.; Gilbert, A.; Roeth, P.; Nair, H., Purification of human immunoglobulin G: a new approach to plasma fractionation. *Vox Sang* **2002,** 83, (4), 332-8.

150. Sauvaigo, S.; Guerniou, V.; Rapin, D.; Gasparutto, D.; Caillat, S.; Favier, A., An oligonucleotide microarray for the monitoring of repair enzyme activity toward different DNA base damage. *Anal Biochem* **2004,** 333, (1), 182-92.

151. Weber, P. C.; Ohlendorf, D. H.; Wendoloski, J. J.; Salemme, F. R., Structural origins of high-affinity biotin binding to streptavidin. *Science* **1989,** 243, (4887), 85-8.

152. Pattnaik, P., Surface plasmon resonance - Applications in understanding receptor-ligand interaction. *Applied Biochemistry and Biotechnology* **2005,** 126, (2), 79-92.

153. Lausted, C.; Hu, Z.; Hood, L., Quantitative serum proteomics from surface plasmon resonance imaging. *Mol Cell Proteomics* **2008,** 7, (12), 2464-74.

154. Maillart, E.; Bassil, N.; Lecaruyer, P.; Canva, M.; Levy, Y., Surface plasmon resonance imaging and versatile surface functionalization for real time comparisons of biochemical interactions. *Biophotonics New Frontier: From Genome to Proteome* **2004,** 5461, 69-77 90.

155. Mercey, E.; Sadir, R.; Maillart, E.; Roget, A.; Baleux, F.; Lortat-Jacob, H.; Livache, T., Polypyrrole oligosaccharide array and surface plasmon resonance imaging for the measurement of glycosaminoglycan binding interactions. *Anal Chem* **2008,** 80, (9), 3476-82.

156. Homola, J., Surface plasmon resonance sensors for detection of chemical and biological species. *Chemical Reviews* **2008,** 108, (2), 462-493.

157. Kretschm.E; Raether, H., Radiative Decay of Non Radiative Surface Plasmons Excited by Light. *Zeitschrift Fur Naturforschung Part a-Astrophysik Physik Und Physikalische Chemie* **1968,** A 23, (12), 2135-&.

158. Homola, J., Electromagnetic theory of surface plasmons. In *Surface plasmon resonance based sensors*, Springer: 2006; Vol. 4, pp 3-44.

159. Campbell, C. T.; Kim, G., SPR microscopy and its applications to high-throughput analyses of biomolecular binding events and their kinetics. *Biomaterials* **2007,** 28, (15), 2380-2392.

160. Maillart, E.; Brengel-Pesce, K.; Capela, D.; Roget, A.; Livache, T.; Canva, M.; Levy, Y.; Soussi, T., Versatile analysis of multiple macromolecular interactions by SPR imaging: application to p53 and DNA interaction. *Oncogene* **2004,** 23, (32), 5543-5550.

161.   Chung, B. H.; Ha, T. H.; Jung, S. O.; Lee, J. M.; Lee, K. Y.; Lee, Y.; Park, J. S., Oriented immobilization of antibodies with GST-fused multiple F-c-specific B-domains on a gold surface. *Analytical Chemistry* **2007,** 79, (2), 546-556.

162.   Wong, D. K. Y.; Fowler, J. M.; Stuart, M. C., Self-assembled layer of thiolated protein G as an immunosensor scaffold. *Analytical Chemistry* **2007,** 79, (1), 350-354.

163.   Barbari, T. A.; Ahmed, S. R.; Lutes, A. T., Specific capture of target proteins by oriented antibodies bound to tyrosinase-immobilized Protein A on a polyallylamine affinity membrane surface. *Journal of Membrane Science* **2006,** 282, (1-2), 311-321.

164.   Zhao, W.; Lam, J. C.; Chiuman, W.; Brook, M. A.; Li, Y., Enzymatic cleavage of nucleic acids on gold nanoparticles: a generic platform for facile colorimetric biosensors. *Small* **2008,** 4, (6), 810-6.

165.   Chen, J.; Zhang, J.; Yang, H.; Fu, F.; Chen, G., A strategy for development of electrochemical DNA biosensor based on site-specific DNA cleavage of restriction endonuclease. *Biosens Bioelectron* 26, (1), 144-8.

166.   Venkatesh, S.; Wower, J.; Byrne, M. E., Nucleic acid therapeutic carriers with on-demand triggered release. *Bioconjug Chem* **2009,** 20, (9), 1773-82.

167.   Wang, Z.; Lee, J.; Cossins, A.; Brust, M., Selective enzymatic cleavage of gold nanoparticle-labelled DNA on a microarray. *IEE Proc Nanobiotechnol* **2005,** 152, (2), 85-8.

168.   Glass, J. R.; Dickerson, J. C.; Schultz, D. A., Enzyme-mediated individual nanoparticle release assay. *Anal Biochem* **2006,** 353, (2), 209-16.

169.   Ma, C.; Tang, Z.; Huo, X.; Yang, X.; Li, W.; Tan, W., Real-time monitoring of double-stranded DNA cleavage using molecular beacons. *Talanta* **2008,** 76, (2), 458-61.

170.   Hillier, S. C.; Frost, C. G.; Jenkins, A. T.; Braven, H. T.; Keay, R. W.; Flower, S. E.; Clarkson, J. M., An electrochemical study of enzymatic oligonucleotide digestion. *Bioelectrochemistry* **2004,** 63, (1-2), 307-10.

171.   Pingoud, A.; Jeltsch, A., Structure and function of type II restriction endonucleases. *Nucleic Acids Res* **2001,** 29, (18), 3705-27.

172.   Protein Data Bank website. a) 2OXV: Structure of the A138T promiscuous mutant of the EcoRI restriction endonuclease bound to its cognate recognition site;.b) 3KSK: Crystal Structure of single chain PvuII. http://www.pdb.org/pdb/home/home.do

173.   Corne, C.; Fiche, J. B.; Gasparutto, D.; Cunin, V.; Suraniti, E.; Buhot, A.; Fuchs, J.; Calemczuk, R.; Livache, T.; Favier, A., SPR imaging for label-free multiplexed analyses of DNA N-glycosylase interactions with damaged DNA duplexes. *Analyst* **2008,** 133, (8), 1036-45.

174.   Lee, H. J.; Wark, A. W.; Corn, R. M., Creating advanced multifunctional biosensors with surface enzymatic transformations. *Langmuir* **2006,** 22, (12), 5241-50.

175.   Pogacnik, L.; Franko, M., Detection of organophosphate and carbamate pesticides in vegetable samples by a photothermal biosensor. *Biosens Bioelectron* **2003,** 18, (1), 1-9.

176.   Moro, T.; Takatori, Y.; Ishihara, K.; Konno, T.; Takigawa, Y.; Matsushita, T.; Chung, U. I.; Nakamura, K.; Kawaguchi, H., Surface grafting of artificial joints with a biocompatible polymer for preventing periprosthetic osteolysis. *Nat Mater* **2004,** 3, (11), 829-36.

177.   Fuchs, R.; Blakesley, R., Guide to the use of type II restriction endonucleases. *Methods Enzymol* **1983,** 100, 3-38.

178.   Kozlowski, L. Calculation of protein isoelectric point. http://isoelectric.ovh.org/

179.   Stobo, J. D.; Rosenthal, A. S.; Paul, W. E., Functional heterogeneity of murine lymphoid cells. I. Responsiveness to and surface binding of concanavalin A and phytohemagglutinin. *J Immunol* **1972,** 108, (1), 1-17.

180.   Schwendel, D.; Dahint, R.; Herrwerth, S.; Schloerholz, M.; Eck, W.; Grunze, M., Temperature Dependence of the Protein Resistance of Poly- and Oligo(ethylene glycol)-Terminated Alkanethiolate Monolayers. *Langmuir* **2001,** 17, (19), 5717–5720.

181.   Cerruti, M.; Fissolo, S.; Carraro, C.; Ricciardi, C.; Majumdar, A.; Maboudian, R., Poly(ethylene glycol) monolayer formation and stability on gold and silicon nitride substrates. *Langmuir* **2008,** 24, (19), 10646-10653.

182.   Csucs, G.; Michel, R.; Lussi, J. W.; Textor, M.; Danuser, G., Microcontact printing of novel co-polymers in combination with proteins for cell-biological applications. *Biomaterials* **2003,** 24, (10), 1713-20.

183.   Jung, J.; Na, K.; Shin, B.; Kim, O.; Lee, J.; Yun, K.; Hyun, J., A cell-repellent sulfonated PEG comb-like polymer for highly resolved cell micropatterns. *J Biomater Sci Polym Ed* **2008,** 19, (2), 161-73.

184.   Scott, E. A.; Nichols, M. D.; Cordova, L. H.; George, B. J.; Jun, Y. S.; Elbert, D. L., Protein adsorption and cell adhesion on nanoscale bioactive coatings formed from poly(ethylene glycol) and albumin microgels. *Biomaterials* **2008,** 29, (34), 4481-93.

185.   Kira, A.; Okano, K.; Hosokawa, Y.; Naito, A.; Fuwa, J.; Yuyama, H.; Masuhara, H., Micropatterning of perfluoroalkyl self-assembled monolayers for arraying proteins and cells on chips. *Applied Surface Sciences* **2009,** 255, 7647-51.

186.   Okano, K.; Yu, D.; Matsui, A.; Maezawa, Y.; Hosokawa, Y.; Kira, A.; Matsubara, M.; Liau, I.; Tsubokawa, H.; Masuhara, H., Induction of cell-cell connections by using in situ laser lithography on a perfluoroalkyl-coated cultivation platform. *Chembiochem* 12, (5), 795-801.

187.   Falconnet, D.; Csucs, G.; Grandin, H. M.; Textor, M., Surface engineering approaches to micropattern surfaces for cell-based assays. *Biomaterials* **2006,** 27, (16), 3044-63.

188.   Tedder, T. F.; Isaacs, C. M., Isolation of cDNAs encoding the CD19 antigen of human and mouse B lymphocytes. A new member of the immunoglobulin superfamily. *J Immunol* **1989,** 143, (2), 712-7.

189.   Gunter, K. C.; Malek, T. R.; Shevach, E. M., T cell-activating properties of an anti-Thy-1 monoclonal antibody. Possible analogy to OKT3/Leu-4. *J Exp Med* **1984,** 159, (3), 716-30.

190.   Gaus, K.; Chklovskaia, E.; Fazekas de St Groth, B.; Jessup, W.; Harder, T., Condensation of the plasma membrane at the site of T lymphocyte activation. *J Cell Biol* **2005,** 171, (1), 121-31.

191.   Marguet, D.; Lenne, P. F.; Rigneault, H.; He, H. T., Dynamics in the plasma membrane: how to combine fluidity and order. *Embo J* **2006,** 25, (15), 3446-57.

192.   Gilligan, J. J.; Schuck, P.; Yergey, A. L., Mass spectrometry after capture and small-volume elution of analyte from a surface plasmon resonance biosensor. *Anal Chem* **2002,** 74, (9), 2041-7.

193.   Sohn, L. L.; Carbonaro, A.; Mohanty, S. K.; Huang, H. Y.; Godley, L. A., Cell characterization using a protein-functionalized pore. *Lab on a Chip* **2008,** 8, (9), 1478-1485.

194.   Zourob, M.; Elwary, S.; Turner, A. P., *Principles of Bacterial Detection: Biosensors, Recognition Receptors and Microsystems*. Springer: 2008.

195.   Elad, T.; Lee, J. H.; Belkin, S.; Gu, M. B., Microbial whole-cell arrays. *Microb Biotechnol* **2008,** 1, (2), 137-48.

196.   Yagi, K., Applications of whole-cell bacterial sensors in biotechnology and environmental science. *Appl Microbiol Biotechnol* **2007,** 73, (6), 1251-8.

197.   Melamed, S.; Ceriotti, L.; Weigel, W.; Rossi, F.; Colpo, P.; Belkin, S., A printed nanolitre-scale bacterial sensor array. *Lab Chip* **2011,** 11, (1), 139-46.

198.   Yang, M.; Kostov, Y.; Bruck, H. A.; Rasooly, A., Gold nanoparticle-based enhanced chemiluminescence immunosensor for detection of Staphylococcal Enterotoxin B (SEB) in food. *Int J Food Microbiol* **2009,** 133, (3), 265-71.

199.   Piliarik, M.; Parova, L.; Homola, J., High-throughput SPR sensor for food safety. *Biosens Bioelectron* **2009,** 24, (5), 1399-404.

200.   Gareis, M.; Heidenreich, B.; Pohlmann, C.; Sprinzl, M., Detection of Escherichia coli in Meat with an Electrochemical Biochip. *Journal of Food Protection* **2010,** 73, (11), 2025-2033.

201.   Zordan, M. D.; Grafton, M. M. G.; Park, K.; Leary, J. F., The design of a microfluidic biochip for the rapid, multiplexed detection of foodborne pathogens by surface plasmon resonance imaging. *Frontiers in Pathogen Detection: From Nanosensors to Systems* **2010,** 7553.

202.   Mazumdar, S. D.; Barlen, B.; Kampfer, P.; Keusgen, M., Surface plasmon resonance (SPR) as a rapid tool for serotyping of Salmonella. *Biosens Bioelectron* **2010,** 25, (5), 967-71.

203.   Dudak, F. C.; Boyaci, I. H., Rapid and label-free bacteria detection by surface plasmon resonance (SPR) biosensors. *Biotechnol J* **2009,** 4, (7), 1003-11.

204.   Paradisi, F.; Corti, G.; Cinelli, R., Streptococcus pneumoniae as an agent of nosocomial infection: treatment in the era of penicillin-resistant strains. *Clin Microbiol Infect* **2001,** 7 Suppl 4, 34-42.

205.   Attali, C.; Frolet, C.; Durmort, C.; Offant, J.; Vernet, T.; Di Guilmi, A. M., Streptococcus pneumoniae choline-binding protein E interaction with plasminogen/plasmin stimulates migration across the extracellular matrix. *Infect Immun* **2008,** 76, (2), 466-76.

206.   Garau, G.; Lemaire, D.; Vernet, T.; Dideberg, O.; Di Guilmi, A. M., Crystal structure of phosphorylcholine esterase domain of the virulence factor choline-binding protein e from

streptococcus pneumoniae: new structural features among the metallo-beta-lactamase superfamily. *J Biol Chem* **2005,** 280, (31), 28591-600.

207.   Kretschmann, E.; Raether, H., Radiative Decay of Non Radiative Surface Plasmons Excited by Light. *Zeitschrift Fur Naturforschung Part a-Astrophysik Physik Und Physikalische Chemie* **1968,** A 23, (12), 2135-2136.

208.   Bakhtiari, A. B. S.; Hsiao, D.; Jin, G. X.; Gates, B. D.; Branda, N. R., An Efficient Method Based on the Photothermal Effect for the Release of Molecules from Metal Nanoparticle Surfaces. *Angewandte Chemie-International Edition* **2009,** 48, (23), 4166-4169.

209.   Lee, S. E.; Lee, L. P., Nanoplasmonic gene regulation. *Current Opinion in Chemical Biology* **2010,** 14, (5), 623-633.

210.   Wu, T. H.; Teslaa, T.; Teitell, M. A.; Chiou, P. Y., Photothermal nanoblade for patterned cell membrane cutting. *Optics Express* **2010,** 18, (22), 23153-23160.

211.   Katayama, K.; Sawada, T.; Shen, Q.; Harata, A., Detection of photoinduced electronic, thermal, and acoustic dynamics of gold film using a transient reflecting grating method under three types of surface plasmon resonance conditions. *Physical Review B* **1998,** 58, (13), 8428-8436.

212.   Kurihara, K.; Nanri, K.; Goto, K., Thermal simulation for a two-dimensional near-field optical recording system using a vertical-cavity surface-emitting laser. *Applied Physics Letters* **2004,** 84, (17), 3415-3417.

213.   Rothenhausler, B.; Rabe, J.; Korpiun, P.; Knoll, W., On the Decay of Plasmon Surface-Polaritons at Smooth and Rough Ag-Air Interfaces - a Reflectance and Photo-Acoustic Study. *Surface Science* **1984,** 137, (1), 373-383.

214.   Xiao, X. J.; Gao, Y.; Xiang, J. A.; Zhou, F. M., Laser-induced thermal effect in surface plasmon resonance. *Analytica Chimica Acta* **2010,** 676, (1-2), 75-80.

215.   Liu, H. Y.; Chen, D.; Yang, L. Q.; Ren, X. L.; Tang, F. Q.; Ren, J., A study of the electron transfer and photothermal effect of gold nanorods on a glucose biosensor. *Nanotechnology* **2010,** 21, (18), -.

216.   Richardson, H. H.; Carlson, M. T.; Tandler, P. J.; Hernandez, P.; Govorov, A. O., Experimental and Theoretical Studies of Light-to-Heat Conversion and Collective Heating Effects in Metal Nanoparticle Solutions. *Nano Letters* **2009,** 9, (3), 1139-1146.

217.   Richardson, H. H.; Hickman, Z. N.; Govorov, A. O.; Thomas, A. C.; Zhang, W.; Kordesch, M. E., Thermooptical properties of gold nanoparticles embedded in ice: Characterization of heat generation and melting. *Nano Letters* **2006,** 6, (4), 783-788.

218.   Yamashita, S.; Fukushima, H.; Akiyama, Y.; Niidome, Y.; Mori, T.; Katayama, Y.; Niidome, T., Controlled-release system of single-stranded DNA triggered by the photothermal effect of gold nanorods and its in vivo application. *Bioorganic & Medicinal Chemistry* **2011,** 19, (7), 2130-2135.

219.   Wu, G. H.; Milkhailovsky, A.; Khant, H. A.; Fu, C.; Chiu, W.; Zasadzinski, J. A., Remotely triggered liposome release by near-infrared light absorption via hollow gold nanoshells. *Journal of the American Chemical Society* **2008,** 130, (26), 8175-+.

220.	Sershen, S. R.; Westcott, S. L.; Halas, N. J.; West, J. L., Temperature-sensitive polymer-nanoshell composites for photothermally modulated drug delivery. *Journal of Biomedical Materials Research* **2000,** 51, (3), 293-298.

221.	Slyadnev, M. N.; Tanaka, Y.; Tokeshi, M.; Kitamori, T., Photothermal temperature control of a chemical reaction on a microchip using an infrared diode laser. *Anal Chem* **2001,** 73, (16), 4037-44.

222.	Miao, X. Y.; Wilson, B. K.; Lin, L. Y., Localized surface plasmon assisted microfluidic mixing. *Applied Physics Letters* **2008,** 92, (12), -.

223.	Maity, S.; Downen, L. N.; Bochinski, J. R.; Clarke, L. I., Embedded metal nanoparticles as localized heat sources: An alternative processing approach for complex polymeric materials. *Polymer* **2011,** 52, (7), 1674-1685.

224.	Pitsillides, C. M.; Joe, E. K.; Wei, X. B.; Anderson, R. R.; Lin, C. P., Selective cell targeting with light-absorbing microparticles and nanoparticles. *Biophysical Journal* **2003,** 84, (6), 4023-4032.

225.	Jain, P. K.; Lee, K. S.; El-Sayed, I. H.; El-Sayed, M. A., Calculated absorption and scattering properties of gold nanoparticles of different size, shape, and composition: Applications in biological imaging and biomedicine. *Journal of Physical Chemistry B* **2006,** 110, (14), 7238-7248.

226.	Reismann, M.; Bretschneider, J. C.; von Plessen, G.; Simon, U., Reversible photothermal melting of DNA in DNA-gold-nanoparticle networks. *Small* **2008,** 4, (5), 607-610.

227.	Jones, M. R.; Millstone, J. E.; Giljohann, D. A.; Seferos, D. S.; Young, K. L.; Mirkin, C. A., Plasmonically Controlled Nucleic Acid Dehybridization with Gold Nanoprisms. *Chemphyschem* **2009,** 10, (9-10), 1461-1465.

228.	Takahashi, H.; Niidome, Y.; Yamada, S., Controlled release of plasmid DNA from gold nanorods induced by pulsed near-infrared light. *Chemical Communications* **2005**, (17), 2247-2249.

229.	Fiche, J. B.; Buhot, A.; Calemczuk, R.; Livache, T., Temperature effects on DNA chip experiments from surface plasmon resonance imaging: Isotherms and melting curves. *Biophysical Journal* **2007,** 92, (3), 935-946.

230.	FrankKamenetskii, M. D., Biophysics of the DNA molecule. *Physics Reports-Review Section of Physics Letters* **1997,** 288, (1-6), 13-60.

231.	SantaLucia, J., Jr., A unified view of polymer, dumbbell, and oligonucleotide DNA nearest-neighbor thermodynamics. *Proc Natl Acad Sci U S A* **1998,** 95, (4), 1460-5.

232.	Berg, J. M. T., J.L.; Stryer L., *Biochemia*. Wydawnictwo Naukowe PWN: Warszawa, 2005.

233.	Wood, T. D.; Chen, L. H.; White, C. B.; Babbitt, P. C.; Kenyon, G. L.; McLafferty, F. W., Sequence verification of human creatine kinase (43 kDa) isozymes by high-resolution tandem mass spectrometry. *Proc Natl Acad Sci U S A* **1996,** 93, (21), 12051.

234. Zhukov, A.; Schurenberg, M.; Jansson, O.; Areskoug, D.; Buijs, J., Integration of surface plasmon resonance with mass spectrometry: automated ligand fishing and sample preparation for MALDI MS using a Biacore 3000 biosensor. *J Biomol Tech* **2004,** 15, (2), 112-9.

235. Ravanat, C.; Wurtz, V.; Ohlmann, P.; Fichter, M.; Cazenave, J. P.; VanDorsselaer, A.; Lanza, F.; Gachet, C., Use of tandem Biacore-mass spectrometry to identify platelet membrane targets of novel monoclonal antibodies. *Analytical Biochemistry* **2009,** 386, (2), 237-243.

236. Buijs, J.; Franklin, G. C., SPR-MS in functional proteomics. *Brief Funct Genomic Proteomic* **2005,** 4, (1), 39-47.

237. Bouffartigues, E.; Leh, H.; Anger-Leroy, M.; Rimsky, S.; Buckle, M., Rapid coupling of Surface Plasmon Resonance (SPR and SPRi) and ProteinChip (TM) based mass spectrometry for the identification of proteins in nucleoprotein interactions. *Nucleic Acids Research* **2007,** 35, (6), -.

238. Stigter, E. C. A.; de Jong, G. J.; van Bennekom, W. P., Development of an on-line SPR-digestion-nanoLC-MS/MS system for the quantification and identification of interferon-gamma in plasma. *Biosensors & Bioelectronics* **2009,** 24, (7), 2184-2190.

239. Wu, H. Q.; Aboleneen, H., Sequencing oligonucleotides with blocked termini using exonuclease digestion and electrospray mass spectrometry. *Analytical Biochemistry* **2000,** 287, (1), 126-135.

240. Li, G.; Waltham, M.; Anderson, N. L.; Unsworth, E.; Treston, A.; Weinstein, J. N., Rapid mass spectrometric identification of proteins from two-dimensional polyacrylamide gels after in gel proteolytic digestion. *Electrophoresis* **1997,** 18, (3-4), 391-402.

241. Wen, N. P.; Brooker, M. H., Ammonium Carbonate, Ammonium Bicarbonate, and Ammonium Carbamate Equilibria - a Raman-Study. *Journal of Physical Chemistry* **1995,** 99, (1), 359-368.

242. Markham, N. R.; Zuker, M., DINAMelt web server for nucleic acid melting prediction. *Nucleic Acids Res* **2005,** 33, (Web Server issue), W577-81 (http://mfold.rna.albany.edu/).

243. Owczarzy, R.; Vallone, P. M.; Gallo, F. J.; Paner, T. M.; Lane, M. J.; Benight, A. S., Predicting sequence-dependent melting stability of short duplex DNA oligomers. *Biopolymers* **1997,** 44, (3), 217-39.

244. Owczarzy, R.; You, Y.; Moreira, B. G.; Manthey, J. A.; Huang, L.; Behlke, M. A.; Walder, J. A., Effects of sodium ions on DNA duplex oligomers: improved predictions of melting temperatures. *Biochemistry* **2004,** 43, (12), 3537-54.

245. Sugimoto, N.; Nakano, S.; Yoneyama, M.; Honda, K., Improved thermodynamic parameters and helix initiation factor to predict stability of DNA duplexes. *Nucleic Acids Res* **1996,** 24, (22), 4501-5.

246. Bourdelat-Parks, B. N.; Wartell, R. M., Thermodynamic stability of DNA tandem mismatches. *Biochemistry* **2004,** 43, (30), 9918-25.

247. Bonner, G.; Klibanov, A. M., Structural stability of DNA in nonaqueous solvents. *Biotechnol Bioeng* **2000,** 68, (3), 339-44.

248.   Herskovits, T. T., Nonaqueous solutions of DNA; denaturation by urea and its methyl derivatives. *Biochemistry* **1963,** 2, 335-40.

249.   Lavelle, G.; Li, A. T., Isolation of intracellular replicative forms and progeny single strands of DNA from parvovirus KRV in sucrose gradients containing guanidine hydrochloride. *Virology* **1977,** 76, (1), 464-7.

250.   Bressan, G.; Rampone, R.; Bianchi, E.; Ciferri, A., DNA conformation in N,N-dimethyl formamide-H2O solutions. *Biopolymers* **1974,** 13, (11), 2227-40.

251.   Liu, J. W.; Dave, N., Fast Molecular Beacon Hybridization in Organic Solvents with Improved Target Specificity. *Journal of Physical Chemistry B* **2010,** 114, (47), 15694-15699.

252.   Kalogianni, D. P.; Litos, I. K.; Christopoulos, T. K.; Ioannou, P. C., Dipstick-type biosensor for visual detection of DNA with oligonucleotide-decorated colored polystyrene microspheres as reporters. *Biosens Bioelectron* **2009,** 24, (6), 1811-5.

253.   Dhawan, S., Design and construction of novel molecular conjugates for signal amplification (II): use of multivalent polystyrene microparticles and lysine peptide chains to generate immunoglobulin-horseradish peroxidase conjugates. *Peptides* **2002,** 23, (12), 2099-110.

254.   Wilson, J. N.; Wang, Y.; Lavigne, J. J.; Bunz, U. H., A biosensing model system: selective interaction of biotinylated PPEs with streptavidin-coated polystyrene microspheres. *Chem Commun (Camb)* **2003**, (14), 1626-7.

255.   Li, S.; Xia, Y.; Zhang, J.; Han, J.; Jiang, L., Polystyrene spheres coated with gold nanoparticles for detection of DNA. *Electrophoresis* 31, (18), 3090-6.

256.   Siiman, O.; Burshteyn, A.; Insausti, M. E., Covalently Bound Antibody on Polystyrene Latex Beads: Formation, Stability, and Use in Analyses of White Blood Cell Populations. *J Colloid Interface Sci* **2001,** 234, (1), 44-58.

257.   WHO-IARC, IARC Monographs on the Evaluation of Carcinogenic Risks to Humans. In 1999; Vol. 71.

258.   Li, X. N.; Du, Z. W.; Huang, Q.; Wu, J. Q., Growth-inhibitory and differentiation-inducing activity of dimethylformamide in cultured human malignant glioma cells. *Neurosurgery* **1997,** 40, (6), 1250-8; discussion 1258-9.

259.   Dexter, D. L.; Barbosa, J. A.; Calabresi, P., N,N-dimethylformamide-induced alteration of cell culture characteristics and loss of tumorigenicity in cultured human colon carcinoma cells. *Cancer Res* **1979,** 39, (3), 1020-5.

260.   Grunt, T. W.; Somay, C.; Ellinger, A.; Pavelka, M.; Dittrich, E.; Dittrich, C., The differential effects of N,N-dimethylformamide and transforming growth factor-beta 1 on a human ovarian cancer cell line (HOC-7). *J Cell Physiol* **1992,** 151, (1), 13-22.

261.   Antoine, J. L.; Arany, J.; Leonard, A.; Henrotte, J.; Jenar-Dubuisson, G.; Decat, G., Lack of mutagenic activity of dimethylformamide. *Toxicology* **1983,** 26, (3-4), 207-12.

262.   Gao, X. Q., C.; Zhang, W., Studies on cell-mediated immunotoxicity of dimethylformamide. *Chinese journal of preventive medecine* **1996,** 30, (5), 269-72.

263. Loris, R.; Hamelryck, T.; Bouckaert, J.; Wyns, L., Legume lectin structure. *Biochim Biophys Acta* **1998,** 1383, (1), 9-36.

264. Krauss, S.; Buttgereit, F.; Brand, M. D., Effects of the mitogen concanavalin A on pathways of thymocyte energy metabolism. *Biochim Biophys Acta* **1999,** 1412, (2), 129-38.

265. Tomar, A.; Bansal, M. P.; Ram, G. C., Maintenance of Concanavalin A stimulated T lymphocytes from peripheral blood of goats. *Small Ruminant Research* **1995,** 18, 89-94.

266. Maezawa, Y.; Okano, K.; Matsubara, M.; Masuhara, H.; Hosokawa, Y., Morphological evaluation of cell differentiation after the isolation of single cells by a femtosecond laser-induced impulsive force. *Biomedical Microdevices* **2010,** 13, (1), 117-22.

267. Huang, X.; El-Sayed, I. H.; Qian, W.; El-Sayed, M. A., Cancer cell imaging and photothermal therapy in the near-infrared region by using gold nanorods. *J Am Chem Soc* **2006,** 128, (6), 2115-20.

268. Piasecka, A.; Leyko, W.; Krajewska, E.; Bryszewska, M., Effect of combined treatment with perindoprilat and low-power red light laser irradiation on human erythrocyte membrane fluidity, membrane potential and acetylcholinesterase activity. *Scand J Clin Lab Invest* **2000,** 60, (5), 395-402.

269. Stadler, I.; Evans, R.; Kolb, B.; Naim, J. O.; Narayan, V.; Buehner, N.; Lanzafame, R. J., In vitro effects of low-level laser irradiation at 660 nm on peripheral blood lymphocytes. *Lasers Surg Med* **2000,** 27, (3), 255-61.

270. Leichle, T.; Lishchynska, M.; Mathieu, F.; Pourciel, J. B.; Saya, D.; Nicu, L., A Microcantilever-Based Picoliter Droplet Dispenser With Integrated Force Sensors and Electroassisted Deposition Means. *Journal of Microelectromechanical Systems* **2008,** 17, (5), 1239-1253.

271. Descamps, E.; Leichle, T.; Corso, B.; Laurent, S.; Mailley, P.; Nicu, L.; Livache, T.; Bergaud, C., Fabrication of oligonucleotide chips by using parallel cantilever-based electrochemical deposition in picoliter volumes. *Advanced Materials* **2007,** 19, (14), 1816-1821.

272. Berthet-Duroure, N. Adressage et immobilisation de biomolécules sur des surfaces : Interaction spot-dans-spot et bioélectrochimie localisée à l'échelle 1-50µm. PhD thesis. Université de Toulouse, Toulouse, 2009.

273. Roupioz, Y.; Berthet-Duroure, N.; Leichle, T.; Pourciel, J. B.; Mailley, P.; Cortes, S.; Villiers, M. B.; Marche, P. N.; Livache, T.; Nicu, L., Individual blood-cell capture and 2D organization on microarrays. *Small* **2009,** 5, (13), 1493-7.

274. Wuister, S. F. K., Y.A.; Dijksman, J.F.; Kruijt-Stegeman, Y.W.: Schram, I. Imprint lithography, United States Patent (US 7,677,877 B2). 2010.

275. Larsen, A. V.; Poulsen, L.; Birgens, H.; Dufva, M.; Kristensen, A., Pinched flow fractionation devices for detection of single nucleotide polymorphisms. *Lab Chip* **2008,** 8, (5), 818-21.

276. Unsworth, C. P.; Holloway, H.; Delivopoulos, E.; Murray, A. F.; Simpson, M. C.; Dickinson, M. E.; Graham, E. S., Patterning and detailed study of human hNT astrocytes on parylene-C/silicon dioxide substrates to the single cell level. *Biomaterials* 32, (27), 6541-50.

277.   Jonghoon, C., Engineered Microdevices for Single Cell Immunological Assay *Interdisciplinary Bio Central* **2010,** 2, 1-8.

278.   Bouchet, A.; Descamps, E.; Mailley, P.; Livache, T.; Chatelain, F.; Haguet, V., Contactless Electrofunctionalization of a Single Pore. *Small* **2009,** 5, (20), 2297-2303.

279.   Grosjean, L.; Cherif, B.; Mercey, E.; Roget, A.; Levy, Y.; Marche, P. N.; Villiers, M. B.; Livache, T., A polypyrrole protein microarray for antibody-antigen interaction studies using a label-free detection process. *Anal Biochem* **2005,** 347, (2), 193-200.

280.   Descamps, E.; Leichle, T.; Corso, B.; Laurent, S.; Mailley, P.; Nicu, L.; Livache, T.; Bergaud, C., Fabrication of oligonucleotide chips by using parallel cantilever-based electrochemical deposition in picoliter volumes. *Advanced Materials* **2007,** 19, (14), 1816-+.

Développement de biopuces dédiées au tri d'échantillons cellulaires

Le présent travail de thèse repose sur la conception d'un système miniaturisé de type biopuce capable d'assurer la capture et le relargage contrôlé de différentes populations des cellules sanguines (*e.g.* lymphocytes). Ce projet a pour objectif la construction d'un outil potentiel de recherche dans le domaine de l'immunologie ainsi que du diagnostic qui permettrait non seulement de réaliser des essais à partir d'une faible quantité d'échantillon, mais aussi de réduire le temps d'analyse. L'approche consiste plus précisément en la fabrication d'une matrice d'oligonucléotides et l'immobilisation de cellules via une molécule hybride composée d'un anticorps IgG couplé à une séquence d'oligonucléotide complémentaire. La synthèse du produit conjugué est mise en place et conduit à l'assemblage fonctionnel sur biopuce. Une fois les cellules spécifiquement capturées sur la surface, deux voies de relargage contrôlé sont explorées. Ainsi, les lymphocytes sont libérés de façon contrôlée et séquentielle par clivage enzymatique d'ADN ou alors par désorption physique possible grâce au chauffage localisé. La détection se fait en temps réel par l'imagerie de la résonance plasmonique de surface (*Surface Plasmon Resonance Imaging, SPRi)* qui présente l'avantage de pouvoir suivre les phénomènes biomoléculaires en absence de marquage et d'apporter une réponse simultanée d'un échantillon biologique sur un grand nombre de sondes. Accessoirement, une approche instrumentale particulière nous permet d'observer les étapes de capture/relargage par microscopie optique classique. La construction de la biopuce permet également l'élargissement à plusieurs cibles et ouvre ainsi la voie à de nombreuses possibilités d'exploration en termes d'application pour l'analyse d'échantillons biologiques plus complexes tels que du sang.

Mots clés : *biopuce, tri cellulaire, imagerie SPR, biomolécules conjuguées, enzyme de restriction, effet photothermique*

Development of biochips for blood cell sorting

This PhD thesis is devoted to conception of a miniaturized system of biochip type able to perform a controlled capture and release of different populations of the blood cells (e.g. lymphocytes). The main objective of the project is to create a potential tool of research, especially in the field of immunology, and medical diagnostics as well, that could perform short-time analyses by using a small sample amount. The approach relies more precisely on fabrication of a DNA matrix and further immobilization of cells through a hybrid molecule composed of an IgG antibody covalently coupled with short oligonucleotide sequence. Synthesis of the conjugated product is developed and demonstrates functional assembly on the micro-platform. Lymphocytes are specifically addressed onto biochip surface and once they are captured, two independent strategies of selective release are proposed. Therefore, immobilized cells are specifically detached either upon enzymatic cleavage of oligonucleotide substrate or physically desorbed by local heating and denaturation of double stranded DNA. The system makes use of *Surface Plasmon Resonance Imaging (SPRi)* to enable real time detection of different biomolecular phenomena in a label-free and high-throughput manner. Accessorily, a particular instrumental approach is developed in order to observe cell capture-release steps directly under optical microscopy. The biochip construction permits to extend its performance to many targets and may be further explored in terms of application to analysis of complex biological samples such as blood.

Keywords: *biochip, cell sorting, SPR imaging, biomolecule conjugation, restriction enzyme, photothermal effect*